

NBSIR 76-1154

Consideration of Fracture Mechanics Analysis and Defect Dimension Measurement Assessment for the Trans- Alaska Oil Pipeline Girth Welds Volume I

October 18, 1976

This is a Final Report

NOTE: This document has been prepared for the use
of the Materials Transportation Bureau,
Department of Transportation. Responsibility
for its further use rests with that agency.

Prepared for

**Materials Transportation Bureau
U.S. Department of Transportation
Washington, D. C. 20590**

NBSIR 76-1154

**CONSIDERATION OF FRACTURE
MECHANICS ANALYSIS AND DEFECT
DIMENSION MEASUREMENT
ASSESSMENT FOR THE TRANS-
ALASKA OIL PIPELINE GIRTH WELDS
VOLUME I**

October 18, 1976

This is a Final Report



Prepared for
Materials Transportation Bureau
U. S. Department of Transportation
Washington, D. C. 20590

TABLE OF CONTENTS

	<u>Page</u>
Foreword	1
List of Symbols.	2
Executive Summary.	6
1. Introduction	9
2. Problem Definition and Scope	12
3. NBS Data on Material Properties.	14
4. Weld Defect Measurement Assessment	79
5. Remarks on Pipeline Design and Stress Analysis	113
6. Assessment of Material Property Data	118
7. Fracture Analyses.	129
8. Weld Defect Summary.	166
9. Conclusions.	174

FOREWORD

The National Bureau of Standards (NBS) received a request in June, 1976, from the Department of Transportation, Office of Pipeline Safety Operations, for technical assistance in evaluating anticipated requests for waivers involving girth welds in the trans-Alaska oil pipeline. To respond to that request, NBS formed a Trans-Alaska Pipeline Project (TAPP) involving a number of NBS personnel. Mr. Harold Berger was named Leader of the TAPP and Dr. John H. Smith was appointed as Deputy. Technical task groups within the project were headed by Dr. Richard P. Reed (Fracture Mechanics Analysis), Dr. M. Linzer (Nondestructive Evaluation), Dr. Robert C. Placious (Assessment of Radiographic Measurements), and Dr. Joan Rosenblatt (Statistics and Mathematical Analyses). Legal assistance was provided by Robert G. Hayes and Gordon Fields. Liaison with the NBS Office of Programs was through Dr. Bruce W. Morrissey.

Major report sections were prepared by M. B. Kasen, J. F. LeBrecque, H. M. Ledbetter, H. I. McHenry, D. T. Read, R. P. Reed, R. E. Schramm, L. L. Sparks, and R. L. Tobler from the NBS Boulder Laboratory and by J. T. Fong, D. A. Garrett, C. G. Interrante, J. A. Lechner, R. C. Placious, J. Rosenblatt, and J. H. Smith of the Washington Laboratory. Critical reviews and analyses were provided by R. deWit, E. Passaglia, and R. Thomson. Many others contributed to this project and report. A partial listing includes the following: F. Biancaniello, G. Birnbaum, C. Brady, B. H. Colvin, N. M. Crockett, C. E. Dick, J. J. Filliben, M. Ganoczy, A. J. Goldman, D. T. Goldman, D. E. Harne, G. E. Hicho, N. Hsu, L. W. Ketron, H. H. Ku, J. W. Motz, J. Moulder, M. Reeve, R. G. Rehm, T. P. Royston, A. W. Ruff, N. Sanchez, R. Schofer, D. Schwab, G. C. Serig, D. Wilson and W. Wilson.

In addition, several consultants contributed ideas, reviews, and in some cases, reports to this project. Consultants included Professor J. A. Begley, Ohio State University; E. L. Criscuolo and D. Polansky, Naval Surface Weapons Center; Professor R. E. Green, Johns Hopkins University; Dr. R. Halmshaw, Royal Armament Research and Development Establishment; Professor G. R. Irwin, University of Maryland; Professor R. C. McMaster, Ohio State University; Professor P. C. Paris, Washington University; and Dean R. D. Stout, Lehigh University.

Fact finding visits were made to several organizations including The Welding Institute, Southwest Research Institute, Rockwell International Rocky Flats Laboratory, and the Alyeska Pipeline Service Company. The open exchange of information and cooperation are gratefully acknowledged.

We are pleased to acknowledge the assistance of all these people and the many others who contributed to this NBS Trans-Alaska Pipeline Project.

Harold Berger
John H. Smith

LIST OF SYMBOLS

For the purpose of this report, the following notation is used. Some extra symbols, used only in certain sections, are defined there;

A	Area under load-displacement curve of test specimen. (Section 3E).
A	Area of separated metal = Bb (Section 3I and Appendix Q).
a	Depth of defect into pipe wall.
a	Crack depth in test specimen.
\bar{a}	Allowable defect parameter of Draft British Standard.
Δa	Crack extension in test specimen.
a^*	Effective crack depth in Begley-Landes-Wilson model.
$\frac{da}{dN}$	Fatigue crack growth rate, which equals $C(\Delta K)^n$ according to the Paris equation.
B	Test specimen thickness.
b	Length of uncracked ligament in test specimen = W-a.
BSI	British Standards Institute.
BWI	British Welding Institute.
C	Empirical constant in the Paris fatigue-crack-growth equation.
CVN	Charpy V-notch
c	$r/2$
CIT	Cranfield Institute of Technology.
COD	Crack opening displacement = δ .
D	Radiographic film density.
D_m	Depth of defect measured by RI technique.
D_t	True depth of defect.
DOT	Department of Transportation.
E	Young's modulus.

F_c	Ligament closing force in the Begley model.
E_D	Total absorbed energy (dial energy).
E_M	Energy to Max Load (initiation energy).
E_p	Propagation energy = $E_D - E_m$.
EPRI	Electric Power Research Institute.
G, G_D	Film gradient.
HAZ	Heat affected zone.
J	J-integral (the energy per unit of new separational area that is released at the tip of a perfect crack in an elastic solid during an infinitesimal, virtual increment of forward crack extension).
J_{Ic}	Measure of fracture toughness derived using the J-integral concept.
K	Stress-intensity factor.
K_d^*	Fracture toughness derived from the equivalent-energy concept.
K_{Ic}	Plane-strain fracture toughness.
K_{Jc}	Static fracture toughness derived from J-integral concept.
K_{Jd}	Dynamic fracture toughness derived from J-integral concept.
ΔK	Stress-intensity range in fatigue.
L	Distance over which residual stresses act in the Begley model.
l	Length of defect parallel to pipe wall.
LEFM	Linear elastic fracture mechanics.
M	Folias correction factor for pipe wall curvature.
m	Plastic constraint factor in conversion between J_{Ic} and δ_c or J and δ .
M_{back}	Special function occurring in the Irwin surface-flaw equation.
N	Number of fatigue cycles, i.e., service lifetimes.
NBS	National Bureau of Standards.
n	Empirical exponent in the Paris fatigue crack growth equation.
OPSO	Office of Pipeline Safety Operations.

P	Applied load.
P_A	Arrest load for fast fracture
P_F	Fast-fracture (cleavage) load
P_{GY}	General-yield load
P_M	Maximum load
P_{max}	Maximum load in fatigue.
P_{min}	Minimum load in fatigue.
Q	Special function occurring in the Irwin surface-flaw equation.
R	Stress ratio = $\sigma_{min}/\sigma_{max}$. (Section 7A).
R	Through-wall reduction (Section 4B and Appendix L).
r	Pipe radius.
RI	Rockwell International.
S	Span in bend test.
SWRI	Southwest Research Institute.
T, t	Thickness of penetrometer and shim.
t	Thickness of pipe wall.
t_{GY}	Time to general yield
t_m	Time to maximum load
W	Test specimen width.
W_M	Absorbed energy associated with maximum load
Δx	Change in thickness of the sample traversed by the x-ray beam.
Y	Special function occurring in the Srawley-Gross equation for stress intensity factor of test specimen.
Δ	Displacement due to residual stress in the Begley model.
δ	Crack opening displacement = COD.
δ_C	Critical COD.
ϵ	Applied tensile strain.

ϵ_y	Yield strain = σ_y/E .
μ	Linear absorption coefficient (x-radiation).
λ	Fong safety factor
ν	Poisson's ratio.
σ	Applied tensile stress.
$\bar{\sigma}$	Flow strength.
$\Delta\sigma$	Stress range = $\sigma_{\max} - \sigma_{\min}$.
σ_c	Ligament closing stress in the Begley model.
σ_{\max}	Maximum σ in fatigue.
σ_{\min}	Minimum σ in fatigue.
σ_u	Ultimate tensile strength.
σ_R	Residual stress.
σ_y	Yield stress (0.2% offset).
σ_{yd}	Dynamic yield stress.
σ_{ys}	Static yield stress.

EXECUTIVE SUMMARY

A number of buried girth welds in the 48 inch diameter trans-Alaska oil pipeline contain radiographically detected defects somewhat larger than permitted by the Department of Transportation (DOT) Regulations, 49 CFR Part 195. The Alyeska Pipeline Service Company (Alyeska) has requested waivers for these welds from DOT. The waiver request is based upon a fracture mechanics analysis. The information presented by Alyeska in support of the waiver request contains proposed allowable defect size curves for the weld defect types involved and descriptions and measurements of the weld defects in terms of both length along the weld circumference and depth in the through-wall direction.

In anticipation of this waiver submission, DOT requested assistance from the National Bureau of Standards (NBS) in evaluating the fracture mechanics analysis and the nondestructive evaluation (NDE) methods used to detect and determine dimensions of specific weld defects. This report is the response to that request.

Material properties needed for the fracture mechanics analysis were determined from samples of field welds. NBS measured a number of properties, for example, elastic, tensile, fracture toughness, and fatigue, to confirm that our data agreed with more comprehensive test program results reported in the open literature or reports from the (British) Welding Institute. In addition, NBS determined the dynamic fracture toughness to assess the effect of high rates of loading on the toughness and allowable defect sizes. The effect of aggressive environments on cracking of the pipe and welds was also assessed.

For this defect size and orientation case, there is no accepted theoretical formulation or empirical data base to determine a specific allowable defect size curve. Therefore, it was necessary to use safety factors and other judgment considerations in modeling the allowable defect size curves. This may lead to a more conservative design approach than would otherwise prove necessary. Future work to provide experimental verification of the allowable defect size curves would permit performance-related regulations to be written. These regulations might provide the same level of safety in a more cost-effective manner.

Taking into account the material properties, the stresses expected in the pipeline and the several fracture mechanics models considered in this report, NBS concludes that the Alyeska allowable defect size curve for nonplanar defects is reasonable. For the planar defects and arc burns, the Alyeska curves are reasonable except for small defect lengths where the Alyeska curves allow unlimited defect depth; the other fracture mechanics analyses do not allow unlimited defect depth.

The waiver request also reported weld defect sizes, both in terms of length and depth, as determined from existing field radiographs of the girth welds. The regulation now calls for defect length measurement from the radiographs. However, there can be differences in reported defect lengths by different interpreters. Comparing results from the several organizations who measured length in this case, there were a number of major discrepancies.

Defect depth measurements are not normally made from radiographs and, of course, were not originally intended from these field radiographs. The depth measurement can be made in cases where good control of the radiographic procedure, particularly in terms of x-ray energy and film processing, can be maintained. With this control, the relationship between film density and the thickness of metal can be predicted. Taking into account the expected variations encountered in field situations, it might have been anticipated that the field radiographs would show large variations from the predicted contrast. This large, observed variation in contrast makes any defect depth measurement which depends on film density observations in the weld and defect area subject to error.

Three methods were used to measure defect depths from the Alyeska radiographs. Southwest Research Institute (SWRI) used both a densitometer method and a visual comparison technique. Rockwell International (RI) employed a visual comparison method involving only the weld and defect area. In both SWRI methods, comparisons were made to the film contrast for the shim-penetrameter image on the pipe wall.

Possible sources of error for the SWRI densitometer method include uncertain values of the shim-penetrameter thickness and the inaccuracy of measuring radiographic film densities in the areas of the weld (which does not have a constant thickness) and the defect (which may not normally have a predictable, uniform shape). The film density measurements used to determine defect depth from the field radiographs were made with a densitometer with measuring aperture of 1 mm. This does not permit the accurate measurement of defect sizes less than about 1.25 mm in width or diameter, a limitation that could have been surmounted by the use of a more sophisticated densitometer. For the depth measurements made by the SWRI densitometer method, estimates of possible errors have been made. For the depth measurements made by the SWRI method of visual comparison of contrast in the defect area and the penetrameter-shim area, no assessment of accuracy was possible.

The visual depth measurements made by RI have been analyzed. Based on laboratory x-ray calibration data, the RI method tends to underestimate the defect depth in increasing amounts for defects of greater depth. However, these corrections are based on laboratory x-ray films. For the Alyeska films, there are many field radiographs whose contrast falls outside the contrast limits predicted by the film response and expected radiographic procedure. This poses a dilemma since the reason for this change in film contrast is not known. If the contrast variations are due to extreme changes in x-ray voltage or changes in film processing, an accurate depth determination by the RI method may not be possible. However, if the contrast changes were caused by shim thickness variations or densitometer reading errors, the accuracy of the RI method may not be affected.

In support of the RI measurements there is information presented to demonstrate that the RI depth measurements tend to be larger (more conservative) than those made by the SWRI densitometer method. This is important because these two sets of measurements were taken by independent approaches and because the SWRI measurements should not be influenced by film contrast variations. It is also demonstrated that RI measurements of several natural defects in welds furnished to NBS by Alyeska, showed good correlation with laboratory radiographic measurements. Since the RI method is the only one used to measure the depth of all weld defects still under consideration for waiver, more comparisons may be desirable in order to set limits on this method.

The effective depth of an arc burn cannot be determined directly by depth measurements from the radiographs. However, a reliable correlation between arc burn diameter or width and the effective depth (which includes the heat-affected zone) has been established. Therefore, the effective depth of the arc burn can be determined from the diameter or width measured radiographically.

In summary, the fracture mechanics analyses provide a method to evaluate the performance of the pipeline girth welds in terms of allowable defect sizes. Defect lengths can be measured accurately, although some discrepancies have been noted. Arc burn diameters or widths can be measured and a method for converting that measurement to an effective depth is described. For other defect types, the depth measurement becomes more difficult and is subject to possible error as described in this report.

1. INTRODUCTION

The trans-Alaska oil pipeline, which stretches 800 miles from Prudhoe Bay to the terminal at Valdez, is being constructed by the Alyeska Pipeline Service Company (Alyeska). Field construction of the pipeline began in 1975 following several years of negotiation between the oil companies involved and the United States Government. The stipulations for the agreement [G-1, exhibit D]¹ between the oil companies and the Department of Interior reached in 1974 provide that the design, material and construction, operation, maintenance and termination practices employed in the pipeline system would be in accordance with safe and proven engineering practice, and would meet or exceed several designated standards, including those set out in the Department of Transportation (DOT) Regulations, 49 CFR Part 195, "Transportation of Liquids by Pipeline".² It was further stipulated that all mainline girth welds would be inspected by radiography, a requirement beyond that normally called for in the DOT regulations for liquid pipelines.

Soon after field welding began, some doubts were raised as reported by Mr. E. L. Patton, Chairman and Chief Executive Officer of the Alyeska Pipeline Service Company, about the quality of the radiographic film interpretation.³ As construction of the pipeline progressed, a number of pipeline girth welds were buried or made relatively inaccessible. Reinterpretation of the radiographs of some of the buried or inaccessible welds showed weld defect sizes beyond those permitted by 49 CFR, Part 195.

On August 30, 1976, Alyeska requested that DOT waive the requirements of 49 CFR Part 195 for some of these girth welds. Documentation supporting Alyeska's request for a waiver consisted mainly of a four-part study entitled: "Fracture Mechanics Study of Buried Field Girth Welds."⁴ The study tracks the DOT published suggested waiver application.⁵ The Alyeska waiver request depends upon fracture mechanics analysis. The analysis leads to a proposed acceptable defect size upon which a decision to accept or reject a pipe weld defect can be based. The analysis requires information which includes the defect type, and dimensions, and the pipeline mechanical properties, operating stresses and projected thermo-mechanical history.

1. See reference G-1 listed in Appendix G (U.S. Government documents).

2. See reference G-2.

3. See reference G-3 for public statement by E. L. Patton dated July 20, 1976.

4. See reference H-1 listed in Appendix H (Alyeska documents).

5. See Vol. 41, Federal Register, pp. 34375-77, (August 13, 1976) [G-4].

In anticipation of the Alyeska waiver request, the Office of Pipeline Safety Operations (OPSO) of DOT approached the National Bureau of Standards (NBS) in June 1976 to request technical assistance in evaluating the fracture mechanics analysis and the nondestructive evaluation (NDE) methods used to detect and determine dimensions of weld defects. The fracture mechanics aspects of the NBS developed program were established shortly after NBS was contacted by OPSO. It was agreed by the Materials Transportation Bureau and NBS⁵ that NBS would evaluate the fracture mechanics analysis and independently assess the material property data.

The NDE aspect of the NBS program has been more flexible because of the changing nature of the anticipated Alyeska waiver request. As initially presented by OPSO, the problem was one of evaluating an ultrasonic system which would be used to inspect welds from inside the pipe. The ultrasonic system, under development as a result of a contract between Alyeska and Holosonics, Inc., presented the inspection information in an image format so that direct comparisons could be made with radiographic inspection. The system was expected to be used to inspect welds for which radiographic information was unavailable or in question.

The Holosonics ultrasonic system was demonstrated to the President's Fact Finding Team on the Trans-Alaska Pipeline System Problem⁷ on July 13, 1976, in Fairbanks, Alaska. Problems with the system were noted, however, and no request for its use has been received by OPSO. The NBS role in regard to the ultrasonic inspection included technical preparation for the evaluation of the system and the preparation of a set of guidelines by which any proposed alternate NDE system could be judged. Those guidelines are included as part of this report.

After it had been established by OPSO that the existing field radiographic inspection records would be used to provide the defect dimensions necessary for the fracture mechanics analysis, NBS agreed to review the methods used to measure these dimensions. An assessment of that methodology is also included in this report.

The NBS fracture mechanics analysis developed alternative procedures to the one used by Alyeska to determine allowable defect size. Bearing in mind that fracture mechanics as applied to this problem is an inexact science, these analyses will assist OPSO to determine if the allowable defect size curves proposed by Alyeska are reasonable. There are several methods by which the fracture mechanics analysis can be made, and therefore, this report includes several such analyses.

6. See NBS Statement of Work dated September 8, 1976 [G-5].

7. See report by J. W. Barnum dated July 17, 1976 [G-6].

The assessment of the radiographic methodology determines limits, where possible, on the accuracy of the defect size measurement. The defect sizes, when coupled with the fracture mechanics analyses, permit the assessment of the likelihood that a given weld defect will result in a failure.

At least three precautionary observations should be made at the outset of this report. One, there is no presently accepted procedure in the United States for fracture mechanics analysis of ductile materials. Additional large scale testing and elastic-plastic analysis research is required to produce a standardized procedure.

A second precautionary observation is that the radiographic measurement of the size of a weld defect in the through-wall direction (hereinafter referred to as the depth dimension) is not a widely accepted practice. Since there is no accepted industry standard for this measurement, one that is critical to the fracture mechanics analysis, the variables that can influence the measurement are described and assessed so that decisions can be made concerning the defect size.

Finally, it is worth noting that when all the technical information on stress, defect size, and material properties is collected and subjected to fracture mechanics analyses to arrive at an assessment of the Alyeska waiver request, it becomes necessary and prudent to adopt several so-called safety factors in engineering-type calculations to account for variables in all phases of measurements ranging from laboratory data to field and fabrication quality control. These safety factors discussed here are independent of the analysis requirements published by DOT. A more detailed discussion of the implications of safety factors in fracture analysis is included in this report.

2. PROBLEM DEFINITION AND NBS SCOPE OF WORK

The Alyeska waiver request consists of several large volumes of supporting documents. These documents contain information on the material properties of the base metal, heat-affected zone, and weld material. Material property data, including fracture toughness, fatigue-crack-growth rate, stress corrosion threshold and tensile properties are used by Alyeska to perform a fracture mechanics analysis and determine allowable defect sizes. A knowledge of the stress spectrum the pipeline will experience over its proposed 30-year lifetime is also required since this is necessary to assure that stress corrosion and fatigue will not cause defects to grow to the point that a through-wall crack occurs. The other major part of the waiver request concerns the specific welds for which a waiver from the requirements of 49 CFR part 195 is being made. The weld data submitted by Alyeska included a description of the defect as to location and type, and dimensional information concerning the defect length and the depth, or amount of steel missing in the through-wall direction. The waiver documents are listed, along with other Alyeska material in Appendix H of this report.

The two major aspects of the waiver justification are: (1) the fracture mechanics analysis which allegedly provides a demarcation between defect sizes that are acceptable (will not cause failure) and those that are not, and (2) Alyeska's measurement of actual weld defect dimensions which, after factors of safety are applied, are compared to the fracture mechanics analysis.

The actual number of welds involved in the waiver request changes as the Alyeska Pipeline Service company continues to repair and/or replace suspect welds in the fields. NBS has been informed that this remedial work is continuing as long as weather conditions in Alaska permit. The types of weld defects for which a waiver is requested include, incomplete penetration, incomplete fusion, elongated slag inclusion, gas pocket, spherical porosity and cluster porosity, wormhole porosity, hollow bead, crater cracks and arc burns. These weld defect types are described generally in the Alyeska Welding and Radiographic Support Manual included in Appendix H of this report. The lengths of weld defects involved in the waiver request vary appreciably between the various types of defects; these are generally a few inches or less. However, a few defect lengths in the Sept. 10, 1976 submission to DOT (see Section 8) are in excess of 7 inches. Weld defect depth dimensions submitted by Alyeska (before NBS analysis of the accuracy of these figures and before a new set of depth figures were obtained by Rockwell International personnel for DOT) are generally small (less than 0.040 in.) but a few are in the range greater than 0.060 in. in depth. The nominal wall thicknesses of the pipe are 0.462 and 0.562 in.

The NBS tasks were to evaluate the Alyeska fracture mechanics analysis and methods of defect measurement. To accomplish that it was necessary to conduct several studies, all of which are described in this report. In Section 3, material property data generated by NBS are given. These tests were necessary in order to verify the material property data used in the fracture mechanics analysis.

The nondestructive evaluation aspects of the problem are discussed in Section 4. Although NBS did not actually measure the sizes of the weld defects, the methods used to obtain these dimensions are reviewed and analyzed so that the accuracy of the measurements may be assessed. Where possible this assessment is given. However, there remain several parts of the measurement methods for which sufficient information for an assessment was not available. These are defined.

In Section 5, the stress spectrum for the pipeline is examined; as indicated above, the stress spectrum is needed to determine the growth of defects during the pipeline's design life. Although the stress spectrum has been established, some of the uncertainties in these calculations are discussed.

The assessment and uncertainty estimates given in Section 6 put the data on material properties in perspective and permit the fracture mechanics analyses to be made using defined data, constants, and conditions.

The fracture mechanics analyses are presented in Section 7. Several analyses are given, representing several different models presently under consideration by the scientific community. For the range of defect sizes under consideration in this case, there is no experimental data base nor a three-dimensional elastic-plastic analysis. The several analyses given are compared to those proposed by Alyeska for the various types of defects. This Section also includes a discussion of the various safety factors involved in the calculations. For each class of defects considered in the waiver request, several theoretical curves are presented for proposed allowable weld defect sizes.

A summary of the weld defect size information is given in Section 8. This section presents defect sizes as given by Alyeska, SWRI, and RI. It also includes RI arc burn measurements after NBS adjustment for depth. Important information concerning the location of welds and the steel material is discussed in this section.

The conclusions are presented briefly in Section 9. The appendices contain many supporting documents, references, consultant reports and explanatory technical material.

In a project of this magnitude and time scale, it is not surprising to find that some aspects of the information are not as complete as one would expect to realize in a longer duration program. Whenever this is true, it has been pointed out and the implications of the missing information described. In spite of this, it is our belief that this report meets our primary objective, namely to provide DOT with the technical data and analyses to permit DOT to make their decisions concerning the Alyeska waiver requests.

The units of measurement are consistent within each section of the report. For example, material property data are given primarily in metric units whereas defect dimensions are given in English units. Multiple units are given in a few parts of this report.

NBS recognizes and has attempted to respond to the urgent need for this study as pressed for by DOT. NBS has responded by forming a Trans-Alaska Pipeline Project Task Force which includes employees throughout the Bureau. The work described in this report was accomplished over the three month period beginning on approximately July 1, 1976.

3. NBS DATA ON MATERIAL PROPERTIES

- 3A. WELDMENT SELECTION
- 3B. SPECIMEN GEOMETRIES AND LOCATIONS
- 3C. ELASTIC PROPERTIES
- 3D. TENSILE PROPERTIES
- 3E. FRACTURE TOUGHNESS OF HEAT-AFFECTED ZONE
- 3F. FATIGUE-CRACK GROWTH RATES
- 3G. SIMULATED-SERVICE FATIGUE PROPERTIES
- 3H. SIGNIFICANCE OF ARC BURNS
- 3I. CHARPY V-NOTCH IMPACT SPECIMEN TESTING
- 3J. STRESS-CORROSION CRACKING TESTS

3A. WELDMENT SELECTION

The following criteria were used to select girth welds from the trans-Alaska pipeline for study by NBS.

- (1) Welds must be 1975 production-line type.
- (2) Welds must be identified positively.
- (3) All welding procedures that enter anticipated variance requests must be represented by two complete girth welds.

Criteria 1 and 2 were met by obtaining the original radiographic films of each weld. Dates on the films confirmed 1975 production. The radiographic "fingerprint," that is, locating radiographic landmarks such as the distances of the longitudinal seam welds from the top button position, confirmed the weld number. This permitted NBS to detect immediately that one of the original radiographs furnished by Alyeska (for NBS weld 2) was incorrect. This clerical error was promptly corrected. Alignment-sheet numbers on the radiographs permit precise location of the weld in the pipeline.

Welding procedures 102A-1 and 104A-1 were expected to enter into waiver requests, according to Alyeska personnel (Mr. Joseph Willing, Alyeska Pipeline Service Company). Two welds of each procedure were, therefore, required. These procedures differ mainly in the type of shielded-arc electrode. The 102A-1 procedure uses AWS E8010-G (Phoenix Cel 80) electrodes, while the 104A-1 procedure uses AWS E7010-G (Lincoln Shield Arc 65+) electrodes. Alyeska records were relied on for weld-procedure identifications. These were checked by chemical analyses of the electrodes and the welds. Both wet-chemistry and emission-spectroscopy results were obtained by Dr. R. W. Burke of the NBS Analytical Chemistry Division. These analyses for nickel content are included in Table 1. They show that Alyeska mislabeled the NBS #4 weldment as 102A instead of 104A. This error made it impossible to meet criterion 3 since time was not available to obtain and analyze a second 102A weld.

Weldments received at NBS are listed in Table 1. Weldment 88070 of procedure 302A-1 will not enter into waiver considerations. However, it had been already cut from the pipeline and was included to provide additional base metal for study. To facilitate specimen preparations, approximately 20 cm (8 in) of base metal was retained on both sides of each weld. All welds were quartered and labeled for shipping as shown in Fig. 1. A photograph of an as-received weldment is shown in Fig. 2.

Welds 88070 and 88119 were selected by M. B. Kasen of NBS, Boulder, during a visit to the pipeline July 15-24, 1976. Arrangements for selecting and delivering the remaining weldments were made then. Quick delivery was sought consistent with the minimum disruption of the Alyeska remedial-weld program.

Table 1. Trans-Alaska-pipeline girth welds received at NBS for study.

Weldment No.		Weld Procedure	Wt. Pct Nickel ^b	Alignment Sheet	Date Radiographed	Date Received at NBS
NBS	Alyeska					
1	88070	302A-1	0.15	122	14 Oct. 1975	26 July 1976
2	88119	104A-1	0.67	123	14 Oct. 1975	26 July 1976
3	79907	102A-1	0.15	123	17 Aug. 1975	5 Aug. 1976
4 ^a	75061	104A	0.90	135	9 May 1975	5 Aug. 1976
5	88503	104A-1	0.79	123	17 Oct. 1975	19 Aug. 1976

- a. Alyeska identified this weldment as a 102A type, but chemical analysis shows it is actually a 104A type.
 b. See Appendix F for details of chemical analysis.

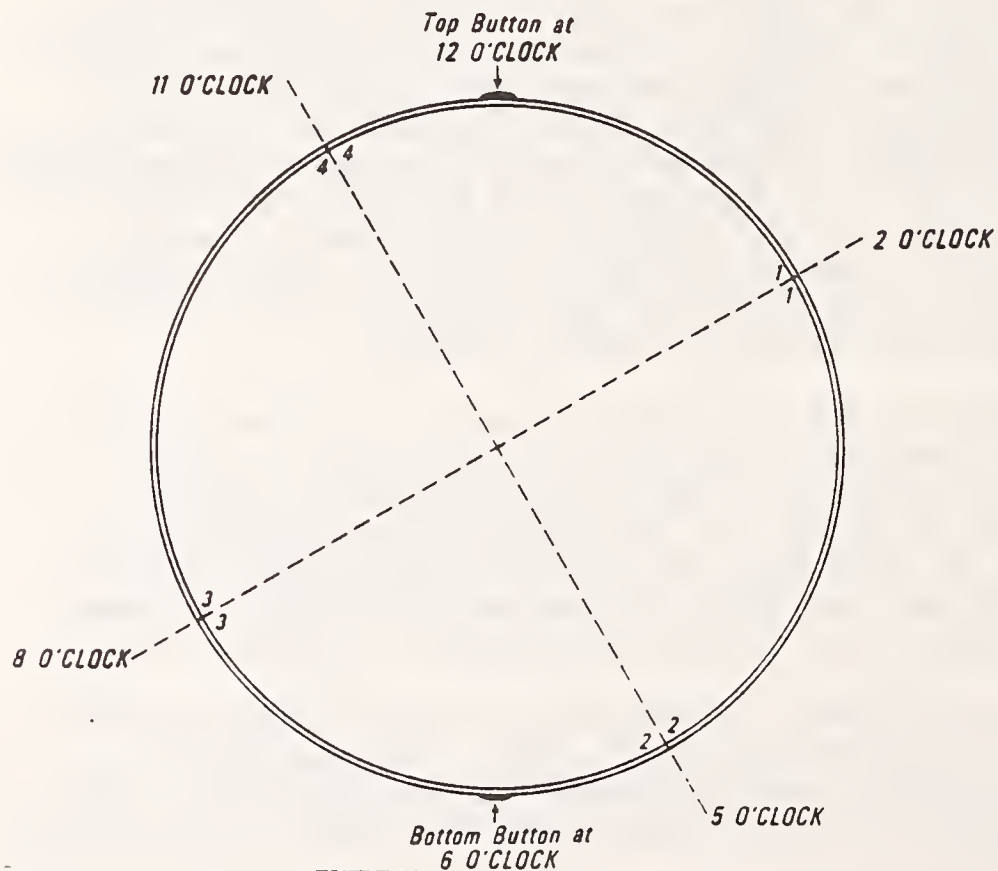


Fig. 1. Schematic of method for quartering and labeling the trans-Alaska pipeline girth weldments for shipping to NBS, Boulder. Each quarter is to be stenciled with the weld number and with markings 1-2, 2-3, etc.

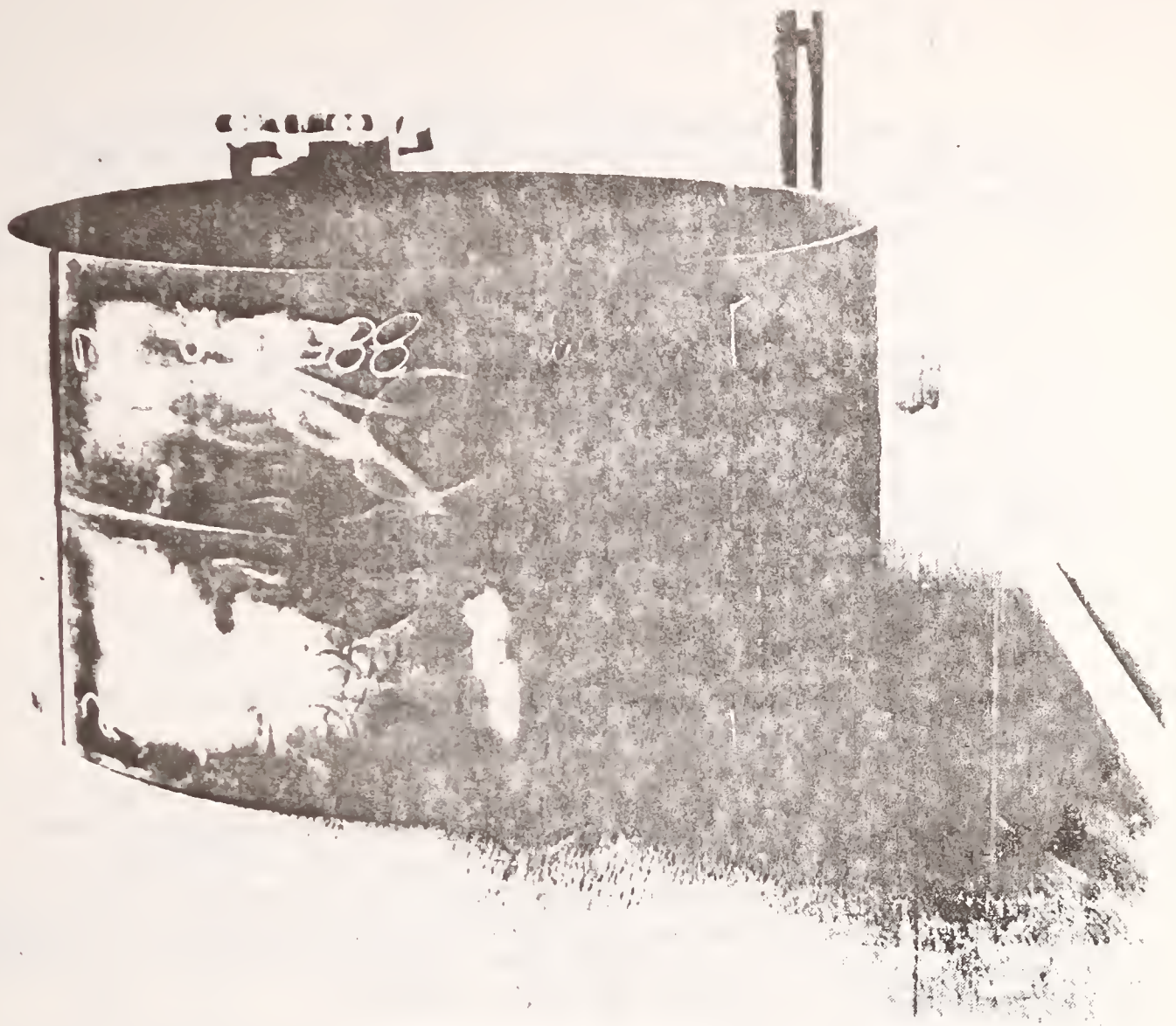


Fig. 2. Quartered Alyeska weldment 88503 received at NBS, Boulder.

3B. SPECIMEN GEOMETRIES AND LOCATIONS

Five cylindrical weldments of the Alaskan pipeline were supplied to NBS, Boulder by Alyeska for testing and evaluation. The weldments are shown schematically in Fig. 3. All five cylinders were cut into quarters approximately the same size.

Ten types of test specimens were prepared from the weldments:

1. Compact tensile (CT) for J-integral tests
2. Tensile (weld) (T)
3. Tensile (base metal) (T)
4. Surface-flaw fatigue (SF)
5. Arc-burn fatigue (AB)
6. Bend fatigue (BF) for crack-growth tests, weld metal
7. Bend threshold (BT) for stress corrosion tests, weld metal
8. Bend (B) for crack-growth tests, base-metal
9. Elastic (E)
10. Charpy impact (CI)

where the abbreviations in parentheses were used to mark the specimens. Diagrams of these specimens are shown in Fig. 4.

Detailed specimen-location maps for all quarters are shown in Figs. 5-9. Shaded areas on each quarter map indicate heat-affected zones from which no specimens were taken. All specimens are located relative to the distance from top-dead-center (TDC) for the particular weld. Top-dead-center indicates the point at which the welding begins and proceeds in opposite directions around the pipe. The distance of each edge from TDC is indicated in the upper corners of each map.

Each specimen is identified by a hyphenated code number. The first digit is the NBS, Boulder number substituted for the Alyeska weld number; NBS numbers 1 through 5 are Alyeska numbers 88070 (302A-1), 88119 (104A-1), 79907 (102A-1), 75061 (104A), and 88503 (104A-1), respectively. The number following the hyphen is the specimen number from the weldment; specimens from each weldment are numbered consecutively in the order they were prepared. Letters following this number indicate the type of specimen. For example, 2-26SF indicates the specimen was the twenty-sixth taken from NBS number 2 (Alyeska 88119, 104A-1) weldment, and the specimen is a surface-flaw type. A summary of the origins of all test specimens prepared at NBS, Boulder is given in Table 2.

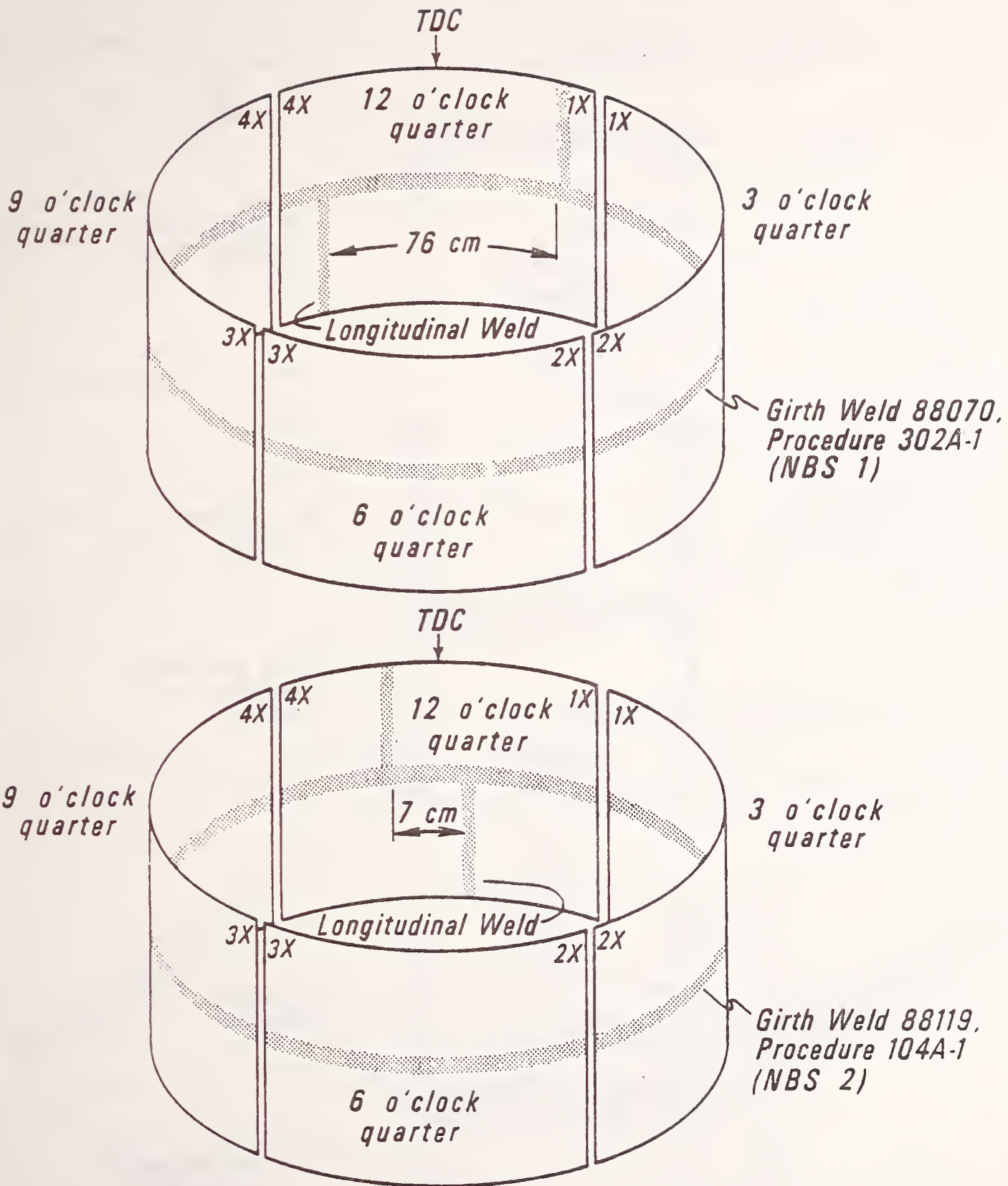
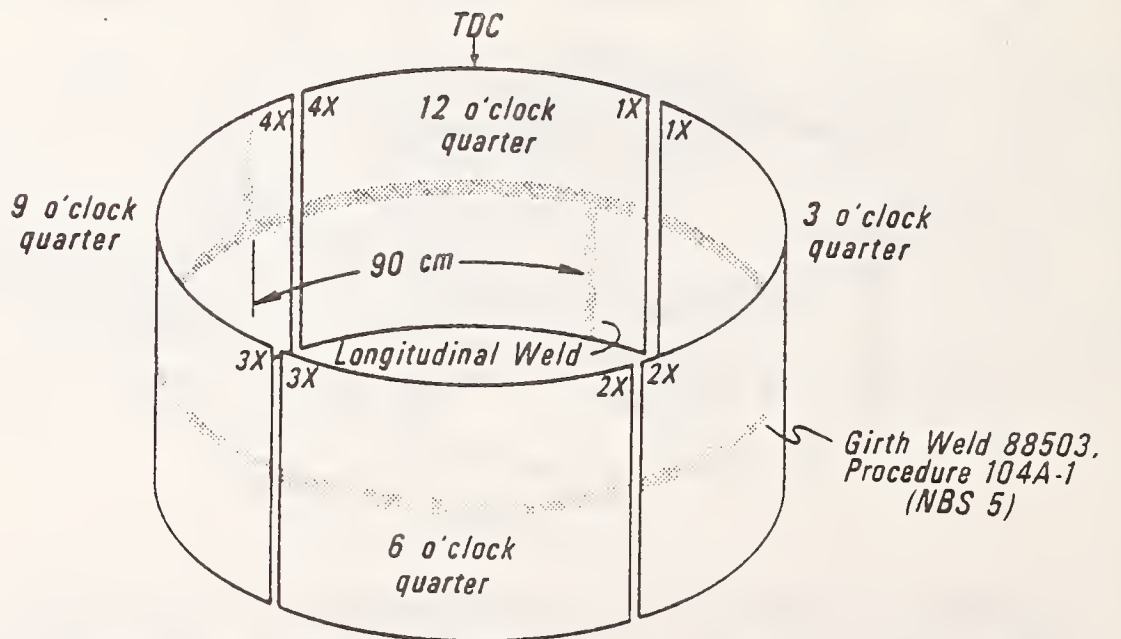
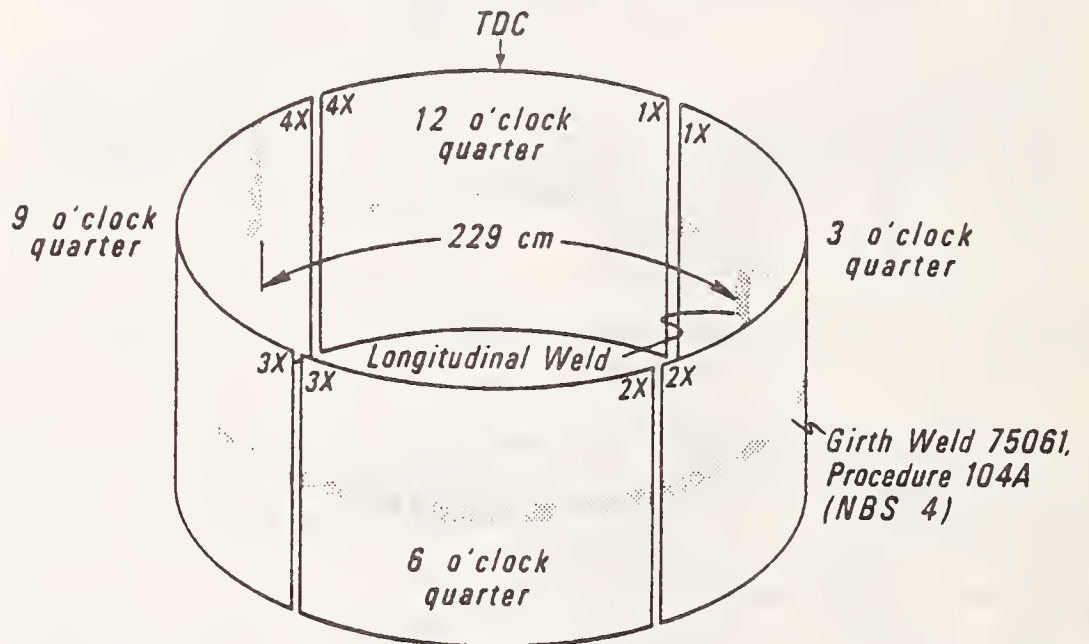
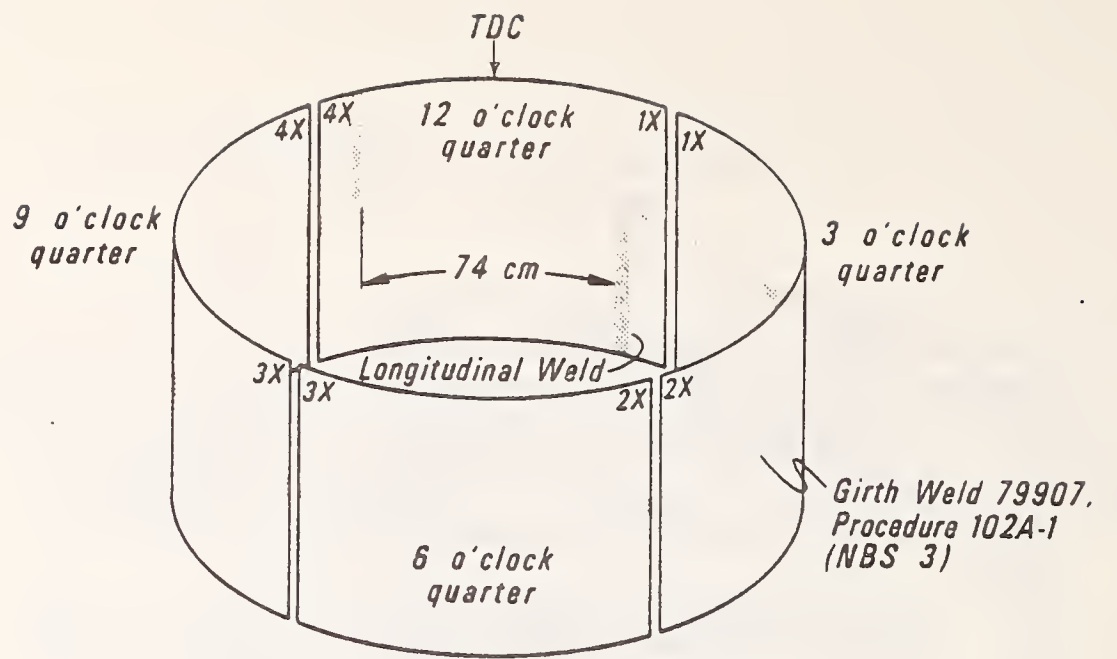
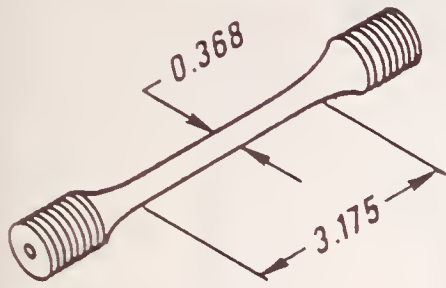


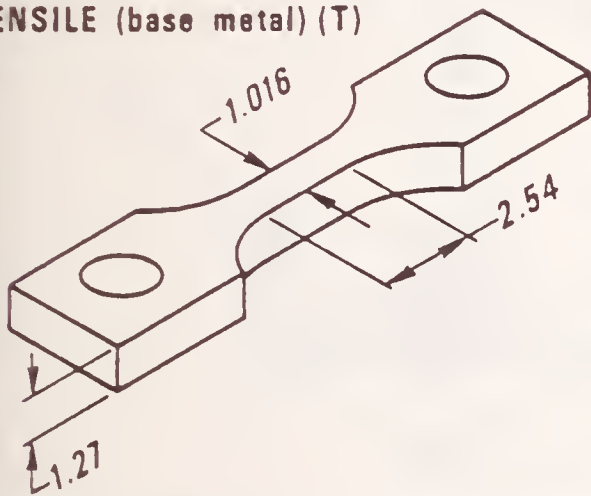
Fig. 3. Schematic diagrams of cylindrical weldments of trans-Alaska pipeline containing girth welds. All welds are shown as shaded areas. Top-dead-center, where the girth welds begin, is marked TDC. Specimen locations within each quarter are shown in Figs. 5-9. See Fig. 2 for a photograph of one of the weldments.



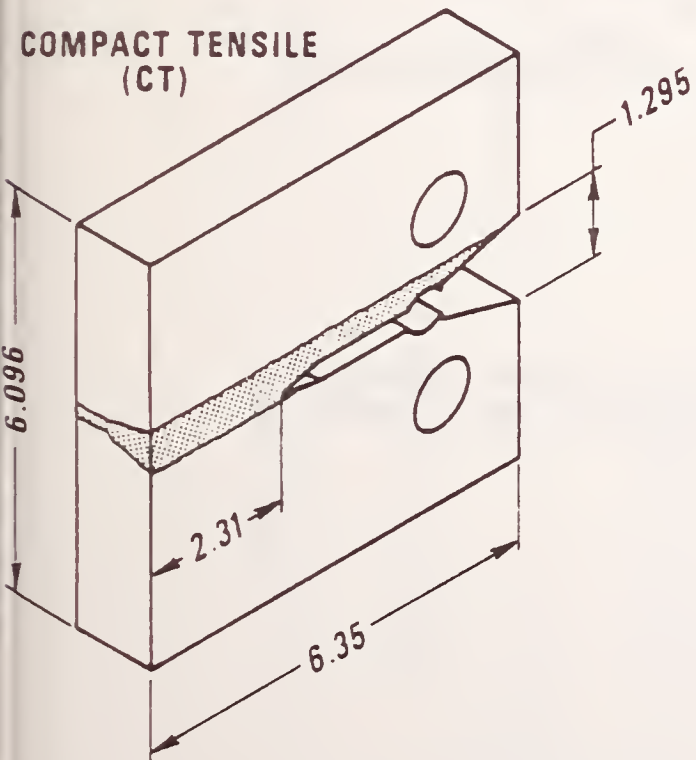
TENSILE (weld metal) (T)



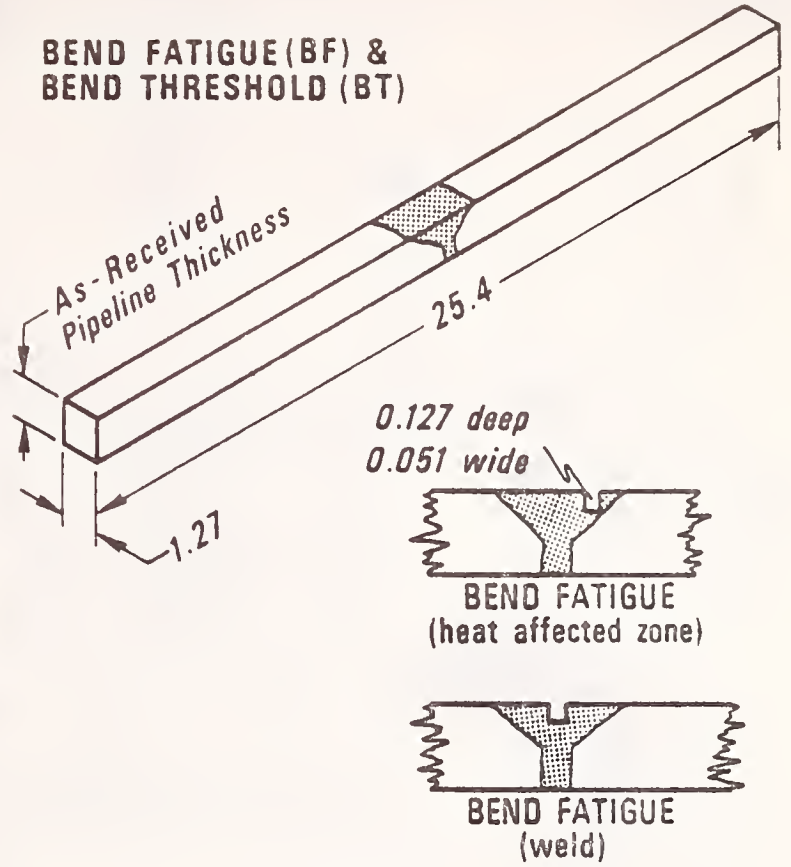
TENSILE (base metal) (T)



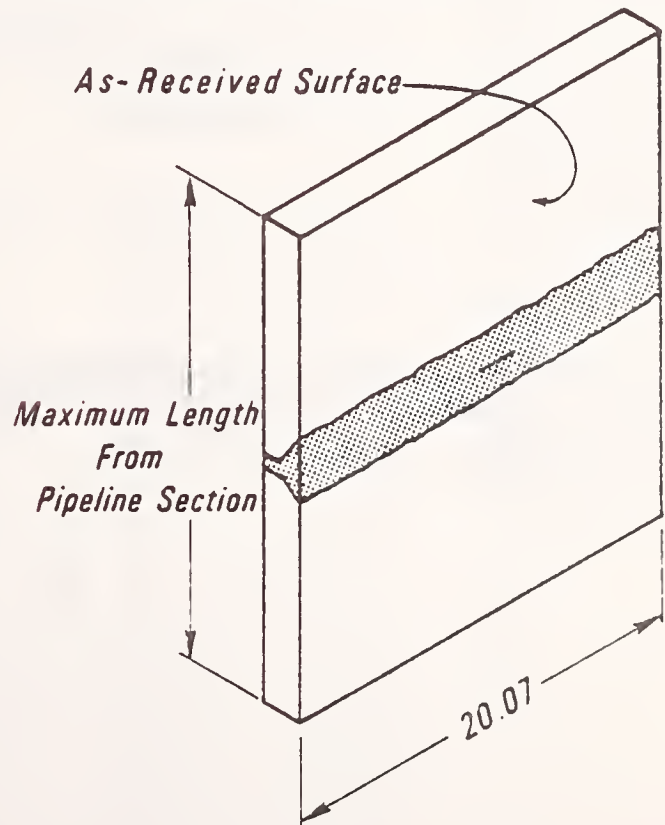
COMPACT TENSILE (CT)



BEND FATIGUE (BF) & BEND THRESHOLD (BT)

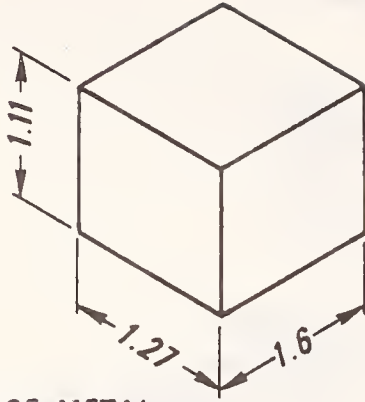


SURFACE-FLAW FATIGUE (SF)

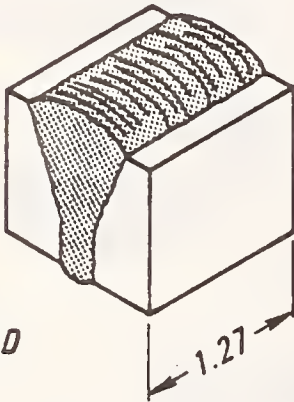


All dimensions in cm.

ELASTIC (E)

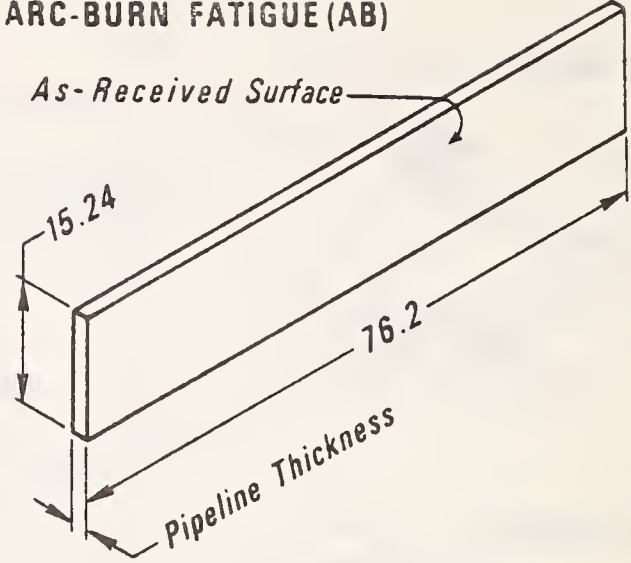


BASE METAL

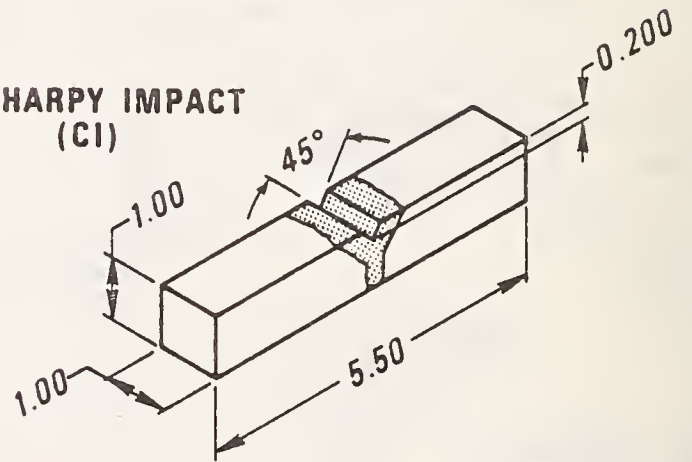


WELD

ARC-BURN FATIGUE (AB)



CHARPY IMPACT (CI)



All dimensions in cm.

Fig. 4. Diagrams of test specimens prepared from trans-Alaska pipeline. Shaded areas indicate weld zone. All dimensions are in centimeters (1 cm = 0.39 in).

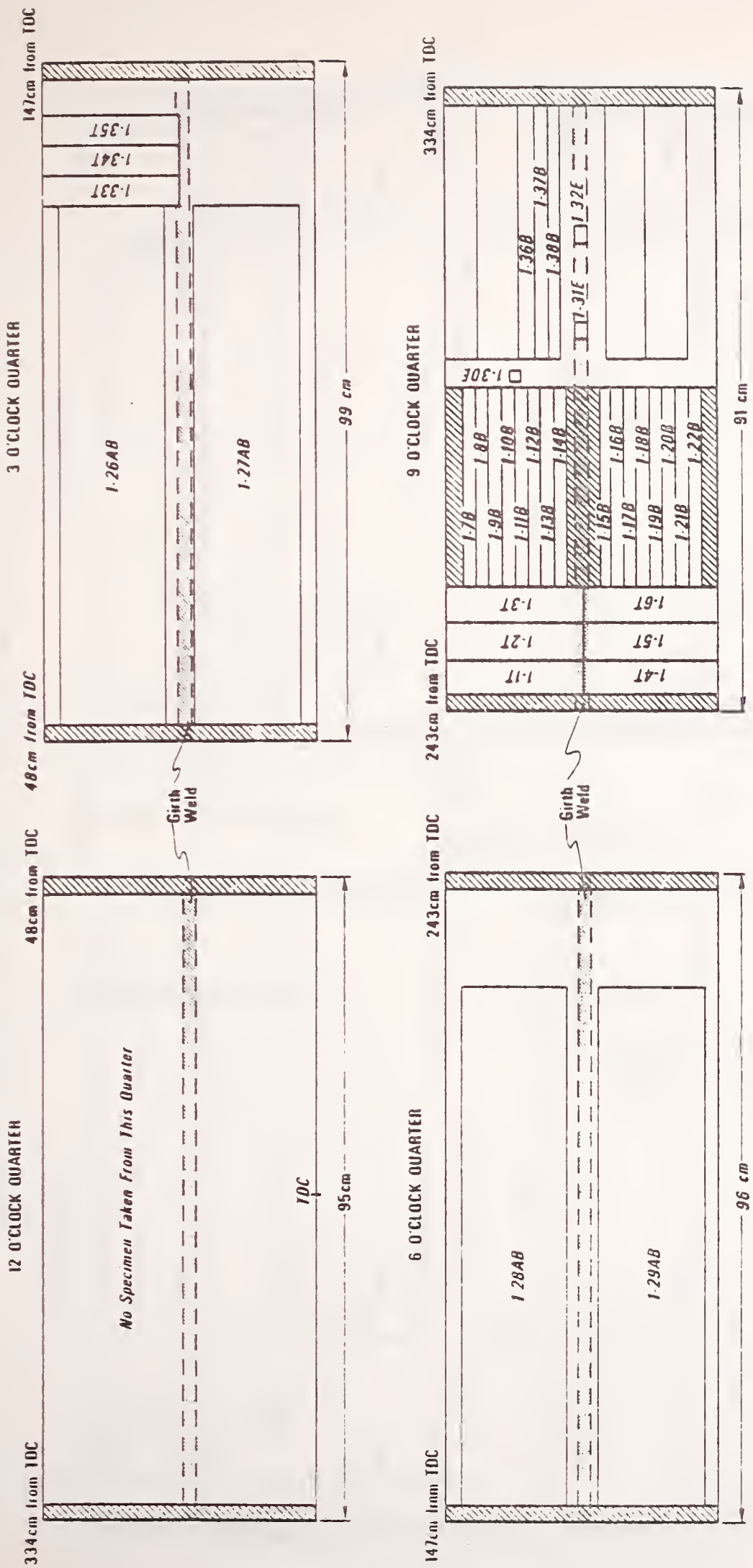


Fig. 5. Quarter maps of Alyeska weldment 88070 (NBS #1), weld procedure 302A-1. Cross-hatched areas are heat-affected zones from which no specimens were taken. Shaded areas indicate girth weld. Locations of longitudinal welds are omitted for simplicity. Meanings of specimen designations are explained in text. Note that all dimensions are in centimeters; 1 cm = 0.39 in. TDC indicates top-dead-center, the beginning of the girth weld.

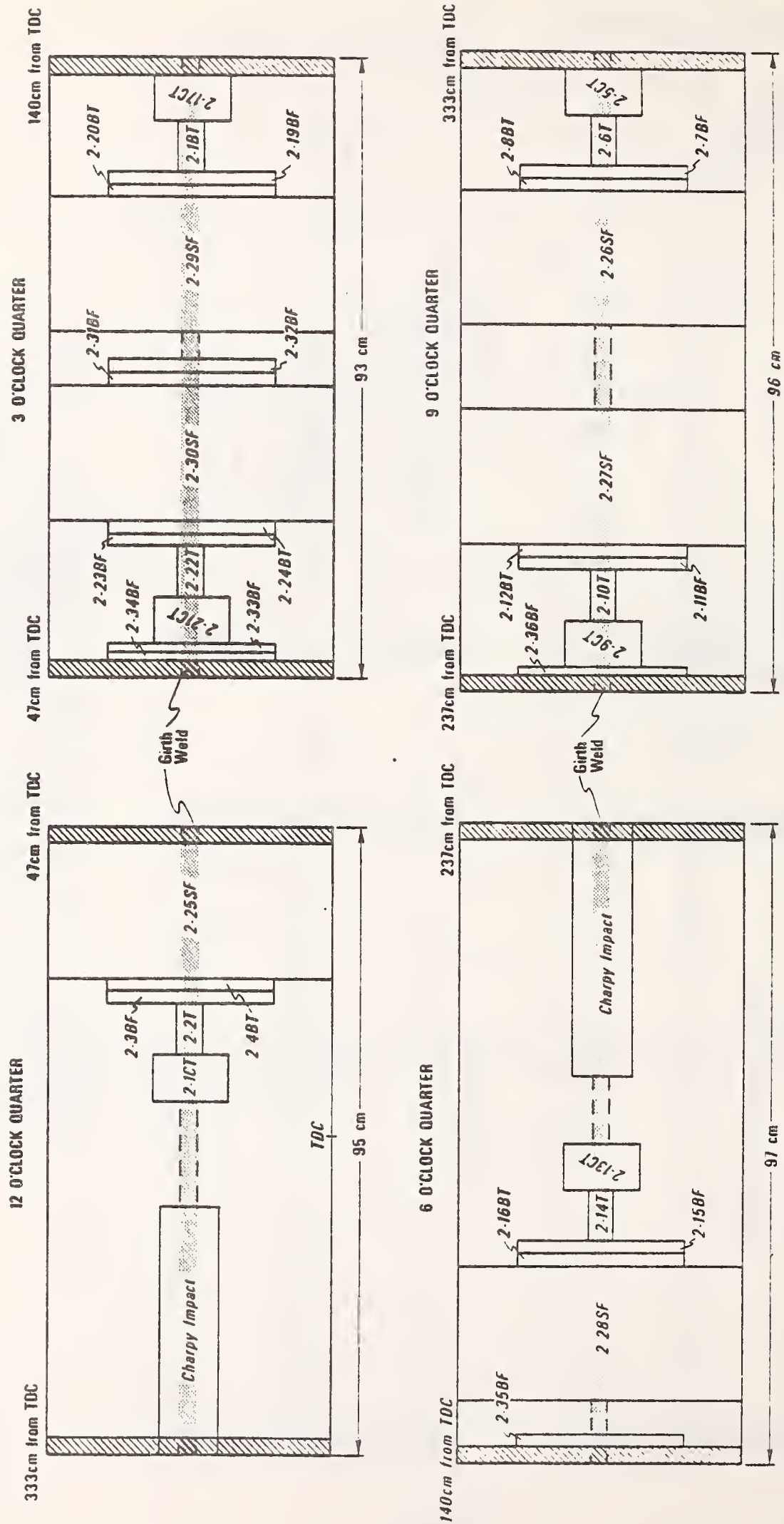


Fig. 6. Quarter maps of Alyeska weldment 88119 (NBS #2), weld procedure 104A-1. See caption of Fig. 5.

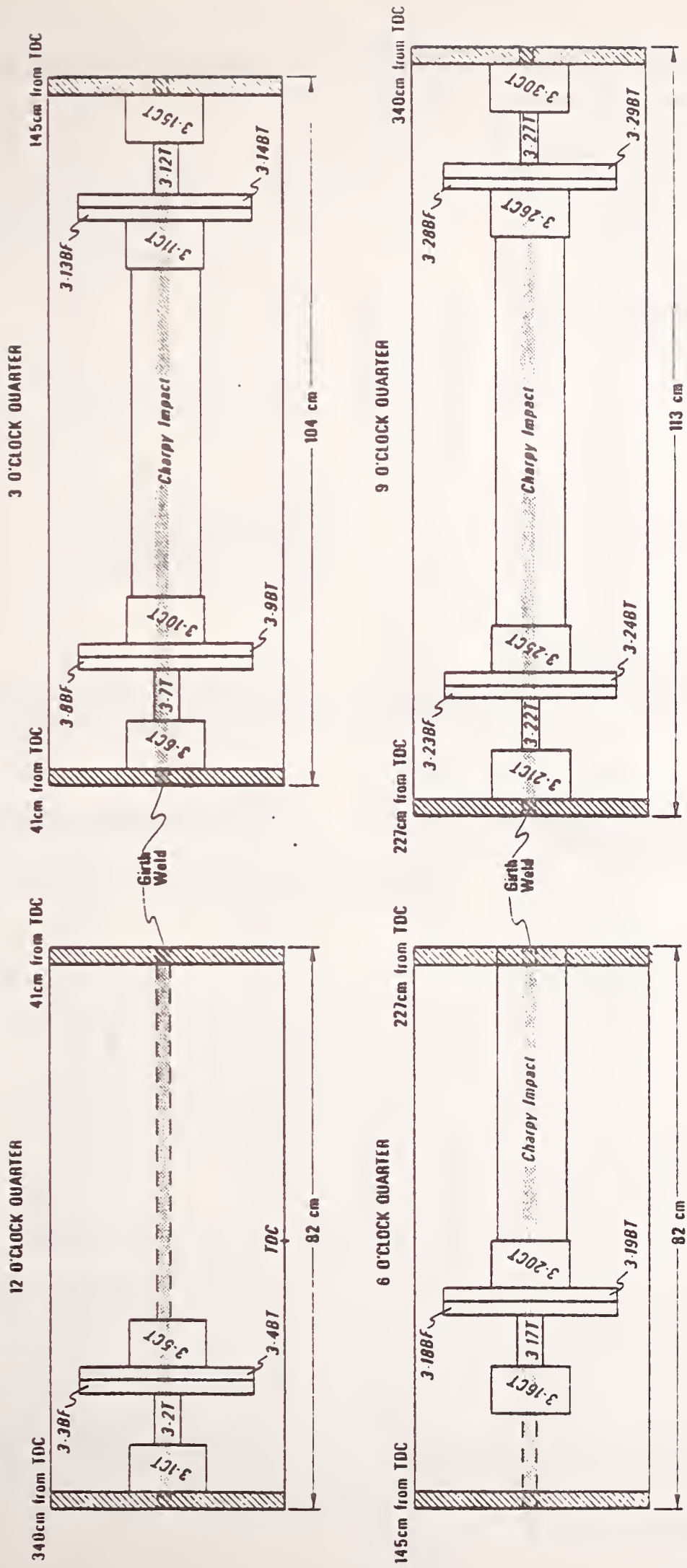


Fig. 7. Quarter maps of Alyeska weldment 79907 (NBS #3), weld procedure 102A-1. See caption of Fig. 5.

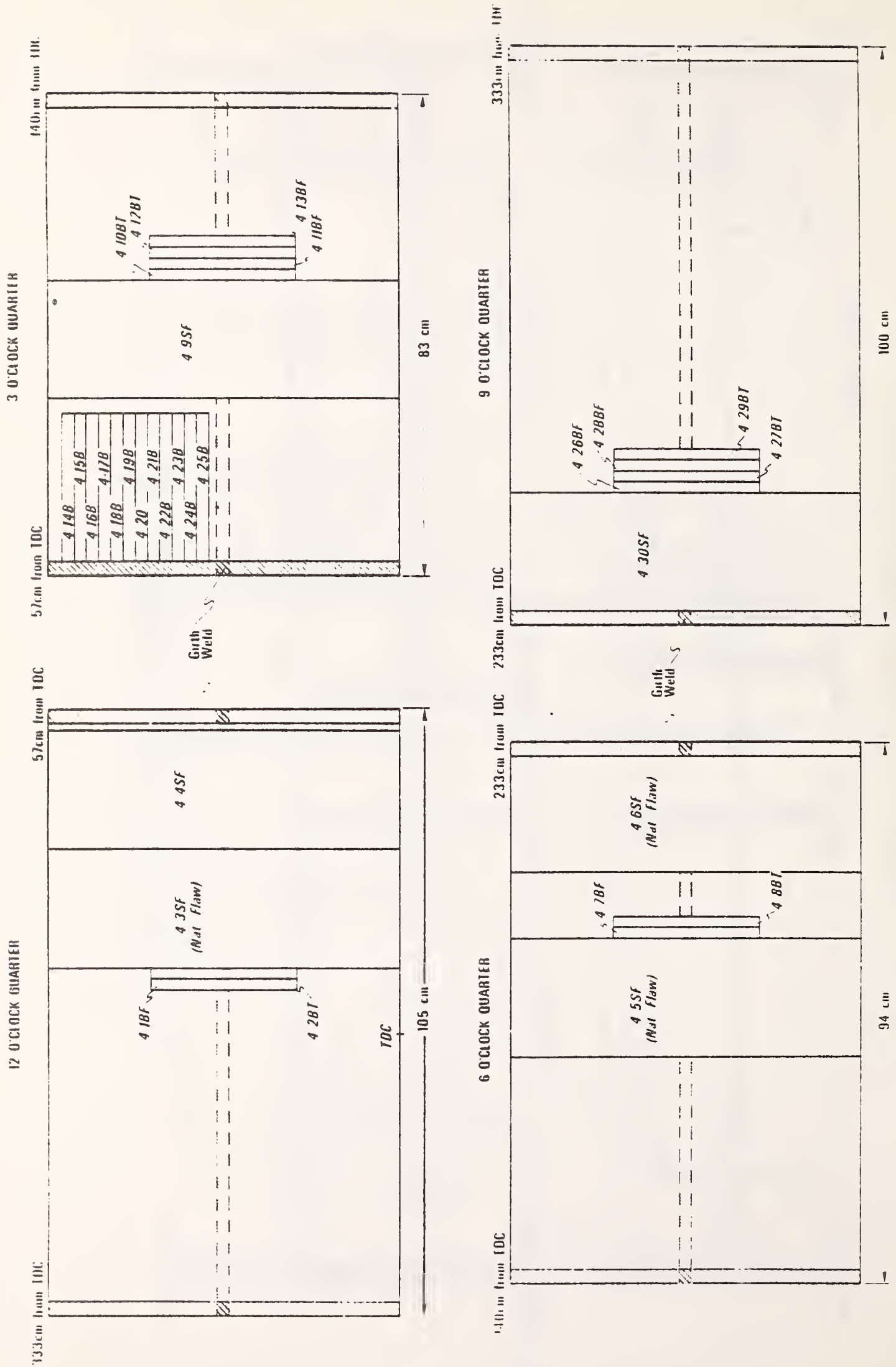


Fig. 8. Quarter maps of Alyeska weldment 75061 (NBS #4), weld procedure 104A. See caption of Fig. 5.

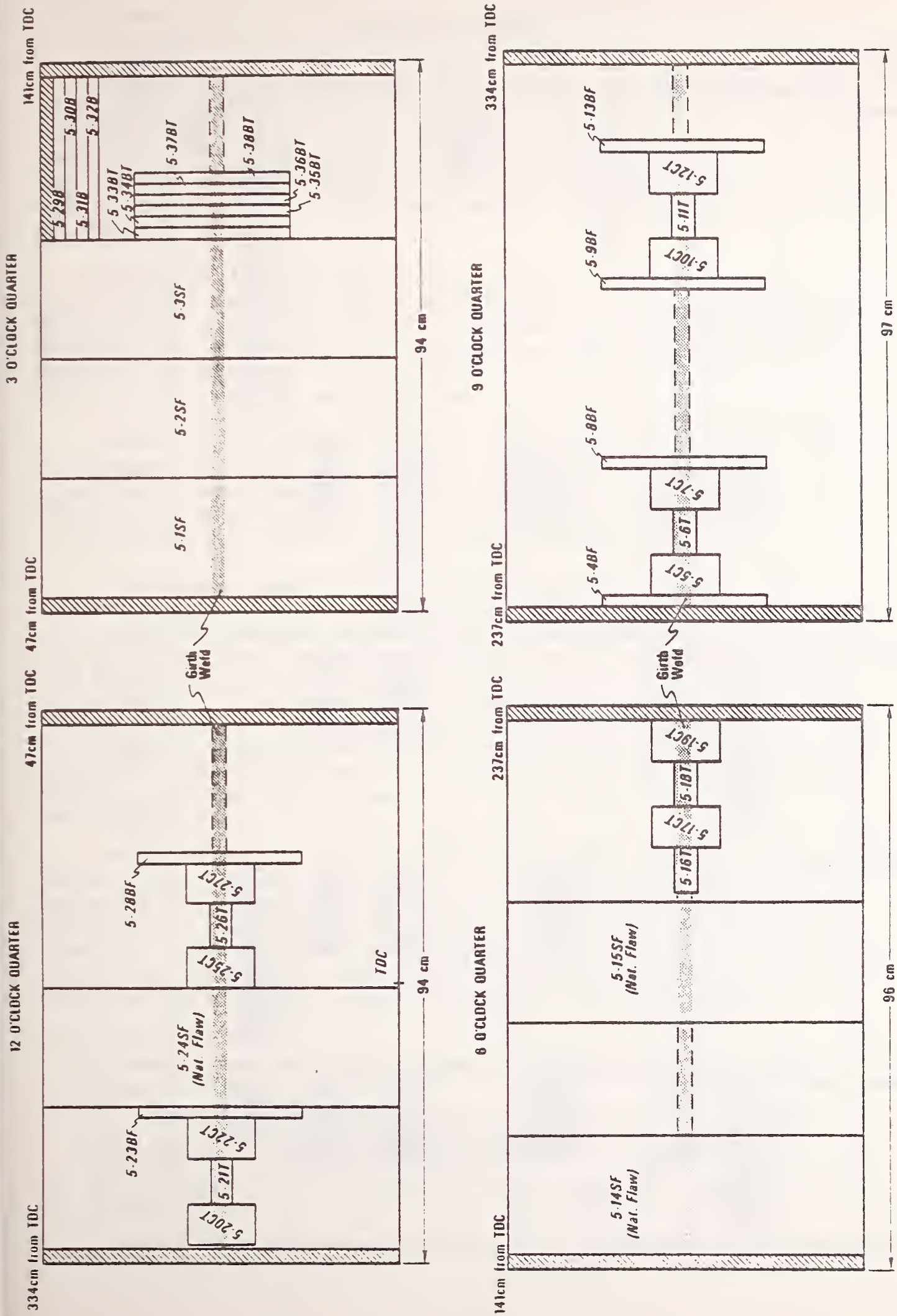


Fig. 9. Quarter maps of Alyeska weldment 88503 (NBS #5), weld procedure 104A-1. See caption of Fig. 5.

Table 2. Specimen-weldment matrix showing origins of test specimens.

WELD IDENTIFICATIONS			SPECIMEN IDENTIFICATIONS									
			Compact Tensile	Tensile (weld)	Tensile (base)	Surface- Flaw Fatigue	Arc-Burn Fatigue	Bend Fatigue	Bend Threshold	Bend (base)	Elastic	Charpy Impact
NBS	Alyeska	Procedure										
1	88070	302A-1			1-1T 1-2T 1-3T 1-4T 1-5T 1-6T 1-33T 1-34T 1-35T		1-26AB 1-27AB 1-28AB 1-29AB			1-7B 1-8B 1-9B 1-10B 1-11B 1-12B 1-13B 1-14B 1-15B 1-16B 1-17B 1-18B 1-19B 1-20B 1-21B 1-22B 1-36B 1-37B 1-38B	1-30E 1-31E 1-32E	
2	88119	104A-1	2-1CT 2-5CT 2-9CT 2-13CT 2-17CT 2-21CT	2-2T 2-6T 2-10T 2-14T 2-18T 2-22T		2-25SF 2-26SF 2-27SF 2-28SF 2-29SF 2-30SF		2-38F 2-78F 2-118F 2-158F 2-198F 2-238F 2-318F 2-328F 2-338F 2-348F 2-358F 2-368F	2-48T 2-88T 2-128T 2-168T 2-208T 2-248T		A-1 through A-50	
3	79907	102A-1	3-1CT 3-5CT 3-6CT 3-10CT 3-11CT 3-15CT 3-16CT 3-20CT 3-21CT 3-25CT 3-26CT 3-30CT	3-2T 3-7T 3-12T 3-17T 3-22T 3-27T				3-38F 3-88F 3-138F 3-188F 3-238F 3-288F	3-48T 3-98T 3-148T 3-198T 3-248T 3-298T		B-1 through B-29 C-1 through C-26 D-1 through D-35	
4	75061	104A				4-3SF 4-4SF 4-5SF 4-6SF 4-9SF 4-30SF		4-18F 4-78F 4-118F 4-138F 4-268F 4-288F	4-28T 4-88T 4-108T 4-128T 4-278T 4-298T	4-148 4-158 4-168 4-178 4-188 4-198 4-208 4-218 4-228 4-238 4-248 4-258		
5	88503	104A-1	5-5CT 5-7CT 5-10CT 5-12CT 5-17CT 5-19CT 5-20CT 5-22CT 5-25CT 5-27CT	5-6T 5-11T 5-16T 5-18T 5-21T 5-26T		5-1SF 5-2SF 5-3SF 5-14SF 5-15SF 5-24SF		5-48F 5-88F 5-98F 5-138F 5-238F 5-288F	5-338T 5-348T 5-358T 5-368T 5-378T 5-388T	5-298 5-308 5-318 5-328		

3C. ELASTIC PROPERTIES

Elastic constants of samples of the trans-Alaska pipeline were determined between -40°C (-40°F) and 60°C (140°F) using dynamic methods. Room-temperature measurements were made with a 10-MHz pulse method,¹ and temperature effects on the elastic constants were determined with a pulse-superposition method.² The elastic constants reported here are: Young's modulus, the shear modulus, the bulk modulus (reciprocal compressibility), and Poisson's ratio.

Room-temperature elastic constants of the pipeline base metal (specimen 1-30E) and the pipeline weld metal (specimen 1-32E), measured along the weld direction, are shown in Table 3 together with the elastic constants of unalloyed iron.³ For practical purposes, the elastic constants of the base metal and the weld metal are identical; and these materials are slightly softer elastically than unalloyed iron.

Changes of the elastic constants with temperature are shown in Fig. 10. As expected for an iron-base material in this temperature region,³ all the elastic stiffnesses decrease linearly with increasing temperature, and Poisson's ratio increases linearly. The elastic constants of the pipeline base metal are given in Table 4 for selected temperatures.

The measured quantities v_l = longitudinal wave velocity and v_t = transverse wave velocity are believed to have systematic errors between 0 and +1% and 0 and +2%, respectively. This estimate is based on previous studies in our laboratory using the same experimental conditions and a specimen similar to the pipeline steel. The $\pm 2\sigma$ imprecisions of v_l and v_t are $\pm 1.4\%$ and $\pm 0.66\%$, respectively. The total uncertainty in the mass density is estimated to be $\pm 0.1\%$, and it was neglected. Thus, from standard formulas, the total (systematic plus imprecision) uncertainty in E is +5%, -3% and in ν is +3%, -1%. The point-to-point imprecision in the temperature dependence of the elastic constants is a few parts in 10^4 .

While the results are not reported here, the anisotropy of the base material was studied by measuring nine ultrasonic sound velocities in three mutually perpendicular directions. A definite anisotropy was detected; for example, the shear modulus varied about ten percent with direction. This anisotropy is probably related to the mill rolling of the steel. The elastic constants reported in the tables were determined by averaging the anisotropic elastic constants over all directions.

-
1. E. R. Naimon, W. F. Weston, and H. M. Ledbetter, *Cryogenics* 14, 246-249 (1974).
 2. W. F. Weston, E. R. Naimon, and H. M. Ledbetter, in: *Properties of Materials for Liquefied Natural Gas Tankage*, ASTM STP 579 (Amer. Soc. Test. Mater., Philadelphia, 1975).
 3. H. M. Ledbetter and R. P. Reed, *J. Phys. Chem. Ref. Data* 2, 531-618 (1974).

Table 3. Room-temperature elastic constants of the trans-Alaska pipeline base metal compared to those of unalloyed iron.

	Iron	Base Material	Weld-Zone Material (302A)
Young's modulus, 10^{11} N/m ² (10^6 psi)	2.130(30.9)	2.050(29.8)	2.060(29.9)
Shear modulus, 10^{11} N/m ² (10^6 psi)	0.828(12.0)	0.794(11.5)	0.797(11.6)
Bulk modulus, 10^{11} N/m ² (10^6 psi)	1.680(24.4)	1.640(23.6)	1.660(24.1)
Poisson's ratio, dimensionless	0.289	0.291	0.294

Table 4. Elastic constants of the trans-Alaska pipeline base metal at selected temperatures; primary units are 10^{11} N/m²; secondary units in parentheses are 10^6 psi, Poisson's ratio is dimensionless.

Temp. °C(°F)	Young's Modulus	Shear Modulus	Bulk Modulus	Poisson's Ratio
-40 (-40)	2.09 (30.3)	0.810 (11.7)	1.65 (24.0)	0.290
-20 (-4)	2.08 (30.1)	0.805 (11.7)	1.65 (23.9)	0.290
0 (32)	2.07 (30.0)	0.800 (11.6)	1.64 (23.8)	0.291
20 (68)	2.05 (29.8)	0.794 (11.5)	1.64 (23.8)	0.291
40 (104)	2.04 (29.6)	0.789 (11.4)	1.63 (23.7)	0.292
60 (140)	2.03 (29.4)	0.784 (11.4)	1.63 (23.6)	0.292

ELASTIC CONSTANTS RELATIVE TO 22°C=72°F

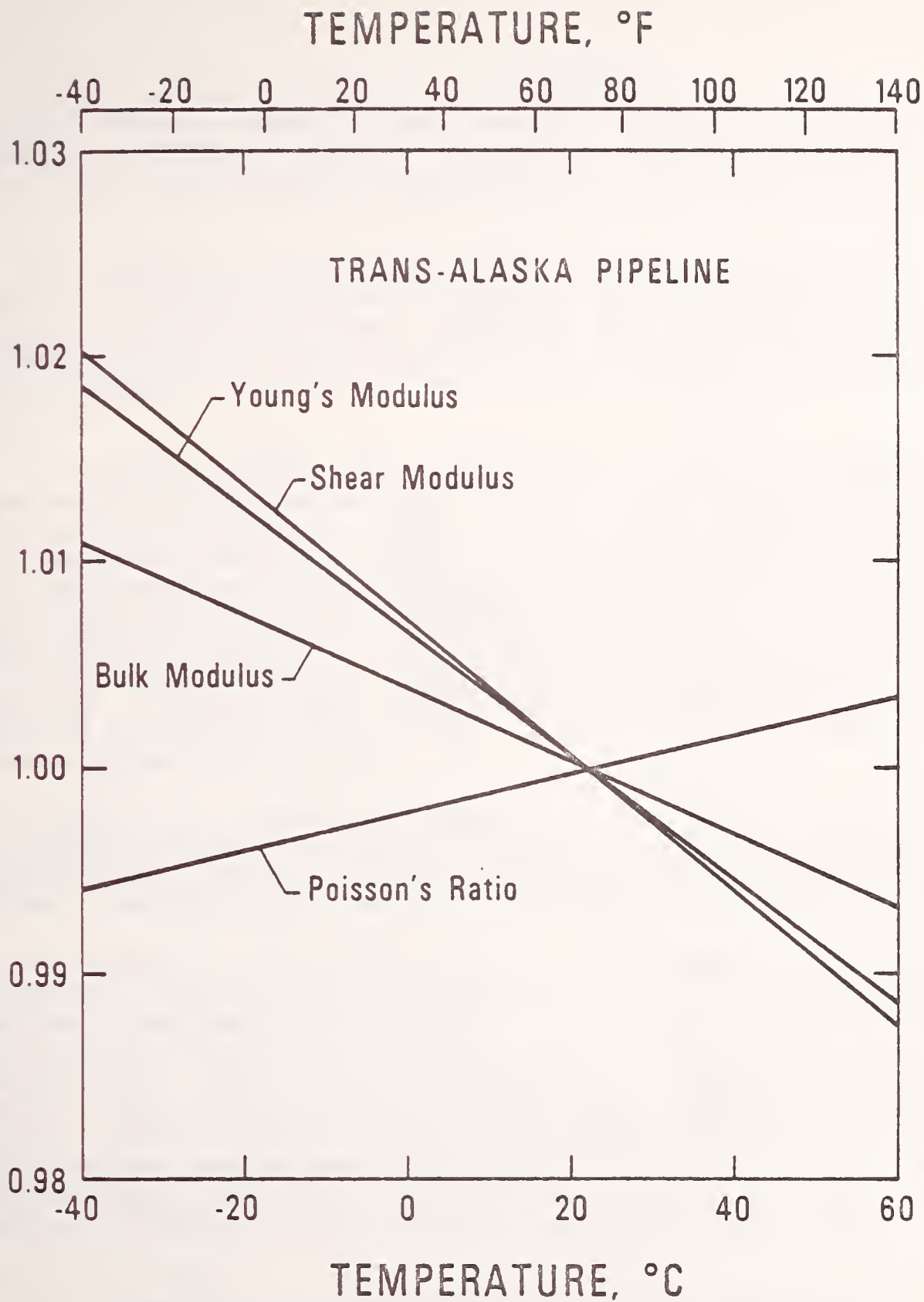


Fig. 10. Temperature variations of the elastic constants of the trans-Alaska pipeline steel. Data points, which were determined at 5°C intervals, are omitted for clarity. Room-temperature (22°C = 72°F) values of the elastic constants are given in Table 3.

3D. TENSILE PROPERTIES

Several tensile properties - yield strength, ultimate strength, elongation, and reduction in area -- were determined for the trans-Alaska pipeline base metal and welds (102A-1 and 104A-1) with test procedures used previously in this laboratory.¹

Flat base-metal specimens oriented parallel to the pipe axis were 1.1 cm (0.43 in) thick with a reduced section 2.5 cm (1.0 in) long and 1.0 cm (0.43 in) wide. Weld-metal specimens from the two welding procedures had their axes along the pipe girth; their reduced section length was 3.2 cm (1.25 in) and their diameter was 0.4 cm (0.14 in).

The important experimental details are as follows: Crosshead speed on the test machine was constant at 0.1 cm/min (0.04 in/min). Three test environments were used: (a) air at 60°C (140°F) achieved by a surrounding electrical heater; (b) air at 20°C (68°F); and (c) the ullage space above liquid nitrogen at -20°C (-4°F). Temperatures were stable within $\pm 0.5^\circ\text{C}$ (0.9°F) except near the finish of the tests when mechanical deformation caused temperature increases up to 2°C (4°F) in the necked region. Two data recordings were made simultaneously: load-cell output versus clip-on-extensometer output, and load-cell output versus elapsed time. Elongation was determined by gage-mark separation.

Inaccuracies in these measurements are estimated to be less than ± 3 percent for load and about ± 5 percent for strains, according to the equipment manufacturers. Relative imprecisions are estimated to be about ± 5 percent. Results of this study are summarized in Table 5 and in Figs. 11-13.

Differences in the yielding behavior of the base and weld metals are shown in the stress-strain curves in Fig. 11. The strain-hardening behavior of the base metal is typical of mild steels.² Small oscillations often occurred in the plastic regions of the weld-metal stress-strain curves. After reaching ultimate load, all specimens necked down locally. Upon fracturing, the base metal usually showed a "delamination," or split, parallel to the original pipe surface; this traveled in both directions from the fracture surface as far as 0.6 cm (0.25 in). Two weld specimens from procedure 102A-1 showed a void on the fracture surface. Examples of fractured tensile specimens are shown in Figs. 14-15.

-
1. K. A. Warren and R. P. Reed, Tensile and impact properties of selected materials from 20 to 300°K, NBS Monogr. 63, U.S. Gov't. Print. Office (1963).
 2. NBS, Cryogenics Div., data reported in Cryogenic Materials Data Handbook, PB 171809-5 (1961).

Table 5. Tensile properties of trans-Alaska pipeline materials; primary units are 10^8 N/m²; secondary units in parentheses are 10^3 psi; elongation and reduction in area are expressed as percentages.

Specimen	Temp. °C(°F)	Yield Strength (0.2% offset)	Ultimate Strength	Elongation at Fracture, % ^a	Reduction in Area, %
Base Metal (x70)					
1-2T	-20(-4)	6.1(88)	6.1(89)	44	68
1-5T	-20(-4)	5.2(76)	5.8(84)	37	70
1-34T	-20(-4)	5.4(79)	6.1(89)	41	70
1-1T	20(68)	5.0(73)	5.7(83)	37	71
1-4T	20(68)	5.1(74)	5.7(82)	35	69
1-35T	20(68)	5.5(80)	5.9(85)	41	70
1-3T	60(140)	4.9(71)	5.0(72)	40	73
1-6T	60(140)	5.0(73)	5.5(80)	34	69
1-33T	60(140)	5.1(74)	5.7(82)	37	75
Weld Metal, Procedure 102A-1					
3-7T ^b	-20(-4)	4.7(68)	5.7(83)	15	55
3-22T	-20(-4)	4.6(66)	5.9(85)	19	69
3-2T	20(68)	4.1(59)	5.2(76)	24	69
3-12T	20(68)	4.1(60)	5.4(78)	23	68
3-17T	60(140)	3.9(57)	5.2(75)	20	69
3-27T ^b	60(140)	4.8(69)	5.0(72)	14	78
Weld Metal, Procedure 104A-1					
2-2T	-20(-4)	4.6(67)	6.0(87)	23	67
2-6T	-20(-4)	4.4(64)	5.4(79)	21	71
5-6T	-20(-4)	4.7(68)	5.7(83)	21	66
5-11T	-20(-4)	5.0(72)	5.7(83)	24	68
2-10T	20(68)	4.8(70)	5.2(76)	23	73
2-14T	20(68)	3.8(55)	5.2(75)	22	69
5-21T	20(68)	4.7(68)	5.5(80)	20	67
5-26T	20(68)	4.1(60)	5.4(78)	21	68
2-18T	60(140)	4.6(67)	5.3(77)	17	70
2-22T	60(140)	4.3(62)	5.1(74)	15	68
5-16T	60(140)	3.5(51)	4.7(68)	17	65
5-18T	60(140)	4.7(68)	5.5(79)	12	42

- a. In 2.54 cm (1 in) gage length.
b. Void visible on fracture surface.

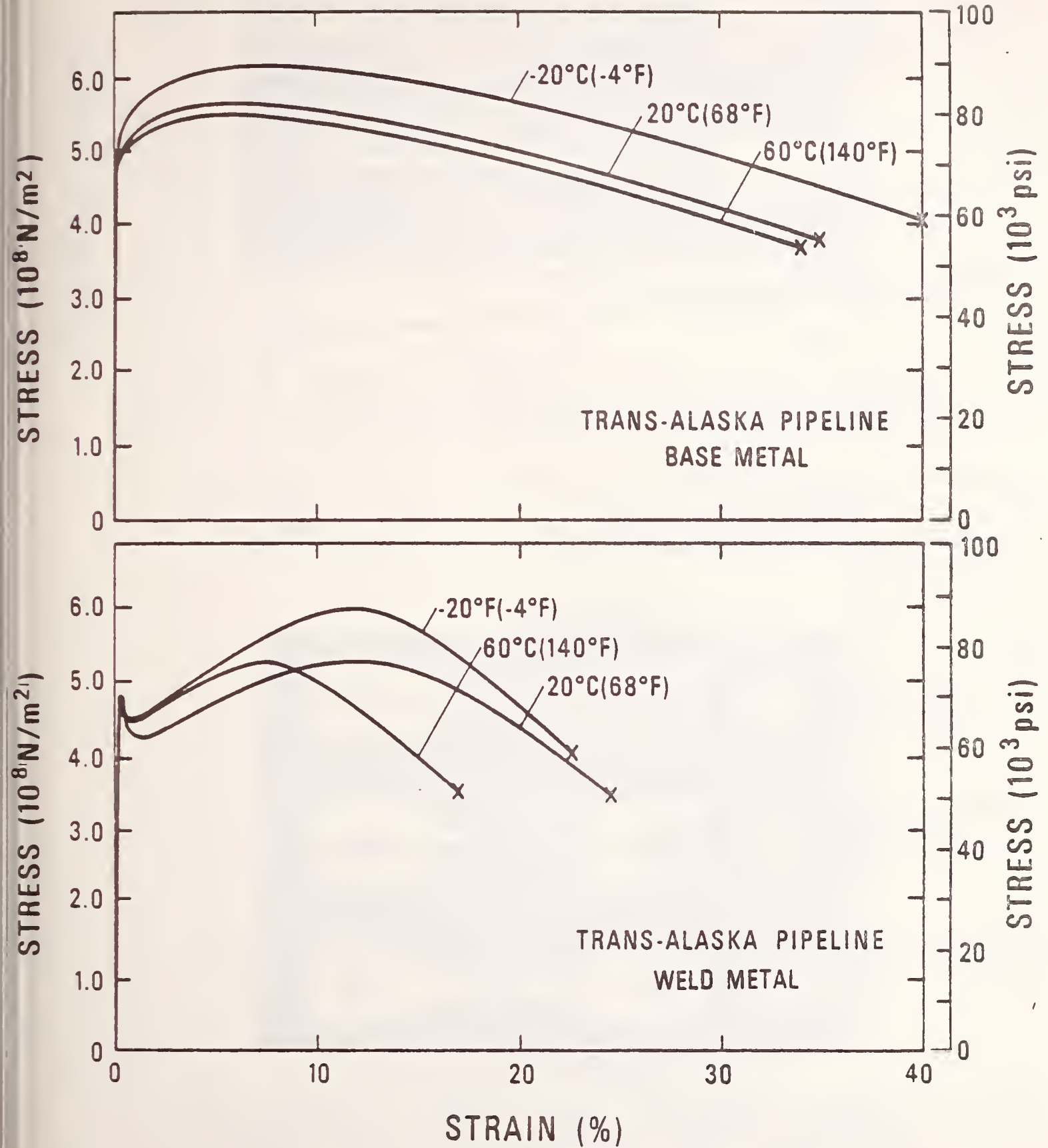


Fig. 11. Typical stress-strain curves for the trans-Alaska pipeline base metal and weld metals from procedures 104-A and 104A-1. Gage lengths was 2.54 cm = 1 in.

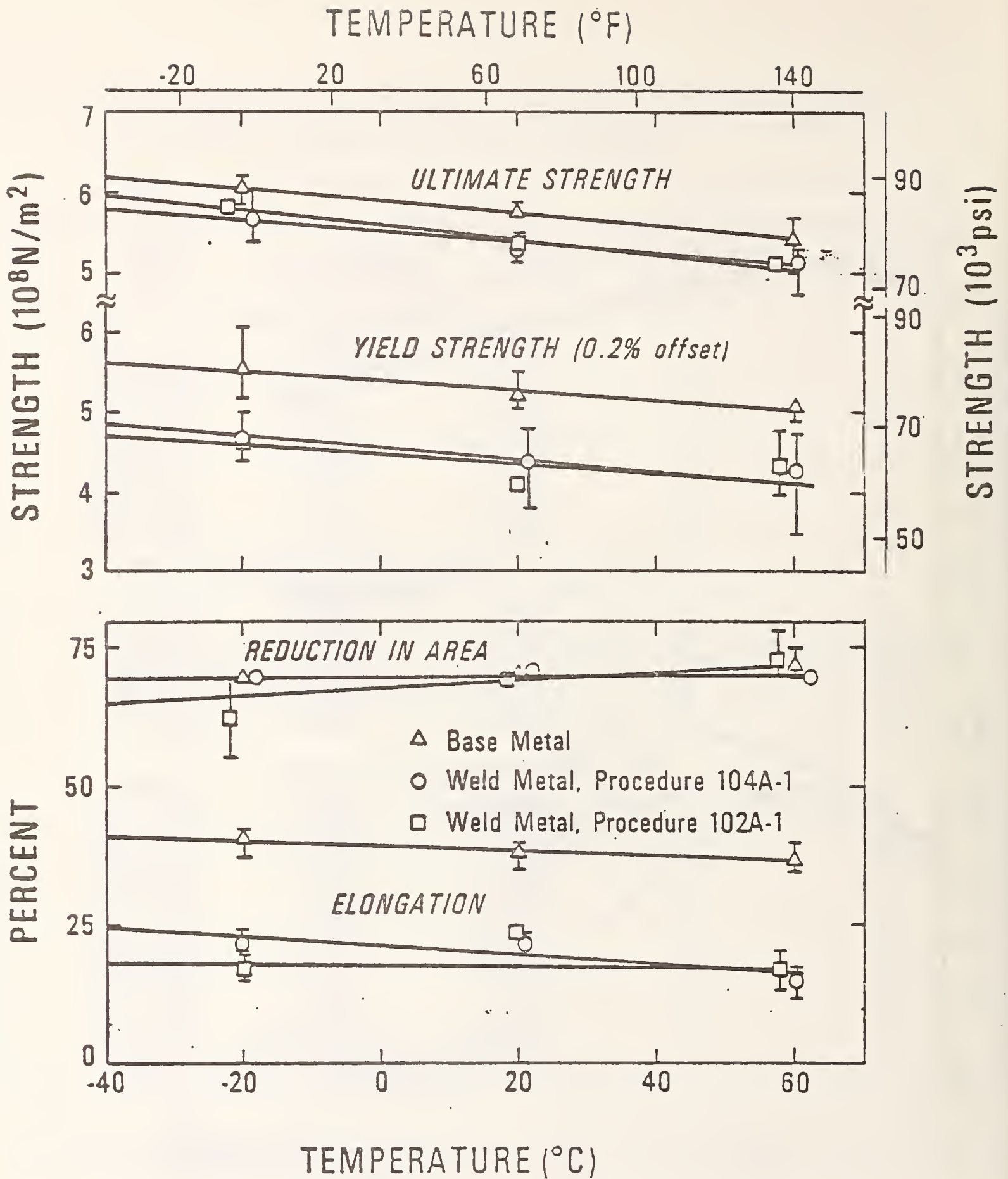


Fig. 12. Temperature variation of yield strength (0.2% offset) and ultimate strength of trans-Alaska pipeline base metal and weld metals. Error bars indicate data spread. Symbols have same meanings as in Fig. 13.

Fig. 13. Temperature variation of the elongation and reduction in area of trans-Alaska pipeline base metal and weld metals.

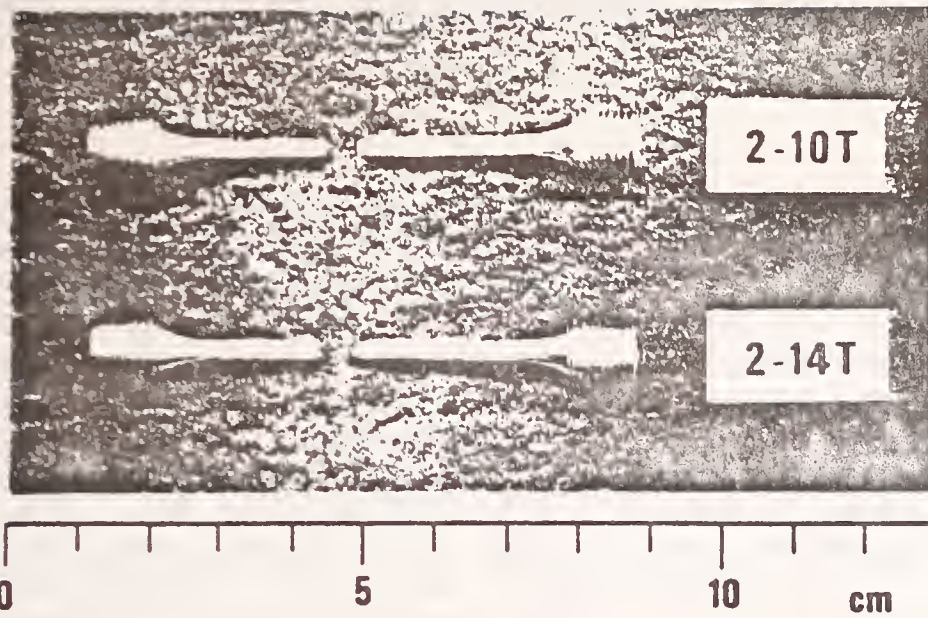


Fig. 14. Examples of fractured weld-metal tensile specimens that were used to determine yield strength, ultimate strength, elongation, and reduction in area.

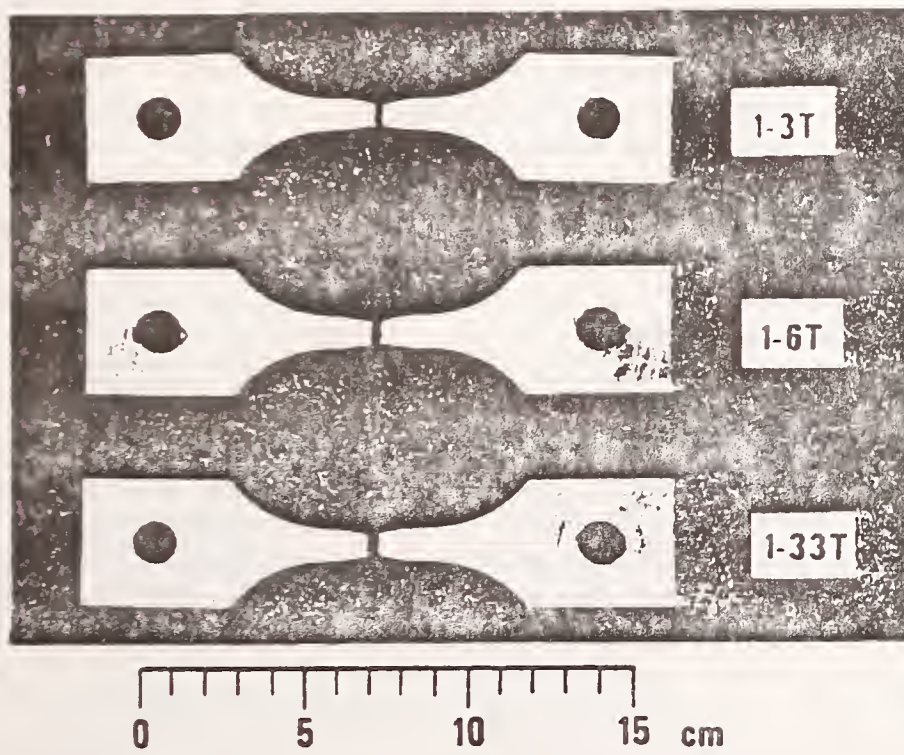


Fig. 15. Examples of fractured base-metal tensile specimens.

3E. FRACTURE TOUGHNESS OF HEAT-AFFECTED ZONE

Tests were conducted to determine the fracture toughness of the heat-affected zones (HAZ) in trans-Alaska pipeline steel weldments. J_{IC} is reported as an index of fracture toughness. J_I is defined as the rate of change of potential energy with respect to crack area, and it is proportional to the energy required to initiate fracture in a flawed specimen subjected to monotonically increasing loads. Using experimental procedures described previously¹, J-resistance curves were determined for specimens of the 104A-1 and 102A-1 weld processes at 20°C and -20°C. The tests at 20°C were conducted in room air, while tests at -20°C were conducted with the specimens immersed in an alcohol bath that was cooled with dry ice. Compact specimens, 1.01 cm thick, were machined with starting notches located 0.38 cm from the weld centerline so that subsequent fatigue cracks would sample the HAZ. (See Fig. 4.) All specimens were then subjected to sinusoidal fatigue load cycling at 15 Hz. Using minimum and maximum fatigue loads of 0.6 and 6 kN, precracks were initiated and propagated at 20°C until the overall crack-length-to-specimen-width ratio, a/W , was about 0.6. The fatigue loads were small, less than half the loads required in subsequent J-tests.

At least five specimens were tested for each weld-process/temperature combination. The J-test procedure first suggested by Landes and Begley, and successfully employed in NBS studies¹⁻³ of ferritic steels and their welds, was used. This procedure involves loading each specimen to a predetermined displacement such that a range of subcritical crack extensions is obtained. The test machine is operated in ram-displacement control. Upon reaching the predetermined displacement, the specimen is unloaded and heat treated to mark the crack extension. The specimen is then fractured into halves and crack extension is measured at three points equidistant across the specimen thickness; the average crack extension is defined as Δa . For each test the J value was calculated using $J = 2A/Bb$, where A = area under load-displacement curve, B = specimen thickness, and b = length of uncracked ligament. Test specimens are shown in Fig. 16, and a macrophotograph of the fracture surfaces is shown in Fig. 17.

The J-versus-crack extension curves are shown in Fig. 18. As recommended by Landes and Begley, the $J/2\bar{\sigma}f_{low}$ line was constructed to account for apparent crack extensions due to crack tip blunting that occurs prior to actual material separation. The flow stress of the material is defined as the average of the yield and ultimate stresses:

$$\begin{aligned}\bar{\sigma} &= \frac{1}{2} (\sigma_y + \sigma_u) \\ &= 496 \text{ MPa (72 ksi)} \pm 5\% \end{aligned} \quad (1)$$

The critical J values are taken at the points of intersection of the $J/2\sigma_{flow}$ line with the J- Δa curves. The critical J values, denoted " J_{IC} ", are listed in Table 6. The uncertainties in J_{IC} values are estimated at $\pm 10\%$ and are due to (1) the uncertainty in fitting curves to the data and (2) the fact that the $J/2\sigma_{flow}$ line is an approximation for crack-tip blunting.

The results show that J_{IC} for the 104A-1 weld process HAZ at 20°C and -20°C is 80 kJm⁻²; J_{IC} for the 102A-1 weld process HAZ at 20°C is 100 kJm⁻², and the temperature reduction to -20°C apparently increases the toughness to 110 kJm⁻².

Direct K_{IC} measurements using the ASTM E 399-74 method were not possible since rapid, unstable crack extension in this material at 20 and -20°C did not occur. However, K_{IC} values can be estimated from J_{IC} data using the approximation:

$$K_{IC} = (EJ_{IC})^{1/2} \quad (2)$$

where E is Young's modulus. Ledbetter's⁴ elastic modulus measurements were used to obtain the K_{IC} values listed in Table 6. These values serve as estimates of K_{IC} , with uncertainties estimated at ± 20 percent. In view of data presented by Read and Reed³ for an aluminum alloy, it appears that K_{IC} estimates based on Eq. (2) may be conservative.

Although the critical crack-tip opening displacement (COD) at the initiation of crack extension was not measured, it can be calculated using the approximation:

$$\delta_c = \frac{J_{IC}}{m \sigma_y} \quad (3)$$

Here, m, the plastic constraint factor, has a value between 1 and 2.1, dependent on materials. For deeply notched I X I bend specimens of trans-Alaska pipeline steel, Harrison⁵ indicated that m has a value near 1.6. This value was used to obtain the critical COD estimates listed in Table 6. The uncertainty in COD is $\pm 30\%$, due primarily to uncertainty in m, which appears to be specimen-geometry dependent.⁵

-
1. R. L. Tobler, R. P. Mikesell, R. L. Durcholz, and R. P. Reed, in Properties of Materials for Liquefied Natural Gas Tankage, STP 579 (Amer. Soc. Test. Mater., Phila., 1975), pp. 261-287.
 2. H. I. McHenry and R. P. Reed, submitted for publication.
 3. D. T. Read and R. P. Reed, Intern. J. Fracture, forthcoming.
 4. H. M. Ledbetter, Elastic properties section of this report.
 5. J. D. Harrison, in Fracture Mechanics Study of Buried Field Girth Welds, Part 3 (Alyeska Pipeline Service Company, August 1976).

Table 5. J-integral fracture-toughness results for trans-Alaska pipeline HAZ specimens.

Specimen	a/W	Δa mm(in)	J kJ/m ² (in·lb/in ²)	J_{Ic} kJ/m ² (in·lb/in ²)	COD ^a mm(in)	K_{Ic}^b MPa·m ^{1/2} (ksi·in) ^{1/2}
Procedure 104A-1, T = 20°C (68°F)						
2-5CT	0.619	0.0254(0.001)	49.5(283)			
2-9CT	0.594	0.0508(0.002)	70.2(401)			
2-13CT	0.586	0.2032(0.008)	120.7(690)			
2-17CT	0.596	0.3048(0.012)	160.4(917)	80(457)	0.114(0.0045)	128(117)
2-21CT	0.577	1.1938(0.047)	285.2(1630)			
5-20CT	0.626	0.4064(0.016)	181.6(1038)			
5-22CT	0.613	0.2286(0.009)	128.3(733)			
5-25CT	0.626	0.5588(0.022)	200.9(1148)			
Procedure 104A-1, T = -20°C (-4°F)						
5-5CT	0.597	0.1016(0.004)	89.6(512)			
5-7CT	0.610	0.2540(0.010)	133.7(764)			
5-10CT	0.616	0.5334(0.021)	189.2(1081)	80(457)	0.107(0.0042)	128(117)
5-19CT	0.619	0.0889(0.0035)	66.5(380)			
5-27CT	0.622	0.1270(0.005)	99.4(568)			
Procedure 102A-1, T = 20°C (68°F)						
3-5CT	0.608	0.4826(0.019)	182.3(1042)			
3-6CT	0.625	0.6350(0.025)	264.2(1510)			
3-10CT	0.615	0.1270(0.005)	115.5(660)	100(571)	0.152(0.0060)	143(131)
3-15CT	0.612	0.0381(0.0015)	69.3(396)			
3-16CT	0.595	0.1016(0.004)	103.8(593)			
Procedure 102A-1, T = -20°C (-4°F)						
3-1CT	0.620	0.0508(0.002)	80.0(457)			
3-11CT	0.609	0.1778(0.007)	142.1(812)			
3-20CT	0.610	0.1016(0.004)	113.2(647)			
3-21CT	0.605	0.0381(0.0015)	49.9(285)	110(628)	0.148(0.0058)	151(138)
3-25CT	0.606	0.0254(0.001)	63.2(361)			
3-26CT	0.610	0.0508(0.002)	89.6(512)			
3-30CT	0.618	0.5842(0.023)	231.9(1325)			

a. Calculated from Eq. (3).
 b. Calculated from Eq. (2).

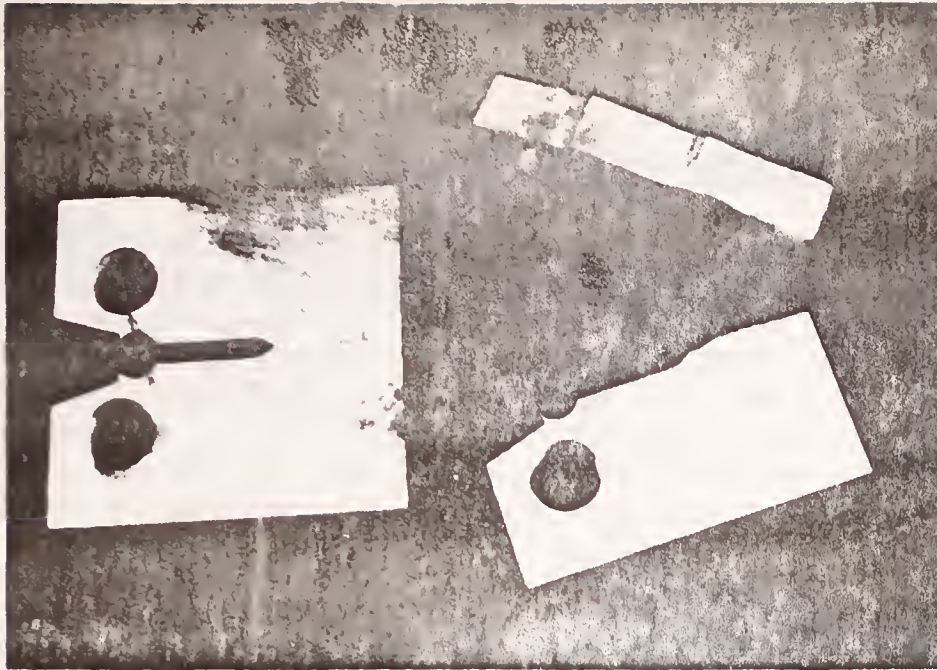


Fig. 16. One-centimeter-thick compact specimens used for J-integral tests.

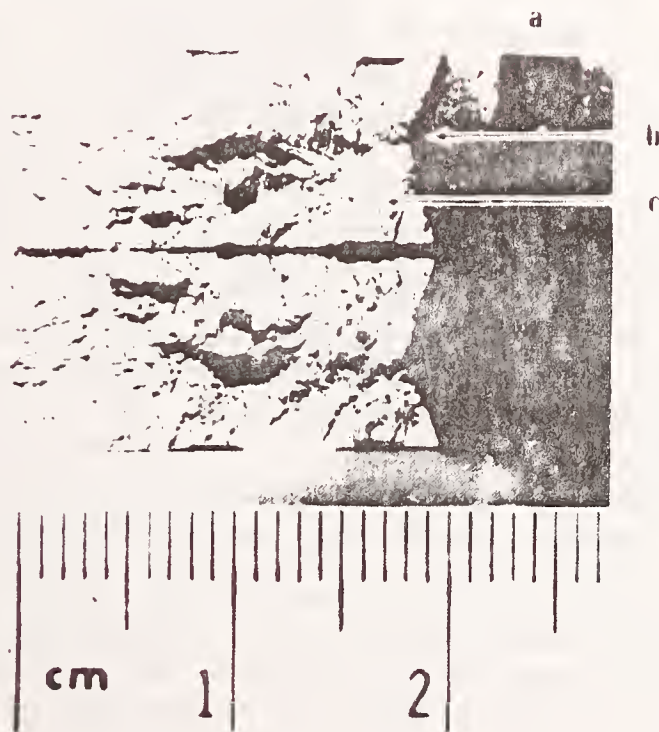


Fig. 17. Fracture surfaces showing: (a) fatigue pre-crack zone, (b) the heat-tinted crack-extension zone due to J test at 20°C, and (c) final fracture zone obtained after cooling to low temperatures to avoid subsequent deformation of (b).

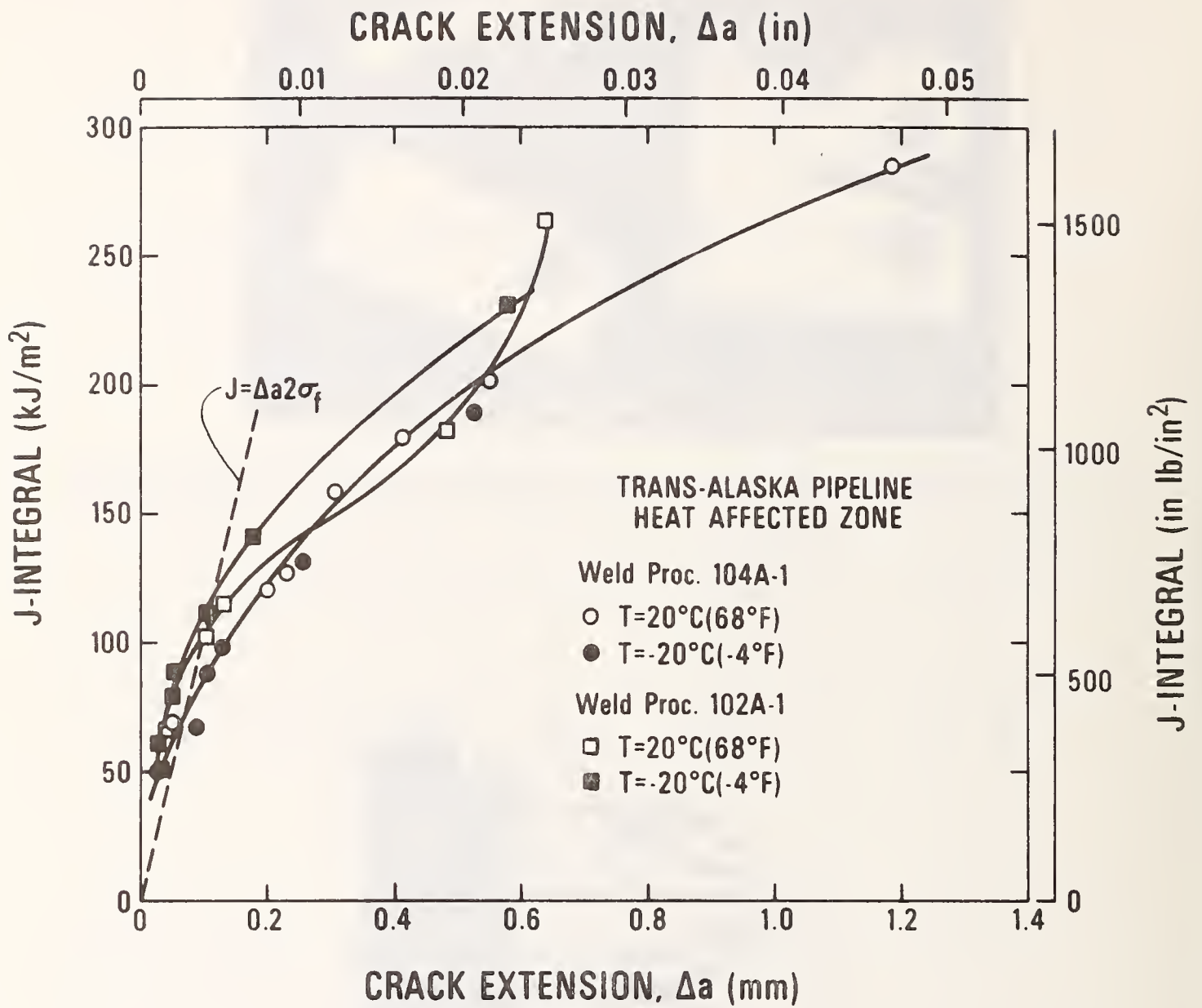


Fig. 18. J-integral results for trans-Alaska pipeline HAZ specimens.

3F. FATIGUE-CRACK GROWTH RATES

Due to a variety of factors, including periodic shut-downs, the trans-Alaska pipeline will experience stress fluctuations during its projected thirty-year service lifetime. The property governing subcritical flaw growth under cyclic loading conditions is the fatigue-crack growth rate, da/dN , where a is the crack length and N is the number of cycles. This report presents fatigue-crack growth rates as a function of the stress-intensity-factor range, ΔK , for the pipeline steel and its welds in air and in a corrosive environment.

The four-point bend specimens, Figs. 4 and 19, chosen for these tests were approximately 1.1 cm wide (W), 1.2 cm thick (B), and 23 cm in span length (S). After etching each specimen, notches were machined in the base metal, weld metal, or heat-affected zones (HAZ). The notch orientation was such that the cracks were propagated in the thickness direction of the pipeline sections. All base-metal specimens were from weld NBS #4. Weld-metal specimens were from welds NBS #2 and NBS #4, and HAZ specimens were from welds NBS #2 and #3. Differences due to welding procedure were not distinguishable from the scatter among replicate tests.

One series of tests was conducted on the base metal, weld metal, and HAZ in room air at 20°C (68°F) and on the base metal in air at $60 \pm 1^\circ\text{C}$ ($140 \pm 2^\circ\text{F}$). The cycling frequency was 10 Hz. A second test series was conducted on base-metal, weld-metal, and HAZ specimens in a corrosive environment at both specimen temperatures of 20°C and 60°C. The corrosive environment consisted of Groenveld and Elsea's¹ electrolyte: a 0.004 wt. pct. H_2SO_4 solution, to which 5 drops per liter of a 5g phosphorous/40 ml carbon-disulfide "poison" was added. The frequency was 0.1 Hz, except for one base-metal test at 0.01 Hz. A constant-current power supply was used to produce a current density of about 0.1 mA/cm² at the crack-growth region. This procedure charges the crack-tip material with hydrogen and creates a simulated stress-corrosion environment that tends to enhance fatigue-crack growth.

The specimens were first pre-cracked in room temperature air, using sinusoidally varying loads. The minimum/maximum load ratio (P_{\min}/P_{\max}) was constant at 0.05. P_{\max} ranged between 1.3 and 3.1 kN, but was constant for each test. The da/dN values were calculated

1. G. P. Groenveld and A. R. Elsea, in Hydrogen in Metals, I. M. Bernstein and A. W. Thompson, Eds. (Amer. Soc. Metals, Metals Park, Ohio, 1974).

by the central-difference method and crack lengths were monitored by compliance measurements.

Using methods described by McHenry and Reed², the functional relationship between relative crack length (a/W) and specimen compliance, EBC (E = Young's modulus, B = thickness, C = deflection per unit load), was determined using calibration specimens. Calibration correlations are shown in Fig. 20, and a base-metal calibration specimen is shown in Fig. 21. Using a computer program, the crack-length/compliance data were fitted to a four-term power-series equation. Crack lengths were calculated from compliance measurements taken during da/dN tests. The stress-intensity factor ranges were calculated using the equation

$$\Delta K = S(P_{\max} - P_{\min})\sqrt{a} Y(a/W)/BW^2 \quad (1)$$

Here, according to Srawley and Gross³,

$$Y(a/W) = 1.992 - 2.468(a/W) + 2.97(a/W)^2 - 23.17(a/W)^3 + 24.8(a/W)^4 \quad (2)$$

The uncertainty in the da/dN data is estimated at less than $\pm 40\%$.

The da/dN -versus- ΔK data from this study are plotted in Figs. 22, 23, and 24. Also shown in these figures are bands representing the spread of published data from other sources^{4,5} for similar steels and welds. As plotted on log-log scales, the base metal data exhibit a linear trend, having a slope of approximately three. Greater scatter and higher apparent slopes are exhibited by weld and HAZ data, possibly due to effects of residual stress.

Analysis of the findings leads to the following conclusions:

- (1) At 20°C (68°F), fatigue-crack growth rates are higher for base-metal specimens than for weld or HAZ specimens. A temperature increase from 20°C to 60°C (140°F) has no measurable effect on rates for the base metal.
- (2) The pipeline-steel base-metal behavior is typical of ferritic steels in general, as indicated by comparison with the works of Barsom⁴, Maddox⁵, and Vosikovsky.⁶

-
2. H. I. McHenry and R. P. Reed, unpublished report.
 3. J. E. Srawley and B. Gross, Eng. Fract. Mechs., 4, 587-589 (1972).
 4. J. M. Barsom, J. Eng. Ind., Trans. ASME, 1190-1196 (Nov. 1971).
 5. S. J. Maddox, Welding Journal, 401s-409s (Sept. 1974).
 6. O. Vosikovsky, Closed Loop, 3-12 (April 1976).

- (3) Over the range of ΔK investigated, the weld and HAZ data do not exceed the upper bound of Maddox's⁵ data for carbon-manganese steel weldments.
- (4) Vosikovsky⁶ reported that a hydrogen-charging environment that simulates stress-corrosion conditions significantly reduces fatigue-crack growth resistance of base metal specimens at 20°C. The limited data available for the trans-Alaska pipeline at 0.1 mA/cm² imply that the (unreported) current densities of Vosikovsky were significantly higher.

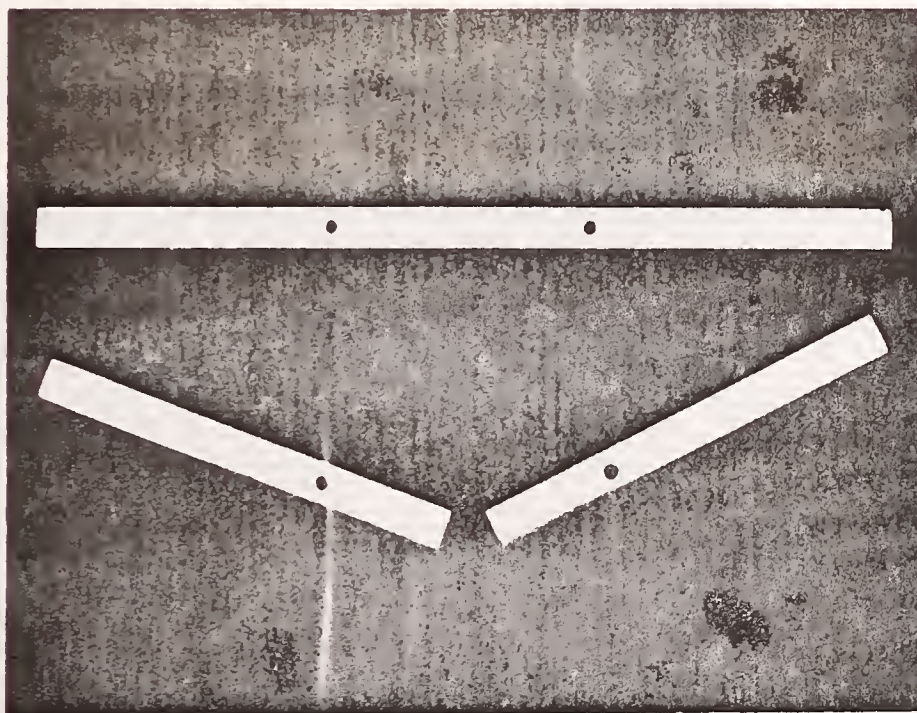


Fig. 19. Four-point bend specimens before and after testing.

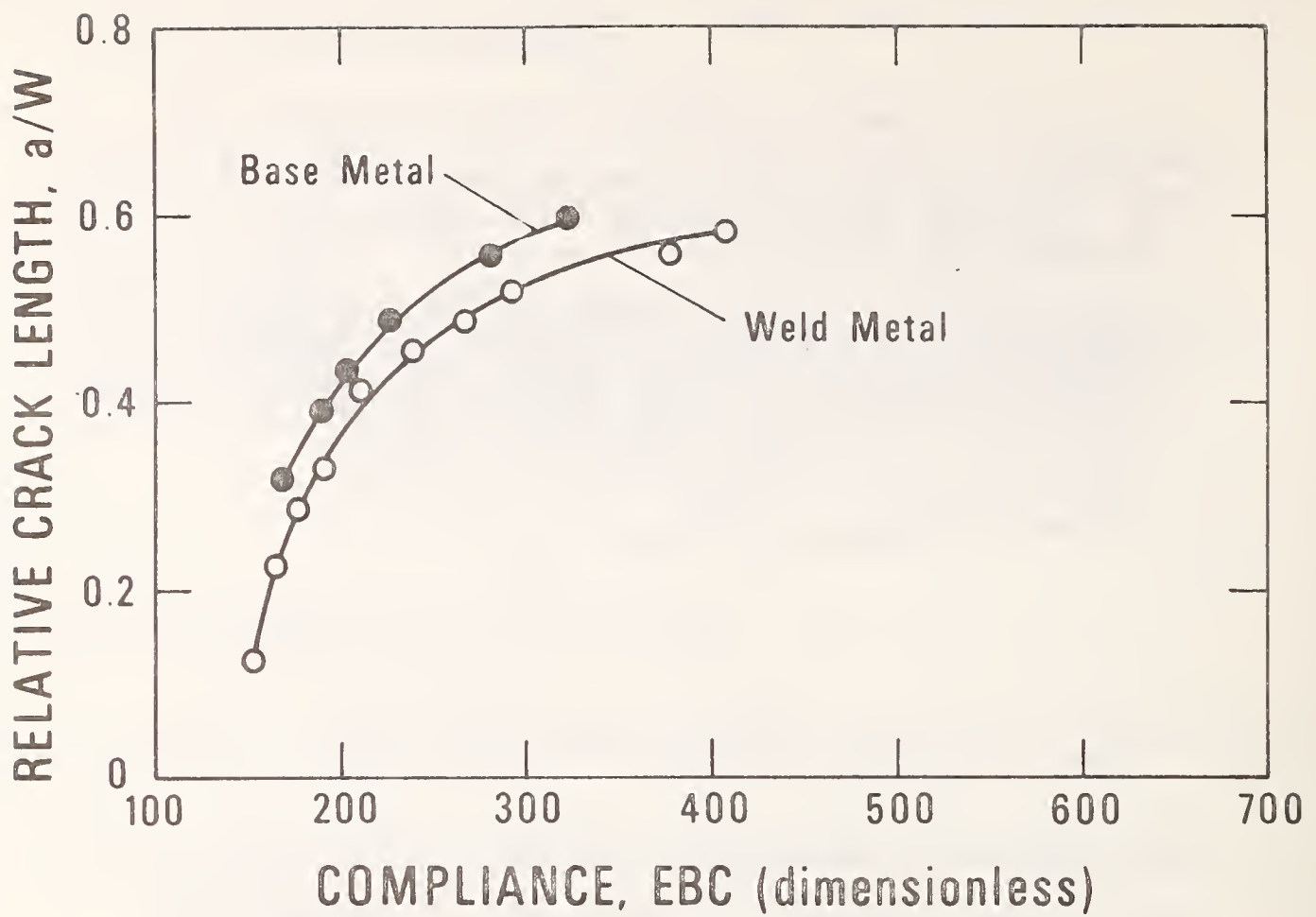


Fig. 20. Crack-length/compliance correlations used in crack-growth-rate tests.



Fig. 21. Base-metal crack-length calibration specimen used in determining the correlation shown in Fig. 20.

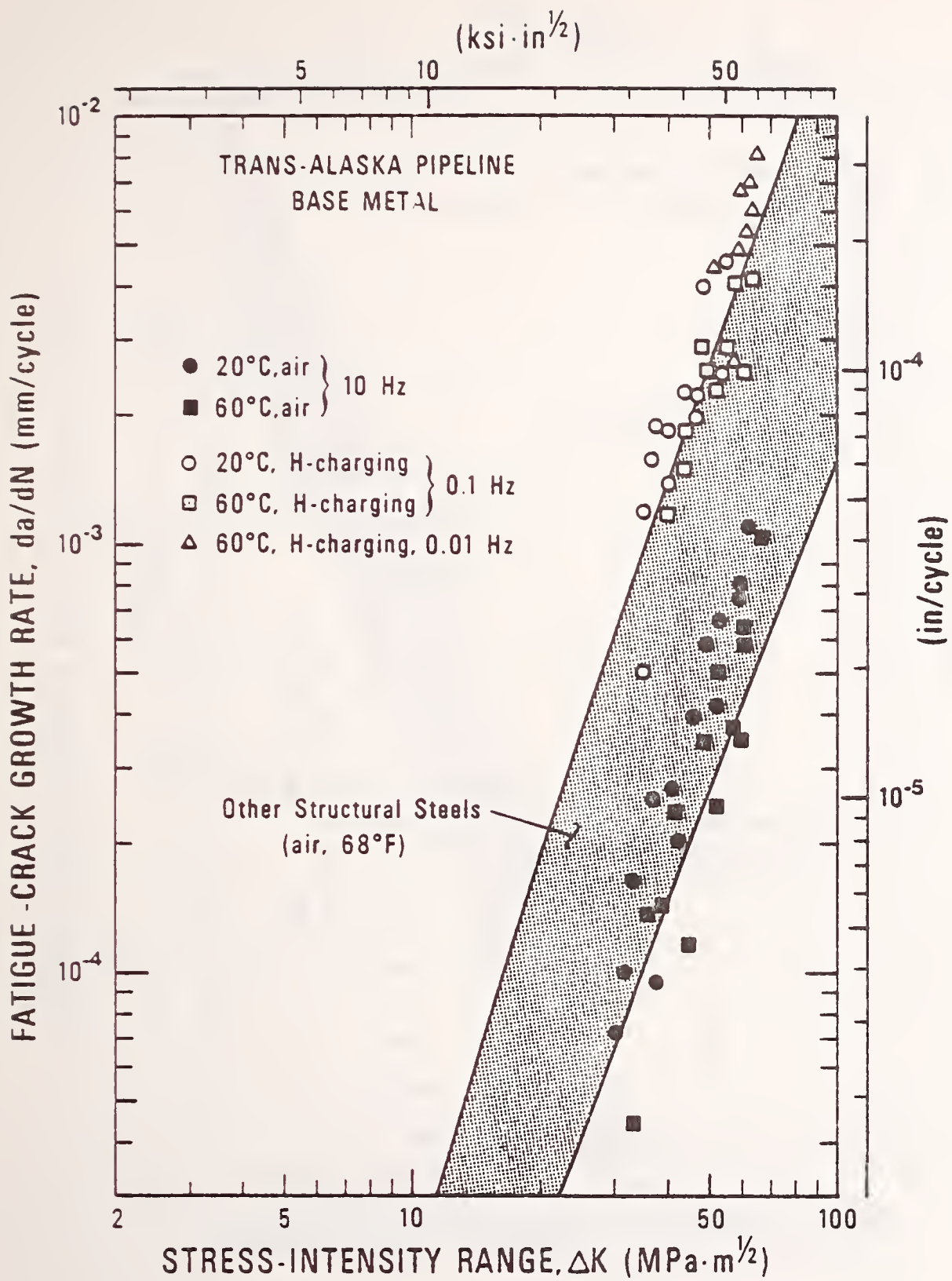


Fig. 22. Fatigue-crack growth rates for the base metal.

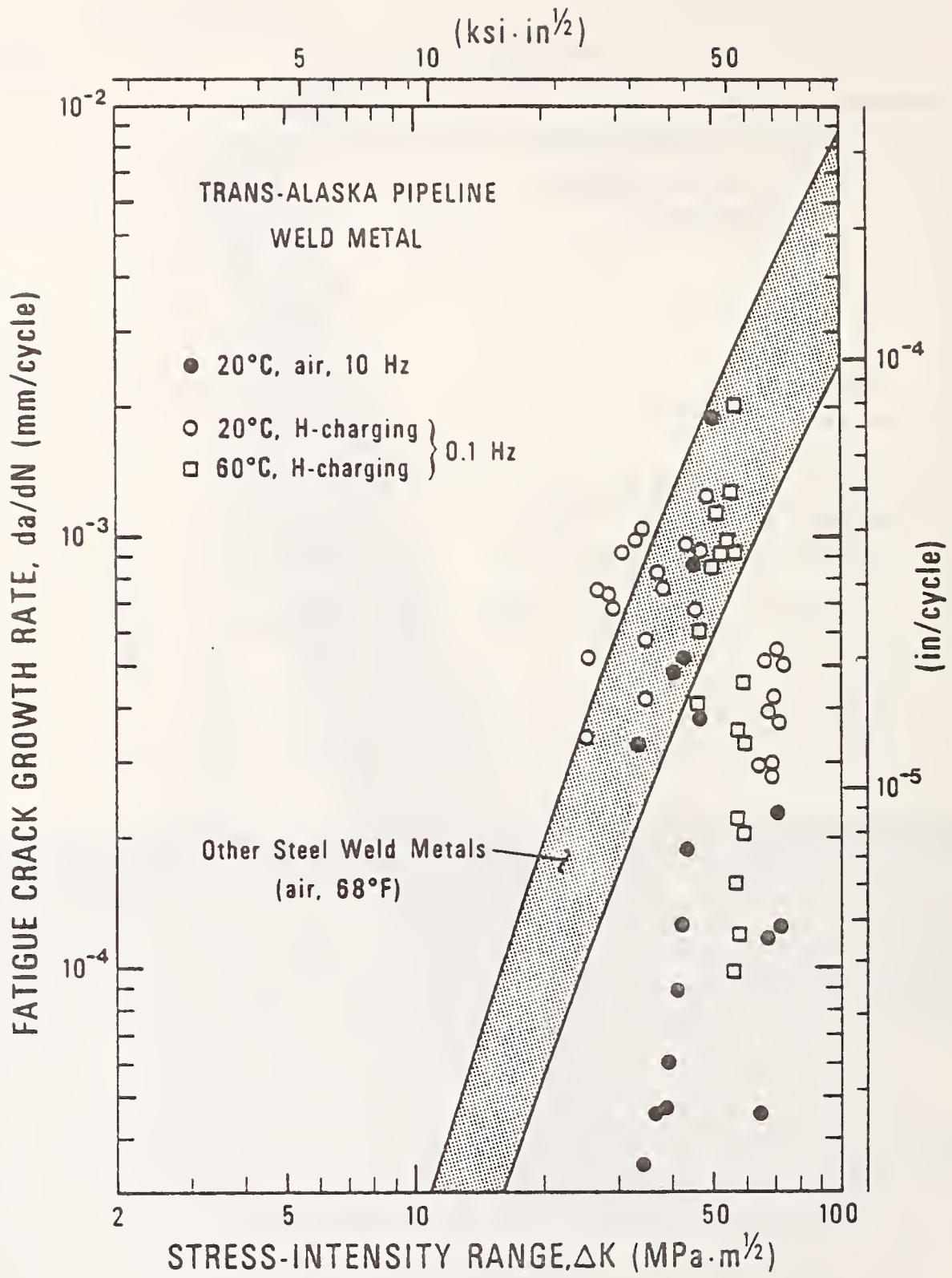


Fig. 23. Fatigue-crack growth rates for the weld metal.

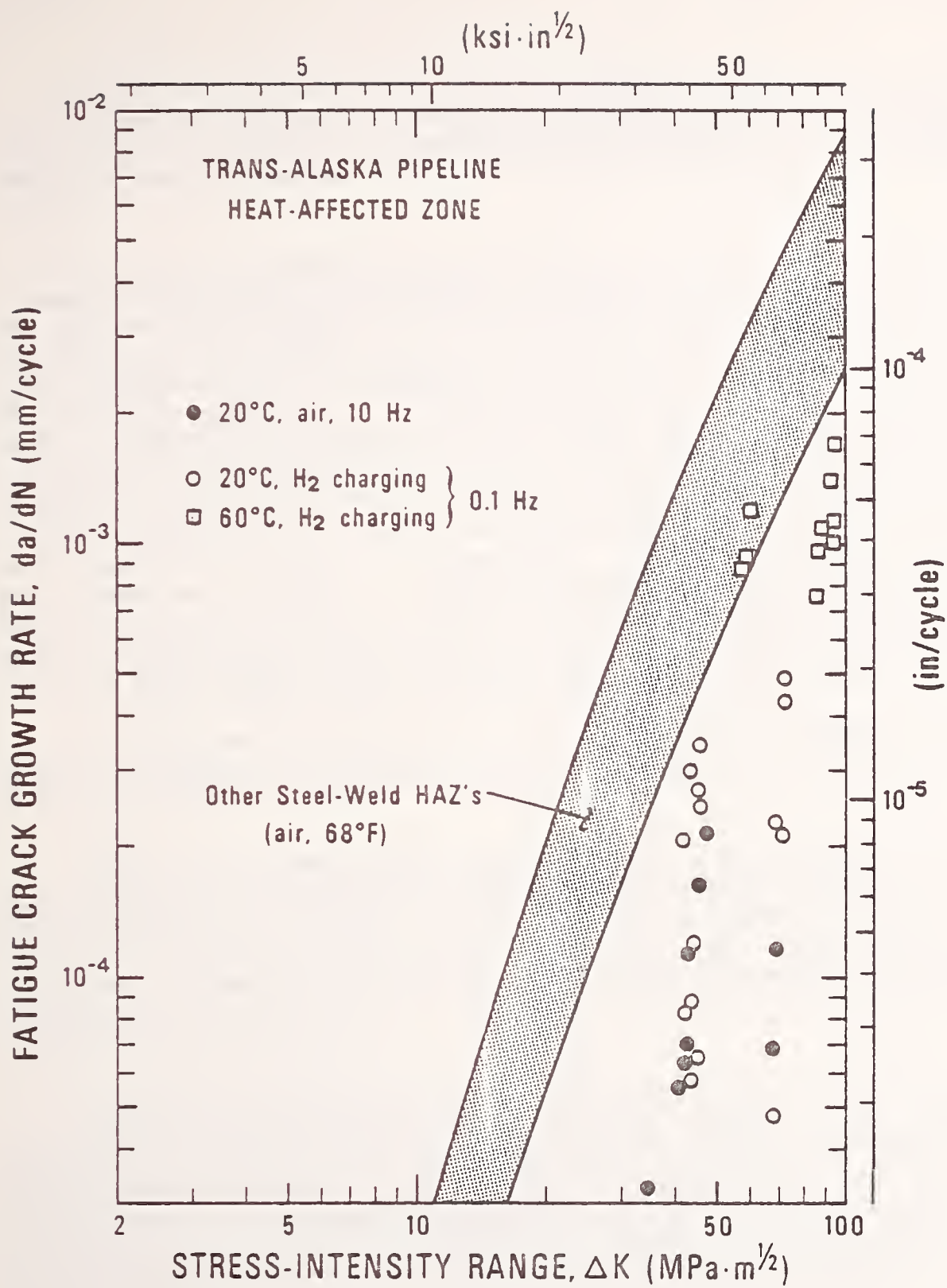


Fig. 24. Fatigue-crack growth rates for the HAZ.

3G. SIMULATED-SERVICE FATIGUE PROPERTIES

A series of fatigue tests was conducted on samples of trans-Alaska pipeline weldments to determine the fatigue behavior of natural and artificial flaws under simulated pipeline operating conditions. The tests were conducted at the Martin Marietta Corporation, Denver Division.

Test specimens were machined as shown in Fig. 4 from welds 2, 4, and 5. The natural curvature of the pipe was retained throughout the test section; however, the specimen ends were flattened in a hydraulic press to facilitate gripping in the test machine. Artificial flaws were introduced into nine specimens and natural flaws were present in the other two specimens. The artificial flaws were introduced into the weld by electrical-discharge machining (EDM) a notch approximately 0.4 cm deep by 5.8 cm long and subsequently extending the notch by bending fatigue to a nominal size of 1 cm deep by 6.4 cm long. Approximately 100,000 cycles of 0 to 275 MPa (40 ksi) outer-fiber bending stresses were required to precrack the specimens. The actual specimen dimensions are summarized in Table 7. Flaw-size dimensions and bending fatigue cycles are given in Table 8. All artificial notches were introduced into the outer (cap pass) surface of the weld, either in the center of the weld (weld metal tests) or at the edge of the weld (HAZ tests).

The tests were conducted in a 4.4 MN (10^6 lb) - capacity electro-hydraulic fatigue test machine equipped with hydraulically operated friction grips.

The two test-load spectra shown in Table 9 were used. The five-step spectrum was representative of the anticipated loadings for above-ground welds with a factor of ten on number of cycles for each step. Use of the five-step spectrum was discontinued when the eight-step spectrum representative of below-ground welds was supplied by Alyeska; the eight-step test spectrum includes a factor of four on number of cycles for each step.

Tests were conducted either in laboratory air at room temperature or in a simulated-service environment at 60°C (140°F). The simulated-service environment was an acidic solution (0.004% by wt. H₂SO₄) in water, pH = 3.2) with 5 drops per liter of poison (5 g P in 40ml CS₂) coupled with an impressed current of 0.1 mA/cm². This environment was developed by Battelle¹ to simulate the hydrogen-charging conditions that are most representative of a defect or hole in the protective coating of a buried pipe.

1. G. P. Groenveld and A. R. Elsea, in Hydrogen in Metals, I. M. Bernstein and A. W. Thompson, Eds. (Amer. Soc. Metals, Metals Park, Ohio, 1974).

The laboratory air tests were conducted at a cyclic loading rate of 3 Hz. Tests were continued by repeated applications of the load spectrum until the crack extended through the thickness or until a large number of cycles were applied. The environmental tests were conducted at a cyclic loading rate of 0.0167 Hz; the complete spectrum was applied once. After completion of fatigue cycling the specimen was loaded to failure and the maximum load recorded for determination of residual strength.

Results are summarized in Table 10. The results indicate clearly that deep flaws in pipeline welds do not grow appreciably in the anticipated service life of the pipeline - either in laboratory air or in a simulated holiday environment. The net section stress at failure ranged from 580 to 640 MPa (76 to 84 ksi); these results indicate that the flaws introduced reduced the load-carrying capacity of the pipe by less than ten percent. The two natural-flaw specimens both failed in the base metal remote from the weld defect. A photograph of a failed and an unfailed test specimen is shown in Fig. 25. The fracture surfaces of the failed specimen are shown in Fig. 26.

Table 7. Simulated-service-fatigue specimen dimensions.

Specimen No	Weld Procedure	Flaw Type	Specimen Dimensions, cm(in)		
			Width	Weld Thickness	Base
4-4SF	104A	Weld	20.13(7.92)	1.85(0.73)	1.46(0.573)
4-9SF	104A	Weld	20.14(7.93)	1.80(0.71)	1.47(0.577)
4-6SF	104A	Natural	20.32(8.00)	2.01(0.79)	1.47(0.579)
4-5SF	104A	Natural	20.19(7.95)	1.88(0.74)	1.47(0.578)
2-27SF	104A-1	Weld	20.07(7.90)	1.55(0.61)	1.24(0.488)
2-26SF	104A-1	HAZ	20.07(7.90)	1.52(0.60)	1.25(0.494)
2-29SF	104A-1	Weld	20.07(7.90)	1.57(0.62)	1.25(0.491)
2-28SF	104A-1	HAZ	20.07(7.90)	1.75(0.69)	1.24(0.490)
5-1SF	104A-1	Weld	20.07(7.90)	1.52(0.60)	1.21(0.475)
5-2SF	104A-1	HAZ	20.14(7.93)	1.50(0.59)	1.21(0.475)
5-3SF	104A-1	HAZ	20.17(7.94)	1.47(0.58)	1.22(0.480)

Table 8. Pre-crack dimensions and bending-fatigue cycles.

Specimen No.	Pre-crack Flaw Dimensions, mm(in)		Bending Kilocycles	Maximum Stress, MPa
	a	ℓ		
4-4SF	11.9(0.47)	59.4(2.34)	125	310
4-9SF	13.5(0.53)	63.8(2.51)	90	276
			95	310
4-6SF	---	---	--	--
4-5SF	---	---	--	--
2-27SF	9.7(0.38)	64.8(2.55)	55	276
2-26SF	10.4(0.41)	60.2(2.37)	36	276
2-29SF	11.2(0.44)	62.5(2.46)	55	276
2-28SF	10.9(0.43)	68.8(2.71)	102	276
5-1SF	9.7(0.38)	57.4(2.26)	146	276
5-2SF	9.4(0.37)	59.7(2.35)	95	276
5-3SF	9.4(0.37)	61.0(2.40)	81	276

Table 9. Test-load spectra.

Step	Cycles	Stress MPa (ksi)	
		Minimum	Maximum
Five-step spectrum: ^a			
1	50	0	135. (19.6)
2	350	0	104. (15.1)
3	20	0	216. (31.3)
4	550	0	162. (23.5)
5	200	0	180. (26.1)
Eight-step spectrum: ^b			
1	8	36.5 (5.3)	154. (22.4)
2	40	-110. (-16.0)	-21.4 (-3.1)
3	12	-110. (-16.0)	40.7 (5.9)
4	4	-110. (-16.0)	103. (14.9)
5	12	40. (5.8)	203. (29.4)
6	96	141. (20.4)	229. (33.3)
7	36	141. (20.4)	291. (42.3)
8	4	141. (20.4)	353. (51.2)

a. The number of cycles for each step is ten times greater than the number anticipated in thirty years of pipeline operation.

b. The number of cycles for each step is four times greater than the number anticipated in thirty years of pipeline operation.

Table 10. Simulated-service-fatigue test results.

Specimen No.	Crack Extension, Δa mm(in)	Spectrum Steps	Environment	Temp.	Spectrum Cycles	Failure Load MN(kips)	Failure Stress MPa(ksi)
4-4SF ^a	0.76(0.030)	8	Air	RT	14	--	--
4-9SF	0.13(0.005)	8	Air/serv	RT/60°C	1/1	1.21(271)	522(75.8)
4-6SF ^b	--	8	Air	RT	25	1.73(390)	580(84.2)
4-5SF ^b	--	8	Air/serv	RT/60°C	1/1	1.67(375)	562(81.6)
2-27SF ^c	4.06(0.16)	5	Air	RT	28	0.85(190)	521(75.6)
2-26SF ^d	3.30(0.13)	5	Air	RT	14	--	--
2-29SF	0.13(0.005)	8	Service	60°C	1	1.09(245)	527(76.5)
2-28SF	0.46(0.018)	8	Air/serv	RT/60°C	1/1	1.03(232)	533(77.4)
5-1SF	0.13(0.005)	8	Air/serv	RT/60°C	1/1	1.10(248)	544(79.0)
5-2SF	1.78(0.070)	8	Air	RT	50	1.07(240)	551(80.0)
5-3F	0.25(0.010)	8	Air/serv	RT/60°C	1/1	1.14(257)	566(82.1)

- a. Machine malfunction, broke specimen.
- b. Base-metal failure.
- c. Estimated P_{max} .
- d. P_{max} not measured.

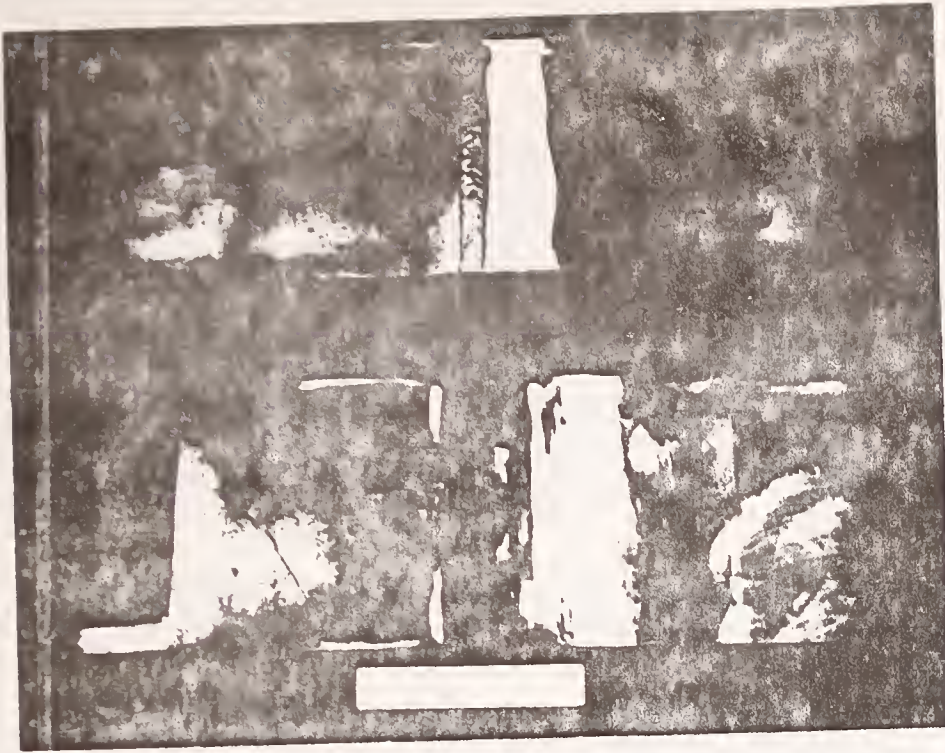


Fig. 25. Failed and unfailed fatigue-test specimens.

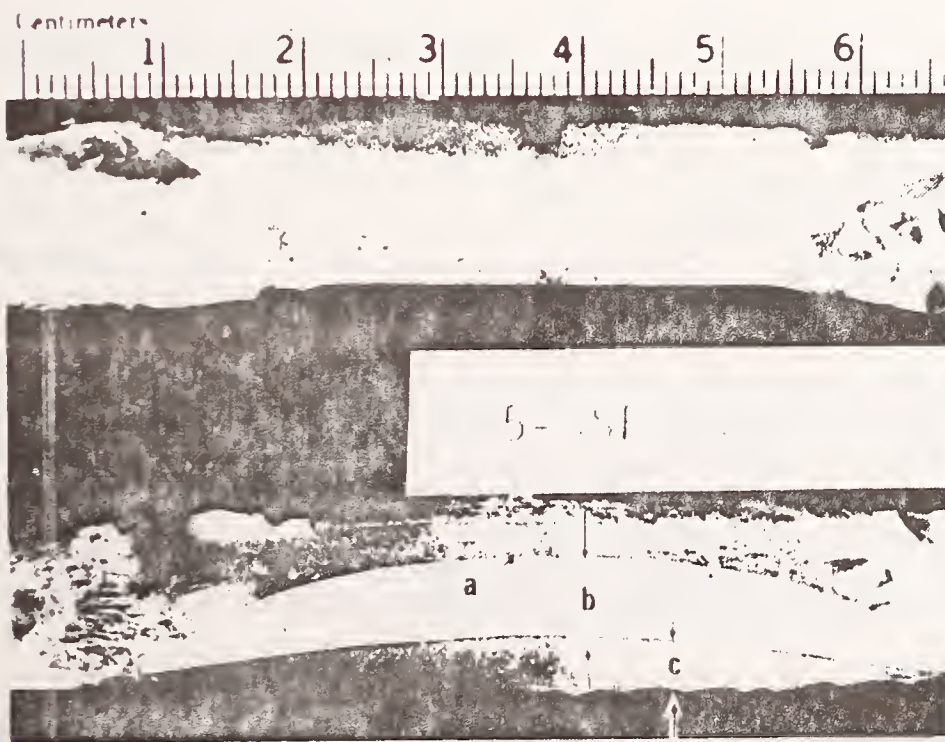


Fig. 26. Fracture surfaces of fatigue-test specimen showing: (a) crack growth due to simulated-service fatigue, (b) bend-fatigue precrack, and (c) EDM notch.

3H. SIGNIFICANCE OF ARC BURNS

The significance of random arc strikes on the base metal of the trans-Alaska pipeline was evaluated under two "worst-case" conditions. One condition simulated the maximum credible hoop-stress spectrum while assuming a defect in the insulation at the location of the burns. This permitted accelerated propagation of any existing surface crack by hydrogen charging due to the cathodic-protection system.¹ The second condition simulated a sustained, static, hoop-tensile stress at the yield point of the steel while assuming hydrogen charging. No evidence of crack propagation into the base metal was seen. Several cracks were found in the arc-burn area after testing; however, the maximum depth was 0.95 mm (0.037 in), confined to the interior of the arc burn.

The arc burns were implanted systematically in four 76.2 cm (30 in) long by 15.2 cm (6 in) wide plates taken from Alyeska pipeline material that was 1.17 cm (0.462 in) thick. The burn pattern and the burn intensities (times) are given in Fig. 27. Arc burns were implanted using facilities at Ohio State University.² Burn times from 0.1 to 0.5 seconds duration resulted in spot burns 0.37 cm (0.145 in) to 1.2 cm (0.47 in) in diameter. Drag strikes were simulated by an overlapping series of spots for total burn lengths of 2.8 cm (1.1 in) to 5.4 cm (1.8 in). Linked spots were oriented perpendicular to the intended stress direction during subsequent tests. The appearance of the panels after burning is shown in Fig. 28.

All panels were radiographed after burning, and no cracks were seen.

Hoop-Stress Fatigue-Spectrum Study

Panels 1-26AF and 1-27AB were subjected to the stress cycles and the hydrogen-charging conditions shown in Table 11. The panels with doublers attached to the tensile grips are shown in Fig. 29. To sustain the tensile load within the arc-burn area, 15 mm (0.6 in) were removed from the panel sides. The testing was done at the General Dynamics Convair Aerospace Corporation, San Diego, California.

The arc burns in the test plates were inspected visually, radiographically, and with dye penetrants for evidence of surface cracking. Metallographic sections prepared from longitudinal cuts through the linked spots of 0.1-, 0.3-, and 0.5-second burn times and through spot burns in the tensile direction failed to show any crack extension from the burn areas into the base material. Occasional small cracks were observed to have propagated from the fusion zone into the heat-affected

-
1. G. P. Groenveld and A. R. Elsea, in Hydrogen in Metals, J. M. Bernstein and A. W. Thompson, Eds. (ASM, Metals Park, Ohio, 1974).
 2. T. J. Natarajan and R. B. McCauley, Welding J., 54, 879-884 (1975).

zone as shown in Fig. 30. Such cracks were only observed in the linked series of spots made at 0.1-second burn time.

Static-Stress Study

Panels 1-28AB and 1-29AB were subjected to static bending stresses (arc-burn side in tension) slightly exceeding the yield point of the material. The panels were subjected to the hydrogen charging conditions in Table 11, except that the test temperature was $20 \pm 3^\circ\text{C}$ ($68^\circ \pm 5^\circ\text{F}$). The method of stressing the plates is illustrated in Fig. 31. Plate 1-28AB was removed after 225 hours of exposure. No surface cracking was observed visually, radiographically, or by dye penetrants. Subsequent examination of metallographic sections, prepared as described previously, indicated a few small cracks confined to the burn area of the 0.1-second linked-spot region shown in Fig. 32. However, no cracks traversed the heat-affected zone into the base metal. Therefore, although some arc burn radiographs show the presence of cracks in the crater, these do not extend into the base metal.

Supplementary Data

These test programs provided an opportunity to establish a correlation between arc-burn diameter and the resulting arc-burn depth and heat-affected-zone depth. These data are shown in Fig. 33, which includes a histogram of the arc-burn diameters reported in the preliminary Alyeska waiver request (Revision 9/6/76). This study also provided an opportunity to determine the hardness profiles from the parent metal through the heat-affected zones and into the fusion zones for burn times varying from 0.1 to 0.5 seconds. These data are shown in Fig. 34.

Table 11. Cyclic hoop-stress spectrum.^{a,b}

Step	Min. Stress	Max. Stress $10^8\text{N/m}^2(10^3\text{psi})$	No. Cycles
1	0	4.26(61.8)	8
2	0	3.23(46.8)	244
3	0	3.58(52.0)	68

a. Environment: 0.004% by weight H_2SO_4 in distilled water plus 5 drops per liter of solution of 5 g phosphorous in 40 ml carbon disulfide; $60^\circ \pm 3^\circ\text{C}$ ($140^\circ \pm 5^\circ\text{F}$); current density 0.97 A/m^2 (90 mA/ft^2); specimen is cathode.

b. Specimen stressed initially in air to $4.26 \times 10^8\text{ N/m}^2$ ($61.8 \times 10^3\text{ psi}$) after which the electrolyte was added and the current impressed. Specimen held 8 hours, after which the prescribed program was completed at a cyclic frequency of 0.17 Hz (1 cycle/min) while maintaining the hydrogen-charging conditions.

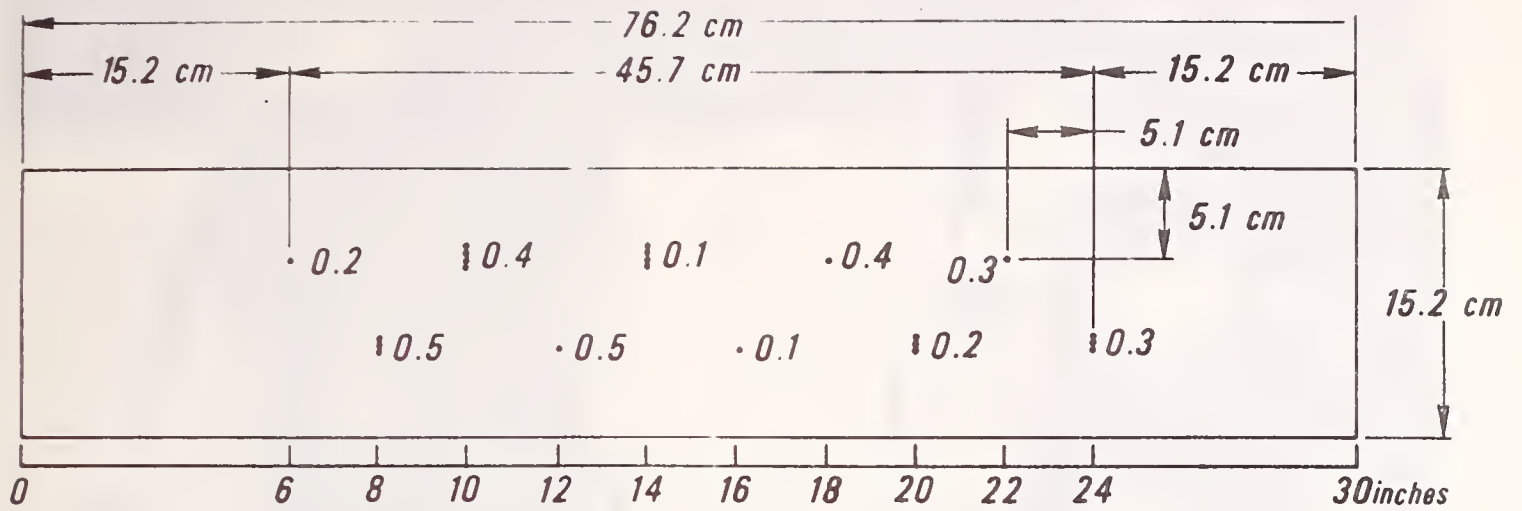


Fig. 27. Distribution of arc burns on test plates.

Test-plate/electrode identifications: 1-26AB = 5/32-in Lincoln 65+ shield-arc; 1-27AB = 3/16-in Lincoln 65+ shield-arc; 1-28AB = 4 mm Phoenix Cel 80; 1-29AB = 5 mm Phoenix Cel 80. Arc-burn times in seconds are shown in Fig. 27.

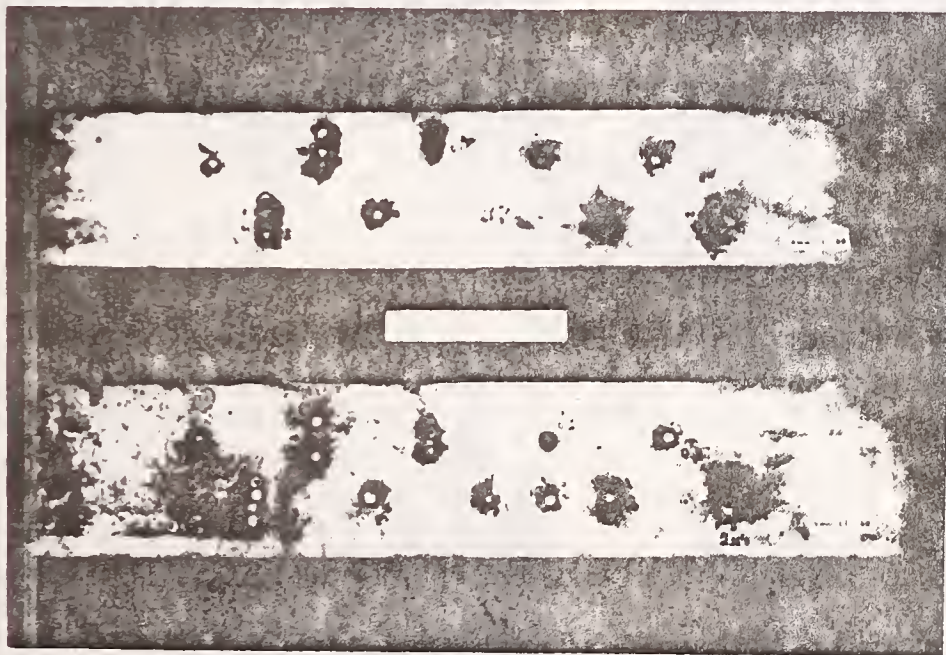


Fig. 28. Completed arc-burn panels.

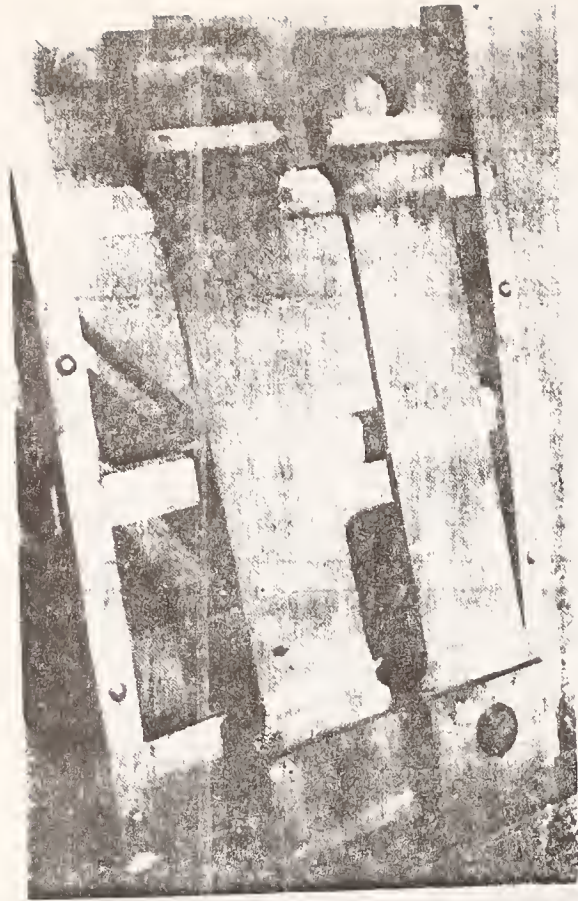


Fig. 29. (Left) Panels prepared for the hoop-stress fatigue-spectrum study.

Fig. 30. (Below) Examples of surface cracks observed in the arc-burn region of plates subjected to maximum credible hoop-stress spectrum while under hydrogen charging conditions. All cracks terminated in the HAZ. Overlapping 0.1-s burns. 200X.



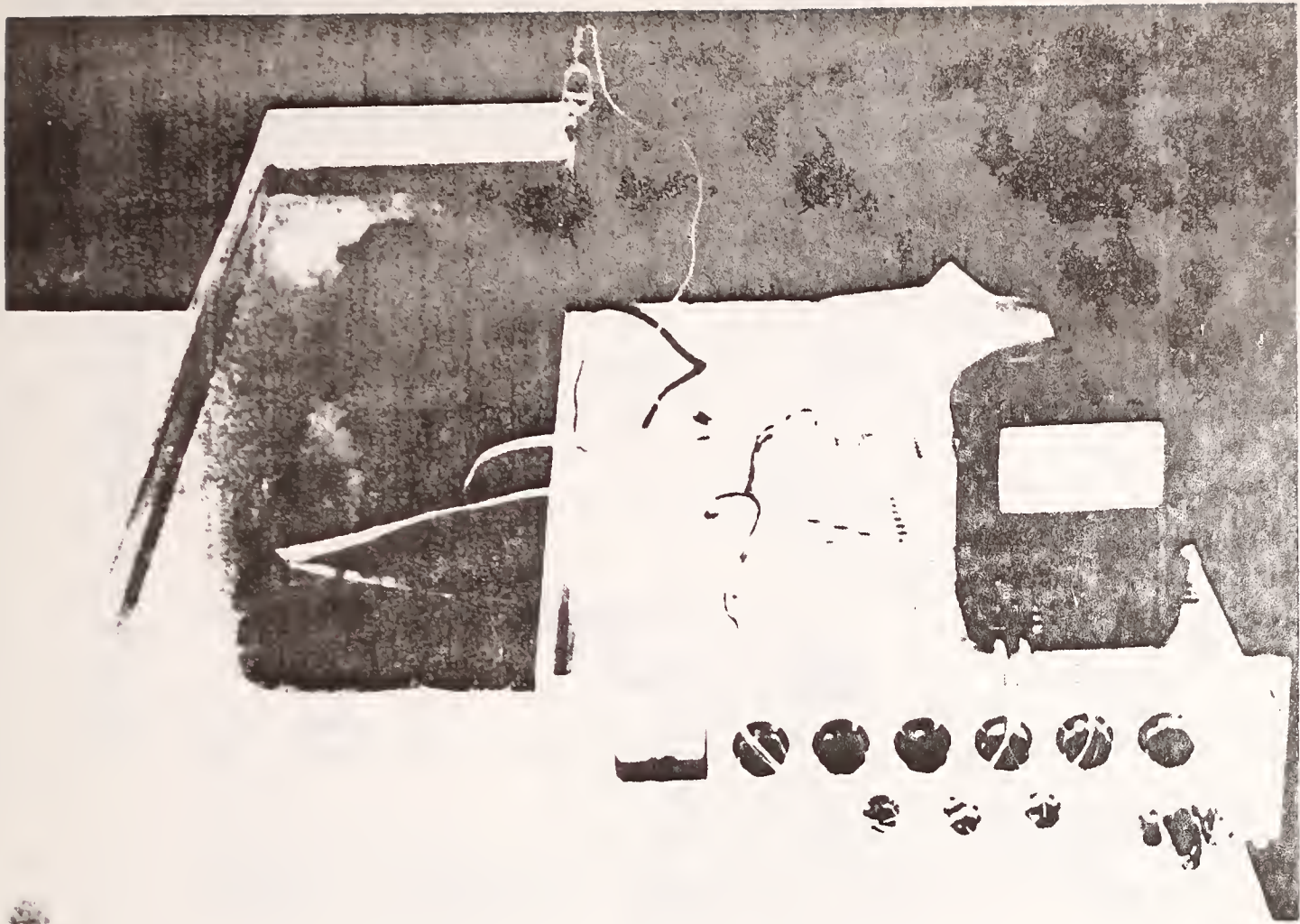


Fig. 31. Test setup for static-stress study.



Figs. 32. Surface cracks observed in the arc-burn region of plates subjected to static bending stress while under hydrogen charging for 225 h. Overlapping 0.1-s burns. 200X.

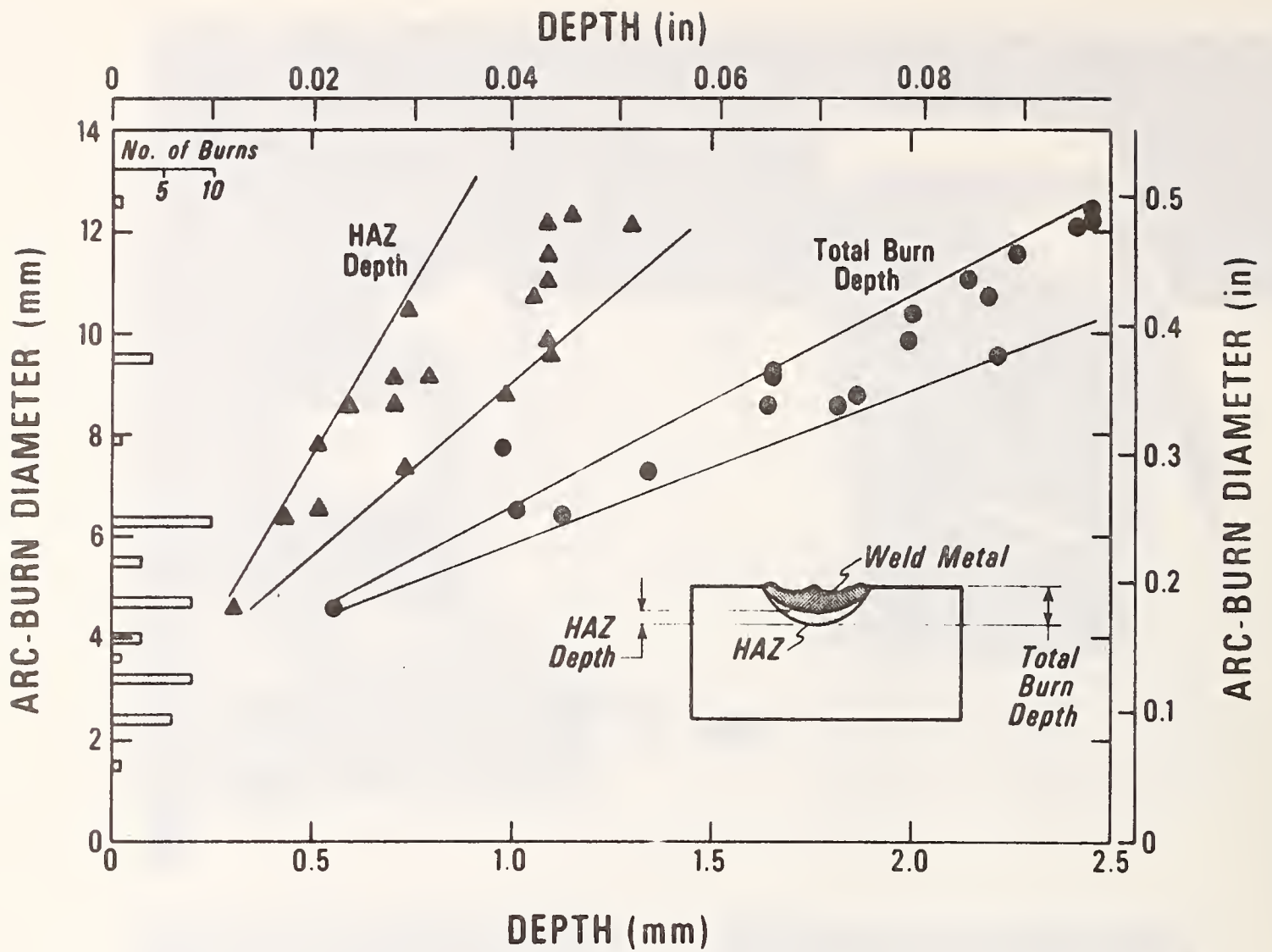
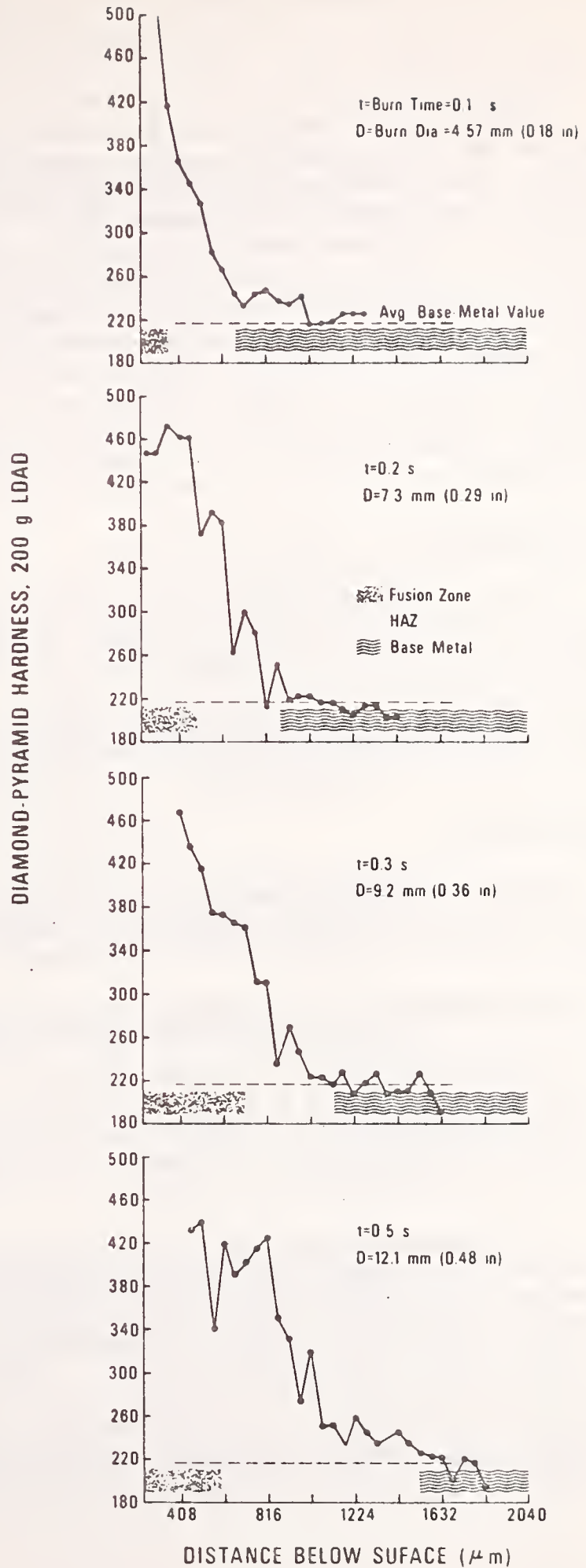


Fig. 33. Variation of total arc-burn depth and heat-affected zone depth as a function of arc-burn diameter.

Fig. 34. Hardness profiles across arc burns of various burn times and diameters.



3I. CHARPY V-NOTCH IMPACT SPECIMEN TESTING

Charpy V-notch impact specimens were prepared from welds made by each of the two welding procedures used (102A-1 and 104A-1). All Charpy V-notch impact testing was conducted using instrumented impact testing equipment that permitted the measurement of impact load versus time to fracture so that the loads and times required to initiate and propagate fracture in a Charpy V-notch specimen could be determined. These instrumented Charpy V-notch tests can be used to determine the "dynamic" fracture toughness of the test material as expressed in terms of energy (such as total energy to fracture) or stress-intensity (such as K_{I_d}). The instrumented Charpy V-notch test has been used extensively to evaluate the dynamic fracture toughness of metals. However, a standard test method has not been established but is still under active development by the American Society for Testing and Materials (ASTM).

Test Materials

Charpy V-notch specimens were obtained from one weldment made using welding process 102A-1 (weld No. 79907) and from one weldment made using welding process 104A-1 (weld No. 88119). All specimens were taken so that the longitudinal axis of the specimen was parallel to the longitudinal axis of the pipe. Four different orientations were used for the specimen notch as shown in figure 35 to determine the effect of notch position on the fracture toughness.

Test Variables

The test conditions were varied to include six temperatures, two types of specimen notches (machined and fatigue precracked) and four notch positions for each of the two weldments.

Testing Procedure for Instrumented Charpy V-Notch Specimens

All test specimens were conventional, full-sized Charpy V-notch specimens (0.394 x 0.394 x 2.165 inches) with a 0.079 inch deep 45° V-notch. Tests were conducted in a standard Charpy impact machine which is fitted with instrumentation for measuring load and time during impact and fracturing of the specimen.

For the specimens with machined notches, the total energy absorbed was measured from the Charpy impact machine dial and the lateral expansion and percent shear fracture were determined after fracture. Only specimens with notch orientation number 1 (crack propagation parallel to the weld axis) were tested with machined notches. From the load-time curves obtained with the instrumented Charpy testing machine, the total absorbed energy (E_D), the energy to initiate fracture (E_M), the energy for fracture propagation (E_p), and the dynamic yield strength (σ_{y_d}) can be calculated as follows.

The total energy E_D is normally taken from the machine dial reading but may also be obtained from the integrated load-time curve. This value is divided by the area under the Charpy V-notch and a normalized total energy value E_D/A , is reported. The energy for fracture initiation, E_M , is equal to $W_M - E_C$, where W_M is the area under the load-time curve up to the maximum load and E_C is a correction for the compliance interaction of the machine which is, $E_C = \frac{1}{2} P^2 C_C$, where P is the applied load and C_C is the compliance of the system.¹ The energy to propagate fracture, $E_P = E_D - E_M$, is obtained by difference. These energy values, E_M and E_P , are normalized by dividing by the area A , similar to the normalized total energy, E_D/A . The dynamic yield strength, σ_{yd} , can also be calculated from the load-time record, as

$$\sigma_{yd} = \left(\frac{3.31W}{B(W-a)^2} \right) P_{GY}$$

where W is the specimen height (0.394 inch), B is the specimen width (0.394 inch), a is the crack length, and P_{GY} is the load at which general yielding occurs. The measured and calculated results of all tests on machine-notched Charpy specimens are shown in Table 12. The measured results of these tests are shown as a function of temperature in figures 36-41.

For precracked specimens, a fatigue crack of approximately 0.10 inch deep was developed under the machined notch. From the load versus time curves, the total energy absorbed (E_D), energy for crack initiation (E_M), energy for crack propagation (E_P), and dynamic yield strength were determined similar to the same measurements made on the machine-notched specimens. In addition, for the precracked specimens, the dynamic fracture toughness, K_{Id} , can be calculated.

When fracture occurs under linear elastic conditions, the dynamic fracture toughness, K_{Id} , is calculated according to linear elastic fracture mechanics assumptions and

$$K_{Id} = \frac{6YP_M}{BW} (a)^{1/2} \quad (1)$$

where P_M is the maximum load measured from the load time curve, a is the crack length, B and W are the specimen thickness and width, and Y is a polynomial function of a/W . Linear elastic fracture applies when the maximum load, P_M , is less than the load required for general yielding, P_{GY} .

¹W. L. Server and R. A. Wullaert, Dynamic Three-Point Bend Analysis for Notched and Precracked Samples, Fracture Control Corporation Report No. 76-8.

Table 12. Results of Machine-Notched Charpy-V-Notch Test

Weld Process	Notch Orientation	Test Temp(°F)	Spec. No.	Measured Results				Calculated Results				Dynamic Yield Strength σ_y (psi)
				Energy Absorbed ft-lb	% Shear Fraction	Lateral Expansion (in)	Total. E_D	Normalized Energy (in-lb/in ²)	Initiation, E_H	Propagation, E_p		
102A-1	1	100	B22-1	88	90	.078	8518	2544	5974	88.3		
			C20-1	69	90	.065	6662	2787	3875	88.3		
			D15-1	82	95	.081	7919	2580	5338	88.3		
		70	B05-1	88	100	.074	8509	2755	5754	95.0		
			C22-1	70	85	.067	6730	2670	4060	91.6		
			D28-1	91	90	.077	8760	2546	6214	92.7		
		32	B03-1	65	55	.055	6323	2833	3490	99.4		
			C11-1	60	55	.059	5840	2872	2968	95.0		
			D05-1	77	70	.060	7426	3023	4402	98.3		
		10	B23-1	71	65	.062	6846	3002	3844	99.4		
			C24-1	47	30	.044	4535	2362	2173	101.6		
			D17-1	68	55	.065	6604	3072	3532	101.0		
		-20	B20-1	61	50	.037	5879	3168	2711	106.6		
			C15-1	40	20	.035	3868	2612	1256	103.2		
			D27-1	81	70	.069	7803	2635	5168	105.4		
-40	C16-1	8	5	.009	793	284	509	103.2				
	D03-1	33	15	.033	3171	2249	923	108.1				
	B01-1	46	25	.037	4457	2500	1950	109.9				
104A-1	1	100	A09-1	72	100	.073	6981	2549	4431	79.8		
			A29-1	73	95	.070	7049	2571	4478	81.7		
		70	A05-1	76	100	.071	7339	2456	4852	82.3		
			A37-1	71	100	.068	6855	2242	4613	90.0		
		32	A41-1	63	85	.059	7542	2287	4754	92.2		
			A20-1	78	90	.072	7542	2787	4754	92.7		
10	A23-1	66	80	.067	6401	2399	4002	95.0				
	A42-1	51	50	.050	4912	2229	2683	95.5				
-20	A32-1	36	15	.035	3519	2345	1174	99.4				
	A45-1	11	15	.011	1073	415	658	96.1				
-40	A03-1	39	15	.031	3781	2162	1618	101.6				
	A31-1	35	15	.021	3423	2182	1240	101.6				

Fig. 3.5 NOTCH ORIENTATIONS FOR CHARPY V-NOTCH TEST SPECIMENS

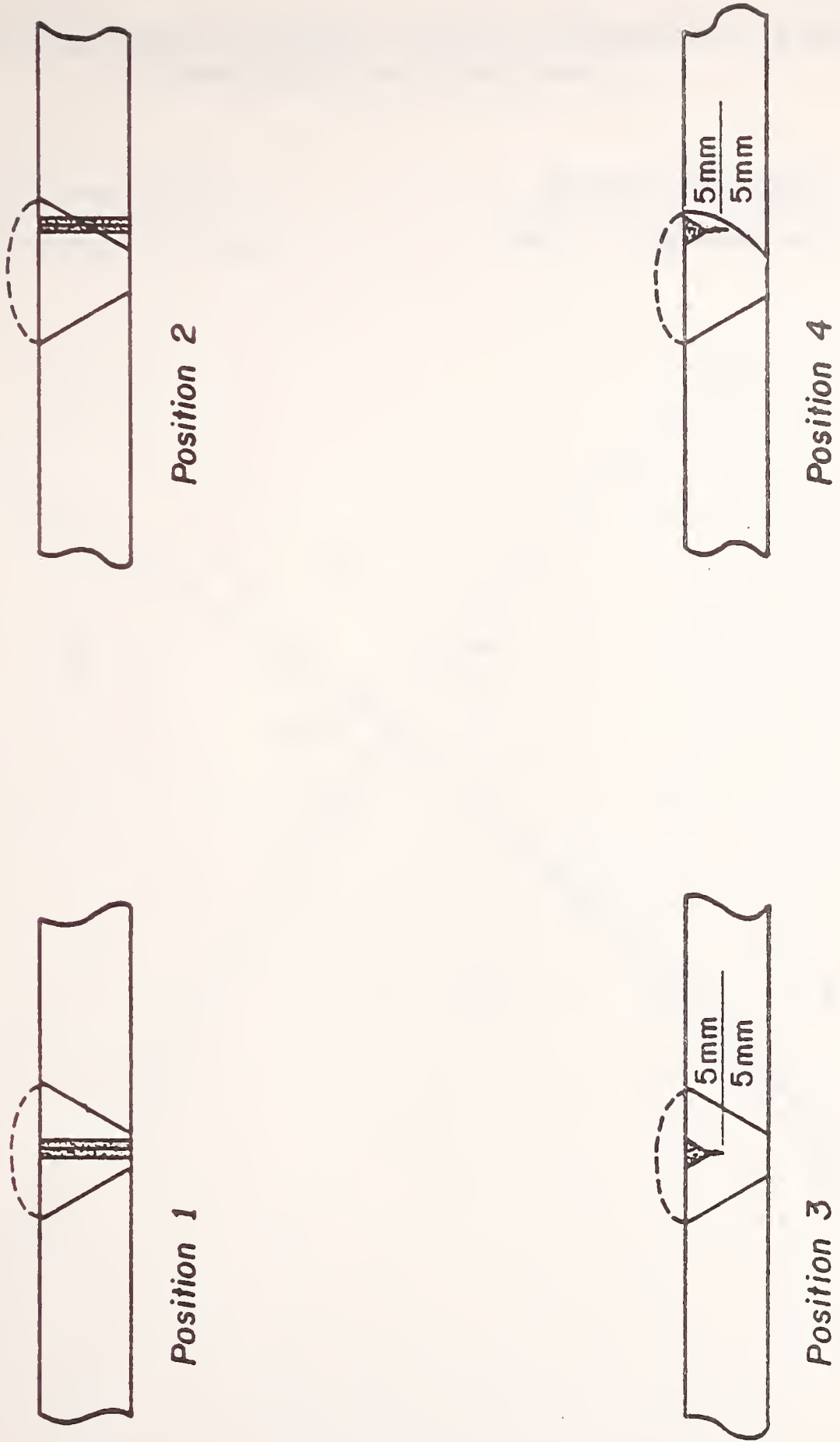


FIG. 36
RESULTS OF INSTRUMENTED IMPACT EVALUATION OF STANDARD CHARPY V-NOTCH
SAMPLES OF NOTCH ORIENTATION 1.

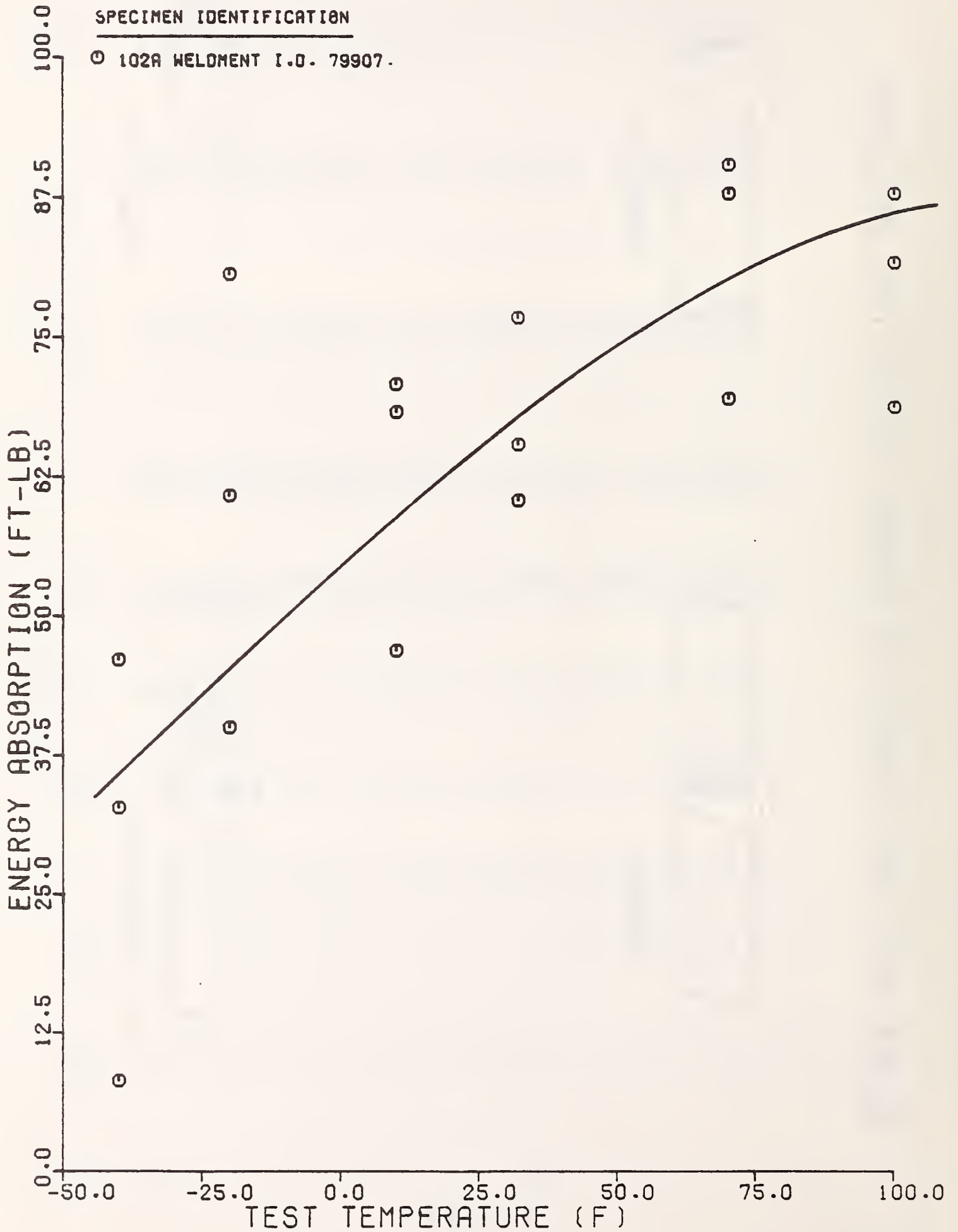


FIG. 37

RESULTS OF INSTRUMENTED IMPACT EVALUATION OF STANDARD CHARPY V-NOTCH
SAMPLES OF NOTCH ORIENTATION 1.

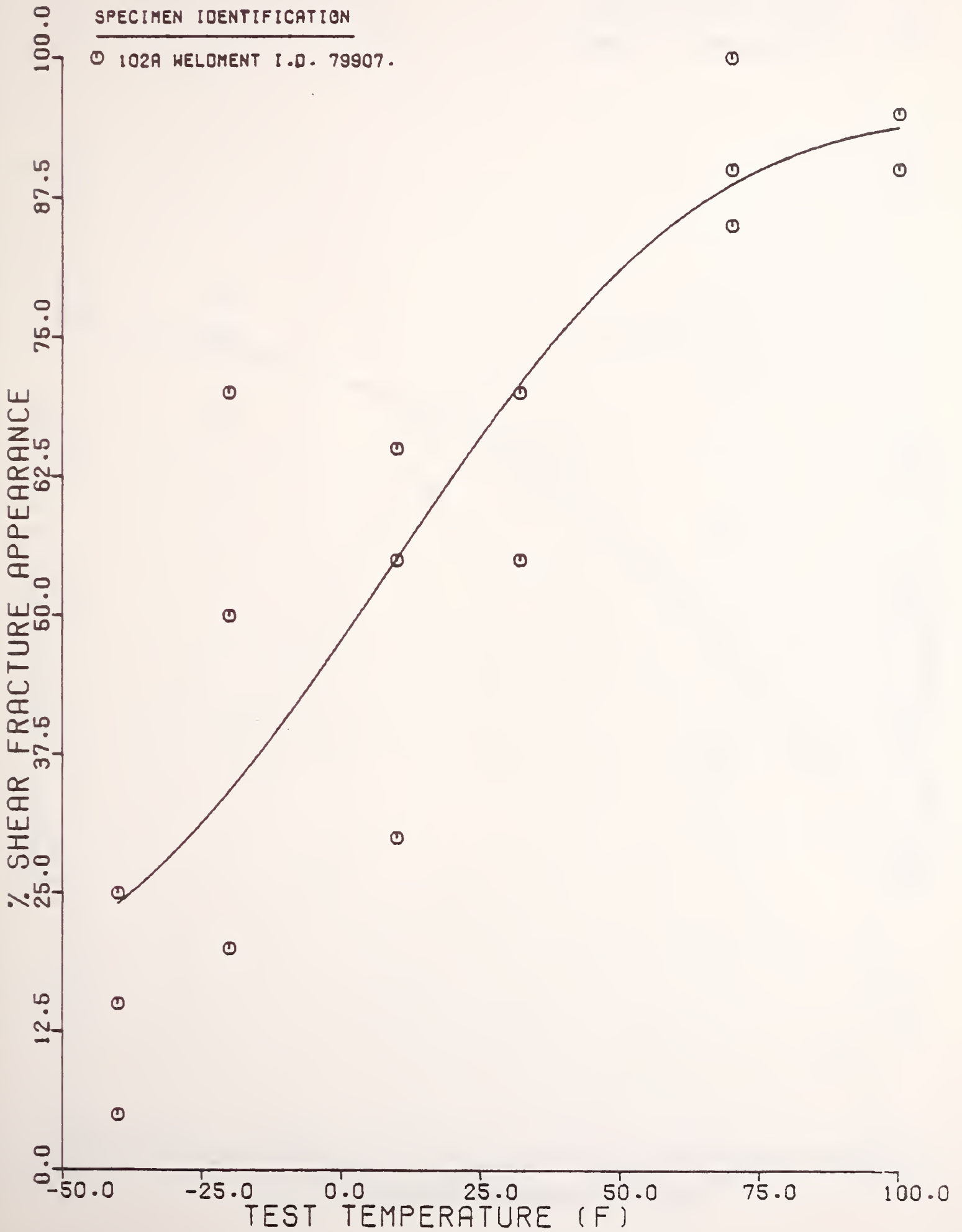


FIG. 38

RESULTS OF INSTRUMENTED IMPACT EVALUATION OF STANDARD CHARPY V-NOTCH SAMPLES OF NOTCH ORIENTATION 1.

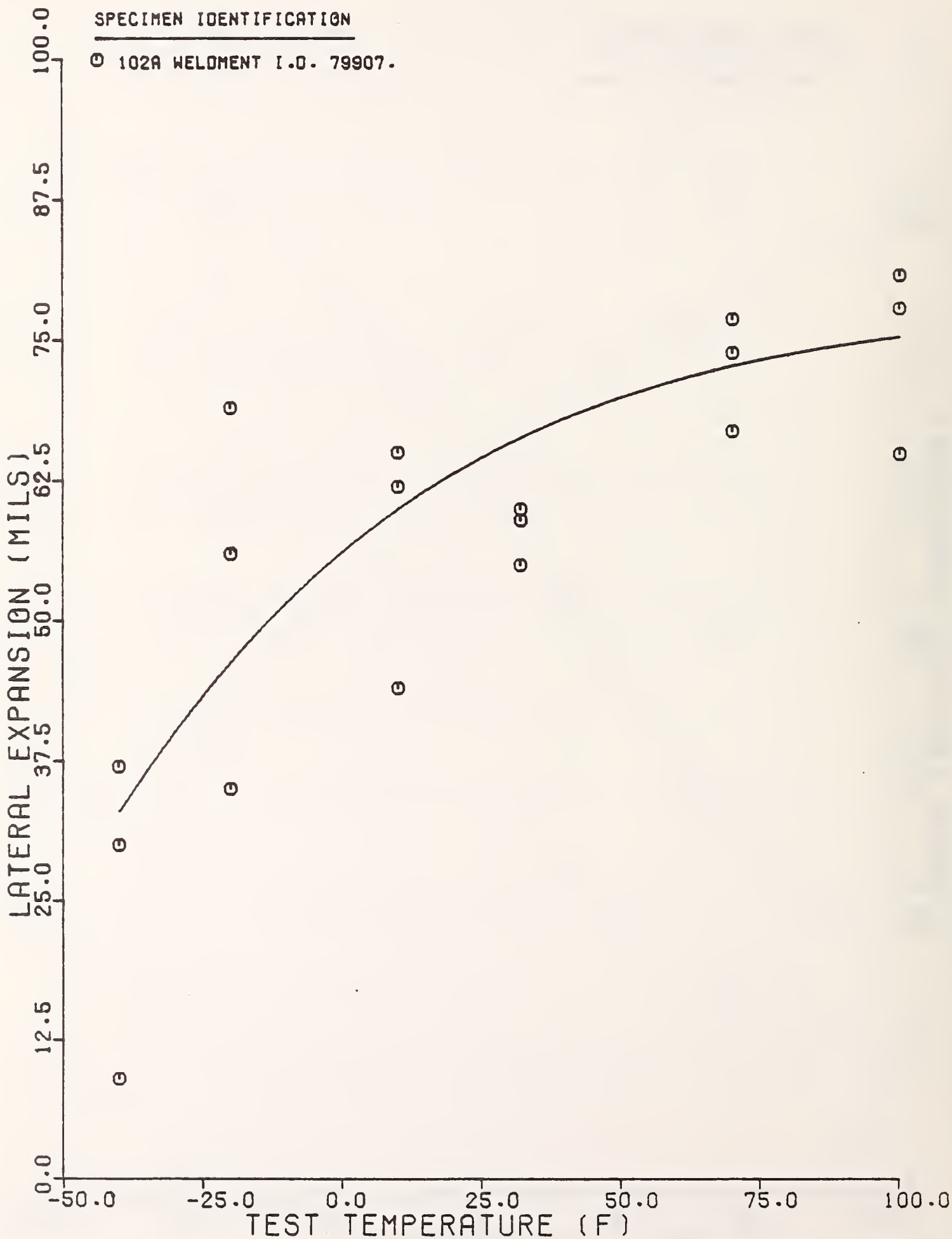
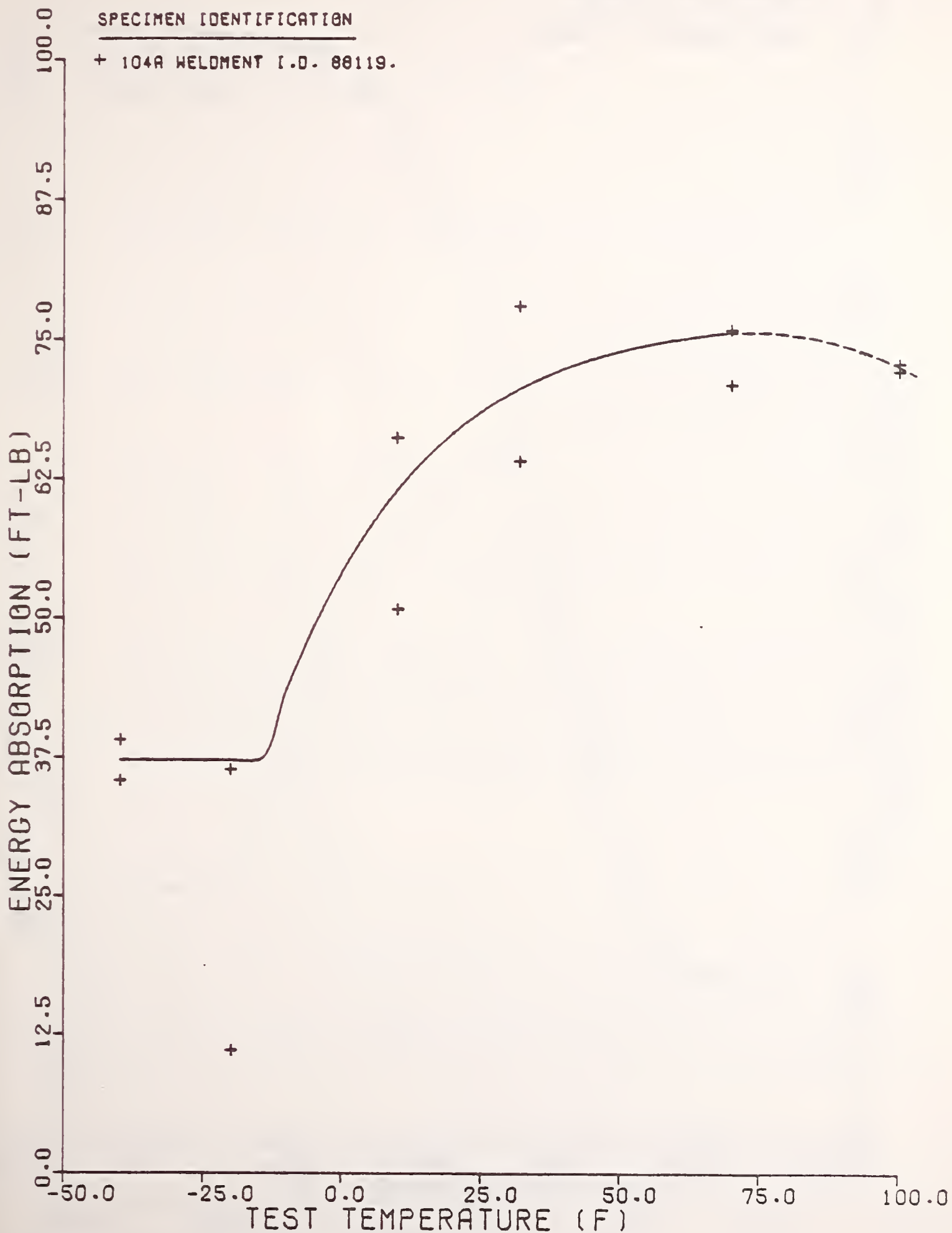


FIG.39 RESULTS OF INSTRUMENTED IMPACT EVALUATION OF STANDARD CHARPY V-NOTCH SAMPLES OF NOTCH ORIENTATION 1.



RESULTS OF INSTRUMENTED IMPACT EVALUATION OF STANDARD CHARPY V-NOTCH SAMPLES OF NOTCH ORIENTATION 1.

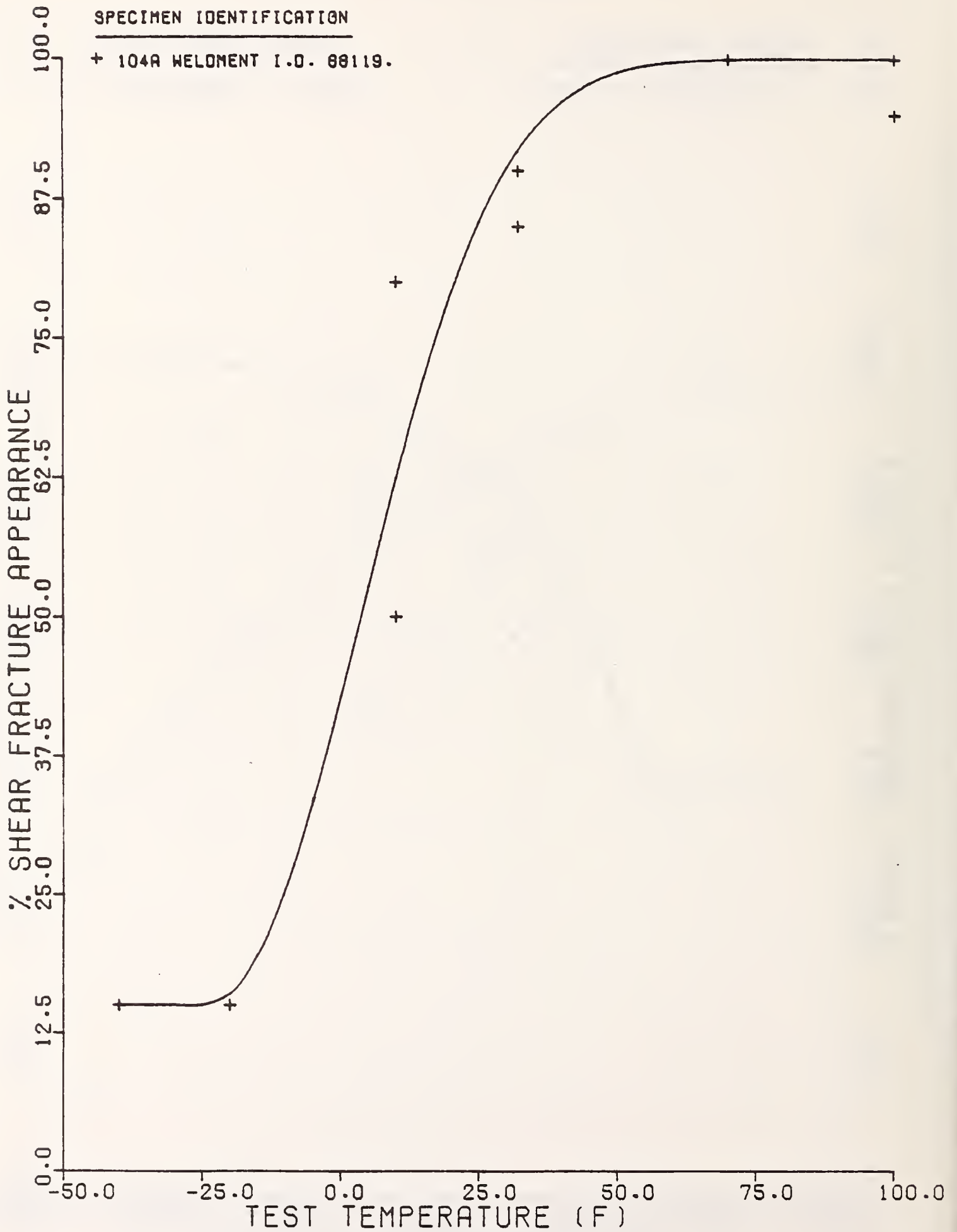
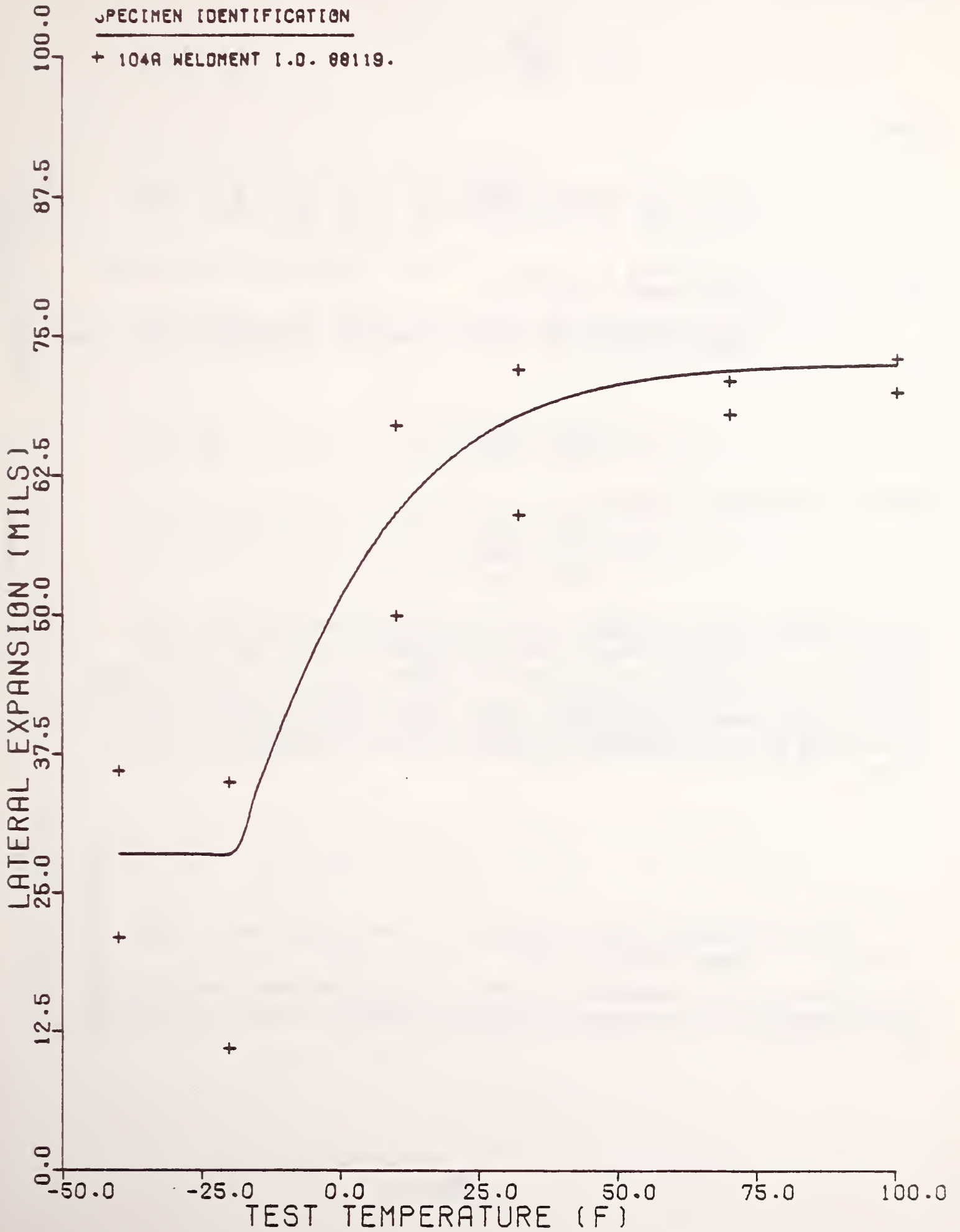


FIG. 41

RESULTS OF INSTRUMENTED IMPACT EVALUATION OF STANDARD CHARPY V-NOTCH
SAMPLES OF NOTCH ORIENTATION 1.



When fracture occurs after general yielding, the method for calculating a correct fracture toughness value has not yet been established. However, two approaches, the equivalent energy method² and the J-integral method³ are used to calculate dynamic fracture toughness after general yielding has occurred. For the equivalent energy method, the dynamic fracture toughness, K_d^* , is

$$K_d^* = \frac{6YP_M^*}{BW} (a)^{\frac{1}{2}} \quad (2)$$

where:

$$P_M^* = \left(\frac{E_m}{C_S} \right)^{\frac{1}{2}},$$

Y, B, W, and a are the same as in eq. (1); E_m is the maximum load energy; and C_S is the elastic sample compliance.

For the J-integral method, the dynamic fracture toughness is calculated as

$$K_{Jd} = (EJ_M)^{\frac{1}{2}} \quad (3)$$

where E is the elastic modulus and

$$J_M = \frac{2E_M}{B(W-a)}$$

The results for all precracked Charpy V-notch test specimens are shown in table 13. Values of dynamic fracture toughness calculated by the linear elastic procedure, K_{Id} , where applicable, or by both the equivalent energy, K_d^* , and J-integral method, K_{Jd} , are presented. In addition, the critical crack opening displacement (COD) value is calculated for each K_{Id} or K_{Jd} value by eq. (2), Section 3E, and by eq. (B-10), Appendix B, of this report.

²F. J. Witt, Equivalent Energy Procedures for Predicting Gross Plastic Fracture, USAEC Report ORNL-TM-3172.

³J. R. Rice, A Path Independent Integral and the Approximate Analysis of Strain Concentration by Notches and Cracks, Journal of Applied Mechanics, 35, 379 (1968).

Table 13. Results of Individual Instrumented Precracked Charpy-V-Notch Tests

Notch Orientation ¹	Test Temp. (°F)	Spec. No.	Fracture Toughness (ksi√in)			Cracking Opening Displacement (COO) (in)	
			K_{ID}	K_D^3	K_D^4	By Eqn. A ⁵	By Eqn. B ⁶
<u>Weld Procedure 102 A-1</u>							
2	10	813-2	---	91.7	93.2	.0028	.0022
		C04-2	---	106.7	107.3	.0036	.0029
		D33-2	---	119.5	120.8	.0045	.0036
	-20	B08-2	---	148.7	153.3	.0073	.0059
		C01-2	---	76.6	77.9	.0019	.0015
		C11-2	46.3	---	---	.0007	.0005
4	10	818-4	---	131.0	132.5	.0055	.0044
		C14-4	---	104.0	104.3	.0036	.0027
		C24-4	---	153.4	157.1	.0077	.0062
	-20	B24-4	---	107.4	110.2	.0038	.0030
		C05-4	---	91.4	91.7	.0026	.0021
		D14-1	---	202.9	202.1	.0127	.0102
3	100	B21-3	---	269.3	272.0	.0260	.0208
		D02-3	---	265.8	271.4	.0258	.0207
		D34-3	---	243.2	246.4	.0213	.0171
	68	B16-3	---	185.2	189.3	.0126	.0101
		D19-3	---	249.2	255.0	.0228	.0183
		D31-3	---	171.8	174.0	.0106	.0085
	32	B28-3	---	122.9	124.7	.0055	.0044
		C17-3	---	194.8	199.1	.0139	.0111
		D16-3	---	235.9	238.0	.0199	.0159
	10	B22-3	54.6	---	---	.0231	.0184
		B02-3	---	---	---	---	---
		B11-3	---	124.9	125.0	.0049	.0039
	-20	C27-3	---	143.3	146.1	.0066	.0053
		D08-3	---	241.2	242.8	.0184	.0147
		B07-3	---	72.9	73.7	.0017	.0014
	-40	C19-3	45.5	---	---	.0006	.0005
		D21-3	---	130.1	131.1	.0054	.0043
		B15-3	53.7	---	---	---	---
		D10-3	44.5	---	---	---	---
		D30-3	39.4	---	---	---	---

Table 13 (Continued)

Notch Orientation ¹	Test Temp. (°F)	Spec. No.	Fracture Toughness (ksi \sqrt{in})			Cracking Opening Displacement (COD) (in)	
			K _{Id} ²	K _D ³	K _{Jd} ⁴	By Eqn. A ⁵	By Eqn. B ⁶
<u>Weld Procedure 104A-1</u>							
2	10	A07-2	---	237.4	239.4	.0177	.0142
		A24-2	---	229.2	232.3	.0166	.0133
	-20	A13-2	---	275.1	279.7	.0241	.0193
		A11-2	---	234.4	233.2	.0168	.0134
4	10	A18-4	---	234.2	235.9	.0172	.0137
		A47-4	49.6	---	---	---	---
	-20	A36-4	---	210.2	209.7	.0136	.0109
		A50-4	---	173.2	173.2	.0093	.0074
3	100	A08-3	---	235.4	237.7	.0186	.0149
		A40-3	---	224.5	226.6	.0169	.0136
	68	A16-3	---	233.7	233.9	.0181	.0145
		A21-3	---	274.7	284.4	.0267	.0214
	10	A48-3	---	188.0	189.2	.0110	.0088
		A49-3	---	237.6	238.1	.0175	.0140
	-20	A44-3	---	160.5	163.3	.0082	.0066
		A40-3	47.6	---	---	.0007	.0006

¹See Figure 35 for details of notch orientation.

²K_{Id} - calculation based on linear elastic fracture mechanics analysis; applies when fracture occurs at maximum level, P_M , prior to general yielding.

³K_D⁴ - calculation based on equivalent energy method of analysis.

⁴K_{Jd} - calculation based on J-integral method of analysis.

⁵Equation A: $\delta_C = \frac{K^2}{1.6 \sigma_y E}$; σ_y = yield strength, E = elastic modulus; calculation based on eqs. (2) and (3) in Section 3E; K_{Jd} is used in the calculation; σ_y used is taken from results in Section 3D.

⁶Equation B: $\delta_C = \frac{K^2}{2.0 \sigma_y E}$; calculation based on most conservative estimate of COD, recommended by Beqley. Appendix B; K_{Jd} is used in the calculation.

⁷Not considered valid values by ERRI procedures, see Appendix Q.

Discussion

The results of the machined notched Charpy V-notch specimens show that weldments made with welding process 102A-1 may be slightly tougher than 104A-1 weldments. A comparison of the total energy absorbed for these two weldments is shown in figure 42. The other parameters measured in the Charpy V-notch test: percent shear fracture, lateral contraction, fracture initiation energy (E_M), and fracture propagation energy (E_P), also do not differ significantly between weldments made with process 102A-1 and weldments made with process 104A-1. These tests show that these weld metals have a minimum upper shelf Charpy V-notch energy of 65 ft-lb and that they reach this upper shelf value at approximately 100°F. These results are consistent with similar results obtained by the British Welding Institute and Cranfield Institute of Technology.

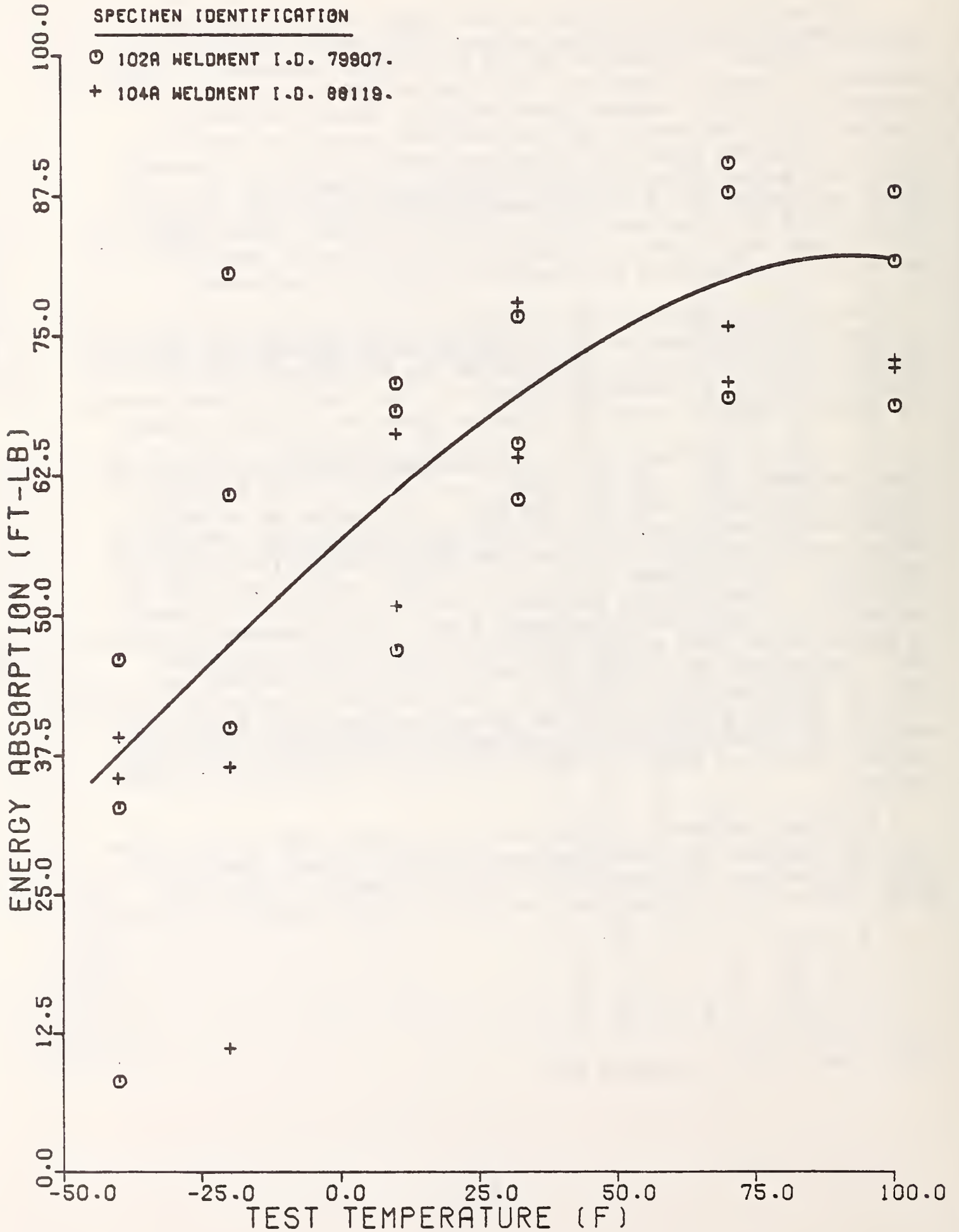
For the instrumented precracked Charpy V-notch tests, the calculation of stress-intensity based on the equivalent energy method (K_{d^*}) gives essentially the same result as the use of the J-integral method of calculation (K_{Jd}). A maximum difference of less than 4% is found between the stress-intensity values calculated by these two different methods.

For tests at 68°F and 100°F, weldments made by both the 102A-1 and 104A-1 processes had a variability of less than 50% in the fracture toughness measured on replicate specimens. This amount of variability in toughness is not unusual for weld metals as seen by the variation in Charpy V-notch energy and COD values measured by the British Welding Institute.⁴ At lower temperatures of 32°F, 10°F, -20°F, and -40°F, the variability in the fracture toughness measured on replicate specimens increases to a factor of approximately 2 to 1. This increased variability is because these tests are at a temperature range below the "upper shelf" temperature for the Charpy V-notch tests, and therefore, the fracture toughness results follow the usual pattern of increased variability when the tests are conducted in the transition temperature range. The variability of the fracture toughness was not affected by the welding process (102A-1 and 104A-1) or the orientation of the notch in the test specimen.

In general, weldments made with welding process 102A-1 had the same fracture toughness as weldments made with welding process 104A-1. At 10°F, for specimens with the notch oriented in position 2 (part weld metal, part HAZ), it appears that the 104A-1 process weldment may have a

⁴ Ref. [H-I], part 3, Appendix [H]

FIG. 42
 RESULTS OF INSTRUMENTED IMPACT EVALUATION OF STANDARD CHARPY V-NOTCH
 SAMPLES OF NOTCH ORIENTATION 1.



higher toughness than the 102A-1 process weldment, but the variability in the data at this temperature does not permit a proper assessment of this difference.

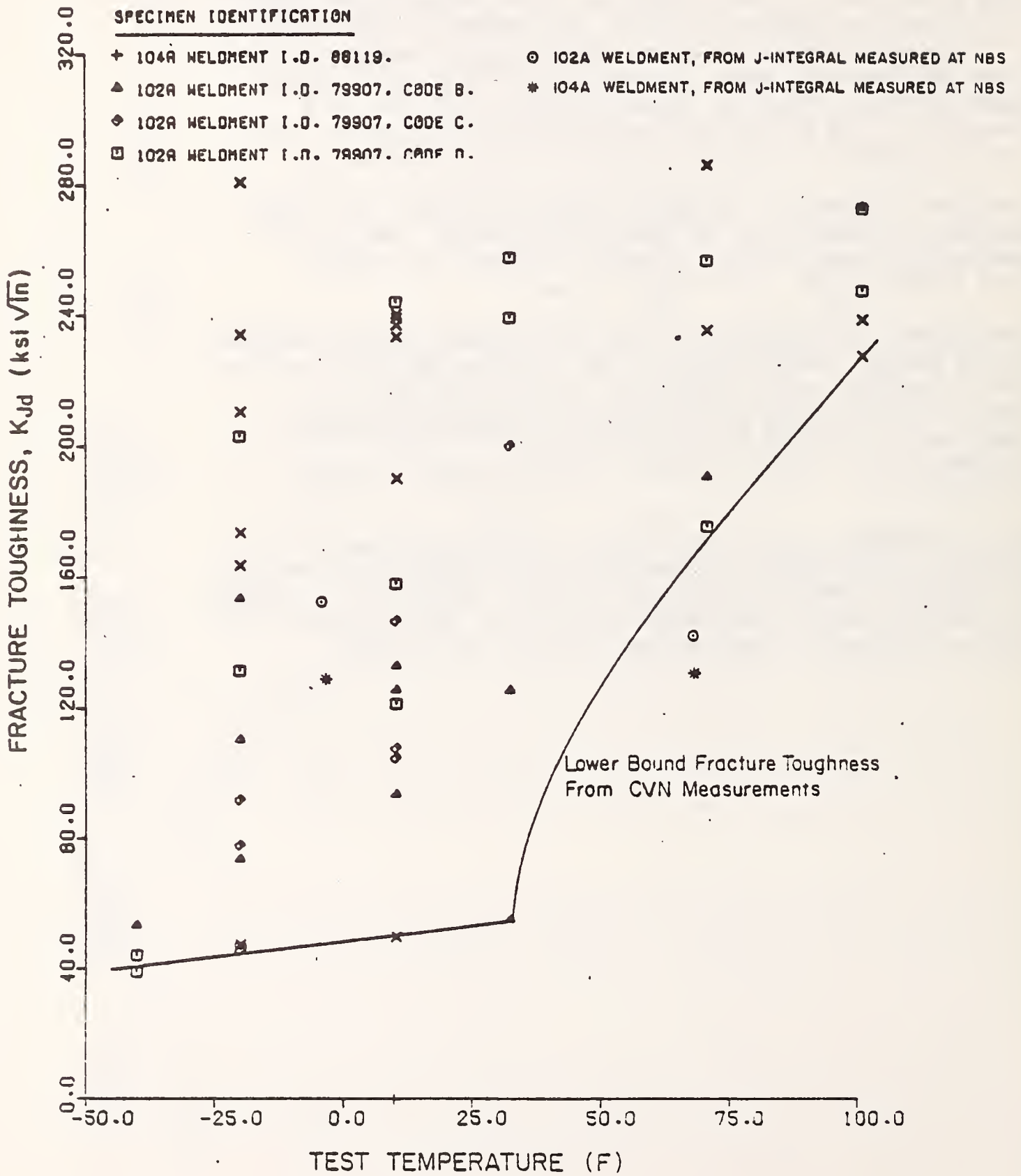
The effect of the anisotropy of the weld metal on the fracture toughness was assessed by comparing the toughness of specimens with notches oriented in positions 2, 3, and 4 at 10°F and -20°F. No measurable effect of the direction of crack propagation within the weld was found. However, if the fracture toughness at 68°F, measured with precracked specimens, is compared with the fracture toughness measured in J-integral tests (Section 3E), the weld metal is found to have a higher toughness in the through-thickness direction (notch orientation 3) than in a direction parallel to the axis of the weld (notch orientation 2). This effect is not as obvious for similar results at lower temperatures.

The fracture toughness for weldments made with process 102A-1 and 104A-1 decreases with temperature as shown in figure 4A. The fracture toughness value calculated by the J-integral procedure is shown in figure 4B and a lower bound limit curve is shown.

For convenience in comparing the fracture toughness results obtained from precracked Charpy V-notch tests with the fracture toughness results obtained with J-integral tests (Section 3E) and with COD tests, all results shown in Table 13 were converted to COD measurements using an analysis described in (Section 3E) and a second analysis described by Begley (Appendix B). These results will be discussed in greater detail in Section 6.

Additional parameters that are obtained from the instrumented precracked Charpy V-notch tests are the total energy to fracture, energy to initiate fracture, energy to propagate fracture, dynamic yield strength, and stress-intensity rate. These parameters are not reported here because they are not used in the fracture analysis for the pipe.

(Fig. 43) FRACTURE TOUGHNESS CALCULATED FROM PRECRACKED CVN SPECIMENS BY J-INTEGRAL ANALYSIS



3J. STRESS-CORROSION CRACKING TESTS

To evaluate the susceptibility to sustained load cracking in an aggressive environment, specimens of weldments made by both weld processes 102A-1 and 104A-1 were tested in a corrosive environment. The environment used was a solution of 0.004 wt. pct. of concentrated H_2SO_4 in distilled water with an applied current sufficient to produce a current density of 0.625 mA/in^2 . A cathode poison consisting of 2 grams of phosphorus in 40 ml of carbon disulfide was added in an amount of 5 drops per liter of test solution. This environment has been used extensively¹ to test the susceptibility of steel line pipe to sustained load cracking and was chosen to represent the most likely "worst case" environment that a pipe will experience. A similar environment was used for fatigue tests (Section 3F).

Test specimens approximately $\frac{1}{2}$ in. x $\frac{1}{2}$ in. by 10 inches long were prepared from sections of weldments made by processes 102A-1 and 104A-1. A notch, similar to that used in Charpy V-notch specimens, was put in the weld metal in the notch orientation position 3 (fig.35) so that cracking would occur in a through-the-wall-thickness direction to simulate a leak in the pipe wall. These specimens were precracked by fatiguing and were then loaded in three-point-bending in the test environment. Tests were conducted at 100°F which is the highest temperature at which the cathode poison was soluble in the test solution. The testing procedure consisted of breaking one specimen of each weldment in air, obtaining a load versus deflection curve for this specimen to failure, and calculating the stress-intensity and net section stress at failure from the maximum load sustained in this test. Additional test specimens were then loaded to various stress levels below that required to cause failure in air, and this load was maintained on the specimen in the test environment for time periods up to 450 hours. At the termination of the tests in the environment, the specimens were cooled in liquid nitrogen, fractured in air, and examined at 50X magnification under a microscope to determine if any sustained load cracking had occurred.

The results of these tests are summarized in Table 14. No evidence of sustained load cracking was found in these tests. Since the applied stress and the stress-intensity used in these tests is well above the maximum levels expected in the pipeline, it is concluded from these tests that crack growth due to an aggressive environment is not likely to be a problem in the Trans-Alaskan Pipeline.

¹T. P. Groeneveld and A. R. Elsea, Hydrogen Embrittlement Testing, ASTM SPP543 (1972).

Table 14. Results of Sustained Load Testing in Agressive Environment

Weld Process	Environment	Time to Failure	Stress-Intensity ² ksi $\sqrt{\text{in}}$, K_I	Net Section ³ Stress, σ_N , ksi
102A-1	air	0	121	209
	cathodic ¹ charging	230*	73	112
104A-1	air	0	78	138
	cathodic charging	456*	59	106
	cathodic charging	431*	58	94
	cathodic charging	431*	56	99

*Test terminated at these times.

¹See text for composition.

² $K_I = \frac{3PS}{2BW^2} \sqrt{\pi a} f(a/w)$; $f(a/W)$ given by G.C. Sih in "Stress-Intensity Factors Handbook."

³ $\sigma_N = \frac{3PS}{2B(W-a)^2}$, P-load, S-span, B-specimen thickness, W-specimen width, and a-crack length.

4A. DESCRIPTION OF ROCKWELL INTERNATIONAL METHOD OF WELD DEFECT MEASUREMENT

Introduction

The procedures used to determine the dimensions of defects in trans-Alaska pipeline girth welds were developed by Mr. Wayne D. Stump and Mr. John L. Summers of the Rocky Flats Plant, Atomics International Div., Rockwell International Corp. The methods were originally employed to determine the depth of defects in welds for nuclear applications. Determinations were made at Alyeska facilities in Alaska. All determinations were witnessed by NBS - Boulder personnel to confirm that no change in measurement procedure occurred.

Arc Burns

The length and the width of arc burns were measured directly from radiographs using either a ruler or a low-magnification eye-piece with a calibrated reticle. Orientation of the defect relative to the girth weld was traced on translucent paper placed over the burn area and retained as a part of the documentation.

Planar and Non-planar Weld Defects

The depth (see fig. 45) of an internal defect within the weld metal was estimated by comparing the radiographic density[†] of the defect to that of the adjacent non-defective weld metal. Density differences were converted to depths using comparison standards. These standards were radiographic-density step wedges reflecting density differences that would be produced on radiographs of Alyeska-type welds. The density differences corresponded to defects ranging in depth from 0.254 to 2.54 mm (0.010 to 0.100 in.). The depth increments in the wedge were 0.254 mm (0.010 in.). Calibration standards were prepared by radiographing a standard step wedge machined from pipeline steel. This standard wedge was nominally as thick as the weld, i.e., plate thickness plus 3.1 mm (0.125 in.). The standard was radiographed at 225 kVp using the film and lead screens reported to be used for the original Alyeska radiography. The standard radiographs were then reproduced on a clear background to facilitate measurement. The comparison standard is placed adjacent to the defect image on the radiograph and moved until a match is obtained between the density of the defect and that on one of the density steps of the standard. Between steps, visual interpolation is used.

[†] Photographic density is a quantitative measure of film darkening defined by the equation $D = \log (I_0/I_1)$ where D is the density, I_0 is the light intensity incident on the film and I_1 is the light intensity transmitted through the film.

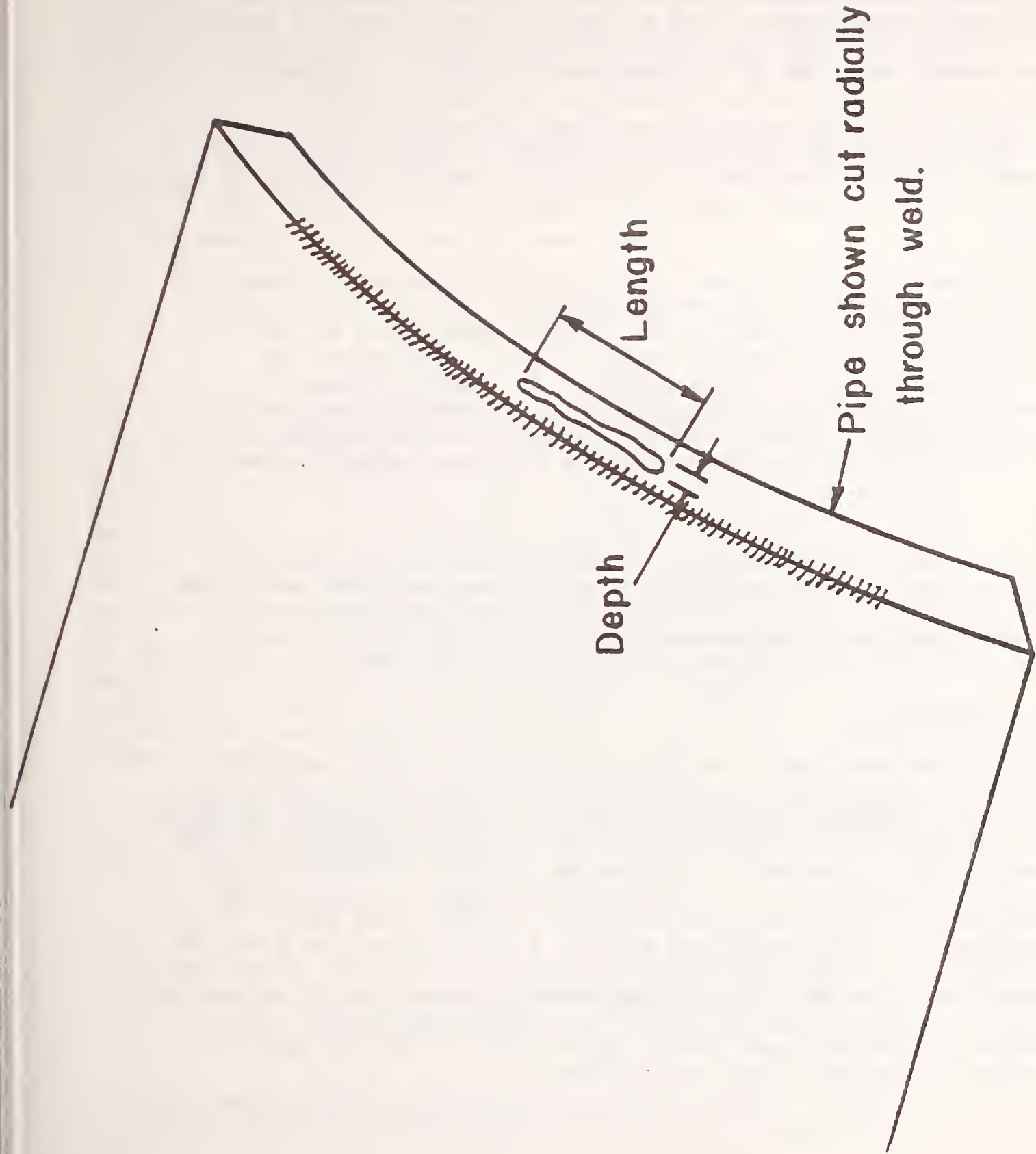


Fig. 45. Orientation of weld defects

The undulating surface of the weld metal causes significant variations in radiographic density along the radiograph. Therefore, it is necessary to select a reference standard having a base radiographic density (density obtained for the full thickness step of the wedge) near the density adjacent to the defect. In the present study, density adjacent to a defect was measured by a microdensitometer, and a reference standard having a base density ± 0.25 units of the desired density was selected. Defect depth was independently estimated by two technicians. Results in reasonable agreement, within 0.102-0.127 mm (0.004-0.005 in.), were averaged. Significant discrepancies suggest a complicated defect (multiple superimposed defects, wormhole porosity, etc.) requiring further study. Five to fifteen minutes were required to characterize a defect, depending on its complexity. Demands on eyes necessitated frequent rest periods for the technicians.

This technique is applicable for determining the maximum thickness of a defect as projected on the radiographic film. For defects lying at an angle to the incident radiation, the resulting measurement will be substantially less than the overall defect height. Correlation with overall defect height will be reasonably good for incomplete penetration, elongated slag, gas pockets, spherical and cluster porosity, and for hollow beads. Height correlation will be only fair for isolated slag and is likely to be very poor for incomplete fusion and wormhole porosity.

Records

All data were recorded in ink in a bound laboratory data book, which was dated and initialed by both technicians. In rare cases the technicians concluded that defects identified as arc burns by Alyeska were actually defects requiring a depth measurement (e.g., incomplete fusion). The depth was measured and the discrepancy documented.

Accuracy Assessment

The bias and precision of the Rockwell International (RI) method of measuring defect depth were evaluated by applying the method to radiographs of seven control specimens. These specimens were sections of pipeline welds containing a series of flat-bottomed holes and slots of known depth milled into the underside of the weld. NBS - Boulder produced test sections from welds in 1.17 cm (0.462 in.) thick pipe and from welds in 1.43 cm (0.562 in.) thick pipe, all flush-ground on the bottom side to facilitate hole or slot depth measurement. NBS - Washington produced a test section from a weld in 1.17 mm (0.462 in.) thick pipe, leaving the bottom side intact. Actual depths were determined by the NBS precision measurements laboratories in Boulder and Washington. The uneven underside of the NBS - Washington section required a high-side and a low-side depth reading for each hole. The hole depth was taken to be the average of these two readings.

The artificial defects were distributed both laterally and longitudinally along the welds as illustrated in Fig. 46. Depth measurements were made by RI personnel, J. L. Summers and W. D. Stump, using the apparatus and standards assembled for use on the Alyeska radiographs. Depths of the defects were unknown to the technicians before testing; however, information on the radiographic procedures was provided.

The measured defect depth is compared to known defect depth in Table 15. Deviations from the true depths are given in Table 15 and plotted versus true depth in Fig. 47.

The equation chosen to best represent the data is

$$D_m = D_t - 0.0028 D_t^2 \quad (1)$$

where D_m is depth measured by the RI technique and D_t is the true depth. The constant 0.0028 was chosen by a least-squares fit. Deviations of the D_m values from the fitted curve have a standard deviation of 3 mils for true depths of 30 mils or less; this standard deviation increases with depth, reaching 10 mils at $D_t = 80$ mils. Furthermore, since the slope of the curve relating D_m to D_t deviates appreciably from unity for large depths, differences in D_t produce even larger differences in D_m . As a result approximate "two-sigma" uncertainty limits for a predicted true depth are ± 7 mils for measured depths less than about 30 mils; ± 14 mils for $D_m = 35$ mils; ± 18 mils for $D_m = 50$ mils; and ± 36 mils for $D_m = 60$ mils. For measured depths between these values, the higher estimate of standard deviation is conservative; for measured depths greater than 60, no information is available. There was no significant effect on either bias or imprecision due to type of defect (hole or slot), plate thickness, or source of specimen.

The curve of D_m vs. D_t is shown in Fig. 48. This curve can be entered on the vertical scale using a value of D_m ; the corresponding estimate of D_t is read from the horizontal scale.

It is possible also to approximate the curve of Fig. 48 with a polynomial in D_m ; e.g.

$$D_t(\text{corr}) = .95 D_m + .0052 D_m^2$$

This equation gives the corrected depth accurate to within 1 mil for D_m up to 60 mils; there are no data to support extrapolation beyond this value.

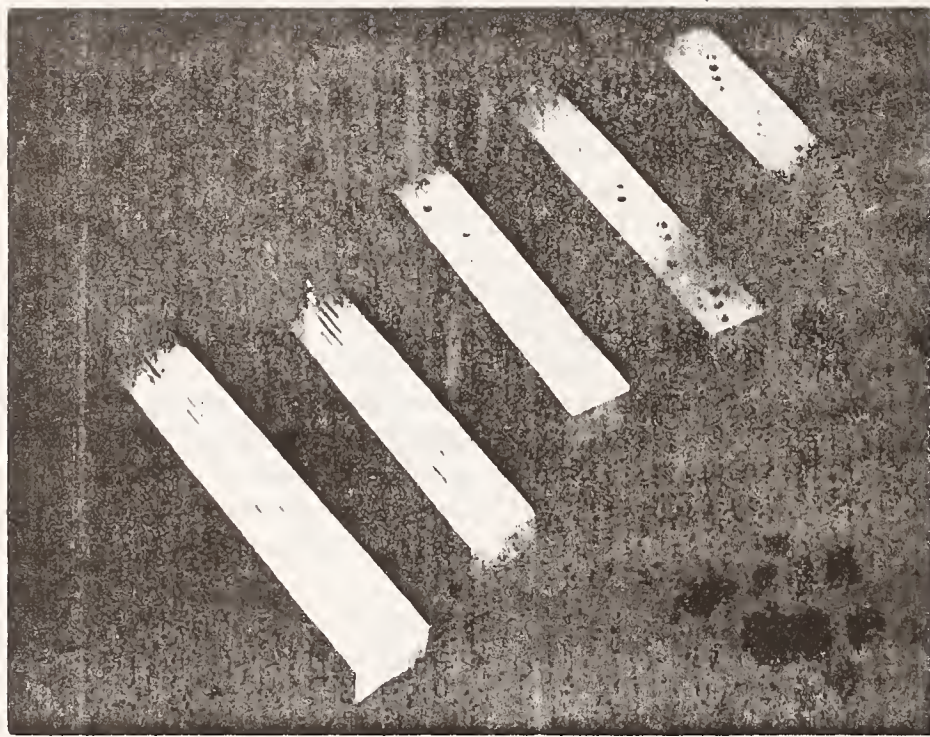


Fig. 46. Specimens used to determine the bias and inaccuracy of the Rockwell International method of measuring defect depth.

Table 15. Results of radiographic determinations of defect depth on standard specimens; all entries in units of 0.0254 mm = 10⁻³ in; Δ = D_{true} - D_{meas.}

Specimen	D _{true}	D _{meas.}	Δ	Specimen	D _{true}	D _{meas.}	Δ
NBS, Boulder:				NBS, Boulder:			
0.462-in weld;	20.2	18	2.2	0.562-in weld;	55.8	48	7.8
1/32-in wide slots.	56.0	38	18.0	1/8-in dia. holes.	15.0	12	3.0
	12.5	15	-2.5		81.0	63	18.0
	21.2	20	1.2		12.0	10	2.0
	15.5	18	-2.5		81.4	63	18.4
	39.0	36	3.0		12.5	13	-0.5
	21.0	20	1.0		38.2	28	10.2
	38.2	43	-4.8		54.2	35	19.2
	55.6	45	10.6		79.3	63	16.3
	81.9	65	16.9		18.2	13	5.2
	39.5	43	-3.5		55.5	45	10.5
	56.4	38	18.4		11.4	9	2.4
	40.5	33	7.5		19.5	20	-0.5
	14.3	10	4.3		15.5	18	-2.5
	81.5	50	30.1		37.5	35	2.5
	13.7	10	-3.2		19.5	20	-0.5
	81.5	50	31.5		37.5	38	-0.5
	20.5	15	5.5		55.5	50	5.5
	56.0	53	3.0		80.0	70	10.0
	80.0	>60	—		37.5	40	-2.5
NBS, Boulder:				NBS, Washington:			
0.562-in weld;	80.7	60	20.7	0.462-in weld;	15.5	21	-5.5
1/32-in wide slots.	20	18	2.0	1/16-in, 1/4-in	23.7	19	4.7
	56.5	38	18.5	diam. holes.	9.8	10	-0.2
	12.1	15	-2.9		40.8	33	7.8
	19.6	20	-0.4		17.5	16	1.5
	15.5	18	-2.5		4.3	<5	---
	38.8	36	2.8		36.5	32	4.5
	19.5	20	-0.5		26.3	23	3.3
	38.0	43	-5.0		30.4	30	0.4
	55	45	10.0		50.2	45	5.2
	80	65	15.0		30.1	33	-2.9
	38.5	43	-4.5		25.5	25	0.5
	55.8	38	17.8		13.8	12	1.8
	38.8	33	5.8		58.9	53	5.9
	12.5	10	2.5		40.0	36	4.0
	80.4	50	30.4		6.0	--	---
	12.7	10	-2.7		72.5	63	9.5
	80.9	50	30.9		38.8	43	-4.2
	20.5	15	5.5		19.4	25	-5.6
	55.0	53	2.0		81.5	73	8.5
					71.4	45	32.4
NBS, Boulder:				Rockwell (Rocky Flats):			
0.462-in weld;	19.0	15	4.0	0.462-in base metal.	54.6	52	2.6
1/8-in diam. holes.	55.5	37	18.5		6.8	9	-2.2
	12.3	15	2.7		32.6	30	2.6
	18.4	18	0.4		19.8	22	-2.2
	11.5	11	0.5		58.8	56	2.9
	38.0	35	3.0		12.9	15	-2.1
	18.5	20	-1.5		49.0	45	4.0
	38.0	40	-2.0				
	55.3	50	5.3				
	38.7	36	2.7				
	54.5	50	4.5				
	38.0	38	0.0				
	12.0	10	2.0				
	81.7	75	6.7				
	11.5	10	1.5				
	80.0	85	-5.0				
	18.3	13	5.3				
	55.3	50	5.3				
	80.2	58	22.2				
	80.7	58	22.7				

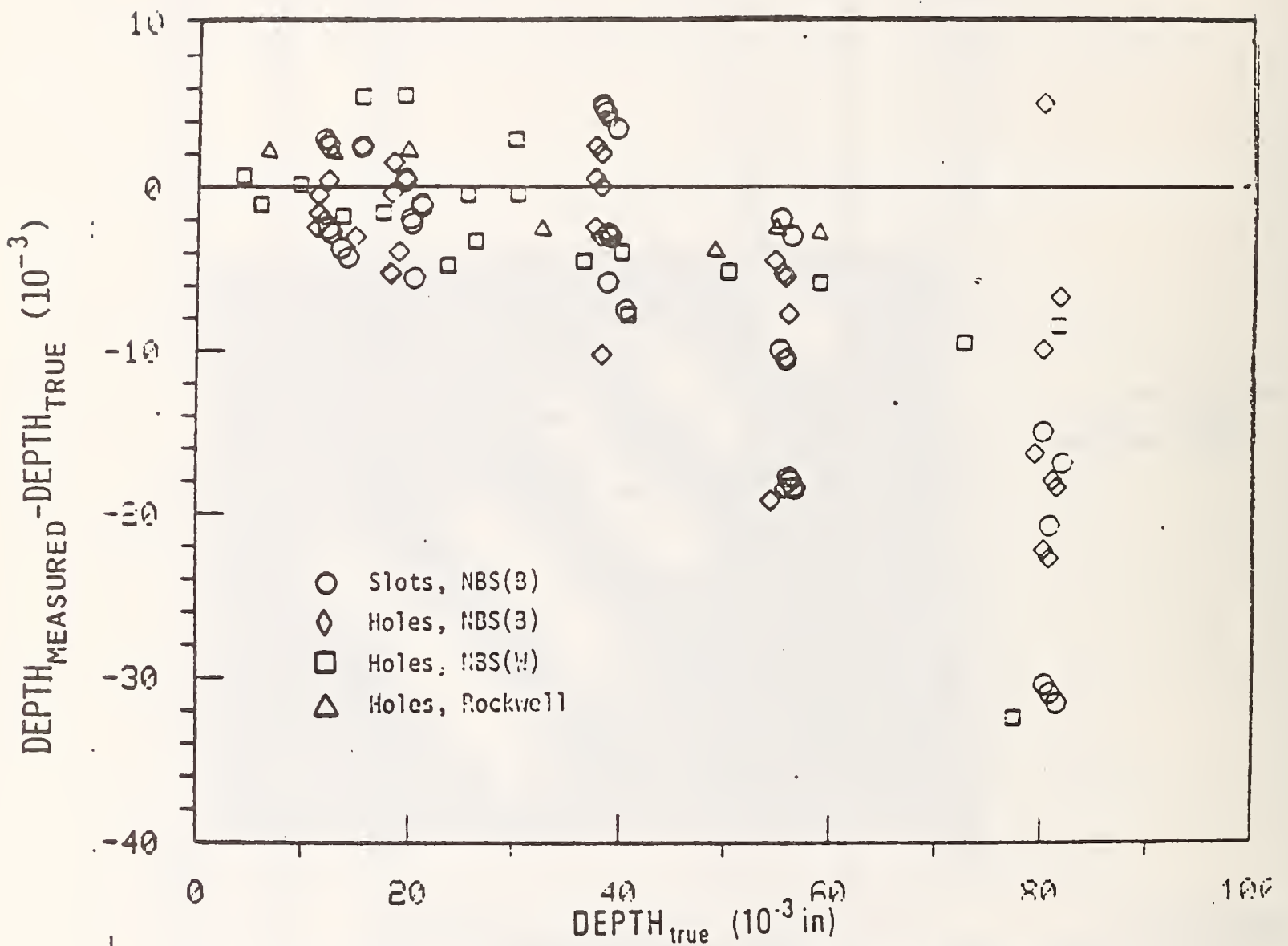


Fig. 47. Deviations of RI radiographic defect-depth measurements from true depths. Defects were produced by machining weld segments from trans-Alaska pipeline.

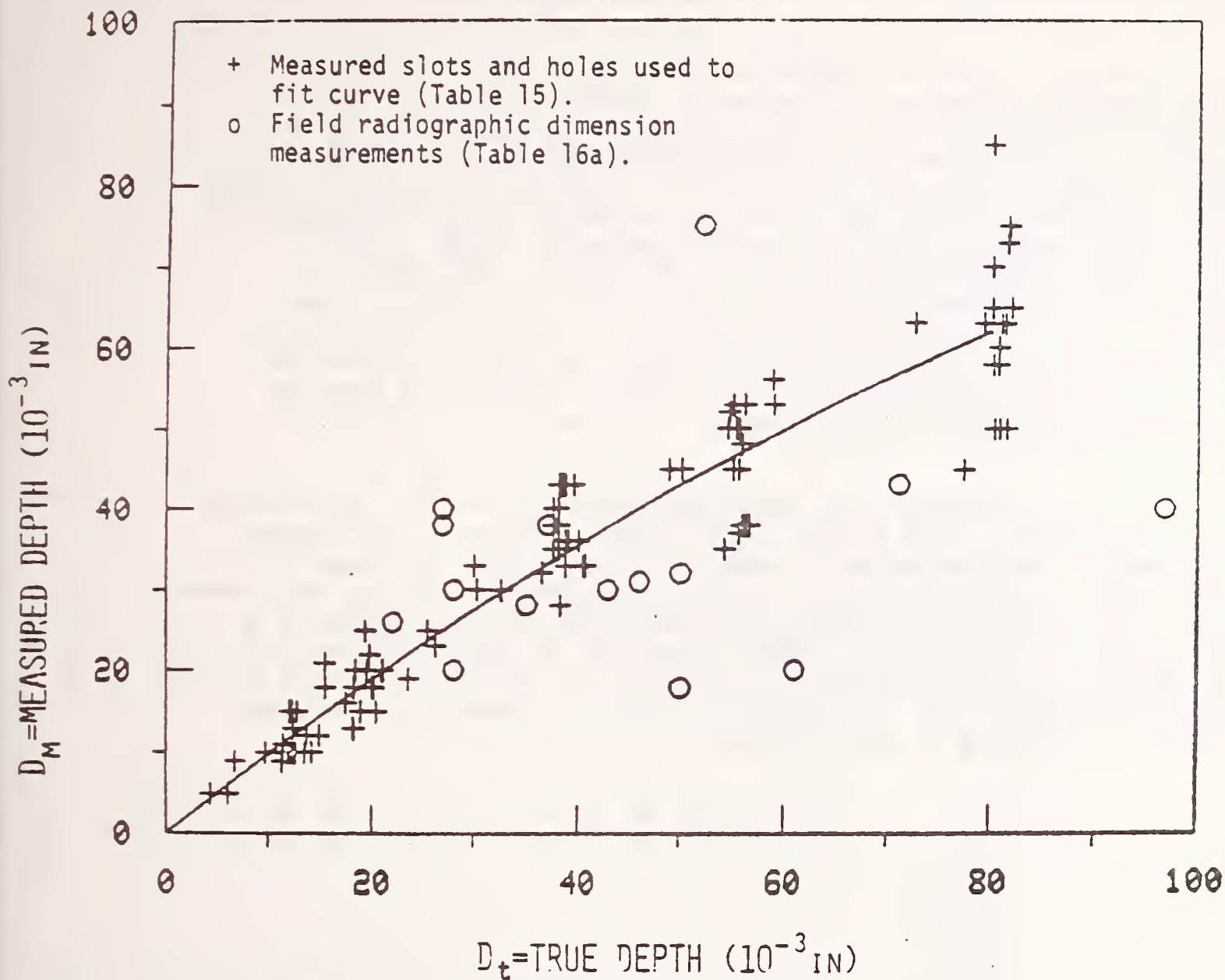


Fig. 48. Bias curve derived from the RI radiographic defect depth experiment based on laboratory radiographs. Additional data from depth measurements of material defects (Table 16a) are plotted as circles.

The above curve and uncertainty limits apply only to the type of defects actually considered in the above well-controlled experiment. However, it is felt that these results can be safely applied to many kinds of defects met in problems. The major exception to this would be those subject to orientation problems as noted above. The depths of such defects are likely to be underestimated by the RI technique, even with the bias correction. The uncertainty for such measurements may well be larger than stated above.

The ability of the RI method to measure the overall height of natural defects appearing in a series of Alyeska radiographs was also evaluated. As discussed previously, any method of converting defect contrast into defect depth will underestimate the overall height of a defect inclined to the axis of radiation. A series of 15 natural defects were identified in six of the Alyeska radiographic films associated with girth welds supplied to NBS for fracture mechanics study. The RI interpreters estimated the depths of these defects. NBS identified sections of the weldments containing the defects and a 0.5 in. long segment of the weld containing each defect was removed. Each segment was ground flat and was radiographed parallel to the axis of the weld to show the defect in profile. Overall defect heights were measured directly from the radiographs using a calibrated filar eyepiece and low-power microscope.

Data from this experiment are summarized in Table 16a. The information has also been added to Fig. 48, plotted as circles. As expected, the RI method underestimates the overall defect height. Although no correlation is observed between apparent film contrast, ΔD , and measurement error, the spread of film contrast values (Table 16A) was generally in the normal, predicted range. After correction for bias according to Fig. 48 and Table 15, the measured values had an estimated relative standard deviation of about 47%. This natural defect experiment gives an added degree of confidence in the RI method.

Table 16A. Measurements of Natural Weld Defects as Confirmed by Laboratory Radiography

Alaska Radiograph #	Projected Defect Height in. *	RI Measured Depth	Difference	% of Difference	Defect Type	Penetra- meter Thickness	Film Density and Contrast**		
							D ₁	D ₂	D ₁ -D ₂
88070	0.071	0.043	0.028	-39	ES	12	2.77	2.00	0.77
(30-110)									
88070	0.052	0.075	0.023	+44	GP	12	2.77	2.00	0.77
(30-110)									
79907	0.027	0.040	0.013	+48	HB	15	3.49	2.35	1.14
(110-0-34)									
79907	0.035	0.028	0.007	-20	HB	15	3.49	2.35	1.14
(110-0-34)									
79907	0.028	0.030	0.002	+7	ES	15	3.49	2.35	1.14
(110-0-34)									
75061	0.050	0.018	0.032	-64	HB	15	3.92	2.89	1.03
(110-0)									
88503R	0.043	0.030	0.013	-30	ES	12	2.98	1.92	1.06
(135-150-22)									
88503R	0.028	0.020	0.008	-28	ES	12	2.98	1.92	1.06
(135-150-22)									
88503R	0.097	0.040	0.057	-60	HB	12	2.98	1.92	1.06
(135-150-22)									
88503R	0.027	0.038	0.011	+41	IF	12	2.98	1.92	1.06
(135-150-22)									
88503	0.046	0.031	0.015	-32	HI-Lo	12	2.61	1.78	0.83
(21-98)									
88503	0.050	0.032	0.018	-36	ES	12	2.61	1.78	0.83
(21-98)									
88503	0.037	0.038	0.001	+3	HB	12	2.61	1.78	0.83
(21-98)									
88503	0.022	0.026	0.004	+18	HB	12	2.61	1.78	0.83
(21-98)									
88503	0.061	0.020	0.041	-67	HI-Lo	12	2.56	1.43	1.13
(100-150-20)									

ES - elongated slag
 GP - gas pocket
 HB - hollow bead
 IF - incomplete fusion

() - indicates the station numbers
 * Was determined by using a filar eye piece and a 0.66X objective in a microscope; calibration of 1 filar unit = 9x10 to the -3 millimeters.

** See Section 4B for a discussion of film density and 4C for a discussion of contrast.

4B. DESCRIPTION OF THE SOUTHWEST RESEARCH INSTITUTE METHOD OF WELD DEFECT DETERMINATION

The Southwest Research Institute (SWRI) method of measuring weld defect dimensions was reviewed in a visit to SWRI on August 16, 1976. Discussions were held primarily with Mr. Sam Wenk. Mr. Wenk discussed the methods used by SWRI to determine defect dimensions. For the length and width indications, a plastic scale was used for the measurement. Wenk felt that, in most cases (as in slag or porosity, for example), these dimensional measurements could be made to an accuracy 0.010 inch. For a planar defect, such as lack of fusion, these dimensions become somewhat more difficult.

For the through-wall dimension measurement, a series of radiographic density measurements or an estimate of density difference as compared to the density difference for the radiographic penetrameter and shim are used. For defects covering an area large enough for a densitometer measurement (densitometer aperture is 1 mm dia.), a formula is used to determine the through-wall reduction (R) (see Fig. 49):

$$R = -T \left\{ \frac{\log\left(\frac{D_4}{D_3}\right)}{\log\left(\frac{D_2}{D_1}\right)} \right\}$$

- where T = thickness of penetrameter and shim;
- D₁ = radiographic density in area under the pipe wall;
- D₂ = density under the penetrameter, shim and wall;
- D₃ = density in the weld area near the defect; and
- D₄ = density in the defect area.

This equation is derived in Appendix L. The derivation of this equation is based on the assumption of narrow beam (non-scatter) conditions. The accuracy of the equation for the assessment of defect depth cannot be determined without a careful investigation of scatter effects.

Since returning from Alaska in July, SWRI personnel have radiographed several steel calibration samples in an attempt to confirm their dimension measurements. These calibrations originally resulted in a uniform correction factor in which 0.025 in. would be added to all SWRI densitometer-determined depth measurements. Present estimates by SWRI are that their depth values are low by varying amounts. Based on recent X-ray calibration tests with the API 1104 grooved plates, SWRI* has informed NBS that they now estimate the depth readings obtained using the above formula are low by 50% for internal surface defects such as incomplete penetration and by 10% for other defect types. They believe the internal defect measurement should be increased by 50% up to a maximum of 0.025 in. correction. No defect densitometer readings (on actual field weld radiographs) were taken for defect widths (or diameters) less than 0.040 in. since the aperture effect was recognized (see Section 4C).

* Telephone conversation October 5, 1976 between E. Ruescher (SWRI) and H. Berger (NBS).

LOCATION of DENSITY MEASUREMENTS MADE by SWRI

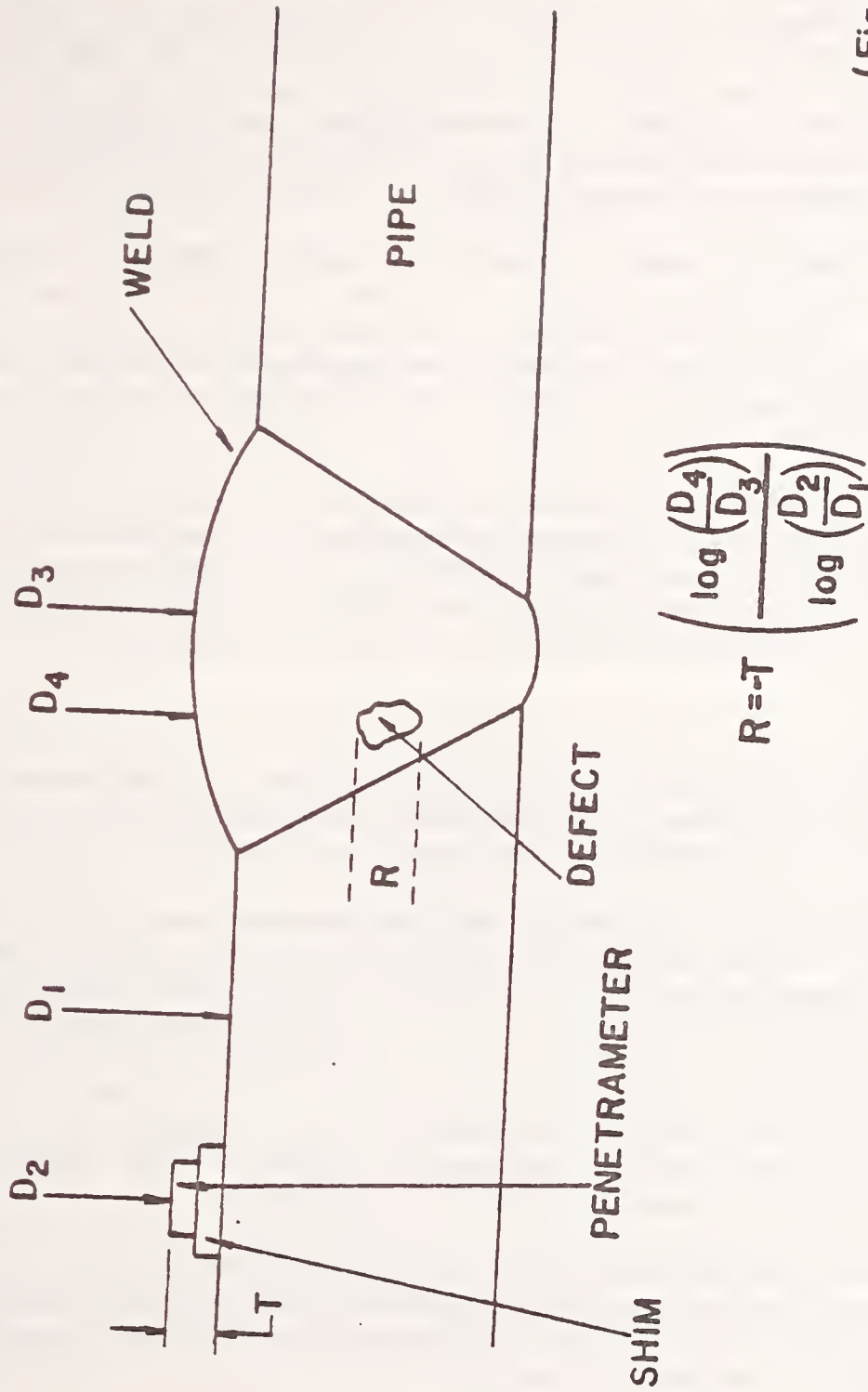


(Fig. 49)

Fig. 49. Schematic: Diagram for Film Density Measurements

There were many defects (an estimated 75%) which were too small for accurate densitometer measurements using the 1 mm aperture. In these cases, an estimate of the change in density was made by a visual comparison with the density change observed for the penetrometer and shim. The accuracy of these so-called eyeball measurements is undeterminable as the methods obviously depend on the individual observer.

Discussions with Mr. Wenk covered some of the problems with regard to these through-wall dimension measurements. Film processing is a variable that is presently not controlled. The film type also varies. The pipe wall thickness itself varies (specifications permit wall variations from -5% to +10%): according to Mr. Wenk, most of the pipe wall runs about 5% high. All these factors introduce difficulties in interpreting the density differences. The density measurement (where it can be done) is also difficult.

Mr. Wenk indicated that SWRI had used this density difference approach (using actual densitometer measurements) in several previous nuclear problems with fair results. In one case, the technique was used to determine wall thickness; the radiographic measurements correlated with other measurements to within 12.5%. This case was not complicated by large thickness changes as is the weld situation.

In considering the SWRI method, it is important to note that the comparisons were always made with the penetrometer-shim image--for both the methods used by SWRI. Therefore, assuming a constant shim-penetrometer thickness, this technique would be less sensitive to changes in film gradient (changes described in Section 4C) than the method used by RI.

Accuracy Assessment

An error estimate for the SWRI visual method will not be given. For the densitometer method, an approach to an accuracy assessment is to consider the possible variations in the density measurements used in the formula for R.

The logarithmic ratio of numerator and denominator produces a large sensitivity to small changes in density and in particular to the densities referring to the defect (D_3 and D_4). Empirically determined or published data lead to estimates for the variability of R. The values of D_1 and D_2 should be capable of being determined to an accuracy of ± 0.03 density units since they are measured over a relatively large area of reasonably uniform density. Density D_3 , which can vary due to weld bead thickness changes has been established by experimental tests of the 3 weld radiographs available for our tests; in these tests the variation did not exceed ± 0.225 density units.

Two methods were used to determine this D_3 variation. The first was a direct scan of several radiographs along the weld bead using a precision micro-densitometer. The other was a calculation of the direct density change by means of the simple equation¹ (neglecting scatter):

$$\Delta D = \frac{\mu_{\text{eff}} G \Delta X}{2.3}$$

¹ R. Halmshaw, "Physics of Industrial Radiology," Heywood Books, London (1966).

Where: μ_{eff} = effective linear attenuation coefficient for the X-ray beam,
G = film gradient (slope of density vs. log relative exposure curve) obtained from published sensitometry data,
 ΔX = change in thickness of the sample traversed by the X-ray beam (i. e. weld peak to weld valley difference).

This equation is derived in Appendix L.

The possible change in D_4 was determined empirically by scanning a known size defect on a radiograph with a precision scanning densitometer and comparing this to a similar measurement with a densitometer of the type and aperture size used by SWRI. The accuracy in D_4 was estimated in this way as about ± 0.05 density units for defect sizes 1.25 or larger times the aperture diameter.

These possible variations in density readings were used in the formula for R to estimate upper values of the determination of R. Two estimates have been made. In what might be called a typical case, D_1 and D_2 have been allowed to vary by 0.03 density units, D_3 by 0.2 and D_4 by 0.05 density units, in each case so as to increase the value of R. Values determined by these typical possible density variations are compared to calculated R values in Table 16b. Also in the table are estimated likely maximum R situations in which variations are 0.05 for D_1 and D_2 , 0.225 for D_3 and 0.1 for D_4 . These calculations of R are only estimates as to possible variations.

Even these estimates of density measurement inaccuracy may be too small particularly for defects that are tear-shaped or sharp and crack-like. In these cases, the measurement of the D_4 with an aperture size of 1 mm would be very difficult, the measurement would normally be much lower than the peak value. Therefore, these estimated R values given in Table 16b are generally useful only for round or flat bottomed defects having a projected area on the film of about 0.050 in. or greater in diameter or width. This might include defects such as gas holes, spherical porosity, and slag. Defects such as incomplete penetration are likely to be too narrow for measurement. Defects such as hollow bead may be tear-shaped. Therefore, care should be exercised in interpreting the values in Table 16b.

An evaluation of the uncertainty of values of R can be made from an approximate statistical analysis of the density readings. Although density varies from film to film, the difference $D_1 - D_2$ should be self-correcting with respect to variability due to film-to-film differences. Using the differences $D_1 - D_2$, the standard deviation of a density reading is estimated to be 0.12 density units. (In addition to errors in density measurements, this may also include variability due to radiography variables such as X-ray energy, film processing, scatter, etc.). Notice that it is larger than the "typical" value of 0.03.

If it is assumed that errors in the four density readings are uncorrelated, a standard propagation-of-error calculation indicates that the relative standard deviation of R is approximately 85%.

In this discussion of the SWRI method it has been assumed that the thickness (t) of the shim-penetrator combination is known. Shim variations, considered as one possibility for film contrast variations discussed in Section 4C, will also have a bearing on the accuracy of the SWRI method.

Table 16b. Film Density Data and R Calculations

Weld Number	Weld Station	Film Densities				Calculated Values* of R		
		D1	D2	D3	D4	R(SWRI)	Typical Case R	Likely Maximum Case R
W8TRX	0	3.80	2.70	3.47	3.65	16.43	42.49	51.76
W15TRX	43	3.83	2.71	2.77	3.12	37.15	69.29	80.79
	55	3.83	2.71	3.67	3.78	9.22	32.60	40.84
	100	3.83	2.71	4.29	4.36	5.05	24.88	31.85
W16TRX	40	4.16	3.02	3.77	3.86	7.96	32.41	40.98
	70	4.16	3.02	3.96	4.11	12.54	36.02	44.32
W23TRX	45	2.90	2.00	2.71	2.80	9.50	39.62	50.62
75477		3.47	2.53	3.39	3.75	35.46	65.74	77.16
75986		3.46	2.64	3.53	3.62	10.33	43.08	55.36
76332		3.67	2.90	3.68	3.79	13.88	50.36	64.31
80856		2.81	1.95	3.01	3.11	9.93	38.40	48.95
81289R	71	3.10	2.21	3.09	3.39	30.39	61.35	73.07
81312	3 1/2	3.18	2.26	3.35	3.58	21.58	49.37	59.73
81324	65	3.24	2.28	3.24	3.59	32.40	60.77	71.38
81142	49	3.11	1.87	2.93	3.13	14.41	35.06	42.24
	67	2.44	1.86	2.40	2.44	6.76	56.55	76.81
81146	28	2.98	1.91	2.40	2.44	4.12	32.79	42.83
81148	79	3.22	2.33	2.93	3.18	28.09	61.95	74.64
	80	3.20	2.33	3.17	3.23	6.56	37.35	48.65
	93	3.25	2.33	3.00	3.46	47.58	80.73	93.40
	98	3.35	2.33	3.35	3.50	13.39	38.88	48.06
	126	2.90	1.93	2.90	3.12	19.93	46.71	56.51
	130	3.07	1.93	3.07	3.16	6.91	28.31	35.80
	144	2.99	1.93	2.87	3.19	26.80	52.10	61.27
81153	48	3.10	2.61	2.62	2.81	45.17	122.88	158.02
81209	129	3.42	2.26	2.87	2.95	7.37	32.97	41.87
81258	47	2.59	1.77	2.43	2.71	31.80	67.20	80.74
81287	147	2.73	1.86	2.51	2.83	34.71	68.63	81.48

Table 16b. Continued

81299	2	2.63	1.87	2.46	2.73	33.89	33.89	73.29	PA.57
81300	76	3.01	2.06	2.39	2.89	55.60	55.60	92.15	105.87
81301	115	2.87	2.06	2.11	2.71	83.77	83.77	133.26	152.79
81307	14 7/8	3.02	2.15	2.28	2.37	12.65	12.65	53.19	60.03
81311	59	2.99	2.07	2.67	2.75	8.91	8.91	40.55	52.03
81316	50	2.81	1.91	2.56	3.17	61.45	61.45	95.87	100.21
81319	2-14	2.86	1.99	2.15	2.21	8.42	8.42	48.57	63.20
81332	50 1/2	3.25	2.24	2.76	2.97	21.87	32.87	52.47	63.52
81338R	23	2.87	1.86	2.21	2.43	24.29	24.29	57.27	69.11
81397	110	2.49	1.76	1.76	1.95	32.80	32.80	96.74	107.52
81407	17	2.98	2.05	+	+	+	+		
81424		3.17	2.08	2.89	3.08	16.77	16.77	42.30	51.34
81430		2.92	2.03	2.92	3.06	14.30	14.30	43.93	50.89
81434R	32	2.91	1.74	2.38	2.45	6.26	6.26	31.23	30.87
81441	74	3.36	2.15	3.04	3.16	9.63	9.63	32.09	30.88
81442	75	3.16	2.42	3.16	3.34	23.05	23.05	61.47	76.49
	79	3.29	2.42	3.29	3.47	19.25	19.25	50.63	62.39
	97	3.43	2.42	2.83	3.16	35.10	35.10	67.51	79.38
81443	50	2.91	2.09	2.91	3.06	16.86	16.86	49.88	62.34
	58	3.00	2.09	3.00	3.13	13.03	13.03	41.90	52.50
81444		3.14	2.18	+	+	+	+		
81447	57	3.07	2.03	2.40	2.75	36.53	36.53	68.79	80.46
81550	141-144	3.09	2.05	3.09	3.23	11.99	11.99	36.40	45.13
81577	125	2.92	2.07	2.38	2.50	15.87	15.87	54.49	60.79
81586R	81	3.39	2.49	3.39	3.79	40.13	40.13	71.56	83.62
81628	40	3.95	2.88	2.78	2.98	24.41	24.41	59.90	72.54
81643	7-16	3.37	2.60	2.58	2.72	22.61	22.61	70.48	80.74
81670	70	3.07	2.10	2.56	2.72	17.72	17.72	49.98	61.65
81674		2.99	1.60	2.19	2.26	5.59	5.59	27.74	35.20
81701	75	3.21	1.91	3.00	3.09	6.32	6.32	25.74	32.39
81710	58	3.38	2.44	2.89	3.51	64.41	64.41	99.31	112.76
90001	C-3	3.87	3.08	3.89	4.02	15.98	15.98	51.60	65.20
90008R	71	3.96	3.23	4.07	4.21	18.42	18.42	57.02	72.13
W25TRX	76	3.20	2.22	1.74	2.03	45.53	45.53	94.70	112.31
W39TRX	81	3.60	2.53	2.28	2.38	13.14	13.14	50.51	63.61

*Depth values given in thousandths of an inch. See text for conditions for calculations.

+Values of D₃ and D₄ were unreadable on available reader sheet copies.

4C. CRITIQUE OF RADIOGRAPHIC DEFECT SIZE MEASUREMENT METHODS

The assessment of defect sizes from radiographs of the girth welds on the Trans-Alaska Oil Pipeline depends ultimately on two factors:

- (a) the judgment and experience of the radiographic interpreter, and
- (b) the relationship of radiographic film density changes to pipeline steel thickness.

Both factors are complicated by the varying film density due to steel thickness variations introduced by the weld bead.

The radiographic procedure in most cases involves the insertion of the x-ray source into and centered in the pipe and aligned as nearly as possible in the plane of the girth weld. The 70 mm film, lead screens, and steel penetrometer with shim to simulate the weld bead thickness used in the Alyeska procedure¹ are placed on the outer circumference of the weld joint. Two or more strips of film are used on each weld. An overlap of film is used to assure complete coverage. Processing of the exposed film is generally done in a Kodak Model M-7 automatic film processor, modified to reduce the speed of the film transport through the processor. However, our information is that some radiographs from the field radiography work were hand processed.

Two independent teams and techniques were used to assess the weld defect sizes considered in the waiver request. As described in this report, those teams and measurements are referred to as Southwest Research Institute (SWRI) and Rockwell International, Rocky Flats (RI)² (see preceding Sections 4A and 4B).

It should be pointed out that the evaluation of the pipeline field radiography is based on information supplied to NBS by the evaluating teams previously mentioned, the Alyeska radiographic procedure¹, and telephone conversations with the Radiographic Services Division of the Alyeska Pipeline Service Company. The original Alyeska radiographs have not been critically examined by the NBS evaluation team, nor have the defects listed on the waiver request been checked independently by this group. Nevertheless, all information indicates that the radiographs were of good quality.

A list of weld defect locations on the girth weld is given in Appendix A. Defect sizes as evaluated by SWRI and RI are given in Section 8.

-
1. "Radiographic Examination of Pipe Welds," Alyeska Specification 82.1.
 2. J. Landolt, W. Stump, and J. Summers, "Radiographic Determination of Defect Thickness", Sept. 1976, to be published.

The two major radiographic factors indicated above are evaluated in greater detail in the following sections.

Judgment

Both sets of film readers, from SWRI and RI have appreciable radiographic interpretation experience. Visual experiments indicate that experienced observers provide consistent, but not necessarily accurate results³. With the limited number of observers in this case, there is no obvious way to assess the accuracy of the visual measurements as concerned with the Alyeska field radiographs. One would need to make use of more observers and destructive tests on defect weld specimens to define the accuracy as it applies to field radiographs.

It is known⁴ from visual tests that an observer looking at a small high contrast target, such as the radiographic image of a small area but relatively deep wormhole porosity image, would tend to underestimate the greyness relative to that for a larger or lower contrast target. Therefore, large density differences from defects of larger depths would tend to be underestimated by this visual comparison. On the other hand, another factor in the visual comparison method used by SWRI is that the penetrameter shim image, of good sharpness because those objects are on the film side of the pipe, would tend to be visually regarded as of higher contrast than it is. The reader would then tend to overestimate the depth of the defect being examined. The degree to which these factors compensate each other is not known.

The eye has a much better capability for matching two shades of grey adjacent to each other⁵, as used in the RI method of defect measurement. The finer steps in grey-scale used in the RI method also lead to a better visual comparison. Although the error of the RI method as compared to laboratory specimens radiographed under well-controlled conditions has been assessed in Section 4A, the error of the RI method and other visual comparisons as applied to less controlled radiographs is another matter. In the field case, the poorer control between radiographic film density and variations in pipe wall thickness will lead to greater complications in the assessment.

There is also the matter of the film density value itself. For total densities greater than about 4, the accuracy of a densitometer measurement is in question. Some of the measured film densities in the weld area exceed this value. In addition, limitations on available illuminators make it

3. R. S. Woodworth and H. Schlossberg, "Experimental Psychology, "Henry Holt and Co., New York, NY (1960) pg. 746.

4. O. Bryngdahl, J. Opt. Soc. Am. 56, 811 (1966).

5. R. N. Evans, "An Introduction to Color", John Wiley and Sons, Inc., New York, NY (1948) pg. 128.

difficult for an observer to see density changes in this range. Therefore, visual measurements also can be influenced by high film densities.

Relationship Between Film Density and Changes in Steel Thickness

The analytical material which follows relates to Eastman-Kodak Type AA X-ray film. It is our understanding that about 85% of the girth welds were radiographed with AA film; therefore, our efforts were concentrated on that film. The particular film related to any given weld radiograph under consideration for waiver should be determined. If it is AA film, our analysis should be valid. Other comparable speed x-ray films are expected to be similar; however such cases should be treated on an individual basis.

Table 17 lists all of the variables that affect film contrast. One of the variables in relating film density to changes in steel thickness is the effective x-ray energy which is related to tube voltage*. It is our understanding that this is not routinely logged in a field environment so it is unknown in the case of the field weld radiographs. The radiographic procedure¹ permits x-ray equipment with a range of tube voltage from 140 to 300 kVp. From data supplied by Alyeska, it appears that field radiographs were taken over the x-ray tube voltage range of 190 to 240 kVp, with the most likely range being from 190 to 225 kVp.

At the lower voltages, the subject contrast will be greater, thereby producing a relatively larger change in film density for the same defect depth dimension. Figure 50 presents typical curves for inspection of steel at the two extremes of the likely tube voltage range, 190 and 225 kVp. As an example, a defect depth of 0.060 in. will yield a change in density (ΔD) of 0.53 density units for 190 kV versus a ΔD of 0.45 for an x-ray energy of 225 kVp. The slopes of the two curves are 8.81 for 190 kVp and 7.52 for 225 kVp. This represents about a 15% change in slope.

A second variable concerns the linearity of the log film density versus metal thickness plot. This linearity aspect is discussed in the report of consultant R. C. McMaster in the Appendix K. McMaster examined the linearity of this plot as a means of determining the change in metal thickness due to a defect. Note the graphical derivation of the SWRI equation in Fig. K-10 of the McMaster report (Appendix K).

Published Kodak data (Fig. 51) shows significant departures from linearity at higher densities. These data show the departure of linearity for densities greater than 3[†]; many of the Alyeska films measured show densities above this value and even higher than 4. Therefore, this

*Tube filtration used by Alyeska radiographers is of little importance in this discussion.

[†]Kodak data is for a net density of 3.0, etc. The total density including background, etc., would be about 3.2.

Table 17

POSSIBLE X-RADIOGRAPHY VARIABLES

1. X-RAY VOLTAGE
2. PROCESSING
3. SHIM THICKNESS CHANGE
4. FILM TYPE
5. PIPE WALL THICKNESS
6. LEAD SCREENS AND CONTACT
7. SCATTERING EFFECTS
8. SOURCE POSITION
9. FILM TEMPERATURE DURING AND AFTER EXPOSURE.

FILM DENSITY vs. STEEL THICKNESS
FOR TWO DIFFERENT KILOVOLTAGES
USING MODIFIED M-7 PROCESSOR
(COURTESY EASTMAN KODAK CO.)

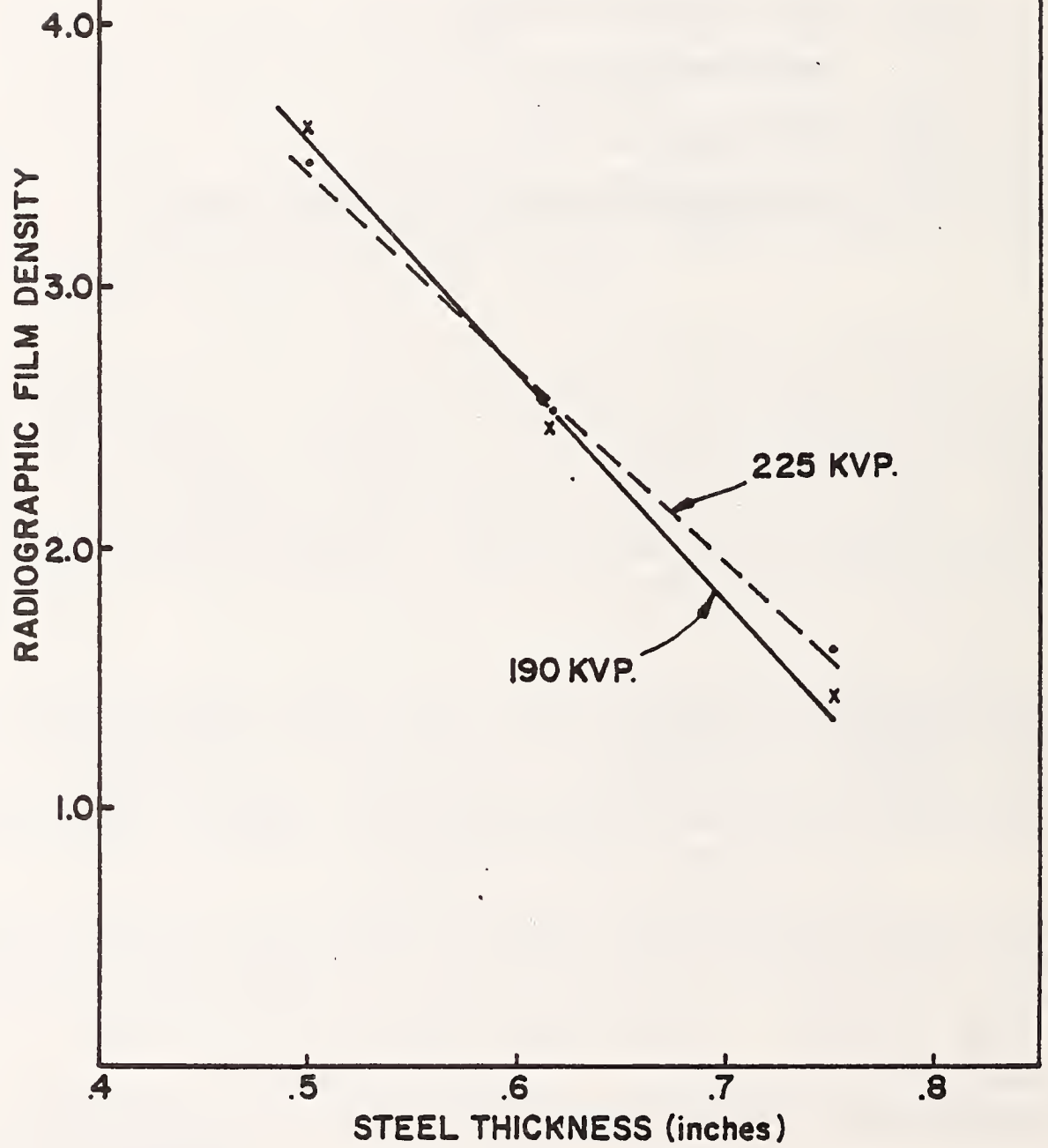


Fig. 50. Film Density vs. Steel Thickness (in.)

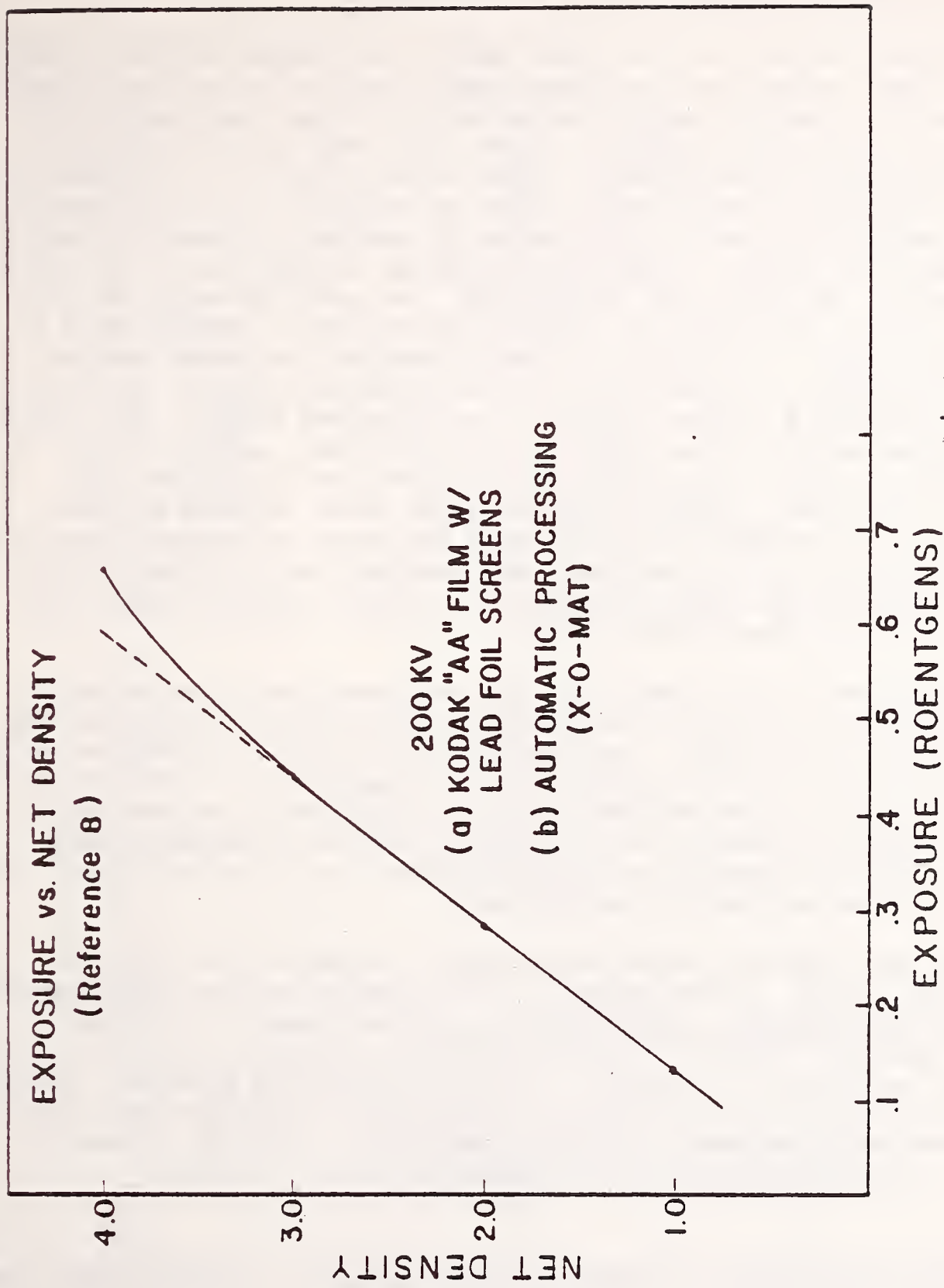


Fig. 51. Net film density as a function of x-ray exposure.

departure from linearity, as much as 10% at a film density of 4, would lead to lower depth measurements using the SWRI equation. However, linearity changes probably have a minor effect.

Another variable is the actual density measurement for small defect sizes, defect indications that approximate the size of the densitometer aperture. For cases in which the aperture is larger than the defect density region, one will obtain a lower peak density, reflecting the averaging effect of the aperture (upper curve, Fig. 52). Only when the aperture diameter becomes smaller than the defect size, will a density reading reflecting the true peak value be obtained. Therefore, density measurements on defect indications determined by SWRI can be in error, depending on the defect indication size. For small defect sizes, the readings would tend to be low, thereby leading to an underestimate of the defect depth. Information in the literature⁶ indicates that an aperture comparable in size to the defect width can give a low reading of about 20% for a rounded versus a flat contoured defect. For defects, not rounded and which show small deep penetrations, such as a tear-shaped hollow bead, this correction factor may be higher than 20%. In recognition of this problem, SWRI personnel* have informed NBS that densitometer measurements were not made for defect sizes that approached the aperture size. An experiment was conducted here to determine what density corrections might be required for density readings made under these conditions (see Section 4B).

Variations in film density in the weld bead due to variations in thickness make it difficult to determine the change in density between a defect and the weld bead. These variations (discussed in Section 4B and Appendix N) limit defect detectability and measurement. One alternative approach to compensate for these density variations is to compare the defect indication density to the lightest part of the adjacent weld image. This will produce the highest contrast on ΔD and will lead to an accurate or overestimate of defect depth.

The most important observation made in regard to film density variations relates to the changes in film density for the shim-penetrator image on the pipe wall. This ΔD^{**} for a known change in thickness should generally increase for increasing film density, because the film gradient increases^{7,8}. However, information obtained from SWRI (Density Data sheets copied at DOT) has been analyzed for the variation in ΔD . For an assumed penetrator-shim thickness value of 0.111, Figure 53 shows a very wide spread in the ΔD observed for this change.

*Telephone Conversation, October 5, 1976, between E. Ruescher (SWRI) and H. Berger (NBS).

** ΔD here means the difference between density values at two points on the radiograph.

6. E. L. Criscuolo, "Radiography and Visual Perception," Nondestructive Testing, 20, 373 (1962).

7. R. Halshaw, "Physics of Industrial Radiology," Heywood Books, London (1966).

8. "Radiography in Modern Industry," Eastman Kodak Co., Rochester, NY, 14650, Chapter 14. See also Figures 55 and 56.

EFFECT OF APERTURE SIZE ON DENSITOMETER SIGNAL

DENSITOMETER SIGNAL

IMAGE OF DEFECT

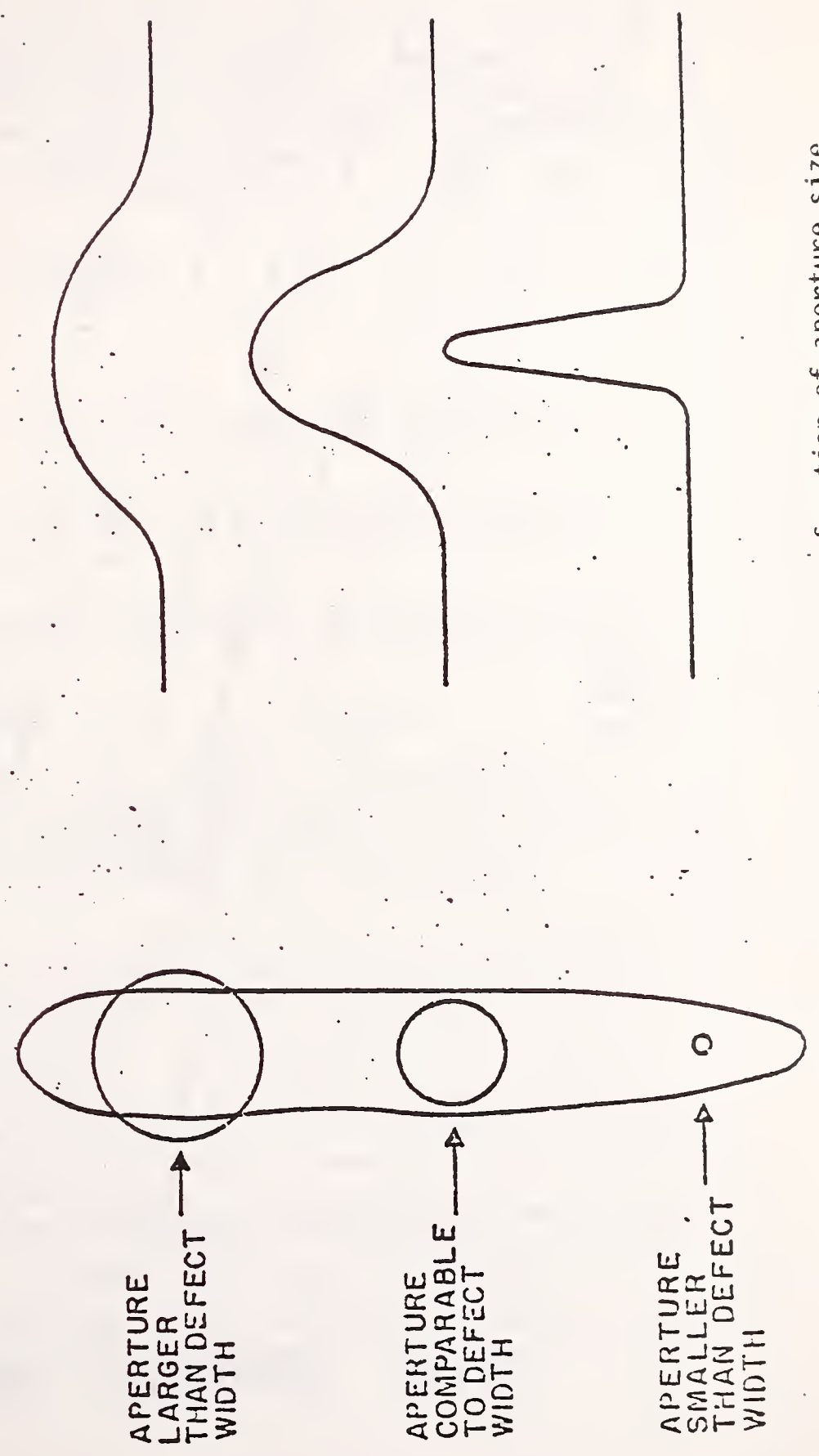


Fig. 52. Relative densitometer readings as a function of aperture size.

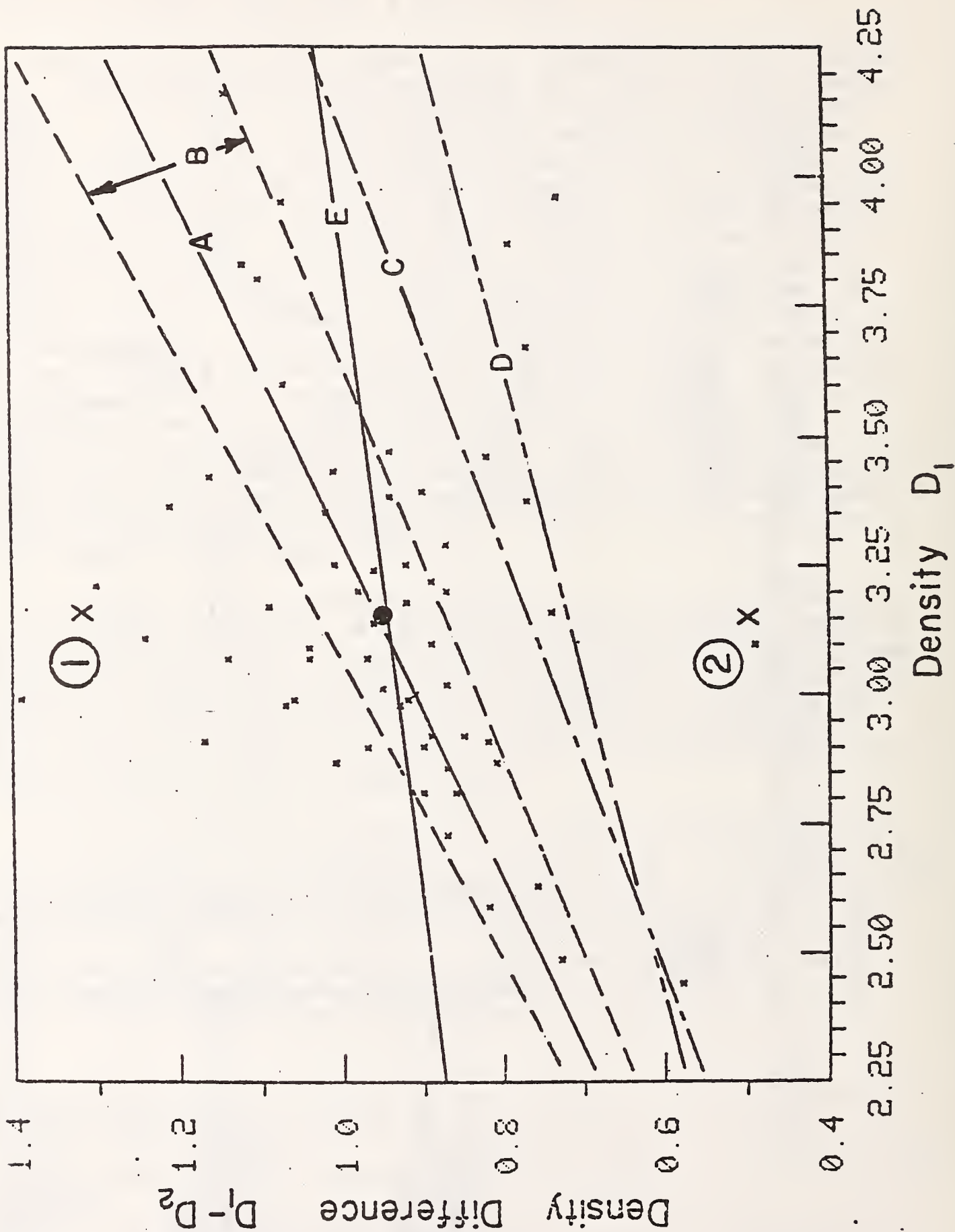


Fig. 53. Film contrast measurements vs. base density for a shim-penetrator thickness of 0.111 in. See text for discussions of the lettered lines.

These same data are plotted in a different way in order to show the general shape of the distribution in the plot (Fig. 54) of frequency of occurrence of a particular value of ΔD .

In the following discussion reference can be made to either plot as desired.

The variation of data shown in Fig. 53 has been analyzed as follows. The average values of $(D_1 - D_2)$ and D_1 were determined. This represents what should be an average condition for the pipeline radiography. At the value of D_1 , the gradient for type AA film (automatic processed) was determined. Then the effective linear absorption coefficient (μ_{eff}) was calculated using equation 1 (see Appendix L):

$$\Delta D = \frac{\mu_{eff} G_D \Delta X}{2.3} \quad (1)$$

where:

ΔD = average value of $D_1 - D_2$ observed from Alyeska film data in Fig. 53.

G_D = film gradient for AA film measured for automatic processed film at the average D_1 value;

μ_{eff} = effective linear absorption coefficient for the pipeline steel;

ΔX = assumed thickness change = 0.111 in. = 0.282 cm.

Using μ_{eff} and actual values of D_1 , values of ΔD were calculated using the above equation. This determined line A on Fig. 53; it represents the ΔD value one should obtain for a 0.111 in. thick steel piece on a 0.562 in. steel pipe wall based on the film response.

That predicted relationship (line A) was broadened by allowing the linear absorption coefficient to vary 15% ($\pm 7.5\%$), as determined from Fig. 50, Band B. An additional variation was determined by allowing the film gradient to vary due to reasonable, possible variations in film processing. Kodak data on variations of film gradient as a function of processing variables are given in Figs. 55 and 56 for automatic and hand processing, respectively. Practically speaking the film gradient only goes down (contrast decreases) as one departs from recommended automatic processing temperature (85°F) or hand processing time (5 min. at 68°F), as shown in Figs. 55 and 56. Curve C, Fig. 53, represents a combination of high x-ray voltage and less than optimum automatic processing (95°F). Curve D represents a combination of high x-ray energy and less than optimum hand processing (2 min. at 68°F). Curve E represents a purely mathematical look at the data points; it is a line that represents a least squares fit to the data points.

FREQUENCY DISTRIBUTION OF CONTRAST MEASUREMENTS

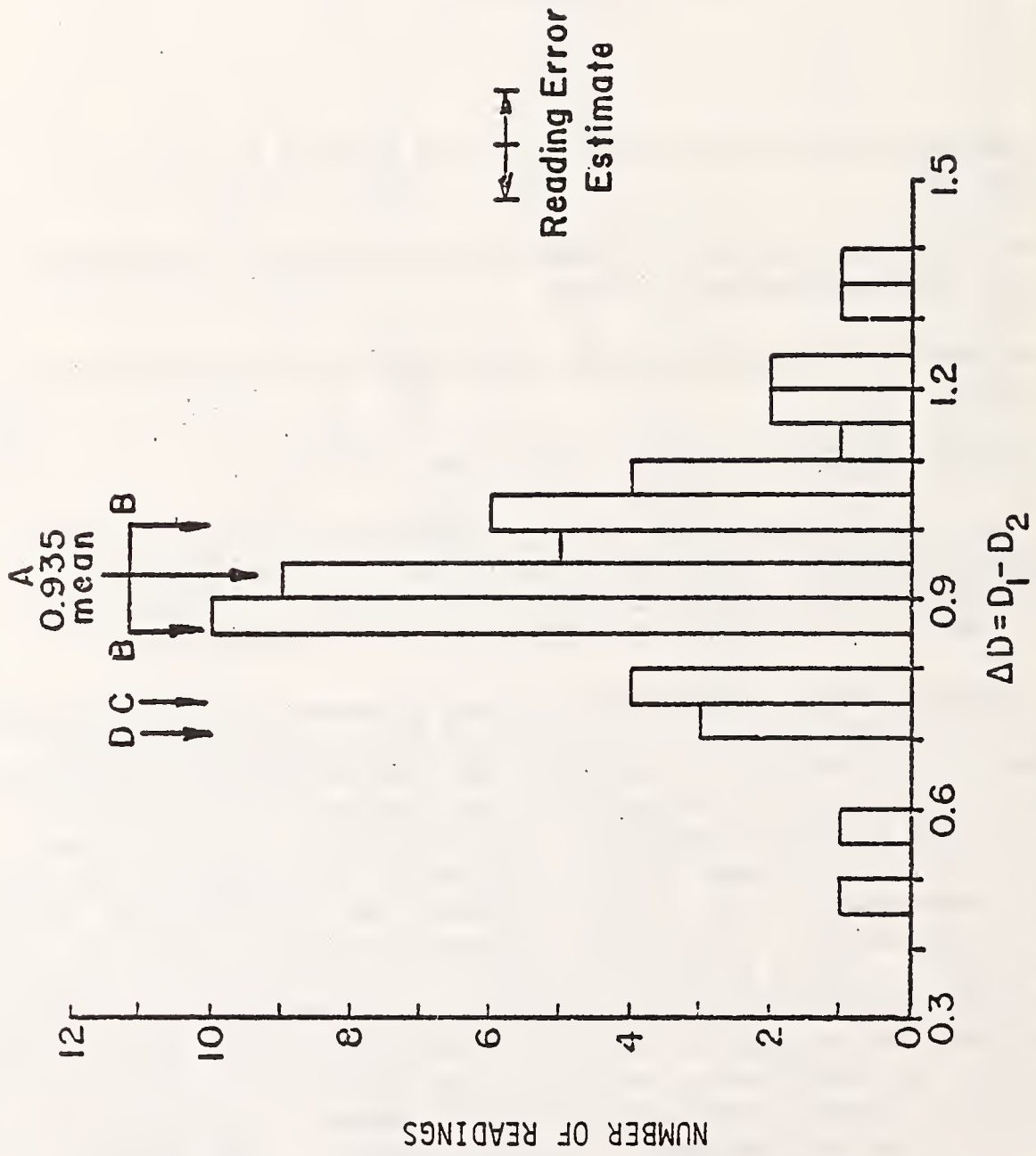


Fig. 54. Distribution of contrast measurements of Alyska radiograph

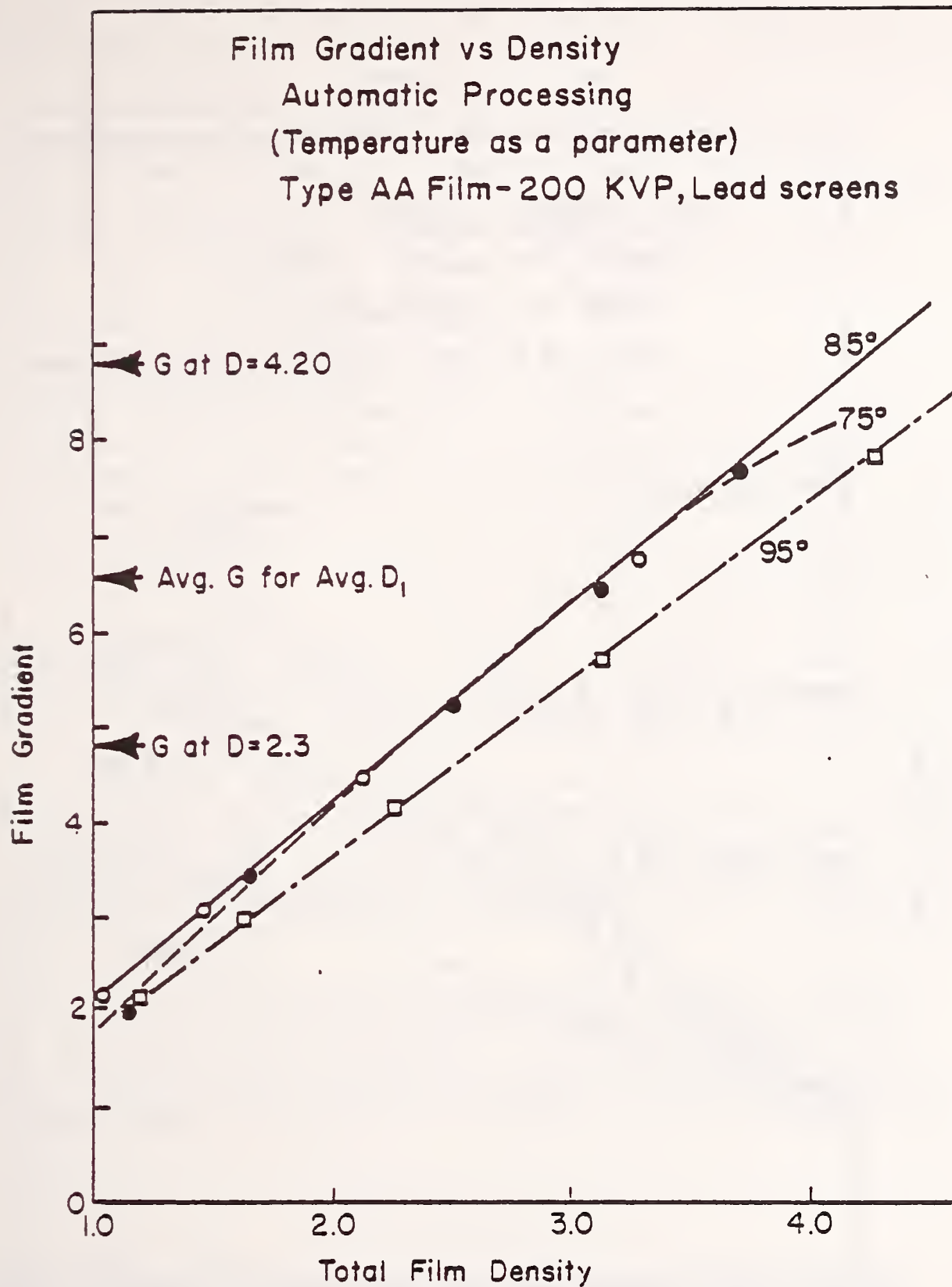


Fig. 55. Film Gradient vs. film density for automatic processing of Type AA Film.

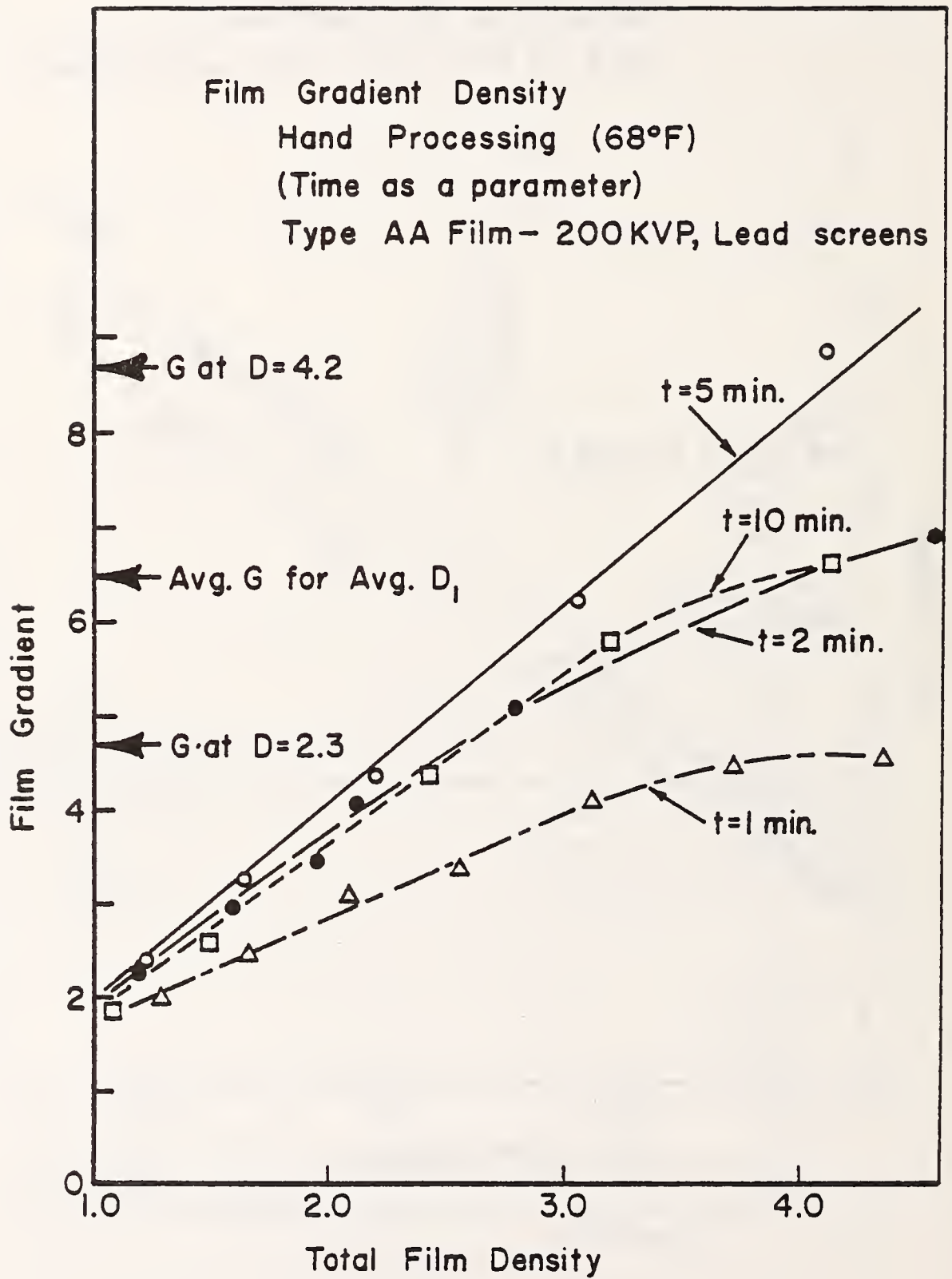


Fig. 56. Film gradient vs. film density for hand processing of type AA film

Two additional points, denoted by 1 and 2, have been added to Fig. 53. Point 1 represents the expected contrast one would obtain if the average radiographic conditions determined from Fig. 53 were applied to a case in which the shim thickness was considerably larger than its normal value (0.158 in. instead of 0.096 in. so that the shim plus penetrameter was 0.173 in.). Point 2 was obtained in a similar way but allowing the shim thickness to decrease by almost a factor of two (0.058 in. plus penetrameter equals 0.073 in.). This shows that the large spread in contrast displayed in Figs. 53 and 54 could essentially be explained on the basis of changes in shim thickness. Said another way, the variation in film contrast means that an observer looking only at the film density change caused by the shim-penetrameter combination might read a value as small as 0.073 in. or as large as 0.173 in. for the presumed actual thickness of 0.111 in. These differences almost cover the extreme values shown in Fig. 53.

Some support for the changing shim thickness explanation of the varying contrast might be obtained from RI measurements of the depth of the penetrameter hole. Once the extreme variation in film contrast was observed, the RI interpreters were contacted in Alaska. They then began to read the penetrameter hole depth using their comparison method. In all these cases, the 0.015 in. deep hole was read as 0.010 to 0.012 in. deep. Of the 31 weld films read in this way, only 10 were among those for which NBS had density data. One low contrast reading was not considered because it involved a tie-in weld. Only two other contrast readings were far removed from predicted film contrast values. It turned out that both these low and high contrast values were for a single weld (#81142), strongly implying that there were two different thickness shims on that weld radiograph.

It should also be mentioned that in an experiment conducted at the Naval Surface Weapons Center* under conditions very similar to the girth welds discussed here, the radiographic contrast for a shim and penetrameter

0.1 in. thick varied from about 0.6 at 250 kVp to about 1.25 at 140 kVp. These variations are about equivalent to the density changes reported by SWRI.

Table 17 lists the possible explanations for the film contrast variations observed in Figs. 53 and 54. Voltage changes, processing conditions and factor-of-two variations in shim thickness have been discussed.** The film type is known to change; this discussion is valid only for Kodak Type AA x-ray film. The pipe wall can vary -5 to +10%;

*E. Criscuolo and D. Polansky, Naval Surface Weapons Center, Silver Spring, MD, private communication (Oct. 1976).

**Shim thickness changes may be a possibility (the Alyeska procedure 32.1 permits the choice of shim thickness to approximate the height of the weld crown) but NBS has been assured that shim thicknesses remained constant telephone conversation, Sept. 29, 1976, J. Willing (Alyeska), and H. Berger (NBS).

extremes in wall thickness for the 0.562 in. wall would be 0.534 to 0.618 in. A change of steel thickness of 0.111 inches on these two extreme wall thickness values yields a calculated change of about 2% in radiation transmitted for an x-ray voltage of 225 kVp (which has peak in the energy spectrum at about 150 kVp). The other variables do not permit assessment without more information than is presently available. A recognized possibility is an extreme change in radiographic procedure, as in the case of a tie-in or repair weld, where the radiograph may be taken from outside the pipe by a double-wall technique or by the use of a radioisotope source (Ir-192) instead of an x-ray generator. Where this was suspected, the density data were not considered in Fig. 53 or the subsequent calculations.

Since these film contrast variations are an important consideration in establishing a relationship between defect depth (or steel thickness) and film density changes, the information is now presented in an additional form. Figure 57 shows the contrast data plotted as the ratio D_2/D_1 rather than the difference. This ratio permits a calculation of the effective x-ray linear absorption coefficient without having to use an empirically determined average for a given change in metal thickness. The μ value determined in this way is within 7% of the value obtained from the averages of the contrast data on Fig. 53.

These film contrast variations would be expected to most influence the RI measurements since these were taken by observing only the weld-defect area of the radiograph. The data on natural defects presented in Table 16a showed that the RI measurements could be related to defect height measurements (obtained from laboratory radiographs) to within a 2σ limit of a factor of two. Further support for the RI measurements is presented in Table 16c, in which comparisons of SWRI and RI measurements on the same defects are made. These films cover the complete range of contrast values, yet the RI depth measurements are consistently (except in one case) greater than those of SWRI.

TABLE 16C. Comparison of Corrected SWRI Densitometer and RI Data on Specific Defects

Weld No	Defect Type	SWRI			RI SWRI (100)	Apparent Contrast ΔD
		Calculated R Value (in.)	Corrected Value* (in.)	RI** (in.)		
81430	IF	0.014	0.021	0.055	262%	0.89
81153	GP	0.045	0.050	0.052	104%	0.49
81209	GP	0.007	0.008	0.050	625%	1.16
81316	GP	0.061	0.067	0.107	170%	0.90
81338R	GP	0.024	0.027	0.076	292%	1.01
81434R	GP	0.006	0.007	0.027	385%	1.17
81441R	GP	0.010	0.011	0.033	118%	1.21
81447	GP	0.036	0.040	0.069	168%	1.04
81670	GP	0.018	0.020	0.060	300%	0.97
81674	GP	0.006	0.007	0.027	386%	1.39
W25TRX	GP	0.046	0.051	0.086	162%	0.98
W39TRX	GP	0.013	0.015	0.074	493%	1.07
81397	ES	0.033	0.036	0.040	111%	0.73
81710	ES	0.064	0.070	0.046	-152%	0.94
81319	HB	0.008	0.009	0.044	489%	0.87
81643	HB	0.023	0.025	0.043	172%	0.77

IF - incomplete fusion

GP - gas pocket

ES - elongated slag

HB - hollow bead

* corrected as per P. 90

**corrected as per Fig. 48

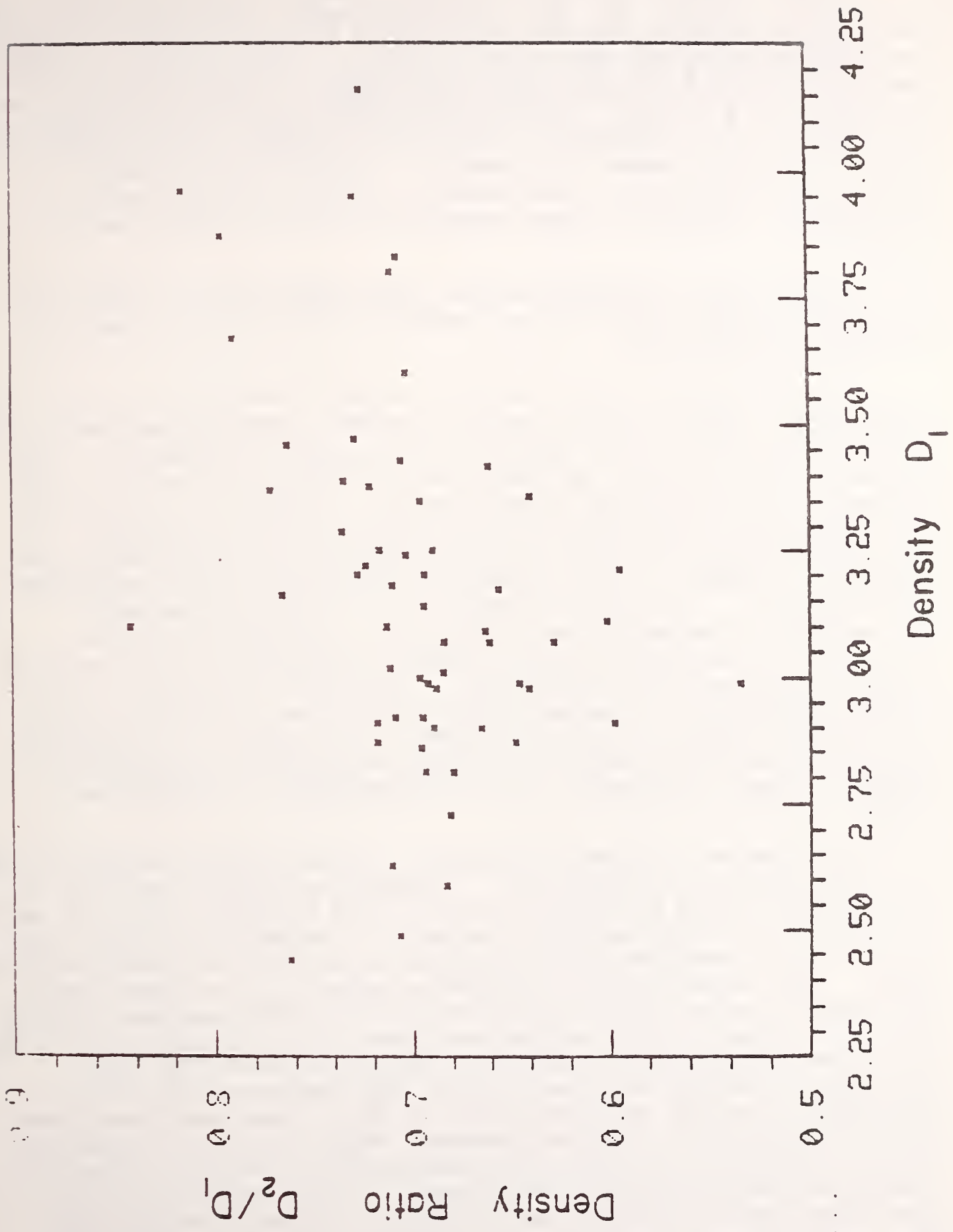


Fig. 57. Film density ratio vs. base density for the Alyeska films

Conclusions

The SWRI methods have been discussed to some extent here and in more detail in Section 4B. The densitometer method is capable of providing reasonable accuracy but depends upon accurate film density measurements. The aperture of the densitometer is an important consideration. For the aperture used for these defect depth measurements, a defect width less than 0.050 in. will lead to an inaccurate defect density measurement. This factor could be improved by the use of a smaller aperture, as in a scanning microdensitometer, for example. The weld bead introduces errors in the densitometer measurement due to the undulating nature of its surface. Estimates of these potential errors have been given in Table 16b.

The SWRI visual comparison method, used because defect widths were too small to measure with the densitometer, is difficult to assess and no attempt has been made.

Large variations in film contrast have been observed for Alyeska field radiographs. Because records were not available regarding necessary radiographic information, such as x-ray energy and film processing parameters, it was not possible to determine the reason for this observed variation in film contrast. If the variations were caused by x-ray energy or non-optimum film processing, the accuracy of the RI method could be influenced. If the contrast changes resulted from such things as inaccurate densitometer readings or changes in shim thickness, the accuracy of the RI method may not be affected. Sufficient information for a rigorous assessment is not available. One would normally state that a film whose contrast falls within a designated predicted range of contrast could be used for a depth determination (with additional variability considered). However, the many combinations of variables that could place a film contrast in an acceptable range have to be considered. For example, it is possible that a thick shim could appear as acceptable contrast if it were radiographed at high x-ray energy or the film processed in a non-optimum manner.

The RI method is potentially capable of good accuracy because the eye can match shades of grey very well. Although the observed variation in film contrast should have most influence on the RI method, there are results that show the RI measurements may be useful. Limited data are available in which the RI measurements are compared to the SWRI densitometer measurements. These comparisons are instructive because, (1) the measurements were taken by two different methods and, (2) the SWRI measurements should not be influenced by film contrast variations. These comparisons show that the RI depth measurements (modified by the bias curve in Fig. 48) are larger (except in one case) than the SWRI measurements (modified according to the SWRI calibration data, p. 90). These comparisons cover the full range of film contrast observed. Additional data in support of the RI measurements is given by the measurements of natural weld defects (Table 16a) from Alyeska field radiographs. It was found that the RI depth measurements of these natural defects (in terms of height rather than depth) showed correlation with laboratory radiographic measurements; the one σ limit was 47%. Since the RI measurements were used for all the weld defects under consideration, DoT may wish to expand these comparisons in order to set limits for the RI measurements.

The reader should recall that the original intent of the field radiographs was to meet the requirements of the API 1104 code. This requires that weld defects be detectable on the radiograph and that lengths of defects be capable of measurement. The variation in film contrast observed in these tests is not inconsistent with those requirements. There was never the intent to use these films for defect depth measurements. If that were the case, much better control of radiographic variables would have been used.

5. REMARKS ON PIPELINE DESIGN AND STRESS ANALYSIS

5.1 Introduction

In Sections 3 and 4, it has been established that two major items of information on girth welds with defects are pertinent to this investigation. One item concerns the nature and size of an identifiable weld defect, and the other an estimate of the fracture toughness and other material properties of the weldment containing a known defect. The former requires a state-of-art investigation in nondestructive evaluation, and the latter leads to an experimental and analysis program in fracture mechanics. There is, however, a third dimension to this technical problem, i.e., the state of stress at any point along the girth weld under investigation during the 30-year design life of the pipeline. For the fracture analysis to be useful as a tool for evaluating a weld with known defects, it is necessary to know not only the maximum stresses in both the hoop and the axial directions, but also the cyclic nature of these stresses due to varying operating and abnormal loading conditions. Maximum stresses are needed in order to identify the "worst loading condition" under which each known defect is required to be stable, and cyclic stress history, also known as the stress spectrum, is required in order to estimate the potential growth of the defect during the pipeline's design life.

The purpose here is not to assess the stress data which Alyeska prepared for the pipeline. Rather, what is presented in this chapter is motivated by a precautionary concern over the uncertainties which are always present in any stress calculations. Since OPSO guidelines [ref. G-4] contain specific references to safety factors on defect sizes and fatigue life as well as minimum or representative material properties, it may be argued that further discussion of adjustment factors for stress, geometric constants for modeling, and materials parameters is unnecessary. As will become clear later in this section and in section 7C, however, we have reason to believe that the physics of the macroscopic behavior of a buried pipeline is not as quantitative and well-understood as that of an above-ground pipeline, partly because of the uncertain nature of the soil-pipe interaction. Furthermore, the present theory of fracture mechanics is based largely on the limiting states of plane stress or plane strain; mathematical modeling of the failure behavior of an elastic-plastic material is still under intensive development, so that today the choice of a particular model and an appropriate set of values for its constants are primarily a matter of judgment. This viewpoint will be substantiated both in this chapter and in section 7C.

5.2 The Physics of the Stress Problem of a Buried Pipeline

A buried pipeline behaves somewhat differently from one above ground, simply because the steel pipe interacts with the compacted granular material backfill through frictional forces not unlike those experienced by steel piling of the friction type. Full understanding of the behavior of the steel pipe when buried underground would require a mathematical model based on the material characteristics of the pipe steel and the surrounding backfill as well as data on the geometry of the pipe alignment, and capable of handling loading cases such as

internal pressure, temperature change, earthquake, and differential settlement. Such a formulation, while technically feasible, is beyond the scope of this investigation. The purpose of this section is to describe qualitatively how the pipeline might be predicted to behave if we had such a mathematical model. This knowledge will then be used to interpret Alyeska's computational results, which were based on a model simplified in ways consistent with current engineering practice. From time to time, elementary calculations are inserted to enhance the qualitative results of this section, but the reader is advised to regard these calculations as purely illustrative because they are not intended either to check or to supplement Alyeska's pipeline design.

For illustrative purposes let us examine a collection of numbers characterizing a typical section of the Alaska pipeline. Let us consider a 2,000-ft long section of 48 in. outside diameter (O.D.), 0.462 in. wall thickness, and horizontally buried pipe with a 4-ft depth of cover from top of pipe to final graded surface. At the two ends of the straight section, a horizontal 45° bend and a vertical 45° bend are designed to change the pipeline alignment. As a grade X-65 material, the pipe steel is designed for a specified minimum yield (SMY) of 65 kips per sq. in. (ksi). For subsequent calculations, we need the cross-sectional area of the pipe ($A = 67$ sq. in.), the plane moment of inertia ($I = 19,500$ in⁴.), and the radius of gyration ($r = 17$ in.). The surface area of contact between the steel pipe and the granular material backfill as specified in Alyeska drawings (see, e.g., Alyeska drawing No. AL-00-65 as listed in [H-11]), is 12.6 sq. ft. per lineal foot. For convenience, numerical quantities are rounded off to emphasize the qualitative aspect of this discussion.

Now assume that this section of pipe is undergoing a hydro-test to 95% of SMY for the maximum stress in the pipe steel. Ignoring the two ends, the state of strain throughout the middle section of the 2,000-ft pipe is a very simple one; namely, zero along the pipeline axis, and uniformly distributed hoop strain along the perimeter of the pipe due to internal pressure. Assuming a Young's modulus of 30,000 ksi, the hydro-test imposes a hoop stress of $0.95 \times 65 = 61.8$ ksi, and a hoop strain of $61.8/30,000 = 0.21\%$. It is a well-known physical fact that when a material is stretched along one dimension it tends to contract in the other two dimensions unless restrained from doing so. For steel, the constraint of zero longitudinal strain introduces a tensile stress along the axial direction equal to $0.3 \times 61.8 = 18.5$ ksi, where 0.3 is the Poisson ratio (assumed). This induces a tensile force along the pipe equal to $18.5 \times 67 = 1,240$ kips which could be provided by the frictional force between a section of the pipe away from the midsection and the backfill material. To estimate that frictional force, Seelye [2, p. 3-29] allows a 35 lb/ft³ equivalent fluid pressure for some common backfill not unlike those encountered in Alaska. A 4-ft cover implies a 6-ft average depth of backfill around a 48 in. O.D. pipe and an average lateral pressure between backfill and pipe equal to $35 \times 6 = 210$ lb/ft². Assuming a coefficient of friction between 0.3 and 1.0, the frictional force can be estimated as between 0.9 and 2.7 kips per lineal foot. This range of values checks very well with values for similar problems recently reported by Kennedy, Chow, and Williamson [1]. To be conservative in estimating the frictional force, we choose to work with the estimate of 2.7 and calculate the length of pipe to develop the tensile force of 1,240 kips to be about $1,240/2.7$ or, say, 500 ft. This means that for about 500 ft. along each end of this pipe, the longitudinal tensile stress decreases from 18.5 ksi at the ends

of the 1,000-ft mid-section to zero at the two bends, with an estimated elongation equal to $0.3 \times 0.21\% \times (1/2) \times 500 \times 12 = 1.9$ inches at each bend. Based on a formula given on p. 6-78 of reference [2], the 45°-bend introduces a longitudinal tensile force of 630 kips for an internal pressure of 1,210 psi which corresponds to the assumed hoop stress of 61.8 ksi. This tensile force develops a longitudinal tensile stress of $630/67 = 9.4$ ksi in the pipe, and an estimated bending stress of 10 ksi at the outer extreme fiber of the bend due to a bearing resistance of 20 kips/sq. ft. in the backfill, over, perhaps, a pipe length of about 20 ft. We have used the bending stiffness ($Z = 810 \text{ in}^3$) of the pipe in this calculation. We now conclude that a safe estimate of the longitudinal tensile stress everywhere along this pipe is about 20 ksi during a hydro-test at the tie-in temperature. This checks very well with Alyeska's estimate for a different, but comparably severe loading condition for the same pipe grade and wall thickness, where the longitudinal stress due to pressure and live and dead loads was estimated to be 19.8 ksi (see Table 10 of Part 3, reference [H-1]).

Similar reasoning can be applied to achieve an understanding of the behavior of the 2,000-ft pipe if it was laid at 35°F (tie-in temperature), and contains oil at 145°F. The net temperature strain would be $110 \times 6.5 \times 10^{-6} = 0.07\%$, where the coefficient of expansion of steel is assumed to be 0.0000065 per °F. With the operating pressure limited to 76% of the hydro-test pressure (i.e., from 0.95 SMY to 0.72 SMY), the induced tensile stress (axial) would have been about 15 ksi. The temperature stress (axial) for zero longitudinal strain would be $0.07\% \times 30,000 \text{ ksi} = 21$ ksi of a compressive nature. Hence the mid-section of the pipe experiences a longitudinal compression of $21 - 16 = 6$ ksi. The net compressive force equals $6 \times 67 = 400$ kips. By the Euler buckling criterion, if the backfill provided no resistance, the critical length of the pipe would equal

$$(\pi^2 \times 30,000 \times 19,500 / 400)^{1/2} = 3,800 \text{ in. or about 320 ft.}$$

Clearly, the backfill pressure provides an excellent deterrent to the problem of instability due to temperature-induced compressive loads on a long buried pipe. One can then go through a similar illustrative calculation for the two ends of the pipe to check the stress behavior as influenced by the temperature change and the backfill-steel frictional force estimated in the last paragraph. The result is that if a girth weld is located near a bend (6 ft. away from the point of tangency), there is a strong likelihood that a longitudinal tensile stress of the order of $10 \text{ ksi} \pm 5 \text{ ksi}$ may be encountered by some portion of the weld under normal operating conditions. This estimate is higher than the comparable Alyeska estimate (3.2 ksi), and may be explained by the difference in the two approaches underlying the estimates.

5.3 Variability in Stress Spectra for Girth Welds

The OPSO requirements specify that proposed alternative-allowable weld-defect sizes and proposed alternative-allowable arc-burn sizes must be supported by fracture mechanics analyses using the worst-cast fatigue-stress spectrum. An axial-stress spectrum is used for girth-weld flaws and a hoop-stress spectrum is used for arc burns. A detailed discussion of the fatigue crack propagation problem appears in section 7(A). The purpose of this section is to show the

variability of stress spectra by comparing Alyeska's worst case spectrum with two of the weld stress spectra provided to NBS by Alyeska. Once again, the intent is to show the qualitative difference between Fig. 58 (worst case spectrum) and Fig. 59 (weld no. 42R, sta. 0192+32, mile post 731, alignment sheet 0013), or Fig. 60 (Alyeska synthesized spectrum no. 23A, sta. 1111+11, mile post 78, alignment sheet 126). In all three cases, the stress ranges denote longitudinal stress differences due to all the pressure cycles, thermal cycles, and earthquake loadings anticipated during the 30-year life-time of the pipeline. Information for Fig. 58 (worst case) came from Part 4, reference [H-1], and that for Figs. 59 and 60 from references [H-6] and [H-7]. For the NBS fatigue analysis given in section 7(A), the stress spectrum corresponding to Fig. 60 has been adopted. If we assume for this qualitative purpose, that the fatigue damage, when measured by crack growth due to cyclic stresses, is proportional linearly to the number of cycles and varies approximately as the third power of the stress range (ΔK) based on the following equation (section 7(A)):

$$\frac{da}{dN} = C (\Delta K)^3,$$

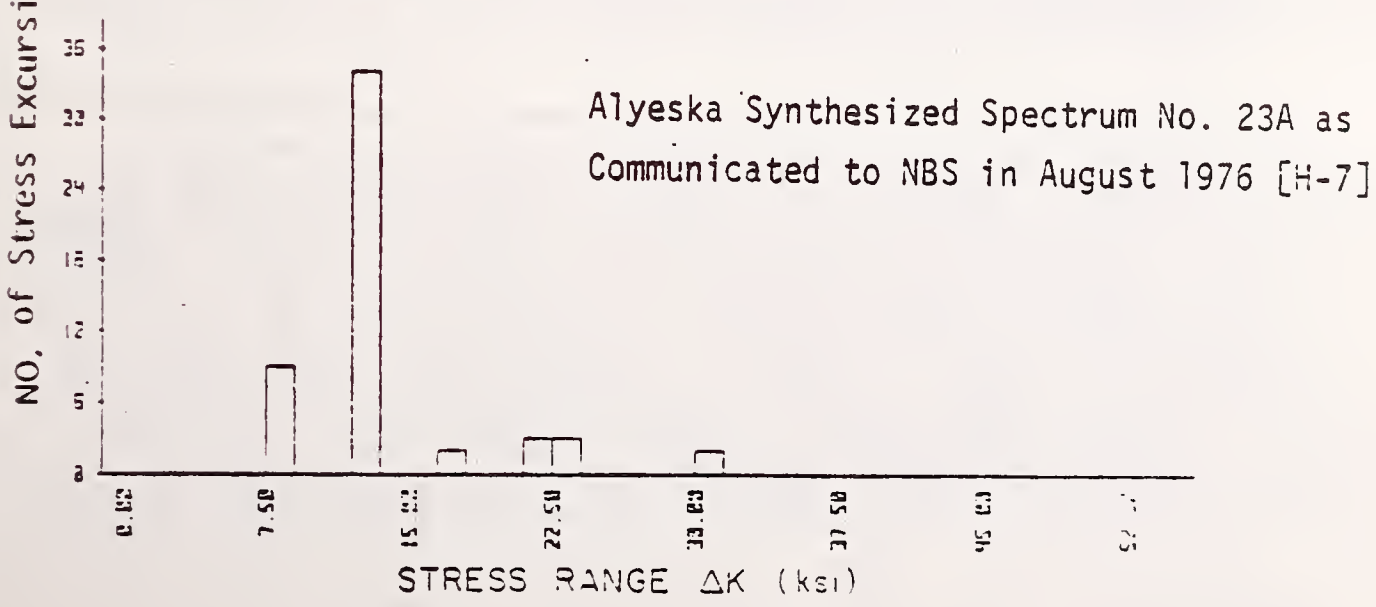
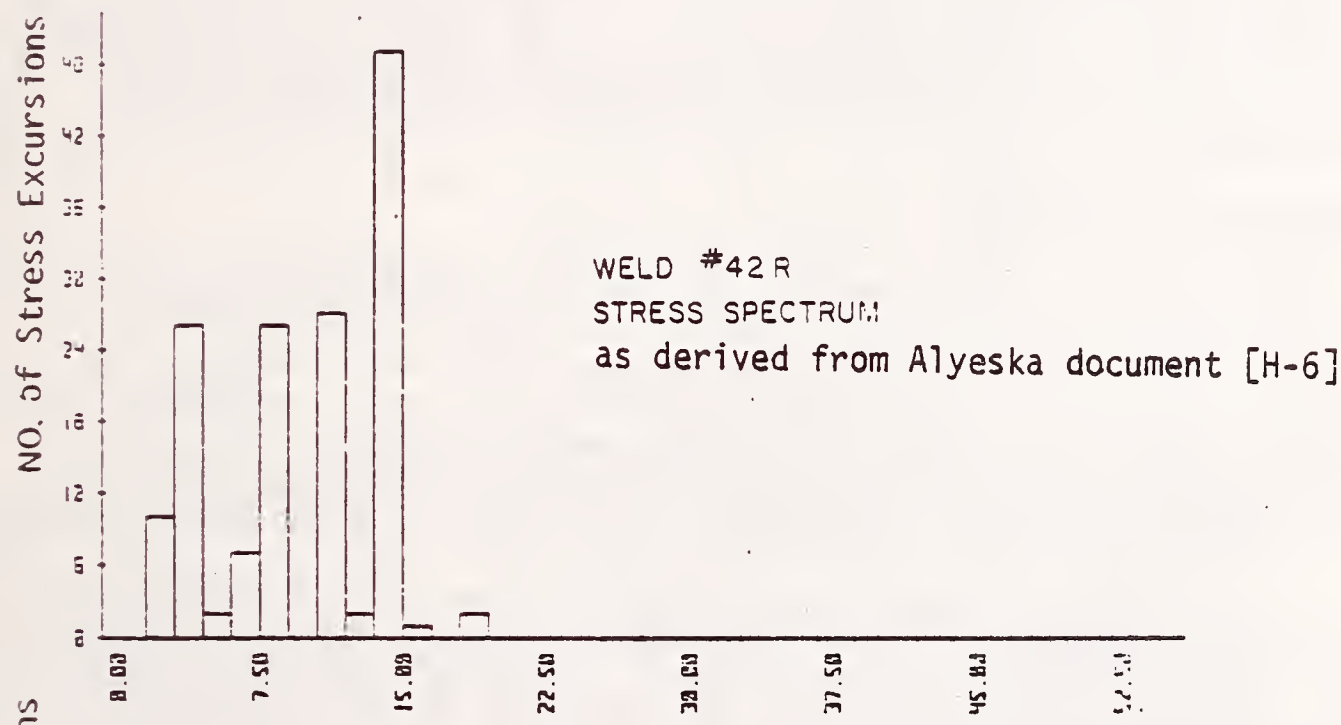
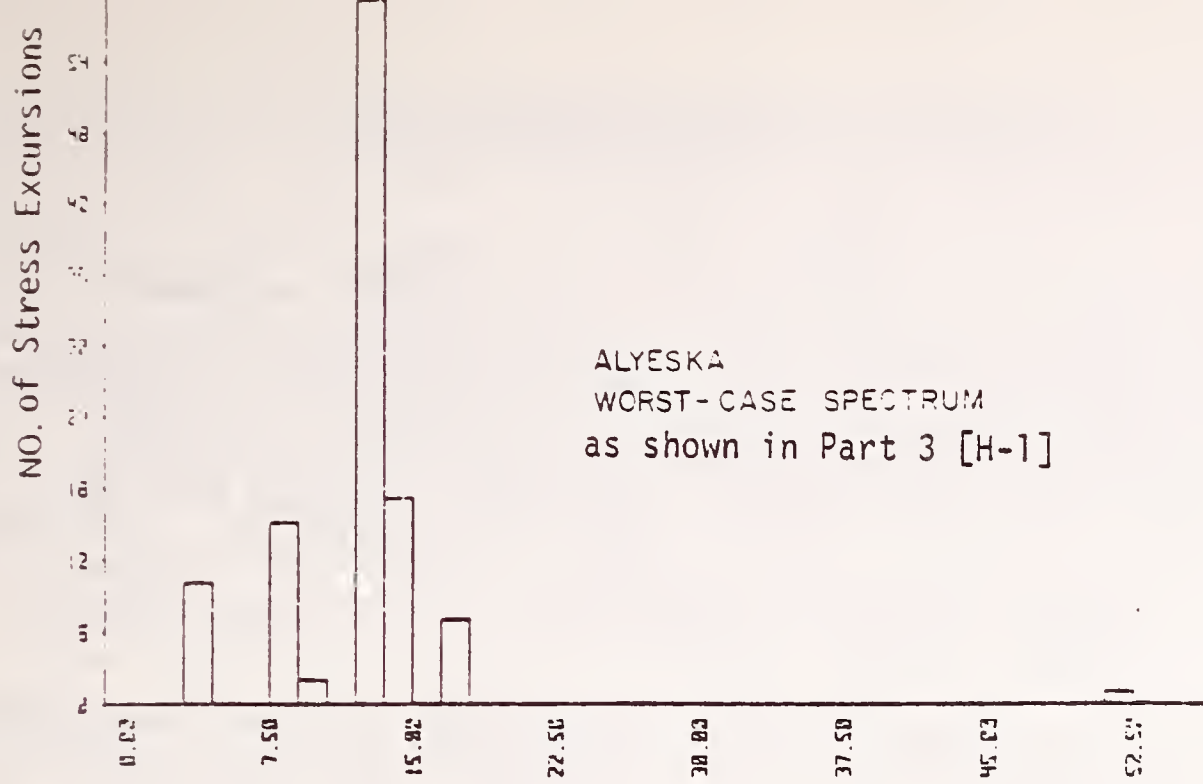
then it is possible to estimate that the worst-case spectrum differs from either of the two specific weld spectra (Figs. 59 and 60) by a factor of 1.75 to 1.0.

5.4 Concluding Remarks

The preceding qualitative analyses of the physics of a buried pipeline (section 5.2) and of the spectra of cyclic stresses during the 30-year life-time of the pipeline illustrate the variability one would confront in choosing a set of stresses to represent the states of stress in all welds under investigation. The variability is particularly hard to estimate when the pipeline is underground. For arc burn problems, there is also a definite cause for concern in the uncertainty of any stress estimate based on a single nominal thickness for a pipe wall which, according to Alyeska material specification [H-2], has an allowable variability of +10% and -5%. Since the stress calculation is only valid to the accuracy of the hydraulic analysis, uncertainties due to surge estimate (see reference [3]) and fluid properties should also be accounted for in fixing a stress level for fracture analysis. These uncertainties on applied stress will be further discussed in section 7(C) under the title: Sensitivity Analysis and the Use of Safety Factors.

5.5 References

- [1] Kennedy, R. P., Chow, A. W., and Williamson, R. A., "Fault Movement Effects on Buried Oil Pipeline," a technical paper presented at 31st Annual Petroleum Mechanical Engineering and Pressure Vessel and Piping Conference, Mexico City, Sept. 1976. Preprint available through first author's office at Engineering Decision Analysis Company, Inc., 2400 Michelson Drive, Irvine, California 92715.
- [2] Seelye, E. E., Data Book for Civil Engineers, Vol. 1, Design, 2nd ed. Wiley (1951).
- [3] Parmakian, J., Waterhammer Analysis, pp. 93-100. Dover (1963).



6. ASSESSMENT OF MATERIALS PROPERTY DATA

The determination of allowable defect sizes depends on the availability of reliable mechanical properties data for the weld metal and base metal. The properties required for the allowable defect size determination are: elastic modulus, Poisson's ratio, yield strength, fracture toughness, fatigue-crack growth rate, and environmentally assisted crack growth rate due to stress-corrosion, hydrogen cracking, and corrosion-fatigue. For this program the required mechanical properties data were obtained from measurements made by the National Bureau of Standards (NBS), measurements made for the Alyeska Pipeline Service Company by the Welding Institute (WI) and the Cranfield Institute of Technology (CIT), and from information reported in published technical literature.

Standardized and accepted methods of measurement have been established to determine some but not all of these required mechanical properties. Therefore, the reliability of all data on material properties used in determination of allowable defect sizes will be assessed in this chapter. This discussion will include an evaluation of the selection of materials used for testing, and an evaluation of the test methods used and the testing parameters chosen.

Selection of Test Samples

All weldments used in the NBS, WI, and CIT test programs were obtained from actual field welds made on the Trans-Alaskan pipeline. Therefore, these weldments should be representative of weldments made according to the prescribed welding procedures and should be typical of production welds. This use of production welds is particularly desirable whenever possible because they are more representative of actual welds than weldments made under "laboratory" conditions using the same procedure.

The NBS testing program was conducted on a group of four weldments consisting of one made with welding process 104A, one made with process 102A-1, and two made with process 104A-1. The WI-CIT testing program used 3 weldments made during 1975 and 3 weldments made during 1976. Each group consisted of one weldment made by each of the three welding processes 102A-1, 104A-1, and 302A-1.

Although extensive testing was done on each of the weldments available, the small number of weldments available (10 weldments representing 3 welding procedures) compared with a total of nearly 60,000 girth welds made on the Trans-Alaska pipeline, does not permit an accurate assessment of the weld properties to be made on a valid statistical basis. However, well defined welding procedures and materials were specified by Alyeska to be used for all production welds. If these welding procedures were followed and a high level of quality control was maintained during the welding, it can be expected that the very limited number of weldments tested should yield material properties data that are representative of the production welds in the pipeline. The lack of a sufficient sample

size to establish a suitable statistical base for assessing the material properties data is one reason that safety factors are required in the allowable defect size analysis to account for these uncertainties.

Tensile and Elastic Properties

The elastic constants of the pipeline base-metal measured at NBS were determined with established and accepted measurement procedures. Elastic constants of the weld metal were not determined but base-metal properties are considered to be representative of the weld metal elastic properties. All results are consistent with accepted properties for steels of the type used in the pipeline.

The tensile properties of the base metal and each of the two weld metals were determined at NBS using well established and accepted testing procedures. The minimum yield strength measured at 68° F of all weld-metal samples was 59 ksi for the weld made with process 102A-1 and 55 ksi for the weld made with process 104A-1. The average yield strength of these welds were 60 ksi and 63 ksi, respectively. These values are lower than expected for welds made with the welding electrodes specified as AWS E7010-G for the 102A-1 process and AWS E8010-G for the 104A-1 process. Welds made with these electrodes should have minimum yield strengths of 70 ksi and 80 ksi, respectively. The low yield strengths determined in these tests may be caused by the small specimen size chosen (0.14 in. diameter). Weldments made specifically for establishing the weld metal yield strength allow larger sized specimens to be obtained on the weld metal yield strength.

Fracture Toughness

The fracture toughness of the metal is the key parameter through which the fracture mechanics analysis determines the allowable defect sizes for specified levels of applied stress. For relatively brittle metals that fracture under conditions where linear elastic fracture mechanics analysis applies, the fracture toughness specified as the critical plane strain fracture toughness, K_{Ic} , can be measured by the accepted and standardized method described in ASTM Standard E399-72. From this fracture toughness value for the specified material, and the specified applied stress, the allowable defect size can be determined for any structure that behaves according to the assumptions of linear elastic fracture mechanics.

For more ductile metals that do not obey linear elastic fracture mechanics assumptions in either the structure of interest or in laboratory test specimens, a single standardized method of determining the fracture toughness has not been agreed upon. The measured value of fracture toughness is very sensitive to the test specimen size and geometry and to the specific choice of when fracture initiates. There are presently four test methods under development to measure the fracture toughness of ductile metals that fracture after undergoing substantial amounts of plasticity. Fracture toughness data using each of these four test methods was obtained on the girth welds of interest and was used to assess the welds and develop allowable defect sizes. The test methods considered here are: standard Charpy-V-notch impact tests, instrumented-precracked Charpy-V-notch tests, J-integral tests, and crack-opening-displacement (COD) tests.

Standard Charpy-V-Notch Impact Test Results The Welding Institute and Cranfield Institute of Technology have done extensive testing for Alyeska of standard Charpy-V-notch test specimens taken from welds made during both 1975 and 1976 using welding processes 102A-1, 104A-1, and 302A-1. This test program tested specimens with notches located in 8 different positions within the weld metal or HAZ and over a temperature range from -40°F to +32°F. These results were submitted to DOT as part 3 of the supporting information for the waiver request. NBS tested similar Charpy-V-notch specimens taken from welds made during 1975 using welding procedure 102A-1 and 104A-1. Only one notch position (position number 1, shown in Figure 35) was used in these tests and a full transition temperature curve from -40°F to 100°F was obtained. These results are summarized in Section 3I and in Appendix Q.

The energy absorbed and percent shear fracture determined in the NBS and the Alyeska tests are similar over the temperature range where they are comparable. The Alyeska data did not demonstrate an effect of changes in notch position on the Charpy-V-notch results. The standard CVN tests conducted by NBS showed that "upper shelf" behavior as demonstrated by 100% shear fracture was not obtained even at 100°F for either of the weldments tested. The extensive variability in the test results from both sets of data, due to the heterogeneity of the weld metal and the fact that most data were obtained within the transition temperature range, prohibits more specific conclusions about the effect of welding procedure or notch orientation to be made from the results of these Charpy-V-notch tests.

Although a fracture toughness value that can be used directly to determine allowable defect sizes cannot be obtained from standard Charpy-V-notch tests, the results of these tests are useful for comparison of relative toughness levels for weldments tested at various laboratories. This is done by assessing the effect of temperature on the ductile to brittle fracture transition and to determine the effect of impact loading on the weld metal. The lowest Charpy toughness found in any of the welds was in excess of 40 ft-lb (average of 3 specimens) at 10°F and in excess of 25 ft-lb at -40°F.

Although the standard Charpy-V-notch test cannot be used to measure the fracture toughness, empirical correlations have been developed that permit the estimation of fracture toughness¹ or the allowable failure stress for piping containing defects² when more precise measures of fracture toughness are not available. Since more reliable tests, such as COD, instrumented precracked Charpy-V-notch impact tests, and J-integral, were conducted in this investigation, these empirical correlations to estimate fracture toughness were not used.

1. R. A. Wullaert, D. R. Ireland, A. S. Tetelman, "Use of Precracked Charpy Specimen in Fracture Toughness Testing," Fracture Prevention and Control, ASM, 1974, pg 255-282.

2. W. A. Maxey, "Fracture Initiation, Propagation, and Arrest," 5th Symposium on Line Pipe Research, American Gas Assoc., Cat. No. L30174, Nov. 1974.

Instrumented Precracked Charpy-V-Notch Tests Instrumented precracked Charpy-V-notch tests were conducted over a range of temperature from -40°F to 100°F on specimens taken from welds made using welding procedures 102A-1 and 104A-1 to determine a quantitative measure of fracture roughness to establish a lower bound for the determination of maximum allowable defect sizes under the most unfavorable conditions of high rates of loading. A measure of the dynamic fracture toughness, K_{Id} or K_{Jd} , is determined from these tests.

Since no "static" fracture toughness, K_{Ic} , tests were conducted using instrumented-precracked Charpy-V-notch specimens, the assessment of the effect of dynamic loading on the fracture toughness of the welds must make use of static fracture toughness measurements made by the J-integral procedure at the Welding Institute³ and at NBS⁴. The measured J-integral values were converted to stress-intensity, K_{Ic} , using the equation:

$$K_{Ic} = (E J_{Ic})^{1/2}$$

where E is Young's modulus. These static K_{Ic} values are plotted on Figure 61 for comparison with the dynamic fracture toughness values, K_{Jd} or K_{Id} , determined from the instrumented precracked Charpy-V-notch specimens.

The results in Figure 61 show that up to 32°F, the dynamic fracture toughness has a lower bound that is substantially below the static fracture toughness and, in fact, the dynamic specimens obey the behavior associated with linear elastic fracture and do not exhibit plasticity prior to fracture. A minimum dynamic fracture toughness of $K_{Id} = 55$ ksi $\sqrt{\text{in}}$. was measured at 32°F. This low fracture toughness suggests that only very small defects would be permitted if the pipe welds experienced loading rates as high as experienced in the Charpy-V-notch tests. However, loading rates this high, above 2×10^5 ksi $\sqrt{\text{in}}/\text{sec}$. are not normally experienced in large, compliance structures.

For temperatures above 32°F, dynamic loading does not appear to degrade the fracture toughness of the weld metal. As shown in Figure 61, at 68°F, the static fracture toughness even appears to be less than the dynamic fracture toughness, K_{Jd} . However, this is an apparent rather than real effect because for K_{Jd} values above 110 ksi $\sqrt{\text{in}}$, the dynamic fracture toughness is affected by the small size of the Charpy specimens and an artificially high value is measured. The static, J_{Ic} tests were determined with full wall thickness larger specimens and are, therefore, not artificially affected by specimen size effect the correct values of these parameters.

3. J. D. Harrison, "COD and Charpy-V-Notch Impact Tests on Three Pipeline Butt Welds Made in 1975," The Welding Institute Report LD 22062/5, July 1976, Ref. [H-1] in appendix H of this report.

4. Section 3E, this report.

J-integral and Crack-Opening-Displacement (COD) Tests.

The J-integral test method under development by ASTM requires several specimens to be tested to obtain a single critical J_{IC} value that represents the critical fracture toughness of the metal. This method is the most widely accepted, but not yet standardized, method for testing in this country. The J_{IC} value can be used directly to obtain allowable defect sizes when the stress in a structure is known.

A simplified, single specimen method was used by the Welding Institute³ to estimate J_{IC} from three-point bend specimens. This simplified method, using maximum loads¹ can only be used for specimens that fracture with limited plasticity so that ductile crack propagation does not occur prior to fracture. Therefore, the Welding Institute J-integral test results are only obtained at test temperatures of 10°F and below. Maximum load estimates tend to over-estimate J, as crack initiation may begin below the peak of the load-deflection curve. A summary of the results of the Welding Institute J-integral tests is shown in Table 18. As with all the weld metals tested, there is a large amount of variability in the J_{IC} values obtained. However, since only specimens which fractured without ductile crack propagation could be used to obtain these J_{IC} values, the results reported in Table 18 are used to establish a lower bound level of J_{IC} for these weld metals.

The results of the NBS tests to measure J_{IC} (Section 3E) are also summarized in Table 18. The NBS tests were conducted with larger specimens than the tests of the Welding Institute and used the multiple specimen technique described in Section 3E of this report. This procedure is considered to be the most accurate presently developed to determine J_{IC} because it clearly defines the initiation of fracture even if ductile crack propagation occurs. However, the NBS values of J_{IC} obtained at 4°F (457 and 628 in-lb/in²) are consistent, within the observed variability of the tests, with the Welding Institute test results of 283 and 503 in-lb/in² obtained at the nearest comparable temperature of 0°F. Therefore, the J-integral test procedure used by the Welding Institute seems to be reliable for determining J_{IC} when no ductile crack propagation occurs prior to fracture.

The largest amount of data on the fracture toughness of the weld metal was obtained using the crack opening displacement (COD) test procedure originally developed by Burdekin and Stone⁵ and subsequently adopted as a standard test method by the British Standard Institute. (Draft for Development #19, 1972.) The COD results are the only fracture toughness results actually used in the calculation of allowable defect sizes in this report.

The results of COD testing by the Welding Institute and by Cranfield Institute of Technology³ included tests on welds made by processes 102A-1, 104A-1, 302A-1 and were conducted for 8 different notch orientations over the temperature range from -40°F to 32°F. The heterogeneity of the weld metal resulted in a large variability in the COD results so that the COD values determined varied by as much as a factor of 6. The minimum value of COD of 4 mils (0.004 in.) at +10°F was chosen by Alyeska as the lower bound value for the allowable defect size calculations.

5. F. M. Burdekin, D. E. W. Stone, "The Crack Opening Displacement Approach to Fracture Mechanics in Yielding Materials," Journal of Strain Analyses, 1 (2), 1966, pp. 145-153.

Table 18. Fracture Toughness Results from J-Integral and COD Tests

Weld Process	Test Temp. (°F)	J _{Ic} (in-lb/in ²)	δ _c , COD (in.)	
			Meas. ¹	Calc. ²
<u>NBS Tests-using Compact Tension Specimens</u>				
102A-1	68	571	--	.0048
	- 4	628	--	.0046
104A-1	68	457	--	.0036
	- 4	457	--	.0034
<u>Welding Institute Tests-using Bend Specimens</u>				
102A-1	32	--	.017	--
		--	.015	--
		10	.009	--
	0	--	.004	--
		883	.007	--
		1443	.010	--
		1318	.011	--
		283	.002	--
		503	.004	--
	- 20	291	.003	--
		895	.008	--
		2830	.019	--
	-40	169	.0010	--
		222	.0015	--
		652	.006	--
104A-1	32	--	.012	--
		--	.007	--
	10	--	.013	--
		--	.012	--
	0	--	.015	--
		--	.014	--
	- 20	--	.011	--
		554	.006	--
	- 40	657	.006	--
		652	.006	--
401		.004	--	

1. Two lowest measured values at designated temperature reported by Welding Institute in report submitted with waiver request.

2. Calculated by conversion: $\delta_c = \frac{J_{Ic}}{2\sigma_y}$

It is possible to compare fracture toughness values determined with COD tests with those obtained with J-integral tests. However, this requires a conversion based on an empirically developed relationship of the form:

$$\delta_c = \frac{J_{Ic}}{m\sigma_y}$$

as given in Section 3E of this report. The value of m can range from 1.0 to 2.1 so that in converting from J_{Ic} the resulting value of COD is not precisely defined. Results of tests by the Welding Institute³ suggests that for large specimens $m = 2.1$ is the best value while $m = 1.6$ is suitable for smaller specimens. Sumpter and Turner⁶ show that $m = 2$ for three-point bend geometry specimens, such as used by the Welding Institute for J-integral tests, when substantial yielding occurs prior to fracture. For specimen geometries other than three-point bend specimens, the factor m , may be different from 2.0, but has not been as clearly defined by experiment or by analysis such as the use of finite element calculations. This uncertainty in the value of m makes it difficult to compare fracture toughness values obtained using the COD test method with those made using J-integral procedures. However, to be conservative, whenever converting measured values of J_{Ic} to COD values, the value of m is chosen as equal to 2.0.

To compare the results of NBS J-integral tests with the COD measurements made by the Welding Institute and Cranfield Institute of Technology, the J-integral values were converted to COD values using a value of $m = 2.0$ chosen because of the large size and constraint present in the NBS specimens. The lowest values of COD measured for each weld at each test temperature are plotted in Fig. 62 along with the COD results calculated from the NBS J-integral test and a lower bound COD curve as a function of temperature is drawn. A minimum critical COD value of 3.4 mils (.0034 -m.) at -4°F is obtained by converting the J_{Ic} value measured at NBS to COD using $m = 2.0$. If the m value is chosen as 1.6 instead of 2.0, the minimum COD is 4.0 mils at -4°F .

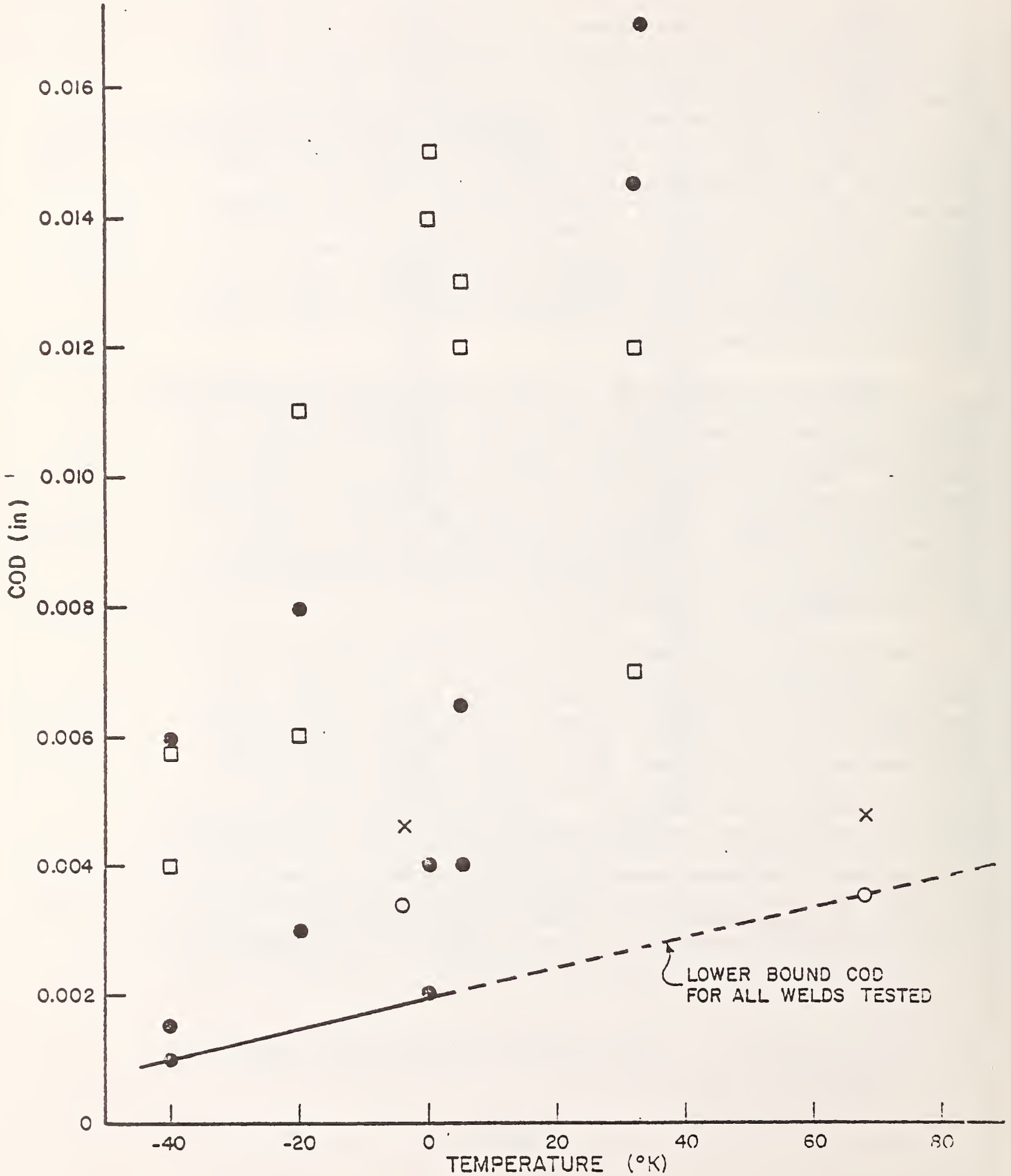
The COD results from Alyeska appear to be higher at 32°F than at $+10^\circ\text{F}$. However this increase was not statistically significant. The comparable results from the NBS J-integral tests at 68°F suggest that the toughness may not increase, but may still be less than the equivalent COD value of 4 mils as shown in Fig. 62. It is possible that the COD measurement made with relatively small specimens (approximately 1/2 by 1/2 inch) exhibit an artificially elevated COD value when extensive plasticity occurs prior to fracture. This would explain why the estimated COD values obtained from the NBS J-integral tests at 68°F are considerably below the Welding Institute COD values determined at 32°F . This effect of specimen size on the minimum value of COD is further substantiated by the result of one test reported by the Welding Institute³, where a COD value of 2 mils was measured at 0°F when a larger (approximately 1/2 by 1 inch) COD specimen was used. This low value of COD was attributed to the high degree of plane strain constraint present in the larger specimen.

6. J. D. G. Sumpter, C. E. Turner, "Methods for Laboratory Determination of J_c ," ASTM STP 601, 1976, p. 1.

(Fig. 62)

FRACTURE TOUGHNESS COD RESULTS

- X 102A-1 WELD, J-INTEGRAL TESTS BY NBS
- O 104A-1 WELD, J-INTEGRAL TESTS BY NBS
- 102A-1 WELD, COD TESTS BY, WI
- 104A-1 WELD, COD TESTS BY, WI



These results suggest that the value of 4 mils used in the fracture analysis is a reasonable value. However, at +10°F, this cannot be considered a lower bound value if the defect is oriented in a direction such that the constraint of the structure increases the amount of plane-strain at the defect location.

Fatigue Crack Growth Rate Data

The fatigue crack growth rate data used in the calculations of allowable defect sizes by NBS was obtained from data published by Maddox⁷ for fatigue crack propagation in carbon-manganese steel weld metal and heat-affected zones. In confirmatory testing done by NBS (see Section 3F), the measured fatigue crack growth rates did not exceed the upper bound of the Maddox data. However, in order to determine the fatigue crack growth rate for a defect growing by fatigue in the through-the-thickness direction, the NBS tests were conducted using relatively small specimens (approximately 1/2 inch square in cross section) so that as the stress intensity range, ΔK , increased, the range of validity for using linear elastic fracture mechanics to calculate ΔK was exceeded. Since all crack growth rate data, da/dN , was determined from compliance calculations, the crack growth rate is overestimated at higher ΔK values due to the nonlinear load-deflection test curve. This has the effect of increasing the slope of the da/dN versus ΔK curve above those measured using larger specimens, as seen in Fig. 23 of Section 3F. However, even when the crack growth rate is artificially elevated due to these small specimens, the maximum crack growth does not exceed the maximum crack growth rate measured by Maddox.

Summary of the Assessment of Materials Properties Data

- (1) A fracture toughness value equivalent to a COD value of 4 mils (for planar defect) and 7 mils (for arc burns) at +10°F as used in calculating the allowable defect size curves are reasonable values.
- (2) Tests with larger sized specimens indicate that a fracture toughness equivalent to a COD value slightly less than 4 mils may apply if the weld metal is sufficiently constrained so that a condition of plane strain can exist. Such a high degree of constraint is unlikely to occur in the thicknesses of metal used in the pipeline.
- (3) The dynamic fracture toughness of the weld metal is sufficiently low that elastic fracture could occur up to temperatures as high as 32°F. However, it is not expected that the loading rates in the pipeline will reach the levels seen in the dynamic fracture testing so that this reduced toughness is not appropriate for evaluating allowable defect sizes in the pipeline. The only other known source of dynamic loading is associated with a fast running crack after "pop-in" such as from an arc burn. This problem has not been evaluated in this report but is not expected to be a significant problem.
- (4) The fatigue crack growth rates used in the calculation of allowable defect size curves are reasonable upper bound values for the weld metals of interest.

- (5) The nominal, rather than minimum, yield strength value of 60 ksi was used in the allowable defect size calculations.

⁷ S. J. Maddox, Welding Journal, pg. 401S-409S, Sept. 1974.

7. FRACTURE ANALYSES

7A. FATIGUE CRACK PROPAGATION

7B. ALLOWABLE DEFECT SIZE ANALYSIS

7C. SENSITIVITY ANALYSIS AND THE USE OF SAFETY FACTORS

7A. FATIGUE-CRACK PROPAGATION

The OPSO requirements, Appendix C, stipulate that surface cracks equal in size to twice the proposed allowable weld-defect or arc-burn size (in both length and depth) must not grow in size such that stressing to the maximum-credible service stress could cause leakage. The crack-growth analysis must account for the cyclic crack growth anticipated during 30 years of operation in the most deleterious service environments and temperatures.

The work reported in this section was undertaken to: (1) independently assess the fatigue-crack growth characteristics of weld defects in the trans-Alaska pipeline, and (2) evaluate the adequacy of the procedures and assumptions used by Alyeska in their assessment of fatigue-crack growth.

Analysis Methods

The NBS fatigue-crack growth analyses were conducted using a computer program developed for the NASA Marshall Space Flight Center.¹ The computer program is based on linear-elastic fracture mechanics and consists primarily of an integration routine that calculates crack growth from an initial defect size to a terminal size -- leakage in this case. The analysis approach used in this investigation was to integrate the Paris equation between the limits of initial flaw size, a_i , and a flaw 95% through the thickness, t :

$$N = \int_{a_i}^{.95t} \frac{da}{C(\Delta K)^n} \quad (1)$$

where C and n are empirical constants that describe the crack-growth behavior of the weld defects under consideration, and ΔK is the stress intensity range calculated as follows:

$$K(\text{at surface}) = [1.12 + 0.11(2a/l)]\sigma\sqrt{\frac{2\pi a^2}{Ql}} \quad (2)$$

$$K(\text{at maximum depth}) = [1 + 0.12(1-a/l)^2]\sigma\sqrt{\frac{\pi a}{Q}} (M_{\text{back}}) \quad (3)$$

$$\Delta K = K\sqrt{T - R} \quad (4)$$

1. M. Creager, "MSFC Crack Growth Analysis Computer Program," NASA CR-143923, September 1975.

$$Q = 1 + 4.593(a/\ell)^{1.65} - 0.212\left(\frac{\Delta\sigma}{\sigma_y}\right)^2 \quad (5)$$

$M_{back} = f(a/t, a/\ell)$ defined in computer program, a = crack depth, ℓ = crack length, $\Delta\sigma$ = stress range, σ_y = 0.2% offset yield strength, and R = stress ratio = $\sigma_{min}/\sigma_{max}$.

The integration of Eq. (1) proceeds incrementally through each step in the fatigue spectrum and continues to repeat the fatigue spectrum until the crack reaches 0.95t. The output of the computer program includes crack-length and crack-depth data at periodic intervals in the fatigue life. These data are plotted as a-vs-N curves, where N is the number of service lifetimes, i.e. number of times the spectrum has been applied.

Fatigue Data

The OPSO requirements state that: "A maximum fatigue crack growth rate for the pipeline shall be established by documenting the fatigue crack growth behavior of the weld metal and heat affected zone that is representative of the pipeline welds and operating conditions and, in the case of arc burns, representative of the base metal. The fatigue crack growth rate used in the fracture mechanics analyses shall be the maximum fatigue growth rate multiplied by an assumed safety factor of four."

The fatigue data used in Eq. (1) were obtained from the open literature, proprietary sources, and the NBS test program. Maddox's² data were used by both NBS and Alyeska for crack growth in a non-aggressive environment. To account for environmental enhancement, NBS used a factor of 10 on Maddox's data and Alyeska used an upper bound of the data obtained by Vosikovsky.³ The Maddox data with a factor of ten provided a conservative upper bound to all the data reviewed by NBS except the data reported by Vosikovsky. The NBS test results on small-scale bend specimens (Section 3F) and large-scale surface flaw specimens (Section 3G) were regarded as sufficient evidence that Vosikovsky's data were not applicable to the trans-Alaska-pipeline welds subjected to a representative current density at a holiday in the corrosion-protection system.

The specific values for C and n in Eq. (1) used in the analyses that follow are summarized below:

2. S. J. Maddox, *Welding Journal*, 4015-4095 (Sept., 1974).
3. O. Vosikovsky, *Closed Loop*, 3-12 (April, 1976).

$$\text{Maddox: } \frac{da}{dN} = 4.94 \times 10^{-10} (\Delta K)^3 \cdot (\text{factor})$$

non-aggressive environment factor = 4

aggressive environment factor = 40.

$$\text{Vosikovsky: } \frac{da}{dN} = 1.56 \times 10^{-5} \Delta K^{.75} \cdot (\text{factor})$$

factor = 4.

Fatigue-Stress Spectra

The OPSO requirements specify that proposed alternative-allowable weld-defect and proposed alternative-allowable arc-burn sizes must be supported by fracture-mechanics analyses using the worst-case fatigue-stress spectrum. An axial-stress spectrum is used for girth-weld flaws and a hoop-stress spectrum is used for arc burns, i.e. the stresses perpendicular to the length dimension of the flaw govern the growth behavior. The spectra employed by Alyeska and by NBS are listed in Table 19.

The worst-case axial spectrum supplied by Alyeska was for 0.462-in thick X-60 pipe operating at 832 psi internal pressure. Subsequently, a spectrum representative of 0.562-in thick X-65 pipe was provided by Alyeska. The differences in axial stresses were considered negligible and the spectrum was not used in the analysis.

The axial spectrum includes all the pressure cycles, thermal cycles and earthquake loadings anticipated during the 30-year life-time of the pipeline. These loadings are superimposed on a pipe-bending stress (tensile in the lower half of the pipe and compressive in the upper half) due to soil settlement that occurs during the first five years of operation. The axial spectrum was given to NBS* in terms of a computer output that included 383 stress excursions in a sequence representing 30 years of anticipated operations. These 383 occurrences were reduced to fatigue cycles using the range-pair counting method described by Dowling.⁴ All cycles with an amplitude less than ± 2 ksi were considered non-damaging and were omitted from the spectrum. Similar occurrences were grouped in the 8-step spectrum shown in Fig. 63. The spectrum included 53 stress cycles, 19 of which were primarily in compression. For analysis purposes, these 19 cycles were treated as zero-to-tension cycles of equal stress range.

The axial stress spectrum used by Alyeska consisted of 151 cycles of zero-to-tension stressing. The significant differences between the Alyeska and the NBS spectra were attributed to the range-pair counting method, which combines stresses in such a way to give fewer cycles and higher amplitudes. The Alyeska approach resulted in a

4. N. E. Dowling, Theoretical and Applied Mechanics Report No. 337, University of Illinois, Urbana (Jan., 1971).

* Provided by Alyeska and described in detail in Section 5.

more conservative spectrum because settlement was treated as a distinct cycle of 0 to 361 MPa (52.4 ksi) instead of a shift in the mean stress. A spectrum severity study, summarized in Fig. 64, was conducted to evaluate the relative severity of the two spectra. The results indicate that the Alyeska spectrum is approximately 25% more severe in terms of predicted life than the NBS spectrum.

A hoop stress spectrum representative of X65 pipe operating at maximum design pressure was used by both NBS and Alyeska. Review of a spectrum that included the lower internal pressures typical of Phase I and II operations (the first 30 months) indicated that the 3-step spectrum was conservative. However, the degree of conservatism has not been established.

Fatigue-Crack Growth: Weld Defects

Several fatigue-crack growth analyses were conducted using the worst-case axial-stress spectrum to independently assess the growth characteristics of weld defects in the trans-Alaska pipeline. The results indicate that cracks up to halfway through the thickness grow 0.001 inch or less in one service life when exposed to a non-aggressive environment as represented by Maddox's data with the required safety factor of 4. In a corrosive environment representative of a holiday in the corrosion protection system, cracks up to halfway through the thickness grow less than 0.010 inch in one service life; Maddox's data with a factor of 40 were used for these calculations. In general, this increment of growth does not noticeably affect the alternative allowable-defect-size curves.

Additional analyses were conducted to evaluate the adequacy of the procedures and assumptions used by Alyeska in their assessment of fatigue-crack growth. The analysis procedures used by NBS and Alyeska are compared in Fig. 65. In this comparison, the Alyeska curve was taken from Part 4 of the Alyeska submittal and the NBS data were generated using the same stress spectrum, fatigue data and thickness. The results indicate that the two analysis methods yield similar results for crack lengths ranging from 50 to 100 mm. The differences in the two methods are attributed to differences in the equations for computing ΔK ; small differences are amplified because growth rate is proportional to the cube of ΔK .

A study of environmental severity was conducted to compare the growth rates computed by Alyeska using Vosikovsky's data with those obtained by NBS using a factor of 10 with Maddox's data. The results, summarized in Fig. 66 indicate that Alyeska's analysis is far more conservative than the NBS analysis. For example, a flaw halfway through the thickness grows 1.2 mm in the Alyeska analysis and the same flaw grows about 0.2 mm in the NBS analysis.

In summary, the NBS growth predictions for weld defects subject to the axial-stress spectrum indicate that growth will be limited to less than 0.010 inch for flaws less than half the thickness in depth. Thus, fatigue is not an important consideration. However, the conservative approach taken by Alyeska can predict substantial growth, e.g. planar flaws analyzed using Vosikovsky's data.

Fatigue-Crack Growth: Arc Burns

Fatigue-crack growth analyses were conducted using the worst-case hoop-stress spectrum to determine the growth characteristics of arc burns in the trans-Alaska pipeline. The results of both the NBS and the Alyeska analyses indicate that substantial fatigue-crack growth occurs in adverse environments.

Comparisons of spectrum severity and analysis methods are shown in Fig. 67. The results indicate that Alyeska's practice of considering all cracks to have infinite length results in only a slight degree of conservatism even though arc burns are generally short. The environmental severity of Alyeska's analysis using Vosikovsky's data results in a 5 mm deep crack growing 2.5 mm in one service life. A similar crack in the NBS analysis grows 1.7 mm.

Since arc burns are generally short, the influence of crack length on fatigue-crack growth was calculated. The results, presented in Fig. 68, indicate that a 5-mm-deep flaw will grow 1.5 mm in a service life when the flaw length is approximately twice the flaw depth and the same flaw will grow 2.5 mm when flaw length is twenty times the flaw depth.

Due to the severity of the hoop-stress spectrum, it may be necessary to consider the actual stresses acting on the location of an arc burn in accordance with OPSO Requirement III. The influence of stress level on fatigue life is summarized in Fig. 69. A 5-mm-deep defect grows 1.7 mm in one service life for the worst-case spectrum (stress factor = 1.0) and the same defect grows 0.5 mm when the stress is reduced to 70%.

Conclusions

1. Fatigue is not an important consideration in establishing alternative allowable weld-defect sizes subject to the pipeline axial-stress spectrum and an environment that causes a tenfold enhancement in fatigue-crack growth rates.

2. Fatigue causes significant growth of cracks subject to the pipeline hoop-stress spectrum and a corrosive environment and must be considered in establishing allowable defect sizes applicable to arc burns.

3. The Alyeska analysis appears to be more conservative than the analysis conducted by NBS, particularly in the area of environment-enhanced fatigue-crack growth.

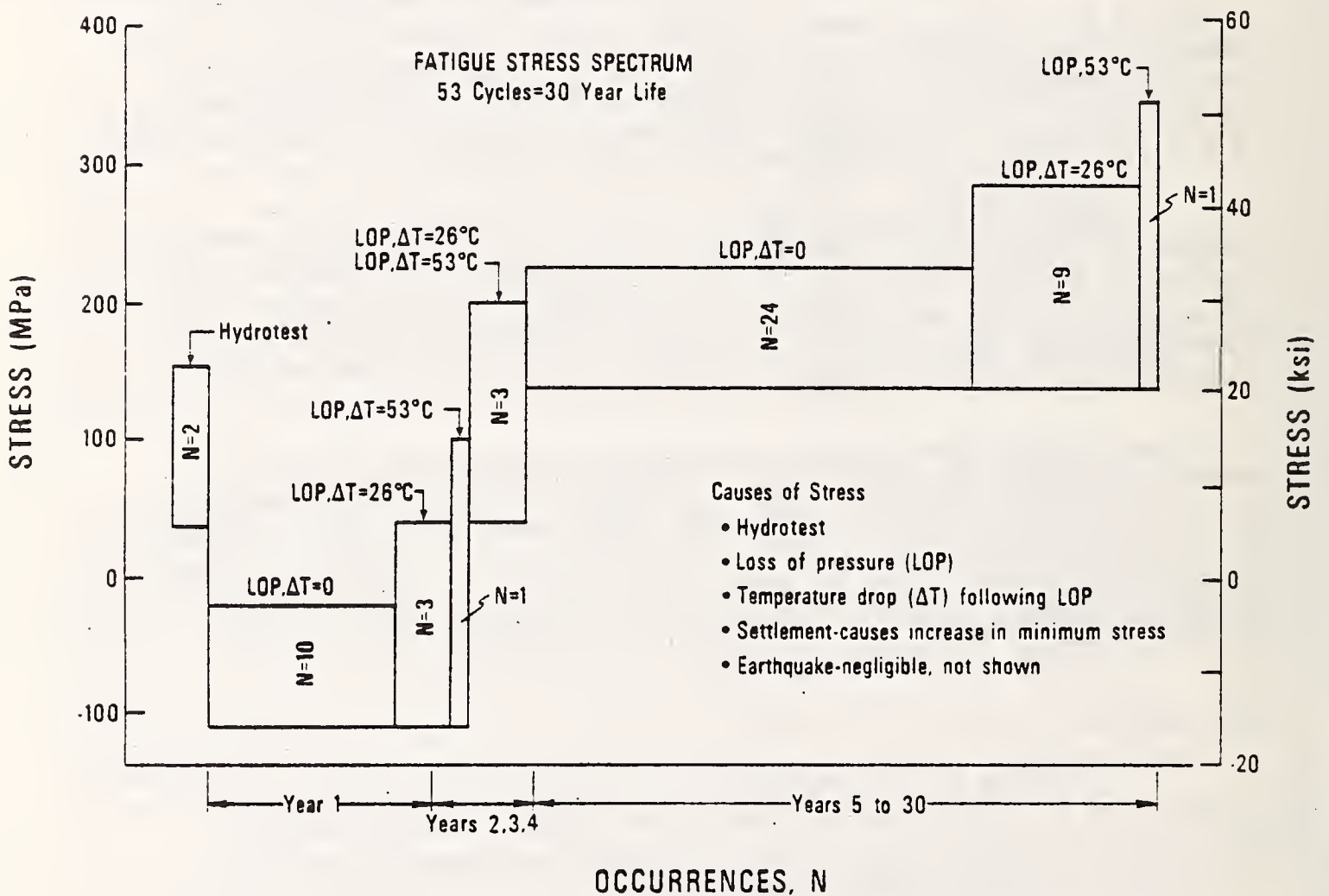


Fig. 63 NBS-derived axial-fatigue stress spectrum.

Table 19. Stress spectra used in fatigue-crack-growth calculations.

Number of Cycles	Minimum Stress (ksi)	Maximum Stress (ksi)
<u>Axial-stress spectrum(NBS)^a</u>		
2	5.3	22.4
10	-16.0	-3.1
3	-16.0	5.9
1	-16.0	14.9
3	5.8	29.4
24	20.4	33.3
9	20.4	12.3
1	20.4	51.2
<u>Axial-stress spectrum(Alyeska)^b</u>		
2	0	17.1
17	0	14.4
59	0	12.97
2	0	9.05
5	0	17.91
15	0	8.86
1	0	52.4
10	0	3.86
10	0	0.96
30	0	0.12
<u>Hoop-stress spectrum^c</u>		
2	0	61.75
17	0	52
59	0	46.8

a. Derived by NBS.

b. From Alaska Pipeline Service Company Report "Fracture Mechanics Study of Buried Field Girth Welds of the Trans-Alaska Pipeline, Part IV."

c. Derived by NBS; used by Alyeska and NBS.

Fig. 64

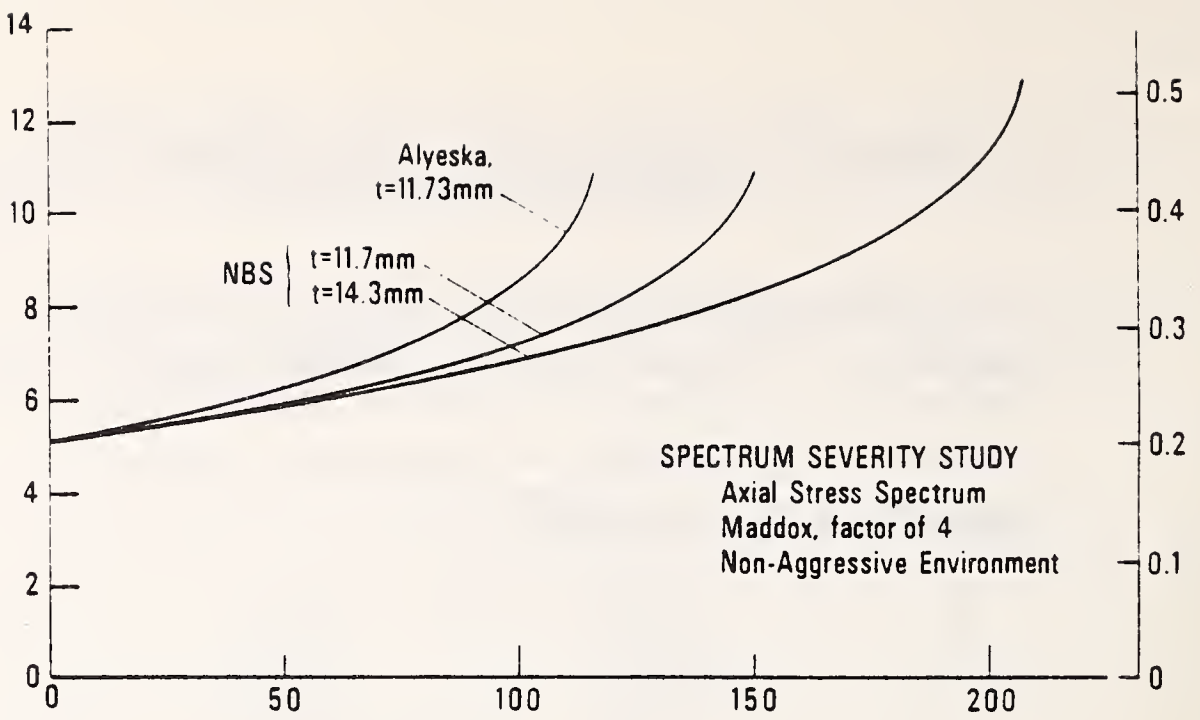


Fig. 65

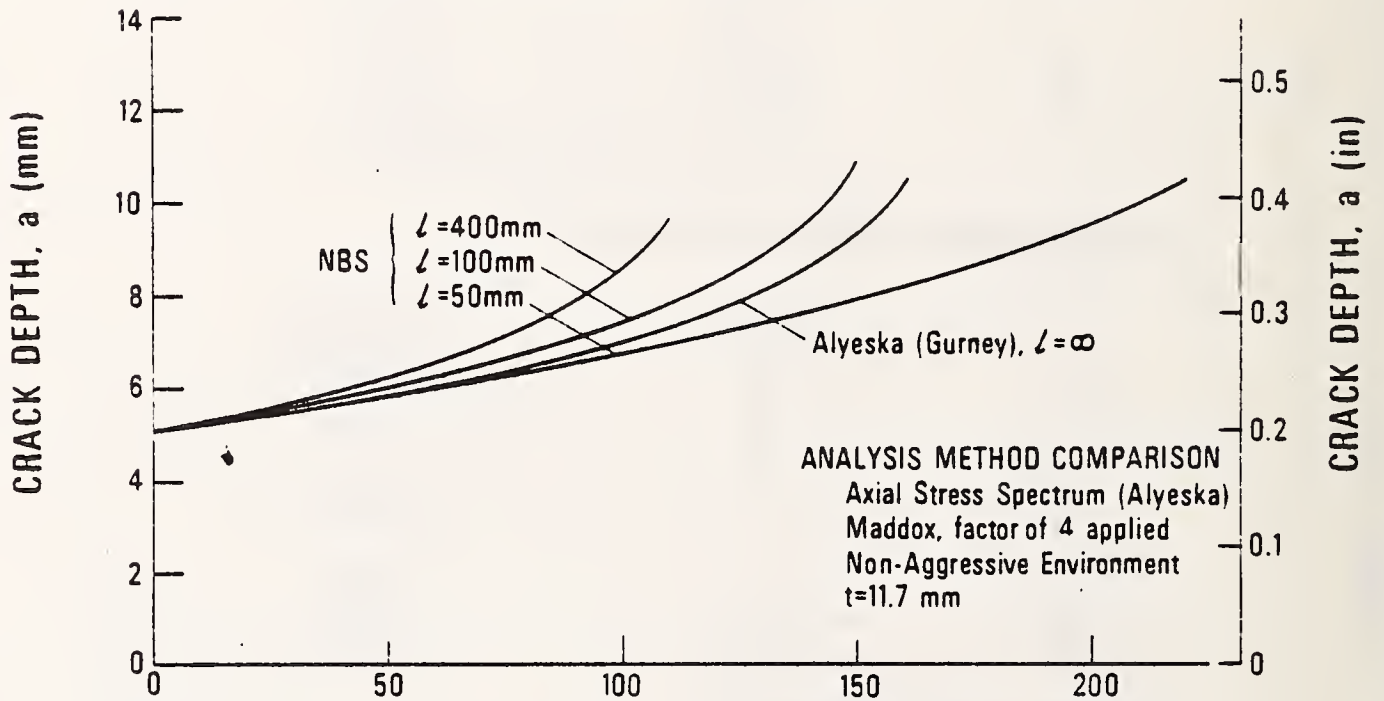
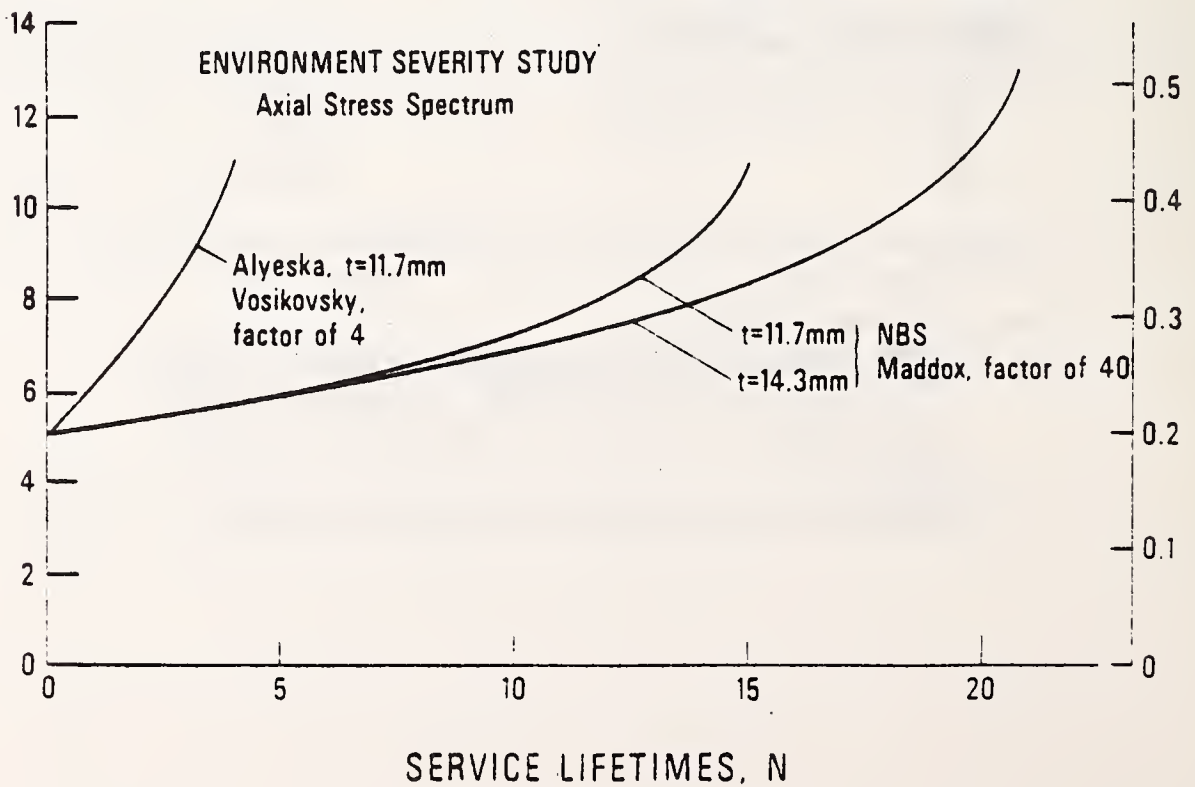
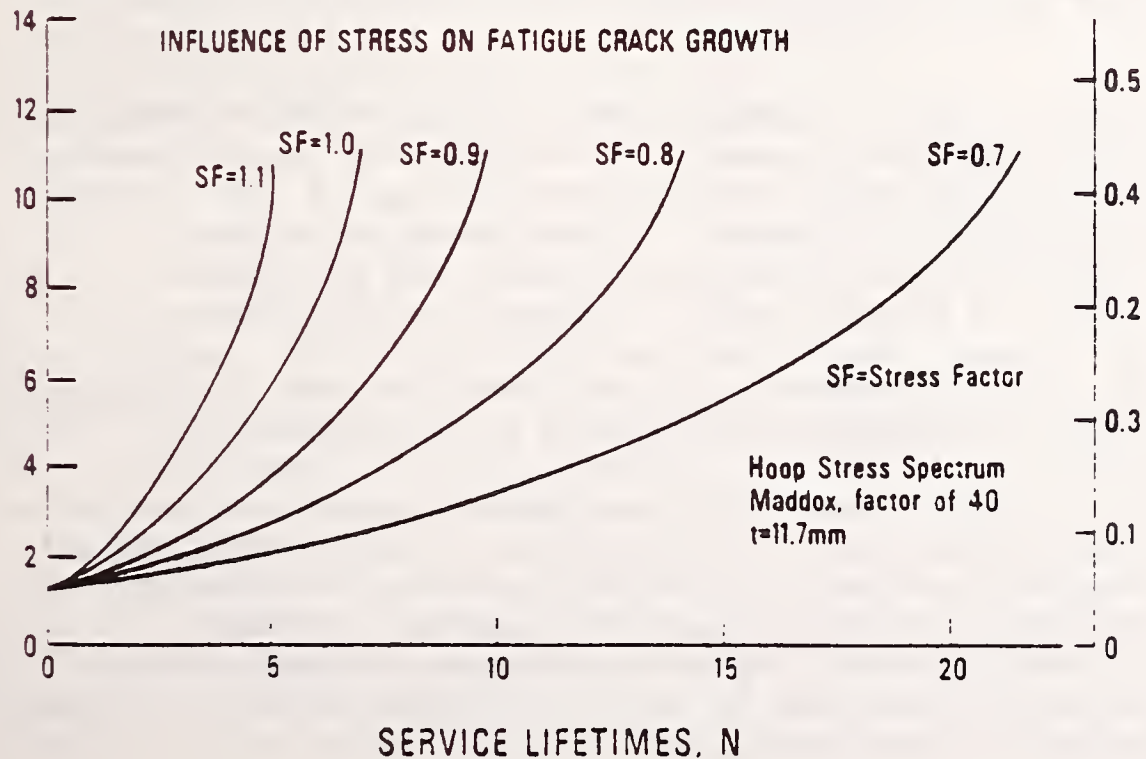
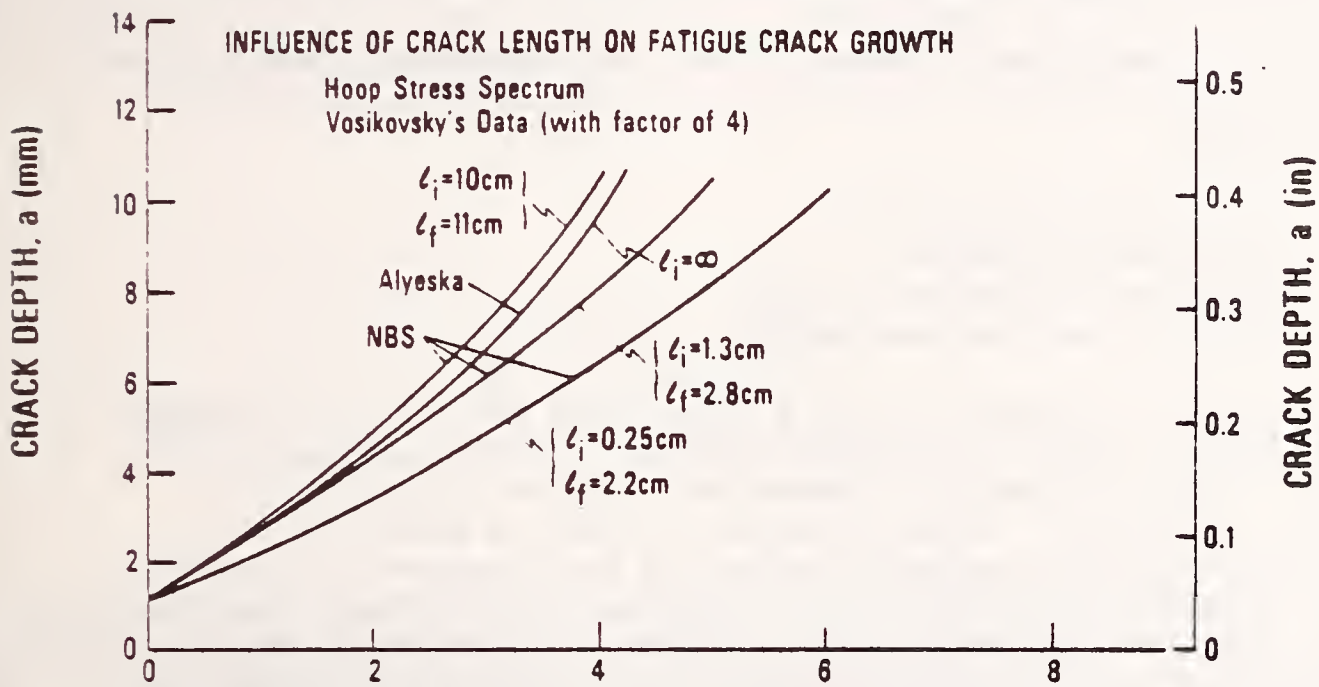
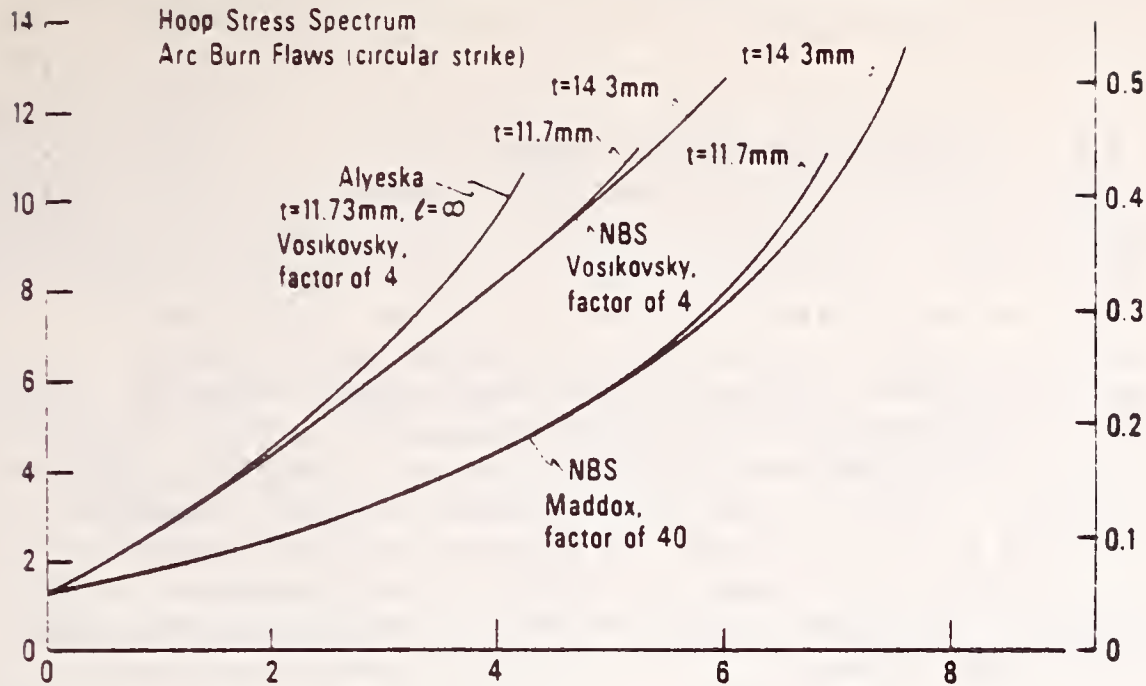


Fig. 66





7.B. ALLOWABLE-DEFECT-SIZE ANALYSIS

1) Introduction

The OPSO notice for anticipated Petition for Waiver states that, "alternative allowable defect sizes should be proposed applicable to each type of defect for which a waiver is being requested. Proposed alternative allowable weld defect and proposed allowable arc burn sizes must be supported by fracture mechanics analysis using the worst case fatigue stress spectrum. For analysis, these defects must be assumed to be surface cracks equal in size to twice the proposed allowable weld defect or arc burn size (in both length and depth). These assumed defects must not grow in size such that stressing to the maximum credible service stress could cause leakage."

In response to these requirements, Alyeska has proposed allowable-defect-size curves applicable to four types of defects for which waivers are being requested:

- Type 1: Non-planar weld defects
- Type 2: Planar weld defects
- Type 3: Arc burns on the weld or HAZ
- Type 4: Arc burns on the base metal

Since all defects are treated as surface cracks, the principal differences in the four types are defect orientation, defect location, and applicable safety factors. Defect orientation determines whether the applicable stresses are axial or hoop. Defect location is used to establish the applicable minimum-fracture-toughness value and the appropriate operating environment (inside or outside the pipe). The applicable safety factors [G-4] include the factor of two on length and depth for all defects plus an additional factor of two on estimated depth (by radiography) of planar defects.

The objective of the work reported in this section is to independently calculate allowable-defect-size curves in accordance with the OPSO notice requirements, and by comparison to evaluate the adequacy of the allowable-defect-size curves proposed by Alyeska. To meet these objectives, calculations of allowable defect sizes were made by NBS consultants (G. R. Irwin of the U. of Maryland and J. A. Begley of Ohio State University) and by McHenry - Read, Fong and Interrante of NBS, and the results were compared with the allowable-defect-size curves submitted to OPSO by Alyeska. Some limited experimental results are also discussed.

This section first describes the Alyeska and other analytic models used to evaluate the Alyeska model. To calculate allowable-defect-sizes from each model requires the use of material-property data representative of the trans-Alaska pipeline; these data are discussed. Following calculations of allowable-defect-size curves, proper assessment of the reasonableness of the Alyeska curve is required. Factors relative to this assessment are detailed in the discussion.

2) Analytic Models

Allowable-defect-size models have been established by Alyeska. Models have also been developed by Begley, McHenry and Read; Fong; Irwin; and Interrante and Kiefner. These approaches are described below.

Alyeska: Alyeska established allowable-defect-size curves by computing a defect-size curve, subtracting the increment of crack growth due to fatigue cycling and then applying the required factors of safety on defect length and depth. A defect-size curve for each type of defect was calculated using the procedures described in the Draft British Standard Rules for Derivation of Acceptance Levels for Defects in Fusion Welded Joints (see Appendix I, Reference I-3). The model is based on an empirical correlation between critical defect sizes and applied stress for through-cracks in welded wide plates. The procedure is to calculate an "allowable-defect parameter" by

$$\bar{a} = \frac{\delta_c}{\sigma_y} \frac{E}{2\pi} \left[\frac{1}{\left(\frac{b + \sigma_R}{\sigma_y} \right) - 0.25} \right] \quad (1)$$

Here the residual stress (σ_R) is assumed equal to the yield stress (σ_y). The maximum credible applied stress is σ . From the ratio \bar{a}/t , and Fig. 14 (applies only when $a/t < 0.5$) of the Draft Standard, several pairs of the two quantities a/t and a/λ are obtained, where a = defect depth, t = thickness and λ = defect length. From these quantities, an a -versus- λ curve can be drawn that the Draft Standard regards as the boundary between the acceptable and rejectable welds. However, in accordance with the notice of Petition for Waiver requirements, each curve (4 types of defects) is subsequently modified by subtracting the increment of crack growth due to fatigue as discussed in the previous section of this report and by applying the required factors of safety on defect length and depth.

Begley, McHenry, Read: Calculations of allowable defect sizes are based on the recommendations of J. A. Begley as described in Appendix B. The model has been adapted to crack opening displacement measurements from a well-known expression regarding the opening of a through-crack under remote tensile stress. In this calculation, a trial defect of a given length and depth is assumed. This defect is allowed to grow over the life of the pipeline by adding calculated increments to the depth and length of the defect for each stress cycle. These increments are computed using the procedures described in the preceding fatigue-crack-growth section of this report (Section 7.A.) The defect is checked

for crack growth through the wall after each stress cycle. If the defect grows through the wall, failure is computed. After all stress cycles of the projected service life have been applied, the maximum credible stress is applied to determine if the critical COD, δ_c , is exceeded. The applied COD is calculated as follows:

$$\delta = \frac{2\lambda}{E} \left(\sigma - \left(1 - \frac{a}{t} \right) \bar{\sigma} \right) \quad (2)$$

Here λ , the effective crack length, is corrected for the plastic zone size, and σ and $\bar{\sigma}$ are the maximum credible applied stress and the minimum credible flow stress respectively. Failure is computed if the applied COD is greater than the critical COD. Residual stress is accounted for by subtracting 0.001 in. from δ_c as recommended by Begley (Appendix B). If the trial defect is computed to fail, its initial depth is decreased and the calculation is repeated until an initial defect depth is reached at which the trial-defect-depth survives. The length and depth of this surviving defect are then plotted; several such points determine the accept-reject curve. The relative position of the curve is strongly dependent on the difference between the applied stress and the flow strength. The use of 70 ksi as the flow stress is considered reasonable based on NBS weld process 102A-1 data and on discussions with Irwin, who developed the equation, and Begley, who recommended its use.

Fong: In order to gain further perspective, a modification of the Begley-McHenry-Read model in the moderately-deep surface crack regime ($0.1 < a/t < 0.5$) is proposed (Appendix P) as an alternative model for the derivation of allowable defect-size curves. The new model is essentially the simultaneous extension of the Begley-McHenry-Read's deep crack model and a shallow crack model due to Begley-Landes-Wilson. As reported by Begley in Appendix B, a shallow crack model ($a/t < 0.1$) for infinitely long surface cracks may be described by:

$$J = E \pi a^* \epsilon_y (2\epsilon - \epsilon_y), \quad \epsilon \geq \epsilon_y \quad (3)$$

where a^* is the effective depth of the surface crack which is related to the critical depth a by:

$$a = \frac{2t}{\pi} \tan^{-1} \left[\frac{\pi a^*}{(1.2)(2t)} \right] \quad (4)$$

The modification consists of introducing a new form of J:

$$J = \lambda E \pi a^* \epsilon_y \left(2\epsilon - \frac{1}{2} \epsilon_y \right), \quad \epsilon \geq \frac{1}{2} \epsilon_y \quad (5)$$

which J is related to the COD by

$$J = m \epsilon \sigma_y$$

The coefficient λ is introduced as a safety factor to insure a no-leak and no-burst condition. The factor of 1/2 is inserted to bring the shallow crack model more in line with the normalized COD design curve than is the case for the original Begley model. A discussion of this model appears in Appendix P.

Irwin: Professor G. R. Irwin of the U. of Maryland, serving as an NBS consultant, has calculated and reported (Appendix D) a set of critical flaw sizes. The calculations are based on a plastic-instability model which features critical ligament strain rather than fracture toughness as a failure criterion. Bulging and curvature (using shell theory) effects are considered in the Irwin analysis, therefore, exterior surface defects are most critical. Buried defects of a given depth can be approximately 30% longer than external surface defects prior to reaching critical size. The increment of crack growth due to fatigue is negligible for the case considered by Irwin, i.e., weld defects subject to axial stress.

Interrante, Kiefner: A series of critical defect sizes were computed by C. Interrante (NBS, Washington) based on the Kiefner equation:¹

$$\sigma = \bar{\sigma} \frac{1 - a/t}{1 - a/tM} \quad (6)$$

$$\text{where } M = \left(1 + 1.255 \frac{c^2}{rt} - 0.0135 \frac{c^4}{r^2 t^2} \right)^{1/2} \quad (7)$$

$c = a/2$ and $r =$ pipe radius. This semi-empirical equation has been developed by Battelle² to model successfully the fracture behavior of longitudinally-oriented defects in full-scale samples of line pipe. Interrante's results, including fatigue and the application of the required factors of safety, are presented only as allowable-defect-size curves of arc burns, representative of longitudinal defects.

-
1. Kiefner, J. F., Maxey, W. A. Eiber, R. J. and Duffy, A. R., ASTM STP (1973), pp. 461-481.
 2. Podlasek, R. J. and Eiber, R. J., Battelle report to Alyeska, 10/9/73.

3) Material-Property Data

The material-property data needed for the analysis include the fracture toughness, the fatigue-crack-growth rate, the stress corrosion threshold, and the tensile properties. Although both 102A-1 and 104A-1 weld process materials were tested, only 102A-1 process defects are presently included in the Alyeska waiver request. The applicable OPSO requirements and the sources of all the data used in the various analyses are reviewed in this section. The values actually used in the analyses are summarized in Table 20. The relationships of these values to the data generated by various programs in support of the trans-Alaska pipeline project are shown in Table 21.

Fracture Toughness: The OPSO notice for the anticipated Petition for Waivers states that: "a minimum fracture toughness value for the pipeline shall be established by documenting the fracture toughness in sufficient notch locations and temperatures for the weld metal and the heat-affected zone that is representative of the pipeline welds and, in the case of arc burns, for the base metal. The toughness value used in the fracture mechanics analyses should be the minimum toughness at 10 °C below the minimum anticipated service temperature."

Alyeska responded to these requirements by submitting fracture-toughness data for nine notch locations in the weld metal, HAZ, and base metal. Tests were conducted at temperatures ranging from -40 to 0 °C using the crack-opening-displacement (COD) method. The temperatures of interest in establishing the allowable-defect-size curves are -12 °C and -22 °C, which correspond to 10 °C below the minimum operating temperature (-2 °C) and 10 °C below the minimum winter start-up temperature, respectively. The toughness values (0.004 in. for non-planar weld defects and 0.007 in. for all other defects) established on the basis of Alyeska's test programs at the British Welding Institute and at Cranfield Institute of Technology were generally used for both the Alyeska and the NBS analyses. These COD values are taken as lower bound values for the toughness at the temperature of interest. However, as discussed in Section 6, a single lower COD value of .002 in. at 0 °F was measured when larger sized COD test specimens were used. The one exception is the case of base-metal toughness applicable to certain arc burns; the Alyeska value of 0.011 in. for COD was not regarded as a well-defined minimum since only one data point was used. Therefore, the Begley, McHenry, Read curve contains a value of 0.007 in. for COD. This value could be justified on the basis of the use of the minimum value of COD at -40 °F, for which the Alyeska submittal contains a number of data points. The 0.004 in. COD value used for non-planar weld defects was confirmed by NBS (see Section 3E), using J-integral test methods and a comparable notch orientation. For weld process 102A-1, the most conservative estimate of COD at 28 °F is 0.0047 in., using $m = 2.0$ in equation 3 (Section 3.E.).

Fatigue-Crack Growth: The requirements for fatigue-crack-growth data and the data used in the analyses are reported in Section 7.A. of this report.

Table 20. Allowable-flaw-size curve parameters.

Source	Material	Type of Defect	Worst Operating Condition	Maximum Stress (ksi)	Temp. (°F)	Critical COD (in)	Yield Strength (ksi)	Flow Strength (ksi)	Young's Modulus (10 ⁶ ksi)	Residual Stress	n	Fatigue Crack Growth C	Fatigue Crack Growth Specimen
<u>Non-Planar Weld Defects, Figure 45</u>													
Alyeska	weld	non-planar	fatigue & extended shut-down	57.7	+10	0.004	65	--	30	$\sigma_R = 65$ ksi	0.75	1.6×10^{-5}	Alyeska Axial
Alyeska	weld	non-planar	winter start-up	20.5	-8	0.002	65	--	30	$\sigma_R = 65$ ksi	0.75	1.6×10^{-5}	Alyeska Axial
EPR	weld	non-planar	fatigue & extended shut-down	57.7	+10	0.004	60	70	30.2	$\epsilon_C = 0.003$ in	3	4.9×10^{-9}	MS Axial
Fort	weld	non-planar	fatigue & extended shut-down	57.7	+10	0.004	65	--	30.2	$\sigma_R = 65$ ksi	3	4.9×10^{-9}	MS Axial
Irwin	weld	non-planar	maximum stress	57	--	--	67	70	--	--	--	--	--
<u>Planar Weld Defects, Figure 46</u>													
Alyeska	weld	planar	fatigue & extended shut-down	57.7	+10	0.007	65	--	30	$\sigma_R = 65$ ksi	0.75	1.6×10^{-5}	Alyeska Axial
EPR	weld	planar	fatigue & extended shut-down	57.7	+10	0.007	60	70	30.2	$\epsilon_C = 0.006$ in	3	4.9×10^{-10}	MS Axial
Fort	weld	planar	fatigue & extended shut-down	57.7	+10	0.007	65	--	30.2	$\sigma_R = 65$ ksi	3	4.9×10^{-10}	MS Axial
Irwin	weld	planar	maximum stress	57	--	--	67	--	--	--	--	--	--
<u>Arc Burns on the Base Metal, Figure 48</u>													
Alyeska	base	planar	fatigue & extended shut-down	52	+10	0.011	65	--	30	$\sigma_R = 65$ ksi	0.75	1.6×10^{-5}	Alyeska Axial
EPR	base	planar	fatigue & extended start-up	52	+10	0.007	65	75	30.1	$\epsilon_C = 0.006$	3	4.9×10^{-9}	Hoop
Fort	base	planar	fatigue & extended shut-down	52	+10	0.007	65	--	30.1	$\sigma_R = 65$ ksi	3	4.9×10^{-9}	MS Axial
Interstate-Kiefner	base	planar	fatigue & extended shut-down	52	--	--	65	75	--	--	--	--	--
<u>Arc Burns on the Weld or HAZ, Figure 47</u>													
Alyeska	weld, HAZ	planar	fatigue & extended shut-down	52	+10	0.007	65	--	30	$\sigma_R = 65$ ksi	0.75	1.6×10^{-5}	Hoop
EPR	weld, HAZ	planar	fatigue & extended shut-down	52	+10	0.007	60	70	30.1	$\epsilon_C = 0.006$ in	3	4.9×10^{-9}	Hoop
Fort	weld, HAZ	planar	fatigue & extended shut-down	52	+10	0.007	65	--	30.1	$\sigma_R = 65$ ksi	3	4.9×10^{-9}	Hoop
Interstate-Kiefner	weld, HAZ	planar	fatigue & extended shut-down	52	--	--	60	70	--	--	--	--	--

177

a. Lowest service temperature less 18°F.
 b. In the Alyeska calculations, the residual stress is added to the maximum stress to correct for residual-stress effects.
 c. In the MS, Boulder calculations, 0.001 in is subtracted from the critical COD to correct for residual stress effects.
 d. Treated using Paris Eq. $da/dN = C(\Delta K)^n$, with ΔK in ksi-in^{1/2}, da/dN in in/cycle, safety factor of 4 not included.
 e. See Table 21.
 f. The thickness of the pipe is t=0.462 inches; its radius is r=48 inches OD. For analyses the fracture strain is taken as 10%.

Table 21. Summary of trans-Alaska-pipeline data for fracture-mechanics analysis.

Property	Conditions	Temp. BMI, (°F) CIT	Alyeska Suppliers	SMRI	NBS	Others	Values Used in Alyeska	Calc. NBS
Tensile								
Young's modulus (10^6 psi)								
base		10	--	--	30.1	--	30.0	30.2
weld		10	--	--	30.2	--	30.0	30.2
weld		-8	--	--	30.3	--	30.0	30.2
Yield strength (a) (10^3 psi)								
base	X65 pipe	10	--	--	80	--	65	65
weld	102A-1, 104A-1	10	--	--	67	--	65	60
weld	102A-1, 104A-1	-8	--	--	68	--	65	60
weld	102A-1, 104A-1	70	--	--	62	--	--	--
Fracture Toughness (b)								
COD base	transverse	10	0.011	--	--	--	0.011	0.007
weld	all notch positions	10	0.004	--	--	--	0.004	0.004
weld	inside surface	10	0.007	--	--	--	0.007	0.007
HAZ		10	0.007	--	--	--	0.007	0.007
J-integral weld + HAZ		-4	--	--	0.004(c)	--	0.004	0.004
Fatigue-Crack Growth Rate, da/dN = C(ΔK)ⁿ								
C, base	aggressive	70	--	--	0.49x10 ^{-8(d)}	0.49x10 ^{-8(f)}	1.6x10 ^{-5(h)}	2x10 ⁻⁸⁽ⁱ⁾
n, base		70	--	--	3	3	.75	3
C, weld	non-aggressive	70	--	--	1.36x10 ^{-6(j)}	0.49x10 ^{-9(g)}	1.6x10 ^{-5(h)}	2x10 ⁻⁹⁽ⁱ⁾
n, weld		70	--	--	3	3	.75	3
C, weld	aggressive	70	--	--	0.49x10 ^{-8(d)}	0.49x10 ^{-8(f)}	1.6x10 ^{-5(h)}	2x10 ⁻⁸⁽ⁱ⁾
n, weld		70	--	--	3	3	.75	3

a. Average values.

b. Minimum values.

c. Converted to C.O.D., see Section 3.E.

d. Upper bound of Maddox data X10 for corrosion effect. NBS data confirms this as a valid upper bound.

e. Upper bound of Maddox data. NBS data confirm this as a valid upper bound.

f. Upper bound of Maddox data.

g. Upper bound of Maddox data X10 for corrosion effect.

h. Upper bound of Vosikovsky data.

i. Includes safety factor of 4.

Sustained-Load Failure: The OPSO notice for the anticipated Petition for Waivers specifies that a minimum threshold for sustained-load failure must be established. Tests conducted by NBS (see Section 3.H. of this report) and by the British Welding Institute for Alyeska indicate that sustained-load failure does not occur in the pipeline welds and base metal for service environments representative of the pipeline.

Tensile Properties: The tensile properties of interest in the analysis are the yield strength, the flow strength and Young's modulus. The flow-strength value for the weld material used is 70 ksi. This was determined by averaging the minimum yield and tensile strengths (see Section 3.D.) at +28 °F, the temperature where the maximum credible stress is applied to the pipeline. From Alyeska data, supplied by Thyssen Stahlunion AG (the supplier of Phoenix Cel 80 electrodes used in the welding process 102A-1) the average flow strength is 83 ksi with a two standard deviation (2σ) value of 7.8 percent. Since in the models the use of a low flow strength is conservative, and since the Alyeska and Begley, McHenry and Read models are very sensitive to flow strength (see Section 7.C.), the lower NBS-determined weld flow strength was used; a reasonable estimate of the possible variations of this flow strength is $\pm 7.8\%$. The base metal flow strength used is 75 ksi, which corresponds to grade x 65 pipe.

4) Calculations from Models and Comparison with Experimental Results

The alternative allowable-defect-size curves submitted by Alyeska and calculated on the Begley-McHenry-Read, Fong, Irwin and Interrante-Kiefner models are summarized in Figs. 70-73. The material property data used to develop the curves are shown in Table 20. Since the various models are based on differing physical pictures and approximations, material property data were used which reflect the requirements and analyses on which the models were based, and on the various safety factors and requirements specified by OPSO. For example, with the minor exceptions noted in Table 20, all the analyses used maximum credible stresses of 57.7 ksi for weld defects and 52 ksi for arc burns. It is apparent from the curves that the different models predict quite different results in some of the regimes of interest, and the implications of these differences are discussed in Subsection 5.

Unfortunately, there are only limited large scale test data available to assist in the substantiation of the analytical models. Fig. 74 displays the actual data from the limited experiments available with the predictions of the models plotted without the OPSO safety factors. Included in Fig. 74 are the NBS data obtained from simulated-service fatigue tests with subsequent stressing to failure. It also includes data from Irwin, Krishna, Yen³ low cycle, flat-plate fatigue tests with flaws transverse to the load axis, stressed to failure or to a chosen maximum stress greater than 60 ksi. NBS specimens failed at stresses higher than the maximum credible operating stress used in the above model calculations (57.7 ksi for weld defects and 52 ksi for arc burns). The observed Irwin, Krishna, Yen defect range represents specimen defect dimensions that failed at applied stresses greater than 60 ksi or were stressed to 60 ksi or more without failure. Since the maximum stresses for these data were larger than the applied stresses used in the model calculations, the data are not precisely comparable to the calculated allowable defect size curves.

Unfortunately, however, we do not believe these results provide adequate information in the region of main interest, where $a \approx 0.15"$, $2 \approx 6"$ on Fig. 74. In order for the model to be fully verified, many more data are needed.

5) Discussion

The purpose of this study is to develop as much independent information as possible in order that DOT may make a judgement regarding the proposed Alyeska allowable-defect size curve. In subsections 3 and 4 of this section, we have developed a number of independent models and reviewed the limited experimental evidence available. In section 7C a discussion will be presented of how sensitive the results of the various curves are for nominal variations in the materials properties and stress parameters.

3. Irwin, G. R., Krishna, V. C., and Yen, B. T., "Flat-Plate Testing of Part-Through Cracks in Line-Pipe Steel Plates," Fritz Engineering Laboratory Report No. 373.1, Lehigh University, March 1972.

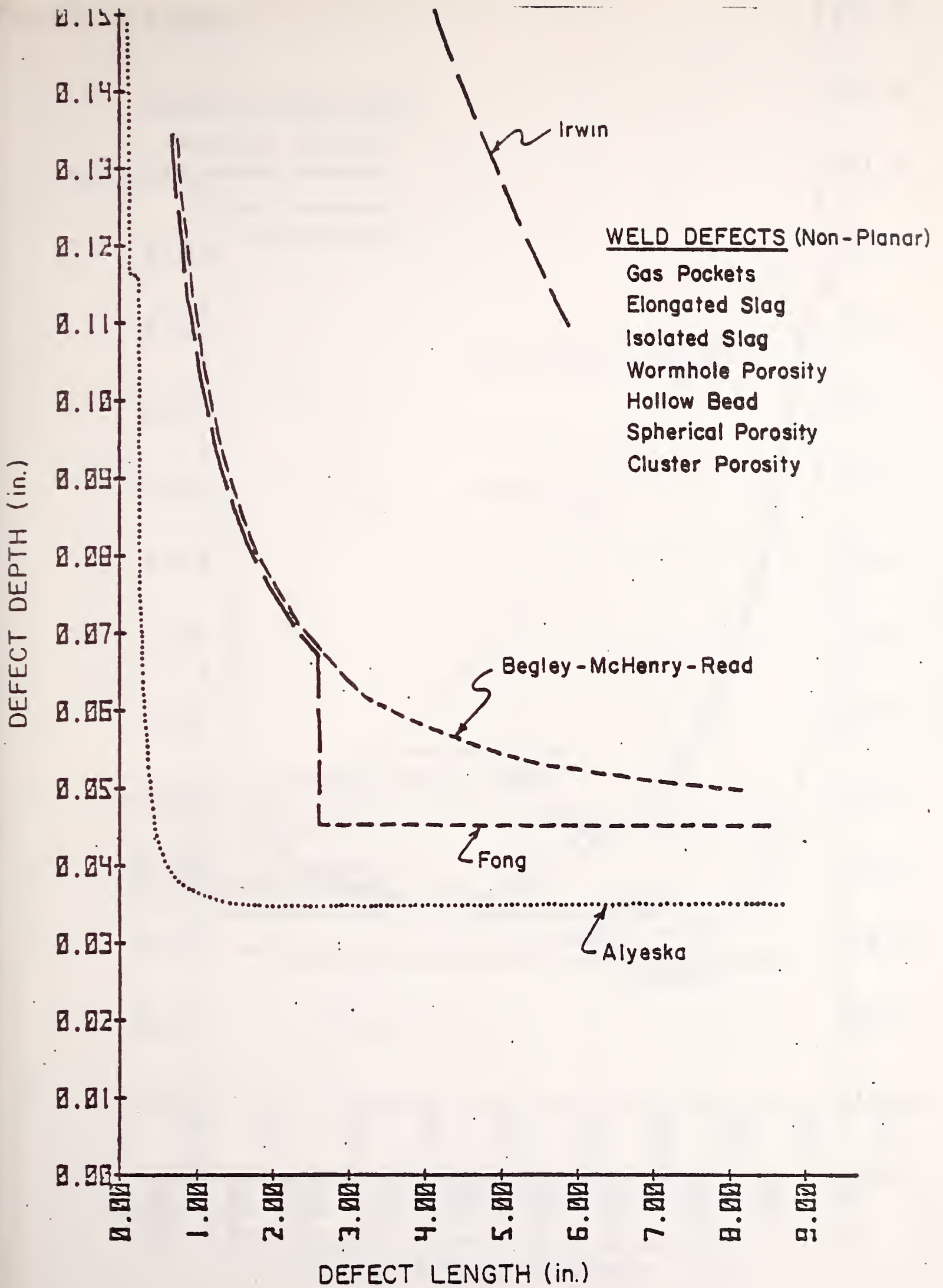


Fig. 70. Allowable defect sizes for non-planar weld defects

WELD DEFECTS (Planar)

- Incomplete Penetration
- Incomplete Penetration (Hi / Lo)
- Incomplete Fusion
- Crater Cracks

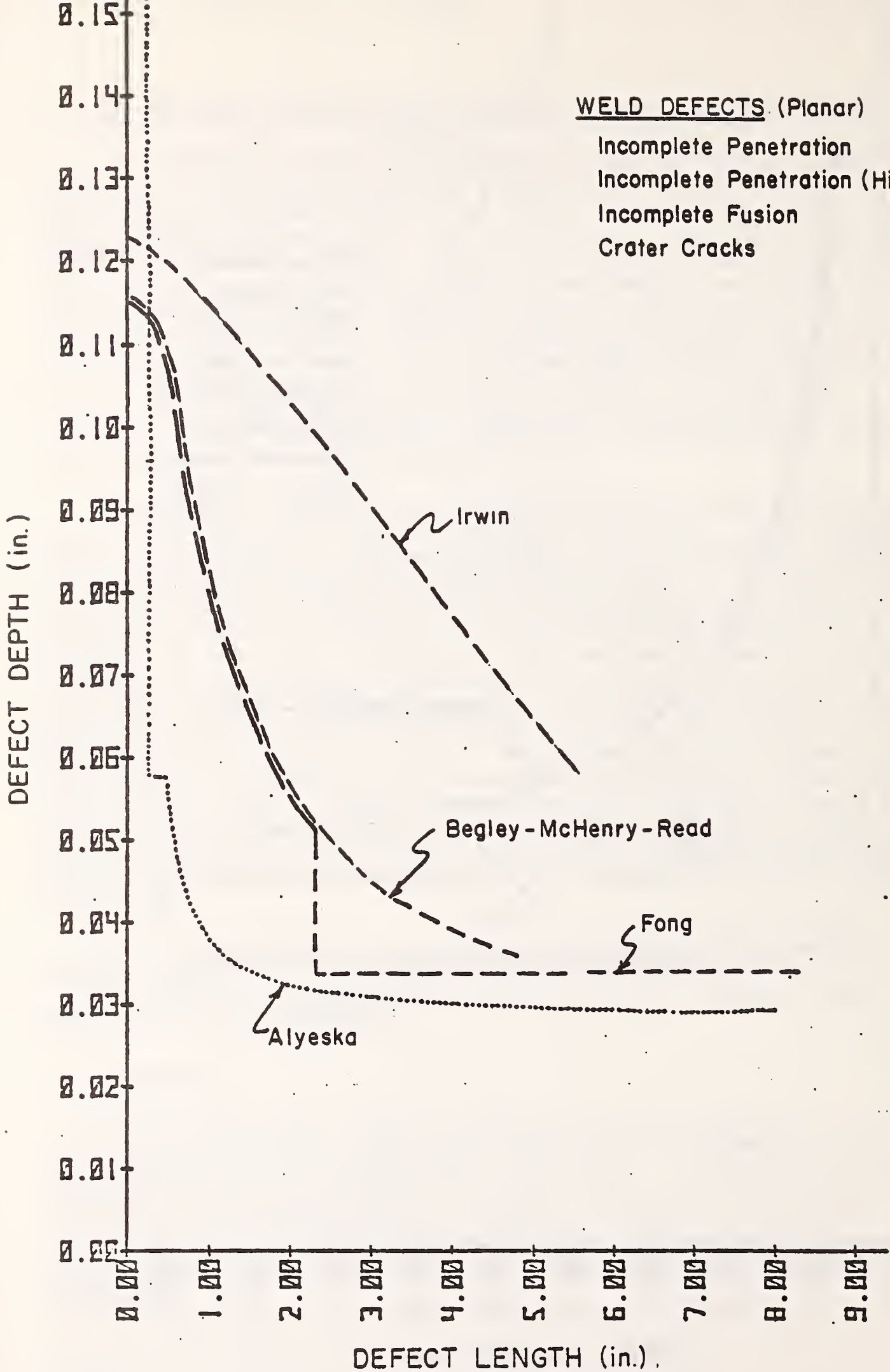


Fig. 71. Allowable defect sizes for planar weld defects.

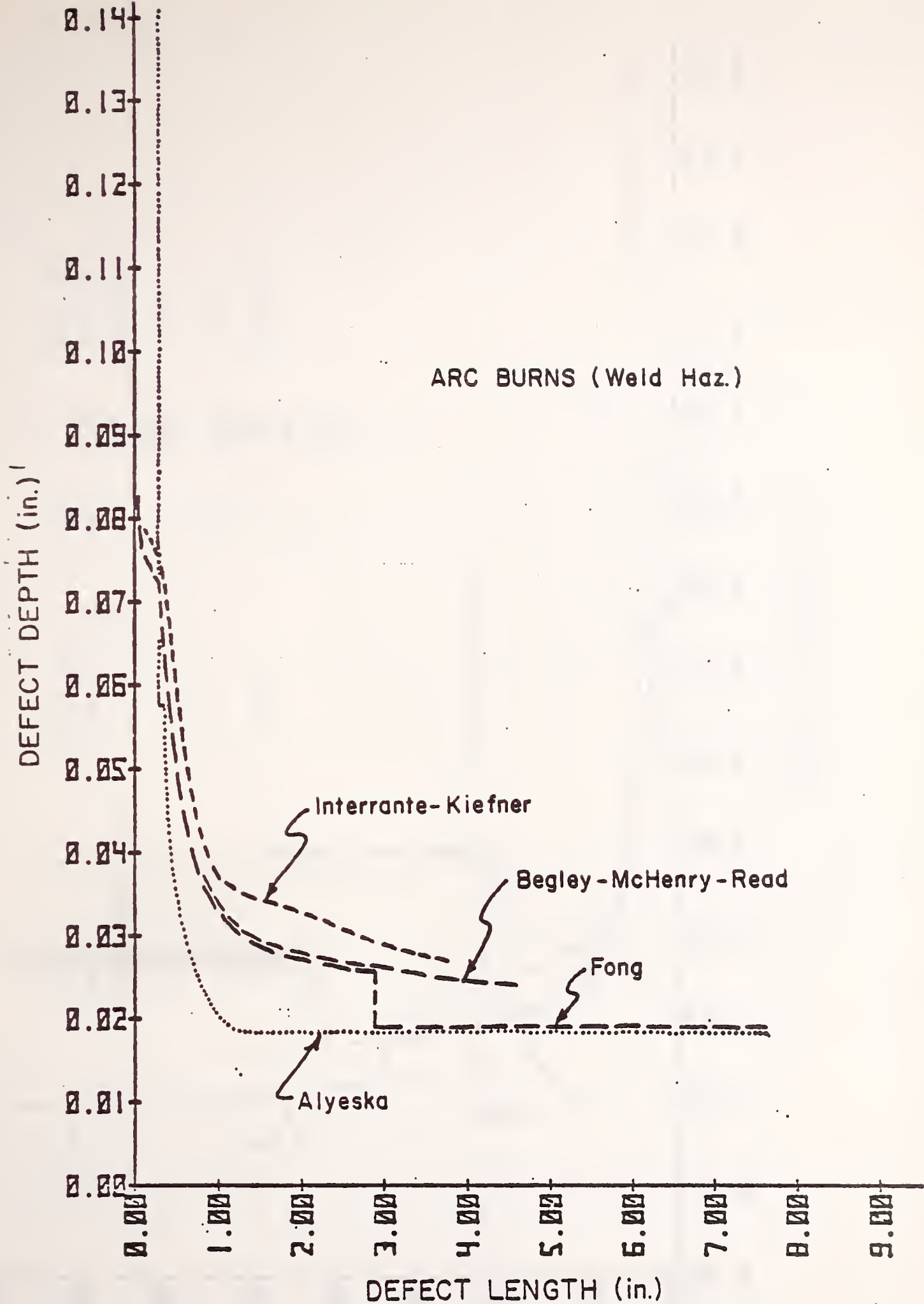


Fig. 72 Allowable defect sizes for arc burns (weld, HAZ).
See Appendix 0 for expanded scale curves

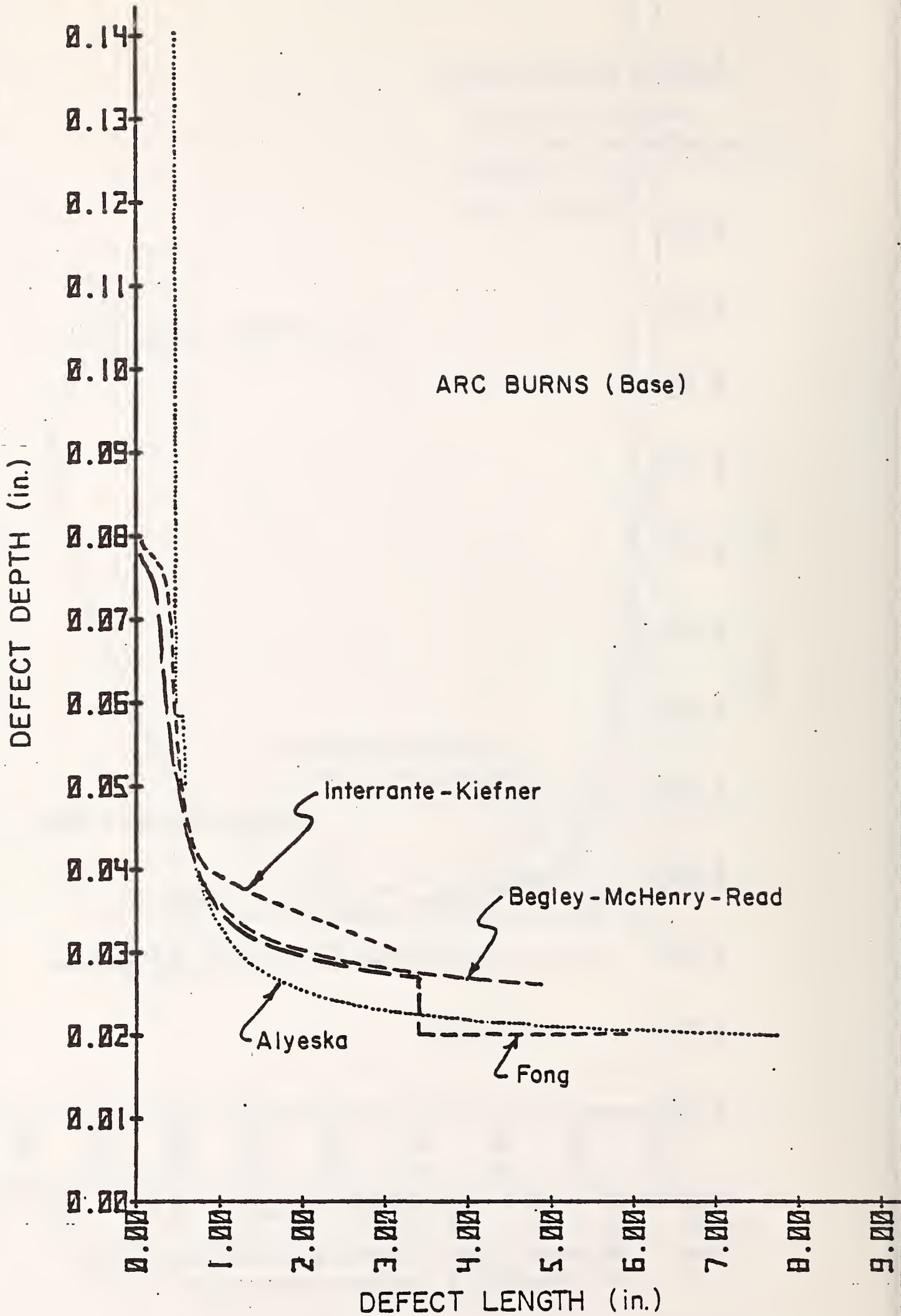


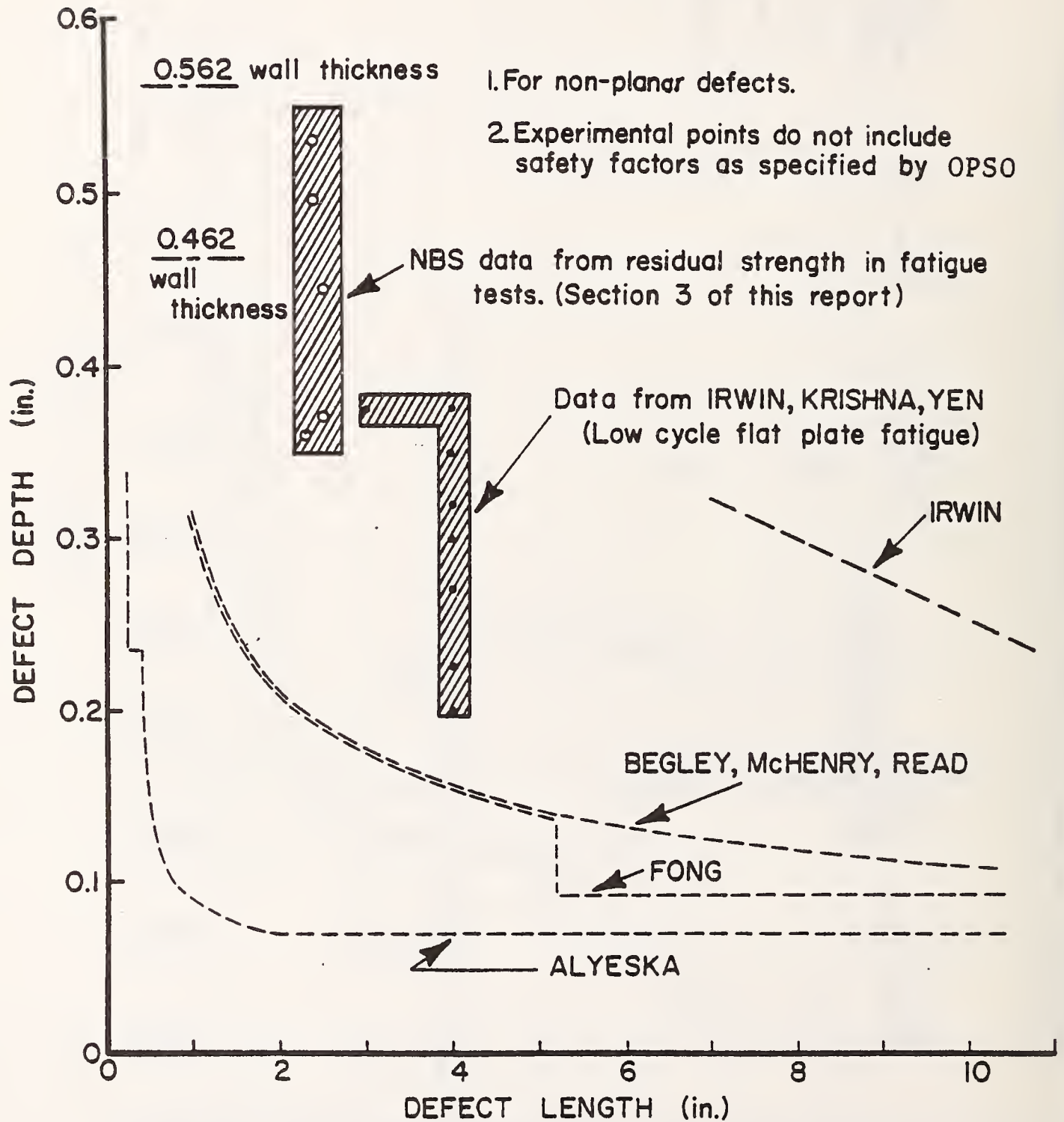
Fig. 73 Allowable defect sizes for arc burns (base).
See Appendix 0 for expanded scale curves.

Table 22. Calculated critical flaw sizes at very long defect lengths

Model	Applied stress (ksi)	Crack opening displacement (in.)	Residual stress (ksi)	Flow stress (ksi)	Critical defect depth (in.)
Alyeska	57.7	.004	65	--	.036
BMR	57.7	--	--	70	.040
Fong ^a	57.7	.004	65	--	=0.0460

^a Length of defect limited to a maximum of 15 in. (see Appendix P).

Fig. 74 Comparison of experimental results with analytic models for part-through cracked specimens.



The first point to be emphasized is that the attempt in our report to reduce the failure problem to a rational analysis does not supercede the use of common sense in quality control during the welding process. In particular, when by visual inspection, a weld does not meet normal welding practice, the weld should be replaced without further question. Our assumptions on material property variability, for example, only apply to good quality material with the natural variability associated with good practice and normal standards of quality. They would not apply to a visibly substandard welding procedure.

The failure problem can be broken into several categories:

- 1) Failure by elastic fracture
- 2) Failure of the ligament
- 3) Failure by plastic fracture

1) Failure by Elastic Fracture

Elastic fracture mechanics provides a relatively well established analytic basis for the three dimensional problem of an elliptical surface crack. For an allowable-defect-size curve, calculated on the basis of elastic fracture weakness, to equal the curve shown by Aleyka, the fracture toughness of the material would have to be about 25 ksi $\sqrt{\text{in.}}$. This is well below even the fracture toughness measured (under dynamic loading conditions) where elastic fracture did occur.

However, if defect sizes can only be measured with a factor of n, and n is used as a safety factor to account for this uncertainty, then the required K_{IC} could be increased by a factor of n^2 . For example, if n is 2, K_{IC} would have to be 100 ksi $\sqrt{\text{in.}}$ instead of 25 ksi $\sqrt{\text{in.}}$ to account for uncertainties in the measured crack length.

2) Failure of the Ligament

In a two dimensional specimen, as a crack grows through the specimen the entire load must be taken up by the remaining "ligament". As the ligament continues to narrow, the stress in the ligament increases, and failure will ultimately occur. In our notation, this condition is written

$$\sigma_u \leq \frac{\sigma}{1-a/t} \quad (8)$$

where σ_u is the ultimate tensile strength of the material. For the nominal operating stress, $\sigma = 57.7$, and $\sigma_u = 80$ ksi, this condition is satisfied for a/t well above the asymptote of the Aleyka curve. The condition is however, very sensitive to variations in the material parameter σ_u , and to the applied stress. However, for the ranges suggested in 7C, the values of a/t fall on the Aleyka curve at long defect lengths.

The failure of a ligament (in two dimensions) might occur for a defect whose COD is too large for the fracture criterion to be satisfied. However, in three dimensions (for lengths small compared to the total pipe diameter) the stress in the ligament will not grow as suggested by Eqn. (8), but the ligament will be partially supported by the rigidity of the pipe beyond the defect length. (See Appendix P).

Hence, because the lower bound of the sensitivity band (Section 7C) falls at the Alyeska asymptotic value, and because of the three dimensional constraints, the Alyeska curve seems reasonable relative to simple ligament failure.

3) Failure by Plastic Fracture

Two dimensional fracture criteria form a special case, because they give a lower bound to the failure criterion -- the asymptotes of the curves of Fig. 70-73.

Where the entire structure is loaded beyond yield, then the model of Begley (Eqn. B-12) applies. Fong's model (Appendix P), and the Alyeska asymptotic expression are all closely related to the Begley model (Eqn. B-12) and are based on similar physical ideas. However, safety factors and residual stress are handled somewhat differently in these models. They all show a relatively minor sensitivity to parameter variability.

When conditions are such that the plastic zone of the crack is small compared to the pipe thickness, then the elastic case already mentioned applies.

In the intermediate case, where $\sigma < \sigma_y$, but where the plastic zone covers the entire ligament, we do not have an adequate model, even though the models of Begley (Eqn. B-12) and Alyeska have been extended empirically into that region as discussed by Merkle.⁴ Various theoretical formulations of this problem have been made, but have not been applied specifically to this problem. By estimating the plastic zone size in a rough way, and taking the average plastic strain in the ligament to be related to the stress from the stress-strain curve, again in two dimensions, an estimate (albeit crude) of failure can be made. We find an expression for the critical defect depth to be

$$a = \frac{F\delta}{2 \left(\sigma - \sigma_y \left(1 - \frac{F}{E} \right) \right) + \frac{F\delta}{t}} \quad (9)$$

F is the linear hardening coefficient defined by

$$\sigma = E\epsilon_y + F(\epsilon - \epsilon_y) \quad (10)$$

4. Merkle, J. G., "Analytical Relations Between Elastic-Plastic Fracture Criteria", *Int. J. Pres. Ves. & Piping*, 4, pp. 197-206 (1976).

From this, with the parameters $\sigma = 57.7$, $\sigma_y = 60$, $F = 3 \times 10^5$, $\delta = .003$ ", $t = 0.462$ ", we find $a \cong 0.1$, which with usual safety factor of 2, becomes about 0.05". Although this is a value above the asymptotic value given by the Alyeska curve, it is very sensitive to small variations in the materials properties and stress parameters.

The Begly-McHenry-Read model was developed independently of the Alyeska model and is a reasonable expression of the present state of analytical development. This model is, however, very sensitive to the values of the parameters, especially for intermediate and long cracks, as shown in Fig. 75.

In summarizing the above discussion, clearly it is not possible to present an allowable-defect-size curve which has a satisfactory quantitative theoretical basis. Each of the models are presented as estimates of reasonable allowable-defect-sizes, and, except for Irwin's model, are not based on a sophisticated theory.

In particular, the great sensitivity to variations in operating and material parameters of some of the models is noted. We have not been able to come to a clear conclusion that this sensitivity is "real", or whether it is an artifact introduced in the models. On the one hand, it seems that the large sensitivity, when it appears, is connected with assumptions about how to estimate the stress in the ligament. As shown in Appendix P a proper three dimensional treatment will lower this ligament stress, and consequently lower the sensitivity. Such calculations have not been carried out, therefore, a clear answer to the problem is impossible. On the other hand, we find that the sensitivity is also related to the very high stress assumed in the pipe in relation to the yield stress. Since the models are all sensitive to the cross-over from elastic-plastic to fully plastic conditions, such sensitivity would be expected to remain "real" in an adequate model, although it might be smaller. It is then a matter of engineering judgement whether the Alyeska curve remains a reasonable allowable-defect-size curve in view of its built-in safety factors, and in spite of the modest overlap between it and the sensitivity band of the Begly-McHenry-Read curve. It is the general opinion at NBS that the Alyeska curve is a reasonable one (except for very short defects -- see below). This conclusion includes those aspects of the problem involving fracture mechanics and materials properties, and does not include considerations of uncertainties in the estimate of operating stresses and in the measurement of defect sizes.

In parallel with the limitations in the models, there is an inadequate base of large scale testing to complement the analysis. Experimental results from the NBS and Alyeska test programs were principally designed to obtain material property data.

In addition to the above general conclusions, we make the following detailed comments relative to Figures 70-73.

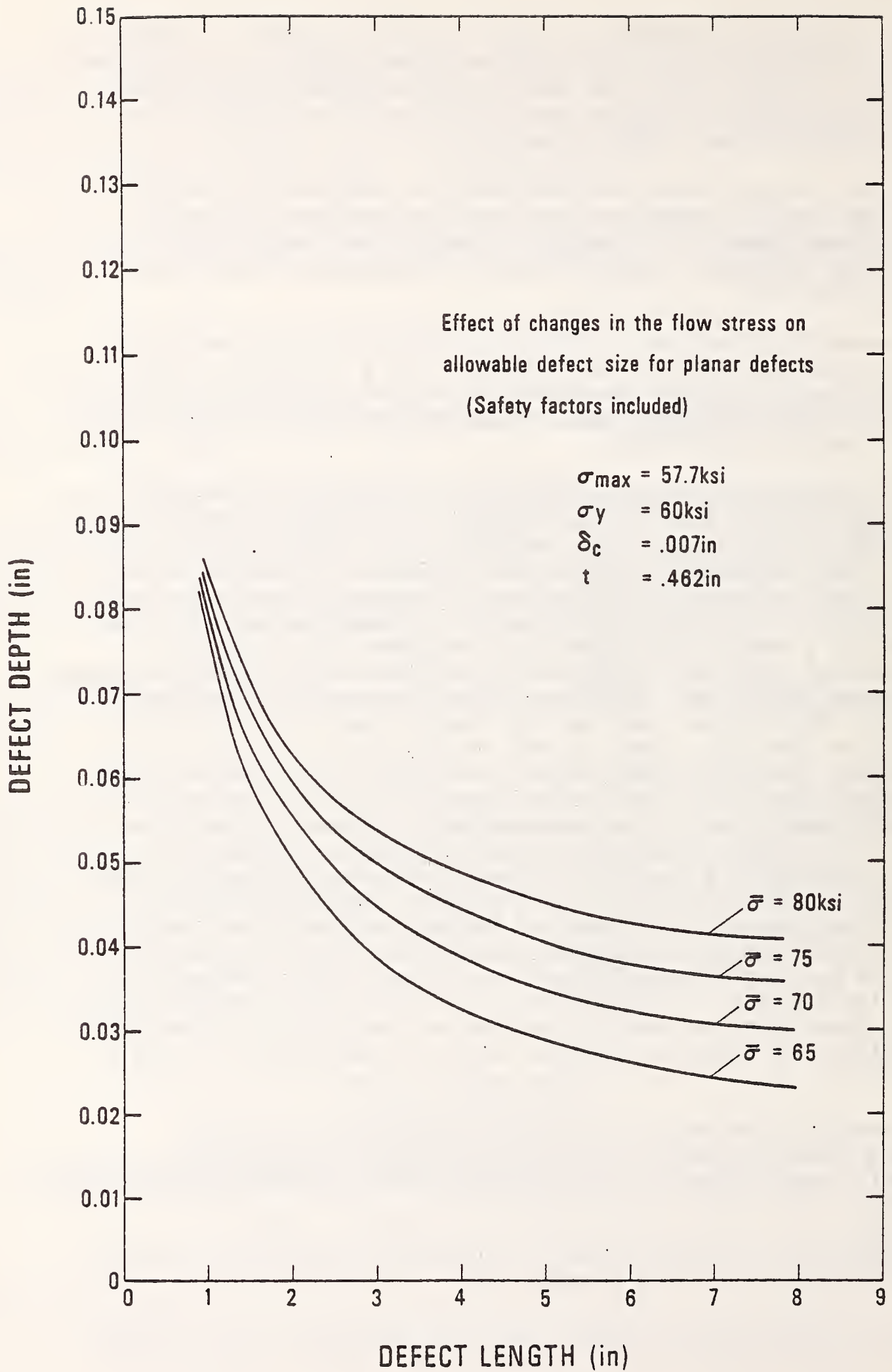


Fig. 75. Effect of changes in the flow stress on allowable defect size for planar defects (safety factors included).

For non-planar defects (Fig. 70) the Alyeska curves seem reasonable. For planar defects (Fig. 71) and for arc burns (Fig. 72) the Alyeska curves also seem reasonable, except for very deep cracks with lengths less than approximately 0.5 inches. In this region, all the curves except that of Alyeska intersect the depth axis at depths between 0.08 and 0.13 inches, while the Alyeska curves show tolerance for unlimited defect depth. This deviation is principally caused by the use of only fracture criteria in the draft British Standards, while the other models consider leakage as well as fracture criteria. In all regions where defect depths on the Alyeska curve are above any of the Begley, McHenry, Read, Fong, Irwin or Interrante, Kiefner curves, the Alyeska curve is then not considered conservative with respect to pipeline leakage. Arc burns on the base material (Fig. 73) constitute a special case. Alyeska, Begley, McHenry, Read, and Interrante, Keifner show close agreement, except at small defect lengths. Therefore, the Alyeska curve is considered reasonable, except for short lengths (< 0.5 in.) where the other curves are more conservative. For lengths shorter than the point where the Alyeska curve rises nearly vertically (Fig. 73) the Alyeska curve is not conservative. For longer lengths the curves are all in general agreement, and the Alyeska curve is reasonable.

Summary Conclusions

The following conclusions include those aspects of the problem involving fracture mechanics and materials properties, and do not include considerations of uncertainties in the estimate of operating stress and in the measurement of defect sizes.

1. The allowable-defect-size curve submitted by Alyeska for non-planar defects (Fig. 70) is considered reasonable.
2. The allowable-defect-size curves submitted by Alyeska for planar (Fig. 71) and arc burn defects (Fig. 72 and 73) are considered reasonable, except for the region of small defect lengths, where the other model curves fall below the Alyeska curve.
3. Through the generation of allowable-defect-size curves, fracture mechanics is a procedure which can be used as a basis for making decisions in accordance with the OPSO notice for anticipated Petition for Waiver requirements. This report indicates that when a more definitive theoretical analysis is available and is supported by adequate experimental studies, a high degree of confidence will be possible in delineating acceptable from unacceptable defects. There are also indications from the work of Irwin that such a study might conceivably lead to a technical basis for less stringent requirements on allowable defect sizes.

7C. SENSITIVITY ANALYSIS AND THE USE OF SAFETY FACTORS

1. Introduction

In addition to specifying the use of both (a) worst case load combinations and (b) minimum material resistance parameters, in fracture mechanics analyses for supporting any weld defect waiver request, OPSO further stipulated [G-4] that:

" . . . these defects must be assumed to be surface cracks equal in size to twice the proposed allowable weld defect or arc burn size (in both length and depth)."

This implies that safety factors of 2 on both defect length and depth were in effect adopted by OPSO in order to cover all uncertainties in design, stress analysis, acquisition and interpretation of laboratory data, inaccuracies in defect sizes, and the use of simplifying assumptions in modeling the fracture behavior of girth welds. For planar defects, OPSO imposes an additional factor of 2 on defect depth because of uncertainty in radiographic estimation of depth.

In deriving the allowable-defect-size curves as shown in the last section, NBS has followed OPSO's choice of defect size safety factors and its guidelines on material properties and stresses. However, during the course of investigation it became necessary to choose additional safety factors or adjustment constants to cover uncertainties in a variety of technical areas. The purpose of this section is to point out the importance of the role of safety factors, whether imposed by OPSO or used by NBS. As observed by participants in an NBS meeting on Safety Factors¹, the choice of safety or adjustment factors is never arbitrary. We present in the following (a) a listing of some important variables in our analysis with variabilities large enough to be worthy of concern, (b) a sensitivity analysis of the allowable-defect-size curves to indicate how the curves may shift under reasonable variation of some of the variables listed in (a), and (c) a listing of additional safety factors or adjustment constants NBS had to introduce to accomplish its contractual objective as stated in reference [G-5].

2. Significance of Variables Included in NBS Analysis

A rational basis for conducting a technical analysis of an engineering problem lies not only in the choice of "relevant" variables for inclusion in the analysis, but also in judging which variable cannot be analyzed for the purpose at hand and how the significance of that variable can be accounted for through the use of an appropriate safety factor. In a real-life project such as the construction of the trans-Alaska Oil Pipeline,

¹ See Appendix M for a summary of the proceedings of a one-day meeting on safety factors held at NBS-Gaithersburg on September 28, 1976.

the number of variables can be so high that any analysis, no matter how careful and complete, may leave out some variables which eventually may prove to be significant. The objective of this section is to show which variables in the NBS analysis are sufficiently significant to motivate a sensitivity analysis, and which ones are important and accounted for through the use of safety factors. The first part leads naturally to sub-section 3 where a sensitivity analysis is documented in detail, and the second part motivates a discussion in sub-section 4 where some of the important safety factors or adjustment constants used by NBS are described.

To begin with, we observe that the following variables are significant enough to deserve a sensitivity study:

- 1) Applied stress (credible variation on worst case: +5%)
- 2) Yield or flow stress (credible variation: $\pm 10\%$)
- 3) Fracture toughness (credible variation on minimum value: -10%)
- 4) Defect length or depth (acceptable criterion as a dependent variable: -50% max.)
- 5) Residual stress (credible variation: same as for yield stress)

There are a number of variables which are known to be significant for the technical problem at hand but are treated in a different way in the NBS analysis because there is not enough data in the literature to support a rigorous analysis within the time constraint of this project. The way to account for them is through the use of safety factors. Aside from those variables on defect size measurements which have been discussed in section 4, the list of variables covered by safety factors may be subdivided into four categories as follows:

Category No. 1: Materials Properties: All of our tests were conducted without the superposition of a biaxial stress state. It is, of course, known that the girth weld is subjected both to a longitudinal stress and a hoop stress, and it is also known that fatigue and fracture resistance of a material is influenced by the existence of a biaxial stress state².

Category No. 2: Stress Analysis: The placement of 62 remotely operated valves, 71 check valves and 9 check and manual block valve combinations along the 800-mile pipeline made the task of hydraulic analysis exceedingly complex, particularly when extreme loading conditions such as the shut-down of a

² See, e.g., Kibler, J. J., and Roberts, R., J. Eng. for INdustry, Trans. ASME, (Nov. 1970), pp. 727-734; Roberts, R., and Pothiraj, S., 2nd Int. Conf. Struct. Mech. React. Tech., Berlin, Sept. 1973, Vol. V - Paper L 8/3; Brown, M. W., and Miller, K. J., Proc. Inst. Mech. Engrs. (UK), 187, 745, (1973); and Zamrik, S., and Shabara, M. A., ASME Preprint 76-PVP-37, presented at Int. J. Conf. Petroleum Mech. Eng. and Pressure Ves. & Piping, Mexico City, Sept. 1976.

pumping station are investigated. Since check valves are designed to close instantaneously when a reverse flow is experienced, the possibility of hydraulic transients is increased when more check valves are installed as in this case of the Alaska pipeline. Two facts may be of interest for future consideration: (a) a comparable oil pipeline, also 48 in. O.D., the trans-Alpine pipeline, which has been in operation for many years, has not a single check valve along its route over mountains and terrains not unlike those in Alaska; and (b) the hydraulic analysis of the trans-Alaska pipeline was completed assuming a mathematical model where the presence of all check valves is ignored. An assessment of the surge analysis was not required of NBS by DOT, and was not attempted.

Category No. 3: Sampling Problem: The selection of welds for laboratory testing was carried out by a method appropriate for choosing a very small number of sample units from a relatively homogeneous collection of potential sample units. In statistical terminology, it was "purposive selection, in which the sample is restricted to units thought by someone to be especially typical of the population or convenient for sampling. Purposive selection may produce good results when the sample is small, but it is not amenable to the development of a theory. . ."³ The selection of test specimens from each sample weld, for material properties measurements, was necessarily guided by the required physical dimensions for test specimens rather than by principles of statistical experiment design. Thus statistical methods are not available for evaluation of weld-to-weld variability in the field nor for discriminating between variabilities in material and those associated with test methods.

Category No. 4: Modeling Problems: In deriving allowable defect size curves, NBS used mathematical models based on sound physical arguments and best judgments in approximating the actual phenomena of fatigue and fracture. Unfortunately, all theoretical models lack full-scale experimental basis in the range of interest where the defect depth to wall thickness ratio lies between 0.1 and 0.4. Some discussion of the current state of art in this specific area appears in Appendix P.

In the next two sections, we shall see how both types of sources of uncertainty were studied.

3. Sensitivity Analysis

As remarked in the last section (7B) on Allowable Defect Size Analysis, the defect sizes predicted by the Begley-McHenry-Read model are very sensitive to a small change in applied stress or flow stress or both in the neighborhood of defect depths from 0.09 in. down to 0.041 in., at which the allowable defect length reaches infinity. The range of defect sizes predicted by this model for small changes in operating and material parameters

³ William G. Cochran, Sampling Techniques, New York, Wiley, 1953, p. 7.

can easily be $\pm 50\%$, and hence cancel the OPSO safety factor of 2. Using physical reasoning, this behavior of the model was investigated to determine whether it arose from a mathematical artifact or was expressive of the true structural behavior. The conclusions were given in Section 7B, sub-section 5. Fig. 76 shows the variability of both the Begley-McHenry-Read and the Fong models for weld defects of the non-planar type. A similar analysis can be performed on planar defects, and the result is shown in Fig. 77. The Fong model is seen in both cases as less sensitive than the Begley-McHenry-Read model so far as variability due to stress, flow stress, and fracture toughness is concerned.

4. Significance of Safety Factors and Adjustment Constants Used in NBS Analysis

As mentioned in the introductory section, in addition to the use of OPSO safety factors on defect sizes and fatigue growth rate, there were numerous occasions when the analysis called for either a safety factor or an adjustment constant or both to complete a specific task. The final conclusion of our analysis depends, in part, on how we choose those factors of safety and adjustment constants. The purpose of this discussion is to illustrate how uncertainties of variables listed in four categories (see sub-section 2) are handled through the use of safety factors.

Regarding Category No. 1, Material Properties, we begin by observing that in addition to a factor of 4 on fatigue growth rate as specified by OPSO, NBS introduced an additional factor of 10 on growth rate in its fatigue analysis (see section 7A). The value of 4 is reasonable for fatigue growth data in general, but because stress corrosion and biaxial stress can be important factors, an extra margin of safety through the value of 10 was used. Turning to uncertainties due to change in fracture toughness from weld to weld, it is worth noting that OPSO requires the use of the minimum value. This led us to waive the use of any additional safety factor on fracture toughness, but we did introduce in our sensitivity analysis a variation of -10% to see how sensitive our allowable defect size curves are to this change.

On Category No. 2, Stress Analysis, we recall that there was a $+5\%$ variation of applied stress in our sensitivity analysis. This is reasonable considering the fact that the applied stress we use is the worst loading case of extremely low probability. We also observe that the NBS stress spectrum for fatigue analysis is not as severe as the Alyeska one. We believe that our choice is realistic and any variability in the stress spectra of different welds can be accounted for by the combination of the values of 4 (OPSO) and 10 (NBS) in safety factors for fatigue crack growth rates. On extra stresses, Alyeska documents asserted that the overstress due to surges will never be more than 10% over the design stress. Our allowance for this type of uncertainty lies in either a 10% reduction of the yield stress or a similar amount for the fracture toughness. The relationship between applied stress and mechanical strength is, in general, nonlinear, but this discussion in qualitative terms illustrates the scope of technical consideration that usually goes with the analysis.

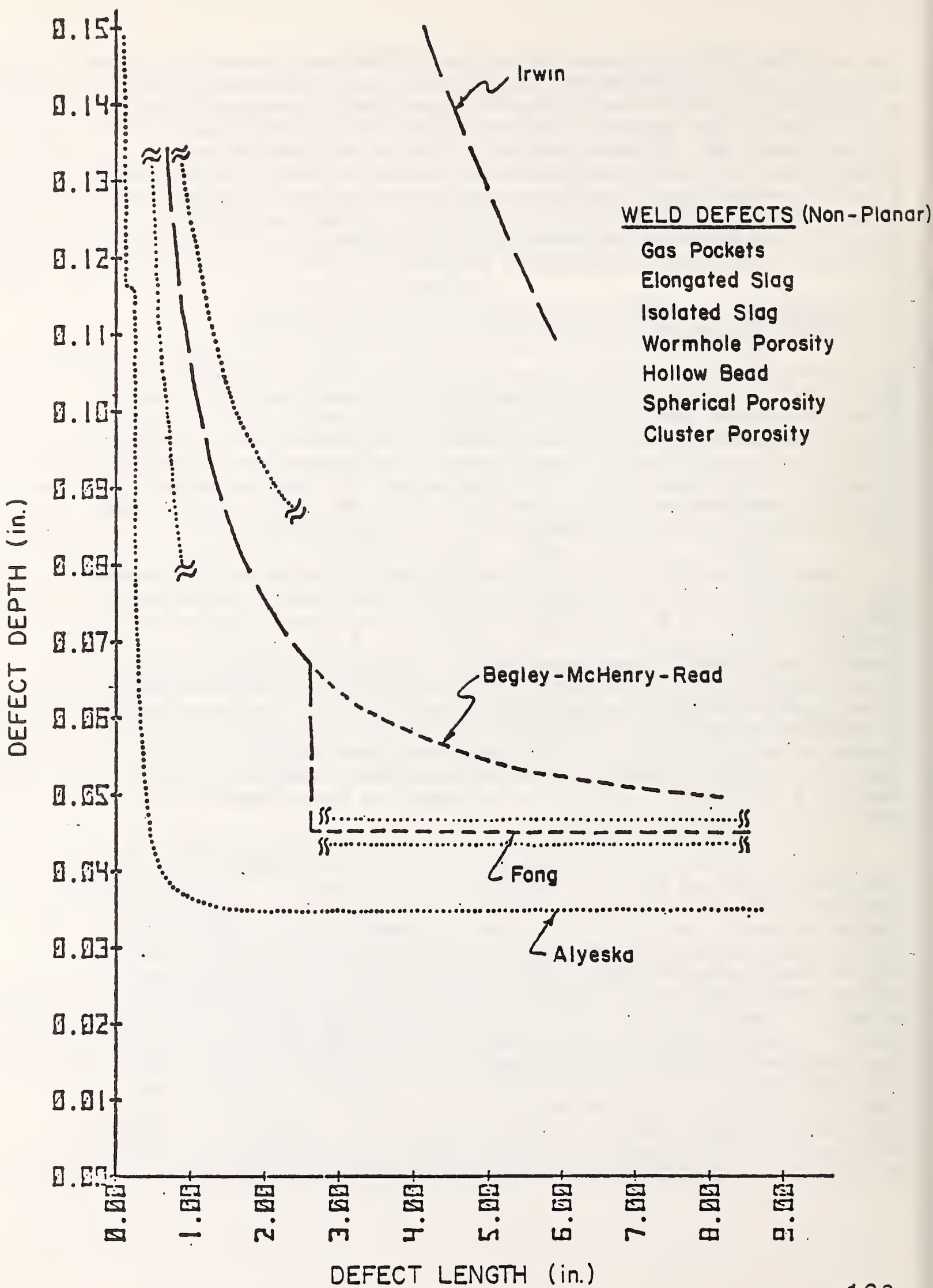


Fig. 7C. Sensitivity Analysis on Allowable Defect Size Curves (Non-Planar)

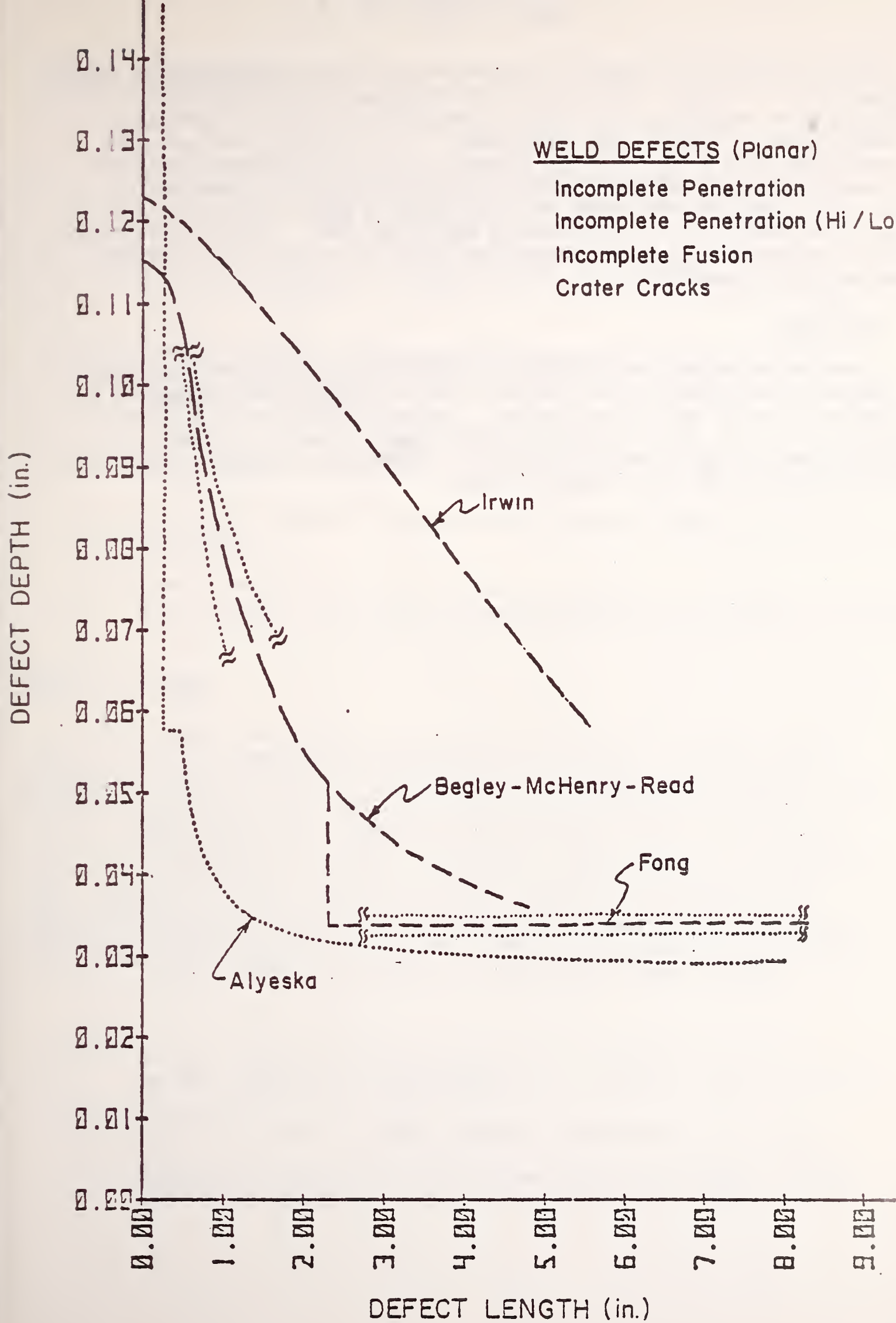


Fig. 77. Sensitivity Analysis on Allowable Defect Size Curves (Planar)

Field variability of material properties and construction quality (Category No. 3 on Sampling Problems) are addressed by applying those safety factors imposed by OPSO such as 2 on defect length and depth and an extra factor of 2 on planar defect depth. To illustrate how we handle uncertainties in modeling problems (Category No. 4), the reader is invited to examine Appendix P where an extra coefficient of 1.5 ($= \lambda$) was introduced when a shallow crack model was extended to a moderately deep crack region and a modification of the theory was called for. As more experimental data and mathematical analysis become available, that factor λ is likely to be adjusted downward.

5. Conclusion

This report summarizes the technical contributions of many investigators. We have shown that the choice of safety factors and adjustment constants is an integral part of this investigation. The conclusion we have arrived at depends not only on the analytical and experimental results of those investigators, but also on their technical judgments as embodied in the usual way through the use of safety factors.

Sources of Information

Defect-size information in this section is from the following sources:

- (1) "Presentation and Analysis of Quality Assurance Audit of 1975 Pipeline Welds/Radiography and Alyeska Engineering Technical Evaluation." (Approximately April 1976).
- (2) "Southwest Research Institute Review of Girth Weld X-Rays," Volumes I, II, and Addenda, S. Wenk and C. Allen (received by Alyeska July 21, 1976).
- (3) "Welds Requested for Exemption," Docket No. 76-12W, Appendices I and III, submitted by Alyeska Pipeline Service Company. (Revised September 10, 1976).

Defect-location and pipeline-variable information in this section is from the following sources:

- (1) Alignment sheets of Alyeska Pipeline Service Company for trans-Alaska pipeline.
- (2) Trans-Alaska Pipeline Project Atlas, Volume I, Livengood to Prudhoe Bay, prepared by M. Baker, Alyeska Pipeline Service Company (June 1976).

Defect-Size Data

Defect-depth measurements and arc-burn length and width measurements are required for assessing the Alyeska defect-size data. Defect size measurements are summarized in Tables 23-25. The measurements made by SWRI and RI are included in this summary without correction factors. For RI arc burn depth measurements listed in Table 25, the depths converted from arc burn widths (using Fig. 33) are included in the RI data. For completeness and for comparison, all data available to NBS from Alyeska (length only), Southwest Research Institute (SWRI), and from the September 10, 1976, Docket No. 76-12W submittal are included in these tables. From the tables, it is apparent that several omissions and discrepancies exist in these defect data; these are itemized in Table 26 and they include:

- (1) Lack of data on defect size from either Alyeska or SWRI to support the data submitted in the Docket.
- (2) Omission of specific defect length or depth data in the Docket.
- (3) Failure to use the most conservative value from Alyeska or SWRI defect-size data base.

During the radiographic measurements by RI, changes of a few defect types were suggested:

Weld #81586, location 81, listed as a gas pocket by Alyeska; described as an arc burn by RI. It is included in both of these categories in the present report.

Weld #81639, location 125, listed as hollow bead by Alyeska; described as both hollow bead and incomplete penetration by RI and SWRI. It is included in this report in both categories.

Weld #81590R, location 143, listed as spherical or cluster porosity by Alyeska; described as an arc burn by RI. This defect is included in this report in both categories.

Weld #90008, location 71, listed as arc burn by Alyeska; described as a "dull tool gouge" by RI. This defect is treated in this report as an arc burn.

Weld #W15TRX, location 55, listed as arc burn by Alyeska; is described as an undercut by RI. This defect is treated in this report as an arc burn.

Weld-Location Data

From the alignment sheets of the trans-Alaska pipeline, supplied by Alyeska, and from the Docket submittal, data are presented in Appendix A pertaining to exact location of the welds that contain the waiver-request defects.

There are several items of concern:

- (1) All previous discussions with Alyeska had established firmly that the pipe grade adjacent to waiver-request weld defects was X65; however from Appendix A it is apparent that the majority of pipe is grade X70. This change is of concern because maximum credible stresses are expected to be larger in grade X70. Also, the worst-case fatigue spectrum probably has greater stresses in X70 pipe areas. While Alyeska has represented the credible stress as a maximum and the fatigue spectrum (Table 19) as a worst case, careful consideration of the effects of X70 grade pipe on these stresses is required.
- (2) Downstream from a pump station, the pipeline is exposed to operating pressure surges that are not represented in the worst-case fatigue spectrum (Table 19). The magnitude of the pressure variations decreases as the distance from the pump station increases. Unfortunately, there are several defects whose location is close to pump station number three (see Appendix A). Documentation of the magnitude of the resulting fatigue spectrum in the pipeline very near, and downstream to, a pump station is needed for accurate assessment of those defects.

Table 23. Defect sizes of all planar defects.

Weld #	Radiographic Location	L E N G T H			SWRI ⁺ (in)	D E P T H	
		Alyeska (in)	SWRI (in)	Final Docket (9/10/76) (in)		Final Docket (9/10/76) (in)	RI ⁺⁺ (in)
<u>PLANAR DEFECTS</u>							
<u>Incomplete Penetration</u>							
90057	2	N.A.	3.50	3.50	N.A.	Est.0.020	0.035
<u>Incomplete Penetration (Hi/Lo)</u>							
81627	111	N.A.	2.00	2.25	Est.0.030	Est.0.030	0.013
81635* ^y	140	N.A.	N.A.	N.A.	Est.0.025	N.A.	0.022
81706	44	3.00	3.00	2.50	Est.0.040	Est.0.035	0.028
	64	3.00	3.00	3.00	Est.0.035	Est.0.035	0.030
90056	0	N.A.	N.A.	5.50	N.A.	Est.0.020	0.035
<u>Incomplete Fusion</u>							
81408	89	5.00	N.A.	5.00	Est.0.015	Est.0.015	0.024
81430**	135	10.00	N.A.	10.00	0.014	0.014	0.046
81448	135	1.50	1.375	1.375	Est.0.035	Est.0.035	0.013
81485	17	2.00	2.00	2.00	Est.0.030	Est.0.030	0.012
81498	124	N.A.	N.A.	2.25	N.A.	Est.0.025	0.028
81499	105	N.A.	2.75	2.75	Est.0.020	Est.0.020	DNF
81506	20	1.25	1.25	1.25	Est.0.035	Est.0.035	0.020
81595	136	2.00	N.A.	2.00	N.A.	N.A.	0.020
81639* ^y	125	N.A.	N.A.	N.A.	N.A.	N.A.	0.038
90008**	124	N.A.	N.A.	0.388	N.A.	Est.0.060	0.048

N.A. - Not available.

Not included in 9/10/76 Docket No. 76-12W submittal.

* Included in 9/10/76 Docket No. 76-12W, Appendix III submittal.

· Hollow bead reported at same location by SWRI, RI, not incomplete fusion.

See P. 90 for recommended correction factor.

+ See Fig. 48 for recommended correction factor.

NF Did not find.

Table 24. Defect sizes of all non-planar defects.

Weld #	Radiographic Location	Alyeska (in)	L E N G T H		SWRI ⁺ (in)	D E P T H		RI ⁺⁺ (in)
			SWRI (in)	Final Docket (9/10/76) (in)		Final Docket (9/10/76) (in)		
NON-PLANAR DEFECTS								
Gas Pockets								
81153	48	0.25	0.15	0.25	0.018	0.018	0.048	
81209	129	0.188	0.175	0.188	0.007	0.007	0.043	
81316	50	N.A.	0.150	0.188	0.057	0.057	0.075	
81321	68	0.375	0.375	0.375	0.015	Est.0.015	0.053	
81338R	23	0.188	0.150	0.188	0.024	0.024	0.060	
81404	18	0.25	0.20	0.25	0.024	0.024	0.038	
81434R	32	0.25	N.A.	0.25	0.006	0.006	0.025	
81441R	74	0.188	0.125	0.188	0.010	0.010	0.030	
81447	57	0.188	0.155	0.188	0.037	0.037	0.056	
81565T	112	0.188	0.150	0.188	N.A.	0.039	0.018	
81577	125	0.188	0.150	0.188	N.A.	0.016	0.035	
81585	0	0.188	0.250	0.188	Est.0.050	Est.0.050	0.078	
81586 ^a	81	0.188	0.375	0.188	N.A.	0.039	0.058	
81628	140	0.188	0.200	0.188	N.A.	0.015	0.045	
81670	70	0.156	0.125	0.312	0.018	0.018	0.050	
81674	28	0.219	0.180	0.219	0.006	0.006	0.025	
81701	75	0.188	0.188	0.188	N.A.	0.006	0.068	
W15TRX	43	N.A.	0.150	0.156	0.038	0.007	0.042	
W25RTRX	74	N.A.	0.135	0.156	0.047	0.047	0.065	
W39TRX	81	N.A.	0.25	0.25	0.014	0.014	0.058	
NON-PLANAR DEFECTS								
Elongated Slag								
81135	115	4.062	7.00	4.562	Est.0.020	Est.0.020	0.037	
81180	10	2.25	1.00	2.25	Est.0.030	Est.0.030	0.043	
81293	24	2.50	2.25	2.50	N.A.	N.A.	0.038	
81397**	111	6.00	0.8125	N.A.	0.033	0.033	0.035	
81401	116	5.00	N.A.	5.00	Est.0.015	Est.0.015	0.026	
81411	145	0.375	N.A.	3.625	Est.0.015	Est.0.015	0.044	
81420	123	2.75	N.A.	3.50	Est.0.010	Est.0.010	0.032	
81424	15	3.375	N.A.	3.375	Est.0.010	Est.0.010	0.035	
81451	146	N.A.	1.00	2.25	N.A.	N.A.	0.053	
81474	105	3.00	3.75	2.50	Est.0.030	Est.0.015	0.030	
	122	3.00	2.375	3.00	Est.0.030	Est.0.015	0.031	
81476	125	3.00	3.50	3.00	Est.0.020	Est.0.020	0.033	
81488	106	4.50	4.00	4.00	Est.0.020	Est.0.020	0.036	
	124	4.50	5.625	5.625	Est.0.020	Est.0.020	0.048	
81498	135	2.50	2.25	2.50	Est.0.025	Est.0.025	0.020	
81499	135	3.50	4.25	4.25	Est.0.020	Est.0.020	0.034	
81503**	123	3.00	3.00	2.50	Est.0.040	Est.0.040	0.038	
	135	3.00	2.062	3.00	Est.0.040	Est.0.040	0.031	
81508	20	3.00	2.312	3.00	Est.0.030	Est.0.030	0.060	
81513	5	2.125	2.625	3.25	Est.0.020	Est.0.020	0.028	
81551	111	3.00	2.875	3.00	Est.0.035	Est.0.035	0.039	
81562	126	2.812	6.00	2.812	Est.0.020	Est.0.020	0.035	
81618	4	3.00	5.00	5.00	Est.0.020	Est.0.020	0.035	
81710**	58	3.375	N.A.	3.375	0.064	0.064	0.040	
90001C**	108	N.A.	2.25	2.25	N.A.	Est.0.040	0.030	
	120	N.A.	2.25	2.25	N.A.	Est.0.040	0.033	

** Included in 9/10/76 Docket No. 76-12W, Appendix III submittal.

a. Estimated by RI to be arch burn, not gas pocket.

N.A. =Not available.

+ See P. 90 for recommended correction factor.

++ See Fig. 48 for recommended correction factor.

Table 24. Defect sizes of all non-planar defects (continued).

Weld #	Radiographic Location	L E N G T H		Final Docket (9/10/76) (in)	SWRI ⁺ (in)	D E P T H		RI ⁺⁺ (in)
		Alyeska (in)	SWRI (in)			Final Docket (9/10/76) (in)	Final Docket (9/10/76) (in)	
NON-PLANAR DEFECTS								
<u>Hollow Bead</u>								
81210	122	2.25	2.75	2.75	Est.0.020	Est.0.020	0.045	
81255	107	2.50	2.375	2.375	Est.0.030	Est.0.030	0.069	
81307	10	2.625	3.625	2.125	0.013	Est.0.020	0.043	
	25	2.625	2.375	0.050	Est.0.020	Est.0.020	0.040	
81316	11	2.375	3.00	2.375	Est.0.020	Est.0.020	0.040	
	25	2.375	2.375	1.75	Est.0.020	Est.0.020	0.030	
81319	8	2.125	3.00	2.125	0.008	0.008	0.038	
81346	101	0.50	1.50	1.50	Est.0.020	Est.0.020	0.032	
81350	26	4.00	N.A.	2.25	N.A.	Est.0.030	0.047	
	125	4.00	7.625	2.25	Est.0.030	Est.0.030	0.041	
81396	23	2.50	2.75	2.50	N.A.	Est.0.030	0.048	
81397**	27	N.A.	2.875	2.75	Est.0.045	Est.0.025	0.045	
81406	20	2.50	N.A.	2.125	Est.0.020	Est.0.020	0.032	
81407	12	2.25	N.A.	2.25	0.013	Est.0.020	0.030	
	26	2.25	N.A.	2.25	Est.0.020	Est.0.020	0.035	
81431	26	2.625	N.A.	2.625	Est.0.020	Est.0.020	0.033	
81432	30	0.375	N.A.	2.375	Est.0.025	Est.0.025	0.040	
81445**	24	N.A.	2.062	2.062	Est.0.040	Est.0.040	0.044	
81451	24	2.50	2.125	2.50	Est.0.035	Est.0.035	0.031	
81473	12	2.125	3.25	3.25	Est.0.020	Est.0.020	0.037	
81500**	135	2.125	2.375	2.375	Est.0.045	Est.0.045	0.034	
81515	14	N.A.	2.75	2.438	Est.0.020	Est.0.020	0.048	
	30	N.A.	2.50	2.312	Est.0.020	Est.0.020	0.038	
81522**	33	2.375	2.562	2.562	Est.0.040	Est.0.040	0.030	
81526**	98	0.50	2.25	2.25	Est.0.040	Est.0.040	0.036	
81532	48	2.188	2.625	2.625	Est.0.020	Est.0.020	0.041	
81535	12	2.125	2.875	2.875	Est.0.020	Est.0.020	0.039	
	141	2.125	2.375	2.375	Est.0.020	Est.0.020	0.045	
81537**	120	2.25	2.688	2.688	Est.0.050	Est.0.050	0.032	
81538**	34	2.375	2.062	2.375	Est.0.040	Est.0.040	0.038	
81540**	124	2.50	2.938	2.938	Est.0.050	Est.0.050	0.045	
81545**	18	2.25	2.75	3.312	Est.0.045	Est.0.045	0.038	
	30	2.25	3.312	2.75	Est.0.045	Est.0.045	0.044	
81548**	30	2.25	2.50	2.50	Est.0.040	Est.0.040	0.043	
81549**	96	2.25	2.25	2.25	Est.0.045	Est.0.045	0.048	
81550**	19	2.50	2.625	2.625	Est.0.040	Est.0.040	0.041	
81552**	28	2.188	2.938	2.938	Est.0.040	Est.0.040	0.051	
81597	45	2.812	2.50	2.50	Est.0.020	Est.0.020	0.054	
81625	135	2.625	3.00	3.00	Est.0.020	Est.0.020	0.022	
81626	55	2.75	2.875	2.625	Est.0.035	Est.0.035	0.030	
	135	2.75	2.625	2.875	Est.0.025	Est.0.035	0.037	
81627	103	2.188	2.50	2.188	Est.0.020	Est.0.020	0.048	
	111	2.188	2.00	2.50	Est.0.030	Est.0.020	0.013	
81630	15	2.50	2.031	2.50	Est.0.035	Est.0.035	0.025	
	125	2.50	3.00	3.00	Est.0.035	Est.0.035	0.028	
81635 ^y	142	2.125	2.031	2.125	Est.0.035	Est.0.035	0.035	
81639 ^z	125	2.125	2.031	2.125	Est.0.035	Est.0.035	0.038	
81642**	15	2.188	2.50	2.188	Est.0.040	Est.0.040	0.034	
81643**	12	2.50	2.875	2.875	0.023	0.023	0.038	
81644	20	2.062	4.375	2.062	Est.0.020	Est.0.020	0.039	
81645	25	3.00	2.625	2.75	Est.0.020	Est.0.020	0.039	
	122	3.00	3.625	3.625	Est.0.020	Est.0.020	0.039	
81646**	48	3.25	2.375	3.25	Est.0.045	Est.0.045	0.041	
81667	42	2.625	2.50	2.625	Est.0.020	Est.0.020	0.025	
	54	2.625	2.50	2.625	Est.0.020	Est.0.020	0.020	
81678	48	2.50	2.50	2.50	Est.0.035	Est.0.035	0.033	
81688	51	2.25	3.50	3.50	Est.0.020	Est.0.020	0.035	
81707**	120	2.312	2.156	2.312	Est.0.045	Est.0.045	0.055	

y. Incomplete penetration (Hi/Lo) also reported at same location by RI and SWRI.

z. Estimated by RI and SWRI to be hollow head, not incomplete penetration.

** Included in 9/10/76 Docket No. 76-12W, Appendix III submittal.

N.A. Not available.

+ See P. 90 for recommended correction factor.

++ See Fig. 48 for recommended correction factor.

Table 24. Defect sizes of all non-planar defects (continued).

Weld #	Radiographic Location	L E N G T H			SWRI ⁺ (in)	D E P T H		RI ⁺⁺ (in)
		Alyeska (in)	SWRI (in)	Final Docket (9/10/76) (in)		Final Docket (9/10/76) (in)		
<u>NON-PLANAR DEFECTS</u>								
<u>Spherical Porosity, Cluster Porosity</u>								
81138	35	0.125	0.047	0.125	N.A.	N.A.	0.023	
	36	0.125	0.047	0.125	N.A.	N.A.	0.005	
	42	0.125	0.047	0.125	N.A.	N.A.	0.028	
	43	0.125	0.047	0.125	N.A.	N.A.	0.040	
81142	47	0.125	0.075	0.094	0.014	0.014	0.050	
	69	0.125	0.075	0.125	0.007	0.014	0.045	
81203	40	0.125	0.25	0.125	Est.0.015	Est.0.015	0.050	
	68	0.125	0.375	0.125	Est.0.015	Est.0.015	0.068	
81252	58	0.125	0.050	0.125	0.065	0.076	0.078	
81258	47	0.094	0.075	0.094	0.032	0.032	0.048	
81299	32	0.219	0.062	0.219	0.034	0.034	0.054	
81300	76	0.125	0.075	0.125	0.062	0.062	0.070	
81301	115	N.A.	0.175	0.219	0.084	0.084	0.082	
81311	59	0.094	0.100	0.094	0.009	0.009	0.055	
81332	50	0.125	0.075	0.125	0.023	0.023	0.098	
81343	88	N.A.	N.A.	0.188	N.A.	N.A.	0.073	
81364	108	0.188	0.094	0.188	N.A.	N.A.	0.055	
81399	35	0.156	N.A.	0.156	N.A.	N.A.	0.042	
81442	97	0.125	0.075	0.125	0.035	0.035	0.067	
81522**	72	N.A.	0.188	0.188	Est.0.015	Est.0.015	0.057	
81544	108	0.125	0.062	0.094	N.A.	N.A.	0.035	
	109	0.125	0.047	0.125	N.A.	N.A.	0.045	
81572	50	0.125	0.075	0.125	N.A.	N.A.	0.052	
81590R ^a	143	0.125	N.A.	0.125	N.A.	N.A.	0.027	
81616	70	0.125	0.100	0.125	N.A.	N.A.	0.050	
81619	98	0.094	0.075	0.094	N.A.	N.A.	0.042	
81660	62	N.A.	0.062	0.062	N.A.	N.A.	0.035	
	70	N.A.	N.A.	0.062	N.A.	N.A.	0.032	
81673	41	0.625	0.25	0.625	Est.0.010	Est.0.010	0.028	
	46	0.625	0.031	0.625	Est.0.010	Est.0.010	0.068	

** Included in 9/10/76 Docket No. 76-12W, Appendix III submittal.
a. Estimated by RI to be arc burn, not spherical or cluster porosity.
N.A. - Not available.
+ See P. 90 for recommended correction factor.
† See Fig. 48 for recommended correction factor.

Table 25. Defect sizes of all arc burns.

Weld #	Radiographic Location	Alyeska (in)	L E N G T H			D E P T H			RI, converted by NBS (in)
			SMRI (in)	Final Docket (9/10/76) (in)	RI (in)	RI diameter (in)	Final Docket (9/10/76) (in)		
<u>Arc Burns (Base Metal)</u>									
81190	68	N.A.	N.A.	0.062	0.250	0.230	Est.	0.020	0.039
81442	75	N.A.	0.50	0.500	0.600	0.160		0.023	0.016
	79	N.A.	N.A.	0.500	0.400	0.140		0.023	0.011
90021	94	N.A.	0.062	0.062	0.340	0.130		0.010	0.008
W22TRX	71	N.A.	0.188	0.188	0.490	0.185		0.025	0.025
81685	77	N.A.	0.250	0.250	0.270	0.210		0.015	0.033
<u>Arc Burns (Weld, Heat-Affected Zone)</u>									
79882	90	N.A.	0.125	0.500	0.305	0.300	Est.	0.010	0.062
81146	28	N.A.	N.A.	N.A.	0.265	0.190		0.007	0.027
81148	79	N.A.	N.A.	0.375	0.365	0.310		0.048	0.065
	80	N.A.	N.A.	0.375	0.535	0.225		0.048	0.037
	93	N.A.	N.A.	0.375	0.480	0.235		0.048	0.040
	98	N.A.	N.A.	0.375	0.270	0.240		0.048	0.042
	126	N.A.	N.A.	0.094	0.335	0.160		0.048	0.015
	130	N.A.	N.A.	0.312	0.340	0.320		0.048	0.068
	144	N.A.	N.A.	0.188	0.335	0.260		0.048	0.049
	36	N.A.	0.020	0.375	0.200	0.160	Est.	0.015	0.020
81248	142	N.A.	0.062	0.312	0.310	0.175	Est.	0.010	0.022
81287	130	N.A.	N.A.	0.375	0.270	0.175		0.035	0.021
81289	71	N.A.	0.025	0.250	0.290	0.200		0.030	0.030
81312	4	N.A.	N.A.	0.250	0.415	0.200		0.260	0.030
81324	65	N.A.	0.020	0.250	0.280	0.240		0.032	0.042
81332	79	N.A.	N.A.	0.188	0.190	0.170		N.A.	0.018
81340	44	N.A.	N.A.	0.125	0.265	0.180	Est.	0.010	0.023
81424	25	N.A.	N.A.	0.094	0.260	0.200		0.018	0.030
81443	50	N.A.	N.A.	0.062	0.360	0.280		0.017	0.055
	58	N.A.	N.A.	0.125	0.280	0.220		0.013	0.036
	58	N.A.	N.A.	0.094	0.220	0.200		0.010	0.030
81444 ^b	58	N.A.	N.A.	N.A.	0.360	0.300		N.A.	0.062
81586 ^a	81	N.A.	N.A.	N.A.	0.400	0.200		N.A.	0.030
81590R ^c	143	N.A.	N.A.	0.250	0.260	0.220	Est.	0.020	0.036
81595	83	N.A.	N.A.	0.188	0.225	0.160		0.016	0.016
90001C ^{**}	3	N.A.	0.188	0.375	0.210	0.200		0.020	0.030
	125	N.A.	0.750	0.750	0.875	0.110	Est.	0.018	0.001
90008R ^{**d}	71	N.A.	0.125	0.375	0.210	0.105		0.038	0.001
W15TRX ^e	55	N.A.	0.125	0.375	0.180	0.150		0.009	0.013
	100	N.A.	0.125	0.375	0.310	0.230		0.008	0.039
W16TRX	40	N.A.	0.375	0.375	1.50	0.125		0.008	0.007
	70	N.A.	0.125	0.375	0.525	0.180		0.020	0.023
W22TRX	36	N.A.	0.125	0.375	0.305	0.220		0.010	0.036
W23TRX	45	N.A.	0.125	0.375	0.280	0.220		0.010	0.036
	75	N.A.	0.125	0.375	0.280	0.220		0.010	0.036

N. A. = Not available
^a Not included in 9/10/76 Docket No. 76-12W submittal.
^{**} Included in 9/10/76 Docket No. 76-12W, Appendix III submittal.
^b Estimated by RI to be arc burn, not gas pocket.
^c Estimated by RI to be arc burn, not spherical or cluster porosity.
^d Estimated by RI to be dull tool mark, not arc burn.
^e Considered by RI to be undercut.

Table 26. Defect-size-data discrepancies.

Special Considerations	Weld # or Number of Defects					
	Planar Defects		Non-Planar Defects		Arc Burns	
	length	depth	length	depth	length	depth
Lack of defect-size data from Alyeska or SWRI to support Docket data.	5	6	2	24	20	1
Lack of defect-size data in Docket submittal.	2	3	1	17	3	4
Alyeska or SWRI defect-size data greater than Docket data.	81706 81448	81706	81585-GP 81586-GP 81628-GP 81135-ES 81474-ES 81476-ES 81562-ES 81307-HB 81316-HB 81350-HB 81397-HB 81406-HB 81545-HB 81597-HB 81626-HB 81627-HB 81644-HB 81645-HB 81142-SP,CP 81311-SP,CP 81544-SP,CP	81321-GP 81474-ES 81307-HB 81397-HB 81407-HB W15TRX-GP.	--	--

GP = Gas pocket
 ES = Elongated slag
 HB = Hollow bead
 CP = Spherical porosity, cluster porosity

9. CONCLUSIONS

The material properties needed for the fracture mechanics analysis of the trans-Alaska oil pipeline base material and welds, have been evaluated. Because of the toughness, yield strength and applied stress in this situation, fracture mechanics is the best available methodology to predict failure and assess girth welds containing defects.

There is no exact method for analyzing fracture conditions involving substantial plasticity. Further, in the region of interest for defect sizes of this project, there are very few experimental results to substantiate any given fracture model. Therefore, several methods were used to calculate allowable defect sizes.

The conclusions are based on allowable defect size curves calculated using maximum credible operating stresses and low rates of loading that are expected to exist in the main line of grade X-65 pipe. Somewhat higher stresses may be expected in sections of X-70 grade pipe and in the fatigue spectrum stress near pump stations due to pressure surges.

Allowable defect sizes calculated using these higher stresses will be lower than those shown in this report. At the expected loading rates in the pipeline, the welds behave in a non-brittle manner at all anticipated operating temperatures. In the unlikely case that a crack of sufficient size is initiated in a hard region, such as an arc burn, propagation or arrest of this crack may be governed by the dynamic fracture toughness of the metal, which is somewhat less than the static fracture toughness used to calculate the allowable defect size curves in this report.

For the stress levels in the X-65 grade of main line pipe and for the expected low rates of loading, the fracture mechanics analyses described in this report indicate the following:

1. The calculated allowable defect size curve and analysis submitted by Alyeska for nonplanar defects is considered reasonable.
2. The calculated allowable defect size curves submitted by Alyeska for planar and arc burn defects are considered reasonable, except for the region of small defect lengths where Alyeska curves allow unlimited defect depth. The other calculated allowable defect size curves developed in this report show a maximum allowable defect depth even for short defect lengths.

When good control is maintained over radiographic variables, defect sizes can be determined with reasonable accuracy. If more precise measurements are required, other nondestructive testing methods such as ultrasonics, should be used to supplement radiographic testing.

In the case of the pipeline girth welds, the radiographs were taken to meet the present workmanship codes. Precise radiographic control is not required and, therefore, it follows that defect size measurements of high accuracy may not be possible. Sufficient radiographic control must be maintained, particularly in terms of radiation energy and film processing, to permit the establishment of a reasonable relationship between radiographic film density and defect depth (or steel thickness). The available data from the pipeline field radiographs show a much greater variability for the radiographic contrast of the supposedly known thickness of the radiographic penetrometer and shim on the pipe wall than can be accounted for with all the considered parameters. This variability makes any depth measurement subject to error.

Three methods were used to measure defect depths from the Alyeska radiographs. Southwest Research Institute (SWRI) used both a densitometer method and a visual comparison technique. Rockwell International (RI) employed a visual comparison method involving only the weld and defect area. In both SWRI methods, comparisons were made to the film contrast for the shim-penetrometer image on the pipe wall.

For the SWRI method in which densitometer measurements were used, the film contrast variability is less important since defect depth was determined by a ratio calculation which makes use of the penetrometer-shim image contrast. The errors then will depend on the accuracy with which the densitometer measurements can be taken. The difficult measurements are those involving the defect image and its contrast with the weld. The densitometer reading of the defect will vary depending upon (1) the ratio of the defect image density area and the area of the densitometer aperture, and (2) the degree of density uniformity in the aperture area. Since each defect may be different, it is not possible to assess the accuracy of this method in a positive manner. Some determinations of defect depth using this densitometer method are given as illustrations of the changes produced in the defect depth calculation for typical variations in densitometer readings.

The SWRI visual method is difficult to assess since no controlled experiment has been done. It is our recommendation that the SWRI visual depth measurements be used only as a means of checking other depth measurements such as those being made by RI. For reasons discussed in this report, we believe the visual method used by SWRI will underestimate flaw depth. The degree of that underestimation has not been assessed.

The visual depth measurements made by RI have been analyzed. Based on laboratory x-ray calibration data, the RI method tends to underestimate the defect depth in increasing amounts for defects of greater depth. However, these corrections are based on laboratory x-ray films. For the Alyeska films, there are many field radiographs whose contrast falls outside the contrast limits predicted by the film response and expected radiographic procedure. This poses a dilemma since the reason for this change in film contrast is not known. If the contrast variations are due to extreme changes in x-ray voltage or changes in film processing, an accurate depth determination by the RI method may not be possible. However, if the contrast changes were caused by shim thickness variations or densitometer reading errors, the accuracy of the RI method may not be affected.

In support of the RI measurements there is information presented to demonstrate that the RI depth measurements tend to be larger than those made by the SWRI densitometer method. This is important because these two sets of measurements were taken by independent approaches and because the SWRI measurements should not be influenced by film contrast variations. It is also demonstrated that RI measurements of several natural defects in welds furnished to NBS by Alyeska, showed correlation with laboratory radiographic measurements to a one σ limit of 47%. Since the RI method is the only one used to measure depth of all weld defects still under consideration for waiver, DoT may wish to expand these comparisons in order to set limits on the RI method.

The length measurements can, in most cases, be made to accuracies of 0.010 in. Exceptions involve defects which gradually diminish in depth so that the ends of the defect are difficult to observe on the radiograph; defects in this category include incomplete penetration, incomplete fusion and elongated slag. An independent length measurement should be provided for those defect types. In addition, some of the large discrepancies noted in defect length should be explained and/or remeasured. These are probably caused by differences in radiographic interpretation.

For arc burns, a method is described for determining effective arc burn depth based on the measurement of arc burn diameter or width, a measurement possible from the radiograph.

In summary, the fracture mechanics analyses provide a method to evaluate the performance of the pipeline girth welds in terms of calculated allowable defect sizes. Defect lengths can be measured accurately, although some discrepancies have been noted. Arc burn diameters or widths can be measured and a method for converting that measurement to a depth is described. For other defect types, the depth measurement becomes more difficult and is subject to possible error as described in this report.

U.S. DEPT. OF COMM BIBLIOGRAPHIC DATA SHEET		1. PUBLICATION OR REPORT NO. NBSIR 76-1154	2. Gov't Accession No.	3. Recipient's Accession No.
4. TITLE AND SUBTITLE Consideration of Fracture Mechanics Analysis and Defect Dimension Measurement Assessment for the Trans-Alaska Oil Pipeline Girth Welds			5. Publication Date October 18, 1976	6. Performing Organization Code
			8. Performing Organ. Report No.	
7. AUTHOR(S) Harold Berger, John H. Smith, Editors			10. Project/Tank/Work Unit No. 3000380	
9. PERFORMING ORGANIZATION NAME AND ADDRESS NATIONAL BUREAU OF STANDARDS DEPARTMENT OF COMMERCE WASHINGTON, D.C. 20234			11. Contract/Grant No.	
			13. Type of Report & Period Covered Final	
12. Sponsoring Organization Name and Complete Address (Street, City, State, ZIP) Department of Transportation 2100 2nd Street, SW Washington, D. C. 20590			14. Sponsoring Agency Code	
			15. SUPPLEMENTARY NOTES	
16. ABSTRACT (A 200-word or less factual summary of most significant information. If document includes a significant bibliography or literature survey, mention it here.) In anticipation of a request for waivers on defective girth welds in the Trans-Alaska oil pipeline, DoT requested assistance from the National Bureau of Standards (NBS) in evaluating the fracture mechanics analysis and the nondestructive evaluation (NDE) methods used to detect and determine dimensions of weld defects. NBS measured the required mechanical properties of the weld metal, developed and evaluated fracture mechanics methods to determine the allowable defect sizes, and evaluated various methods of measuring the size of defects present in the welds from existing field radiographs. Results of this investigation show that the fracture mechanics analysis can be used to determine the allowable defect sizes concerning the integrity of the pipeline, but that these analyses have not been experimentally verified at this time. Defect dimensions can be determined with sufficient accuracy to be useful in the fracture mechanics analyses if the radiographs are made under carefully controlled conditions. If the radiographs are not made with close control, the accuracy of the defect sizes may not be sufficient to permit their use in establishing allowable defect sizes.				
17. KEY WORDS (six to twelve entries; alphabetical order; capitalize only the first letter of the first key word unless a proper name; separated by semicolons) Fracture control; Fracture mechanics; Mechanical properties; Nondestructive evaluation (NDE); Radiography; Welding				
18. AVAILABILITY <input type="checkbox"/> Unlimited <input checked="" type="checkbox"/> For Official Distribution. Do Not Release to NTIS <input type="checkbox"/> Order From Sup. of Doc., U.S. Government Printing Office Washington, D.C. 20540, SO Cat. No. G33 <input type="checkbox"/> Order From National Technical Information Service (NTIS) Springfield, Virginia 22161		19. SECURITY CLASS (THIS REPORT) UNCLASSIFIED		21. NO. OF PAGES 310
		20. SECURITY CLASS (THIS PAGE) UNCLASSIFIED		22. Price

